PHOTO-INDUCED STRUCTURAL CHANGES IN THE Ag-As-S SYSTEM

by

A. P. Firth

A thesis presented for the degree of Doctor of Philosophy

Faculty of Science
University of Edinburgh

June, 1985

DECLARATION

This thesis is the original composition of the author's work, unless stated otherwise, and has not been submitted previously for any other degree.

In memory of my father

CONTENTS

ACKNOWLEDGEMENTS

I would like to thank my supervisors, Professor A. E. Owen and P. J. S. Ewen for their advice and help during the project. Also I would like to thank Miloslav Frumar for his help and advice with the photodarkening experiments, and to Janos Hajto for some useful discussions.

I am grateful to Dr P. J. S. Ewen and Dr J. A. Bruce for proof reading, and to Elizebeth Rogawska for typing the script.

I would like to thank Hugh Vass of the Physics deptartment for his help with the Raman experiments, and also I am grateful to the technical staff of the Electrical Engineering department.

I acknowledge the University of Edinburgh for providing the laboratory facilities and also the SERC for financial support.

Finally I would like to thank my family and friends for their understanding and encouragement.

ABSTRACT

The photodarkening effect in evaporated As_2S_3 films, thin bulk samples and glassy powders has been studied. Optical transmissivity was measured and its dependence on intensity, wavelength, temperature and previous thermal history was found. A structural investigation was also made using Raman spectroscopy. A feature at 231 cm^{-1} in the Raman spectra, Which is associated with hompolar As-As bonds, is enhanced after photodarkening. A model based on the redistribution of chemical bonds under illumination is used to explain the results.

The photodissolution of Ag into As-S films has also been studied. Raman spectroscopy has been used to study the structural changes occurring in films of As-S glasses of compositions $As_{41}S_{59}$, $As_{38}S_{62}$, $As_{30}S_{70}$ and $As_{20}S_{80}$, after photodoping with Ag. Only the photodoped film of composition $As_{30}S_{70}$ produced a single phase homogeneous material which was structurally the same as a bulk glass of similar composition. In the other compositions there is evidence of phase separation. Kinetic experiments indicate that Ag^+ ions are mobile during photodissolution, and that the actinic light which causes photodissolution is absorbed in the photodoped layer, close to the interface between the doped and undoped regions. A proposed mechanism involving a tarnishing type process is used to explain the results.

CHAPTER 1

INTRODUCTION

A fundamental property of an amorphous semiconductor is that the structure and bonding configuration are not determined and fixed by thermodynamic equilibrium conditions: alterations can be produced, sometimes reversibly, by some means which changes the energy of the system. It is therefore possible that light-induced structural changes will occur in amorphous semiconductors.

Chalcogenide semiconductors are a particular class of amorphous semiconductors in which a wide variety of light-induced changes have been observed. These range from reversible optical changes (i.e. photodarkening and photobleaching) caused by small changes in atomic rearrangements to more substantial modifications which completely change the physical and chemical nature of the material (e.g. photopolymerisation, photocrystallisation, photodissolution of metals etc.).

These effects are of interest because of the information they provide on defects and meta-stable structural properties which are unique to the amorphous state. Also, photo-induced effects in chalcogenide glasses are of considerable technological importance.They

have potential applications in optical-imaging, hologram recording, optical mass memories (1, 2, 3, 4), and in particular they have potential as sub-micron photo-resists for the fabrication of integrated circuits (5).

At least seven distinct photo-induced structural or physico-chemical changes have been observed in amorphous chalcogenides, when samples in a suitable form are exposed to light or other irradiation, vis: photocrystallisation; photopolymerisation; photo-decomposition (in compounds); photo-induced morphological changes; photo-vaporisation; photodissolution (of certain metals); and light induced changes in local atomic configuration. In general these changes are accompanied by changes in the optical constants of the material and particularly shifts in the absorption edge, i.e. photodarkening or photobleaching. These photo-induced phenomena may be classified according to whether they are primarily structural or physico-chemical in nature and whether they are reversible or irreversible, in the sense that the system may partly revert to its initial state after some annealing treatment at a temperature higher than that at which illumination took place, or will recover completely on annealing at the glass transformation temperature, Tg.

The reversible effects are generally observed most readily in well-annealed vapour-deposited films, or in

melt-quenched glasses, which are also comparitively well-annealed as a natural consequence of their method of preparation. By contrast, those irreversible changes which are primarily structural are found mainly in poorly -annealed vapour-deposited films, while the irreversible physico-chemical phenomena occur whatever the state of annealing of the amorphous sample. The inter-relationships between the reversible or irreversible, and structural or physico-chemical effects are illustrated schematically in figure 1.1.

The present work is concerned with two particular photo-induced effects: optical darkening (termed "photodarkening") and the photodissolution of metals into chalcogenide glasses (also called "photodoping"). The study is concerned exclusively with chalcogenides in the As-S system and Ag metal phtotodissolution. This system was chosen because amorphous As_2S_3 is the most widely studied of the chalcogenide glasses in which both the photodarkening and photodissolution effects occur. Despite extensive investigation neither of these effects has been fully explained .

The photodarkening effect is best observed in thin evaporated As-S films and in annealed films the effect is fully reversible. An explanation of photodarkening in terms of structural changes has been suggested but as yet no structural evidence as to the origin of photodarkening

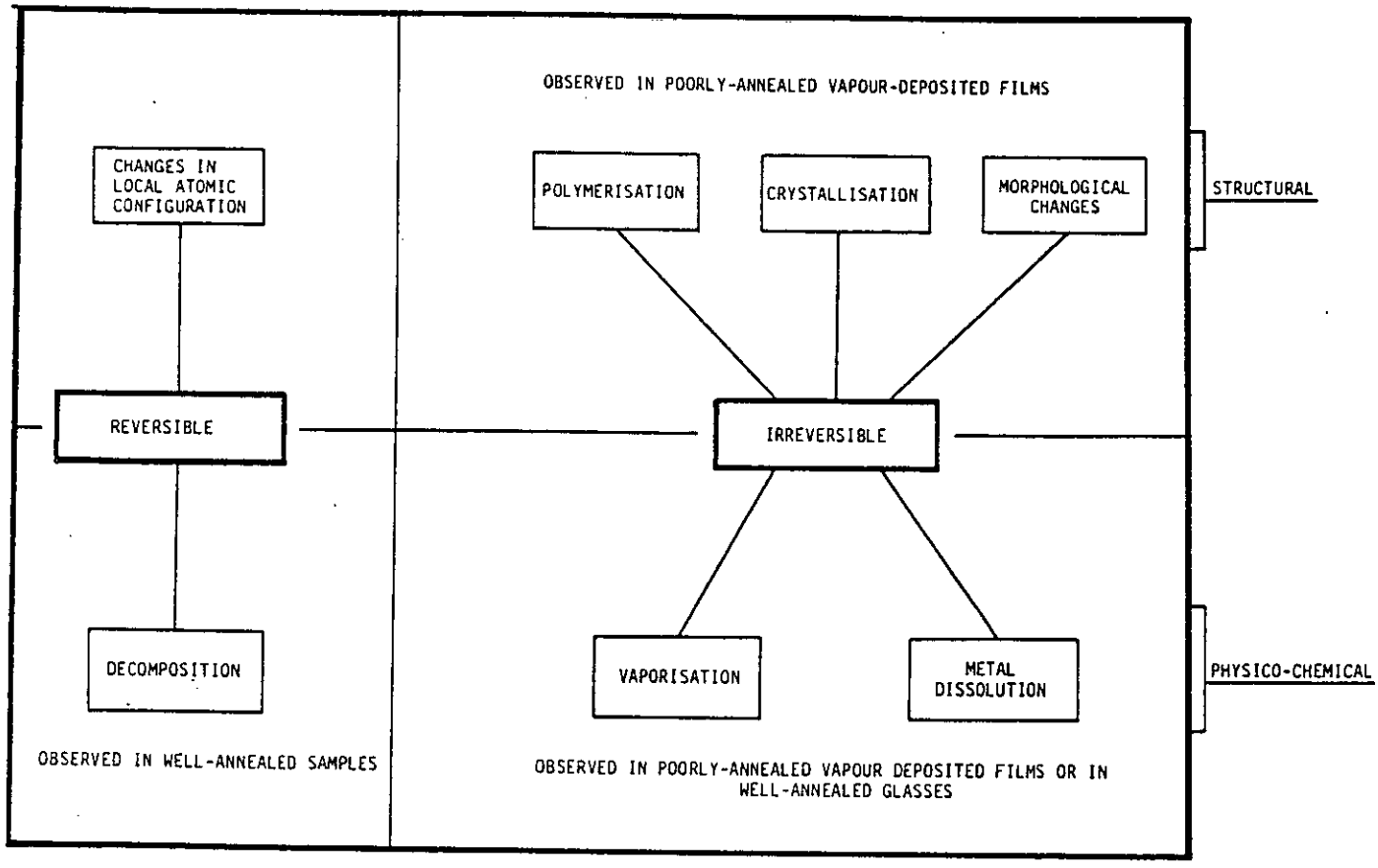

Figure 1.1 Classification of photo-induced strucural and physico-chemical phenomena in amorphous chalcogenide semiconductors.

has been obtained. One objective of this study has been to investigate the structural properties of photodarkening in the As-S system using Raman spectroscopy as the structural probe.

There is also little information concerning the structure of As-S glasses after the photodissolution of Ag. Such information is necessary in understanding the photodoping phenomena and a Raman study was therefore considered important. Kinetic experiments, which measured Ag dissolution rates, have also been used in this investigation and together with the structural work have enabled a mechanism for the photodissolution process to be developed.

References

1. Shimizu, I., Kokado, H. and Inoue, E., Photogr. Sci. and Eng., 19, 136, (1975).
2. Shirakawa, T., Shimizu, I., Kokado, H. and Inoue, E., Photogr. Sci. and Eng., 19, 139, (1975).
3. Asahara, Y. and Izumitani, T., Phys. Chem. Glasses, 16, 29, (1975).
4. Bordogna, J. and Keneman, S. A., "Holographic Recording Media", edited by H. M. Smith (Berlin: Springer-Verlag), P.229, (1977).
5. Tai, K. L., Ong, E. and Vadimsky, R. G., Proc. Electrochem. Soc., 82-89, 9, (1982).

CHAPTER 2

THE STRUCTURE OF Ag-As-S COMPOUNDS

2.1 Introduction

A knowledge of the structure of Ag-As-S compounds is an important prerequisite to understanding their properties and the nature of the photo-induced effects that occur in them. Hence this chapter presents a review of the existing information on the structure of materials in the Ag-As-S system. Both crystalline and amorphous solids can be formed in this system and it is instructive to compare the structural information for both types since it is likely that structural units found in the crystalline compounds will also exist in the amorphous forms of similar composition.

2.2 Crystalline Ag-As-S compounds

The principle ternary crystalline compounds that form in the Ag-As-S system are proustite (Ag_3AsS_3), smithite ($AgAsS_2$), a modification of proustite called xanthoconite and a modification of smithite called trechmanite. Recently another crystalline compound of composition Ag_7AsS_6 has been reported by Blachnik and Wickel (1).

2.2.1 Smithite and trechmanite

Smithite belongs to the monoclinic class of crystals with a space group C2/c (C_{2h}^6). The base-centred unit cell, which is shown in figure 2.1(a), covers two layers and contains 24 $AgAsS_2$ formula units. The layers lie in the xy plane along the (001) direction. The symmetry of the layer is described by the space group C_2^3 . The structure is built up of As_3S_6 units consisting of 3 AsS_3 pyramids joined as a six membered corrugated ring and forming a "chair-like" structure. This is illustrated in figure 2.1(b). The "chair-like" units are joined in pairs by Ag atoms.

Trechmanite is an interesting modification of smithite. Instead of the "chair-like" structures found in smithite, the As_3S_6 ring units form a "boat-like" structure (figure 2.1(c)). Roland (2) reported that $AgAsS_2$ glass crystallised into trechmanite when heated at 290^{o}C for 315 hours. At higher temperatures, between 320^{o}C and 421^{o}C the glass crystallised into smithite after about 24 hours.

2.2.2 Proustite

Proustite belongs to the hexagonal crystal systems and has a room temperature space group of C_{3v}^6 . Figure 2.2 shows a view of its structure looking down the

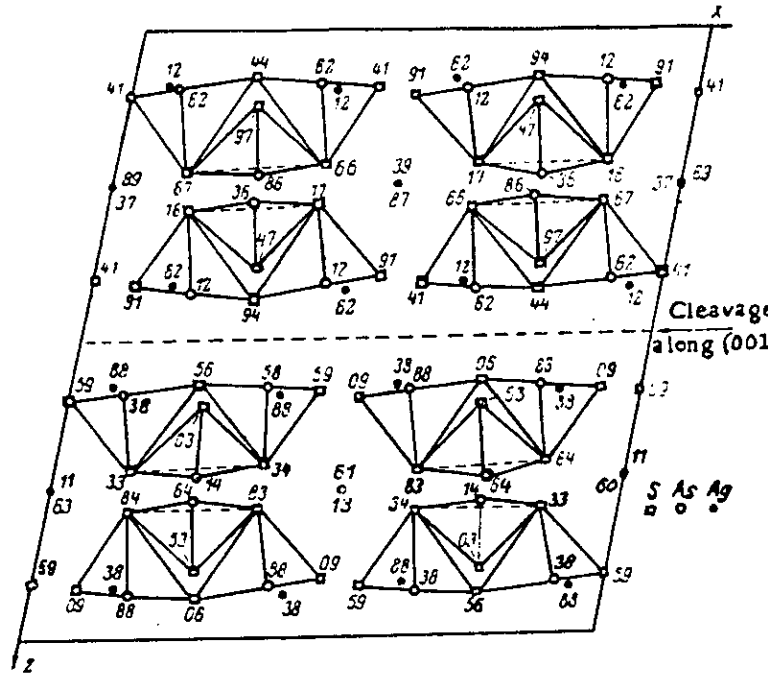

(a)

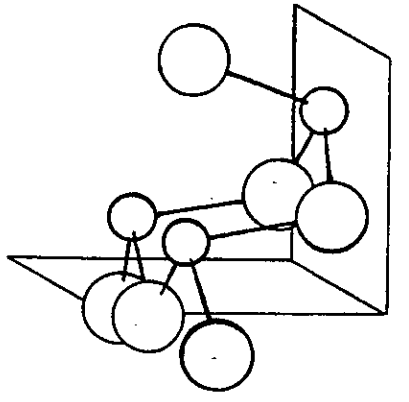

(b)

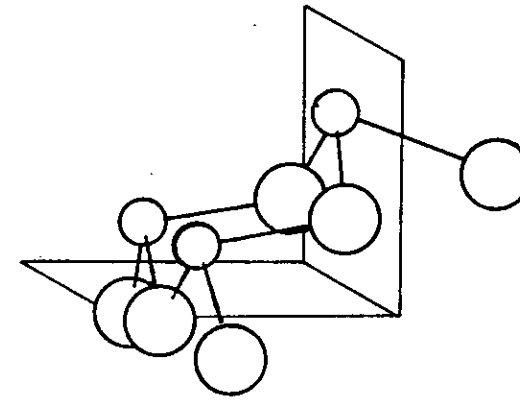

(c)

Figure 2.1 The structure of crystalline $AgAsS_2$: (a) the unit cell of smithite, (b) the "chair-like" uint found in smithite and (c) the "boat-like" unit found in trechmanite.

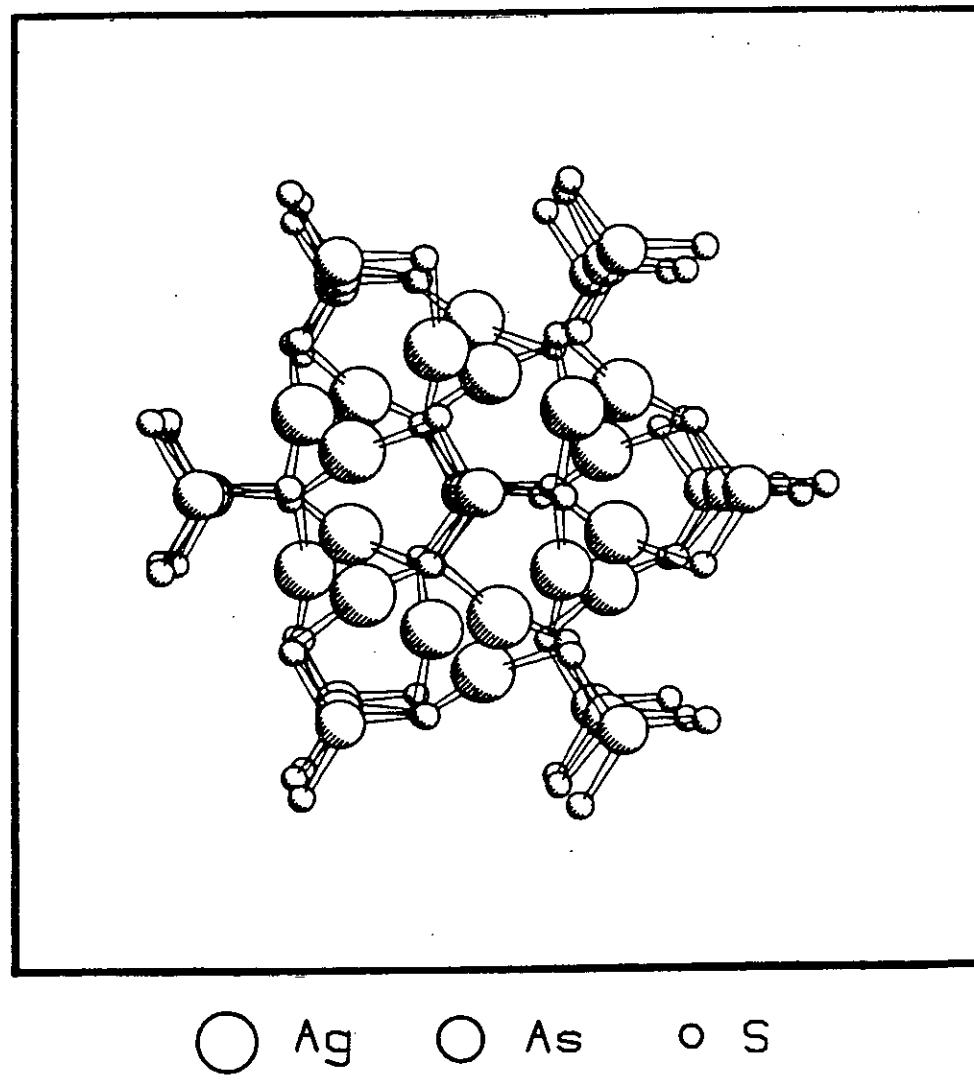

Figure 2.2 The structure of proustite looking down the trigonal axis.

trigonal axis. The basic building block of the structure is again the AsS_3 pyramid but in this case they are more isolated than in the smithite structure and are linked together via Ag-S spirals (3). Proustite crystals are deep red in colour since its absorption edge is near 600 nm. It is interesting to note that a silvery coating is reported (4) to form on the crystal surface when exposed to light.

As regards the electrical properties of the crystal, at room temperature high purity synthetic single crystals of proustite were found to conduct electricity by motion of Ag^+ ions; their transport number was found to be 1.02 ± 0.02 (5).

2.2.3 Xanthoconite

Xanthoconite has the same composition as proustite but it crystallises in the monoclinic system as tabular crystals with a space group C2/c (C_{2h}^6) (6). The structure is composed of double sheets parallel to the (001) direction (=twin plane) consisting of AsS_3 pyramids pointing with their As apices outward. One type of Ag atom has planar threefold coordination, with Ag-S bond lengths of 2.45 - 2.6 Å, and they lie in the plane of the sheets. Another type of Ag atom has pyramidal threefold coordination, with Ag-S bond lengths of 2.48 - 2.76 Å, and these Ag atoms hold the sheets together.

2.3 Glass formation in the Ag-As-S system

2.3.1 As-S glasses

The glass forming region in the As-S system extends approximately from As_5S_{95} to $As_{43}S_{57}$ (7, 8). It has been shown by several workers, eg. Ewen (9), that the short-range order in stoichiometric As_2S_3 is similar to that in the corresponding crystal. This indicates that it has a network structure composed of AsS_3 pyramid units linked by As_2S bridges. Ewen also found homo-polar bonds (i.e. As-As and S-S bonds) to be present in As_2S_3 glass, with about 1% of bonds being "like-atom".

In the S-rich glasses, for compositions with S content between 60 and 65 at. % the extra S atoms were found to form non-planar As-S-S-As bridges and S_8 rings were also found in compositions more S-rich than $As_{37}S_{63}$. The As-As bonds in the As-S network were found to rapidly disappear for a S content > 60 atm. %.

As-S glasses more As-rich than As_2S_3 were found to consist of a glassy matrix into which crystallites of α-As_4S_4 were embedded. The glassy matrix had the same network structure as As_2S_3 glass, but there were no S-S bonds present, only As-As bonds.

2.3.2 Ag-As-S glasses

A detailed study of the glass-forming region in the Ag-As-S system has been made by Kawamoto et al (10). Their results are shown in figure 2.3 and show clearly that the system contains two areas of glass formation. Similar results were obtained by Golovach et al (11). One of the areas of glass formation is situated along the As-S edge and centred on the composition As_2S_3. This area is quite small with a maximum Ag content of about 4 at. %. The other area of glass formation is an island region and extends along the As_2S_3-Ag_2S tie line from about 30 mole % to 70 mole % Ag_2S. It is suggested (10, 11, 12) that the area of glass formation centred on As_2S_3 is based on the AsS_3 pyramidal structural unit and that small amounts of Ag (< 4 at. %) can be incorporated into the As-S network without significant change in structure. This was confirmed by Raman scattering experiments (12) which showed that a Ag-containing glass of composition $Ag_4As_{38}S_{58}$ had a similar structure to an As_2S_3 glass. It is also suggested (10, 11, 12) that the larger island region is based on a structural unit found in the crystal smithite ($AgAsS_2$). This "chair-like" unit has already been described (see figure 2.1). Evidence for this was again provided by Raman scattering experiments (12). Figure 2.4(a) shows a comparison between the Raman spectra of crystalline and amorphous $AgAsS_2$ and figure 2.4(b) shows a comparison between the glassy composition

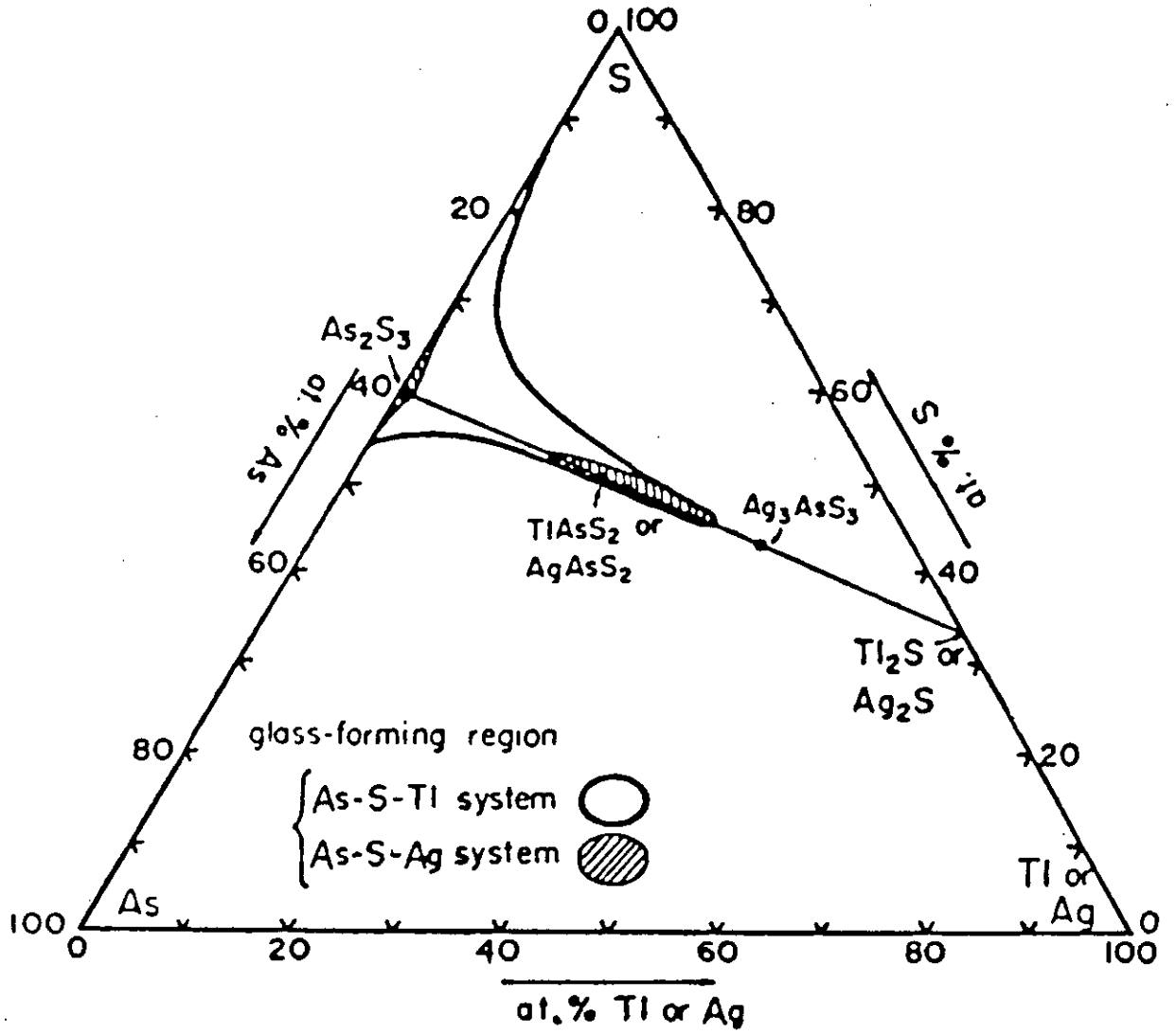

Figure 2.3 The glass-forming region in the Ag-As-S system as determined by Kawamoto (9). Glass formation in the Tl-As-S system is also shown for comparison.

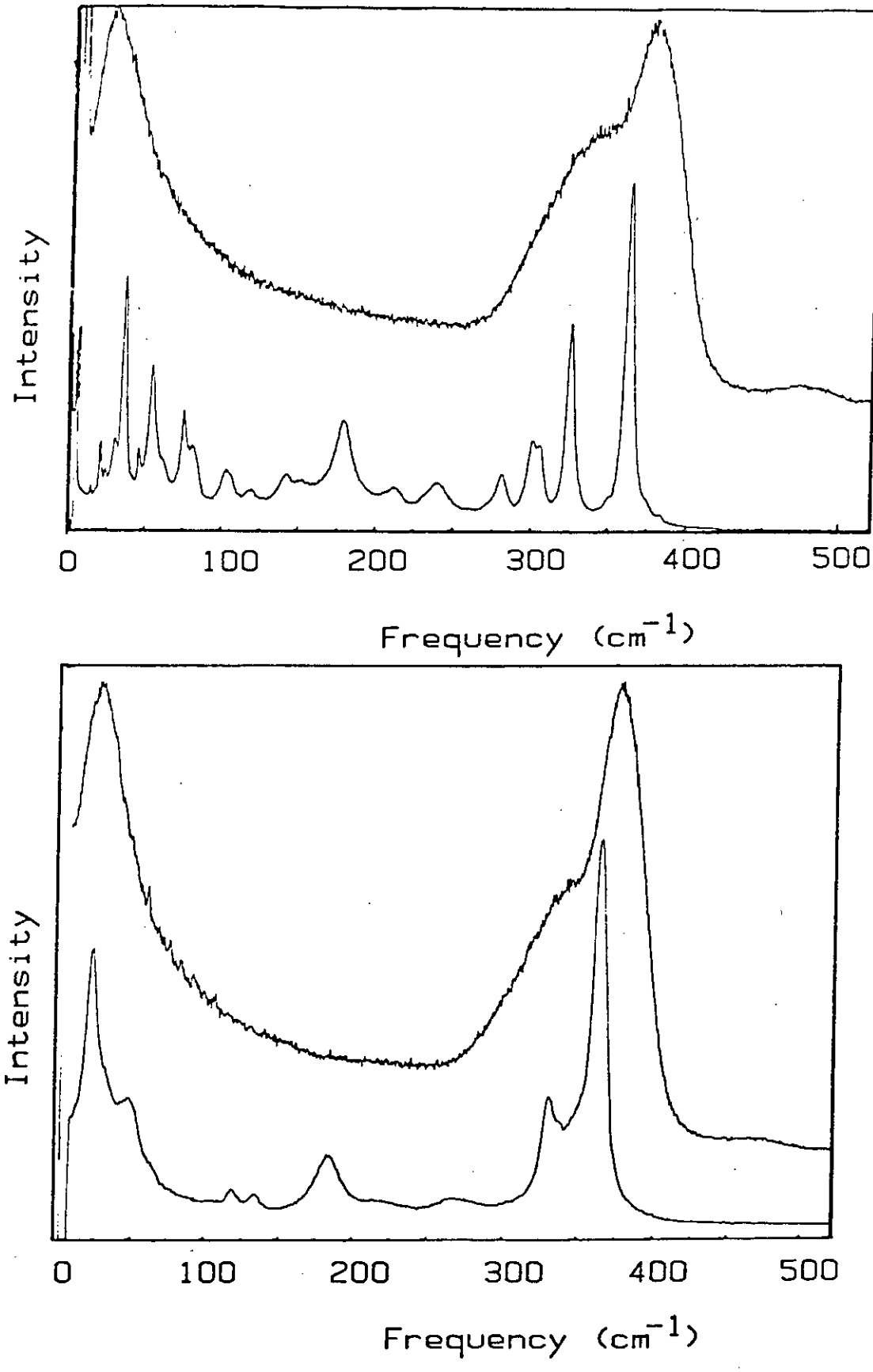

Figure 2.4 A comparison of the Raman spectra of (a) crystalline and amorphous $AgAsS_2$ (smithite composition) and (b) crystalline and amorphous Ag_3AsS_3 (proustite composition).

$Ag_{30}As_{22}S_{48}$ and a crystalline composition $Ag_{40}As_{16}S_{44}$ (which is close to the composition of proustite). These two figures show that the glass spectra are approximately the envelope of the corresponding crystalline spectra. From this it may be deduced that glassy $AgAsS_2$ is formed from structural units found in smithite and that glassy $Ag_{30}As_{22}S_{48}$ contains structural units found in proustite.

Golovach et al (11) explain the region of non-glass formation as a manifestation of the immiscibility of the two glasses based on the two types of glass formers.

2.4 References

1. Blachnik, R. and Wickel, U., Z. Naturforsch, 85b, 1268-1271, (1980).
2. Roland, G. W., The American Mineralogist, 53, 207, (1973).
3. Byer, H. H. and Bobb, L. C., Ferroelectrics, 5, 207, (1973).
4. "Encyclopedia of Minerals and Gemstones", edited by M. O'Donoghue (Orbis Publishing London), p.170, (1976).
5. Davies, P. H., Elliot, C. T. and Hulme, K. F., Brit. J. Appl. Phys. (J. Phys. D) 2, 165, (1969).
6. Engel, W. P. and Movacki, W., Acta Cryst., 24(b), 77-81, (1968).
7. Flaschen, S., Pearson, A. and Northover, W. J., Amer. Ceram. Soc., 42, 450, (1959).

8. Myers, M. B. and Felty, E. J., Mat. Res. Bull.,2, 535, (1967).

9. Ewen, P. J. S., Ph. D. Thesis, University of Edinburgh (1978).

10. Kawamoto, Y., Agata, M. and Tsuchihashi, S., Yogyo-Kyokai-shi, 82(9), 502, (1974).

11. Golovach, I. I., Gerasimenko, V.S., Silvka, V. Y., Dovgoshei, N. I., Bogdanova, A. V. and Golovei, M.I., Fizika i Khimya Stekla 3, 463, (1977).

12. Firth, A. P., Owen, A. E. and Ewen, P. J. S., J. Phys., Paris Colloq., 42, 903, (1981).

CHAPTER 3

PHOTODARKENING IN CHALCOGENIDE GLASSES

3.1 Introduction

The photo-induced changes that occur in As-S compounds can be divided into two categories: irreversible changes produced in as-deposited evaporated thin films, and reversible changes produced in well-annealed films or bulk glassy samples. Irreversible photo-induced changes are mentioned only briefly here, the bulk of this chapter being a review of reversible photo-induced changes.

3.2 Irreversible photo-induced changes

When As_2S_3 films are formed by thermal evaporation they contain the predominant vapour species, which have been found to be (1, 2) As_4S_3 and S_2. As the film forms on a substrate at room temperature it consists of these molecular units, mainly bonded together by weak van der Waals forces. Illumination (or thermal annealing) of the film causes polymerisation and its structure and optical properties are irreversibly changed, becoming similar to those of well-annealed films or bulk glassy samples.

3.3 Reversible optical changes (photodarkening)

It has been widely reported (3, 4, 5) that optical darkening occurs in films of evaporated As_2S_3. The effect has been termed "photodarkening" and is found to be fully reversible; annealing the samples at Tg (~443 K) completely restores the film to the original state.

The particular characteristic of photodarkening is a nearly parallel shift of the absorption edge. This is illustrated in figure 3.1 which shows the change in optical absorption observed in evaporated films and bulk glasses of As_2S_3. (The bulk samples were thin platelets 10-20 um thick). Also shown in the figure is the absorption edge of crystalline As_2S_3. No photodarkening is observed in crystalline samples and this indicates that the effect is unique to the amorphous phase.

The magnitude of the photodarkening effect depends on the temperature of the sample. Figure 3.2 shows the optical transmission of an As_2S_3 film as a function of exposure time, t, for four temperatures: the incident light intensity and wavelength were kept constant and only the temperature at which exposures took place was varied. It can be seen that the initial value of transmission (at t=0) depends on the temperature, but that after a sufficient exposure time the transmission saturates at a value which is independent of temperature.

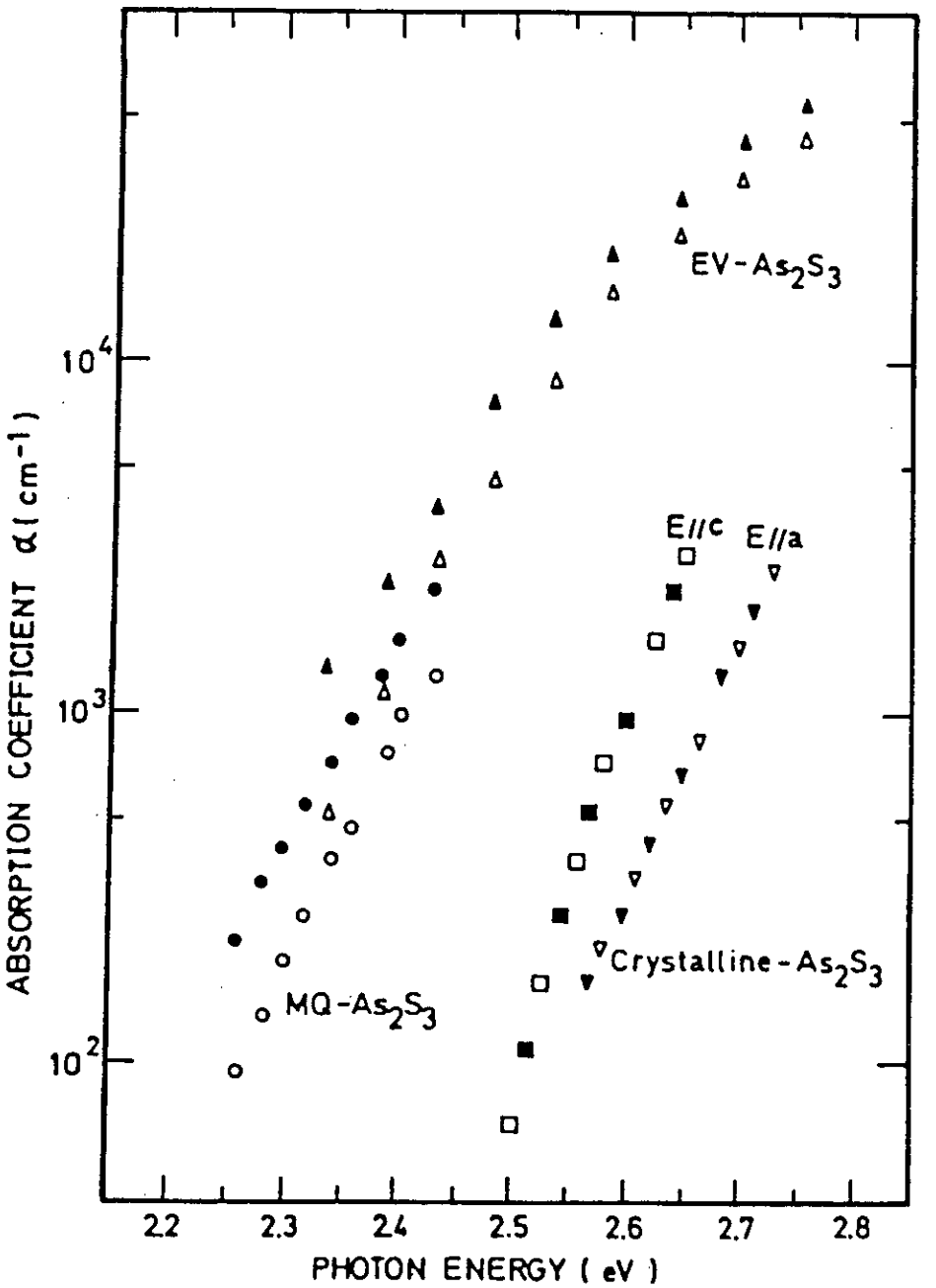

Figure 3.1 Photodarkening observed both in evaporated and melt-quenched As_2S_3. The open and solid symbols represent the data before and after the exposure to light respectively. No change in observed in crystalline As_2S_3. (Ref. 5).

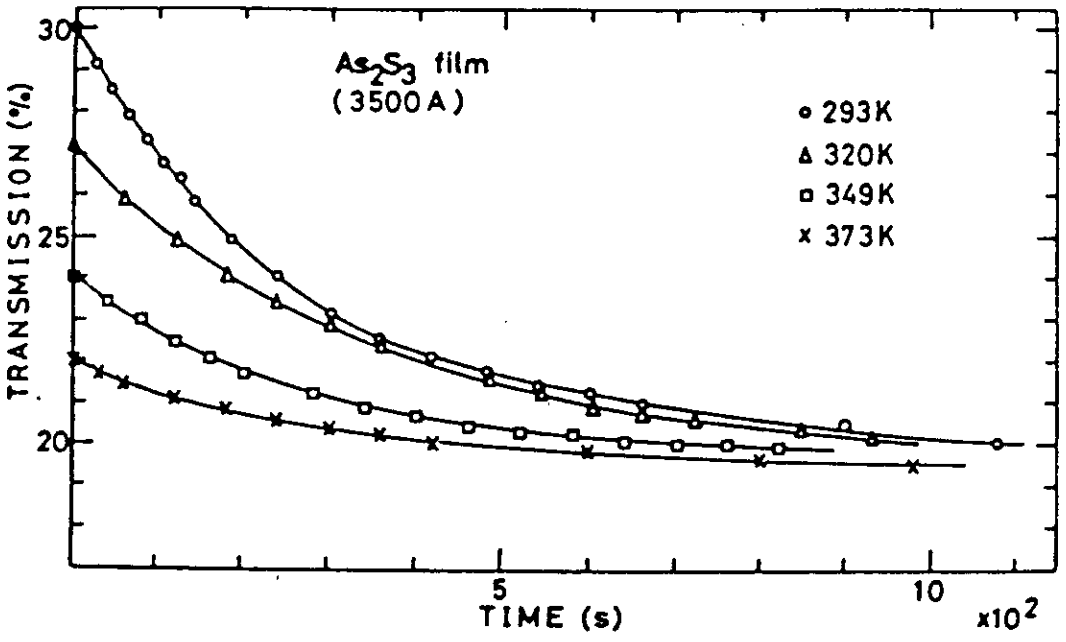

Figure 3.2 Optical transmission (at 470 nm) as a function of illumination time for different illumination temperatures. (Ref.7)

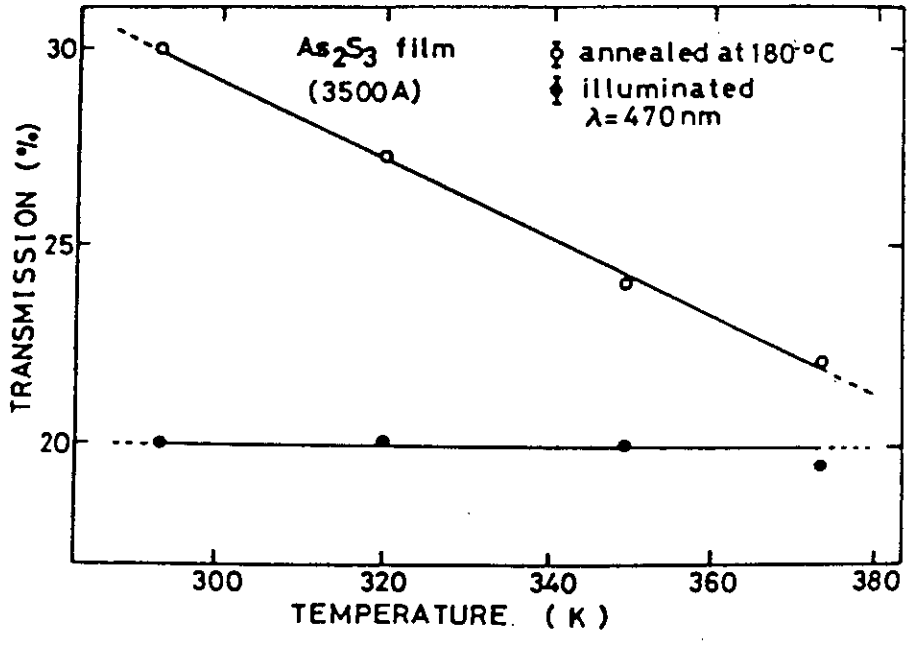

Figure 3.3 Optical transmission (at 470 nm) before and after illumination at different temperatures. (Ref.7)

The initial and saturated value of optical transmission can be obtained from figure 3.2 and replotted as a function of temperature. The results are shown in figure 3.3. The temperature dependence of the optical gap Eo, can be represented by the equation

$$Eo\ (T) = Eo\ (0) - \gamma T \qquad (3.1)$$

where Eo(0) is the optical gap at T = 0 K and γ is a constant.

The transmission values of the photodarkened state remain constant with temperature which seems to suggest that the optical gap of the photodarkened state is independent of temperature. (Similar results have been obtained by Lyubin (6)).

Tanaka (7) has also measured the absorption edge of As_2S_3 (figure 3.4) after exposure at two different temperatures, the absorption measurements being made at 290 K. As shown in the figure, the absorption edge is shifted to lower photon energies after irradiation at 77 K (curve c) when compared to the result for the sample irradiated at 290 K (curve b). It is also interesting to note that the sample photodarkened at 77 K became more transparent when exposed to light again at 290 K (curve c to curve b). This has been termed photobleaching.

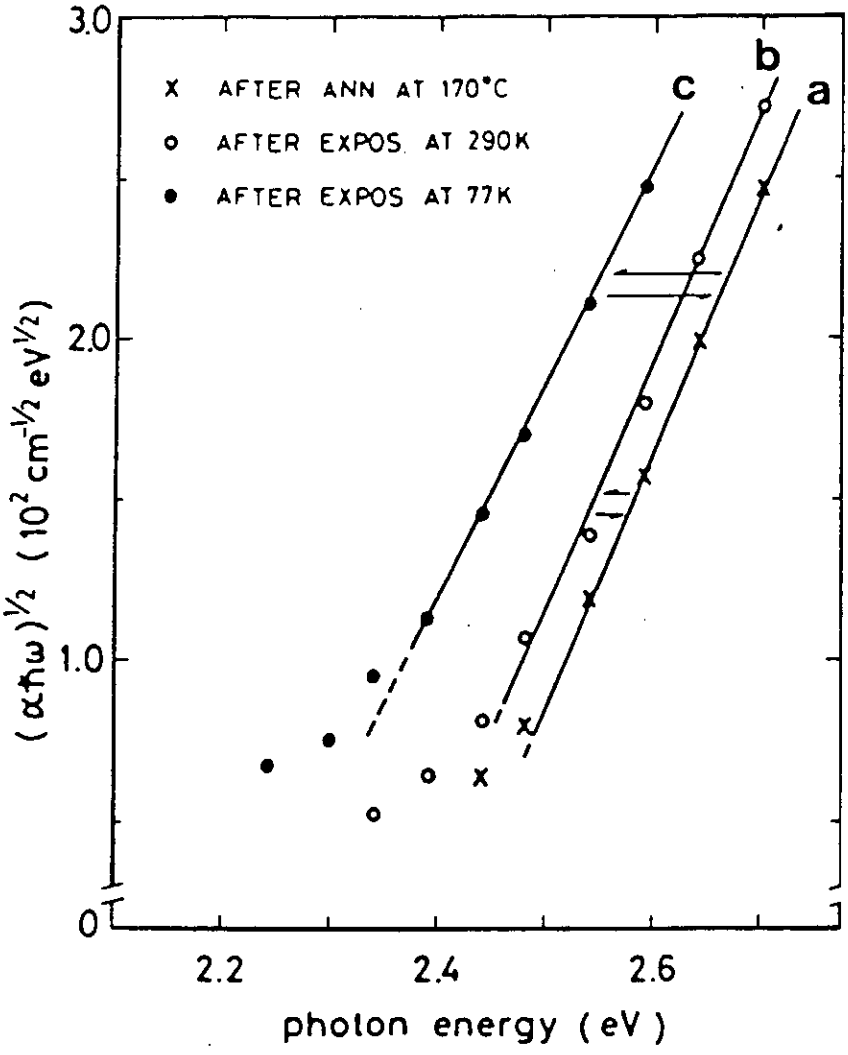

Figure 3.4 Photodarkening (a → b or a → c) and photobleaching (c→b). (Ref.7).

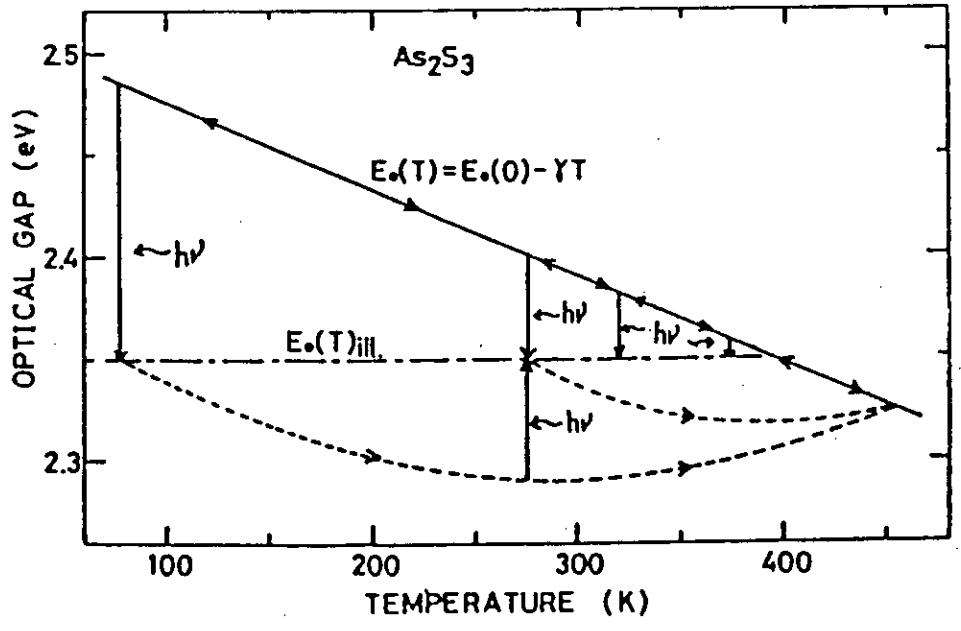

Figure 3.5 Temperature cycling of photodarkening and photobleaching shown on a Eo - T diagram. (Ref.7).

The results shown in figures 3.3 and 3.4 have been summarized by Tanaka (7) into an Eo-T diagram (figure 3.5). The vertical arrows in the figure, represent changes in the optical gap; either photodarkening or photobleaching caused by light irradiation under isothermal conditions. The important feature of the figure is that the optical gap of the illuminated state has the same value irrespective of previous thermal history. The particular value of the optical gap obtained from the figure is not a characteristic value, but depends on the value of light intensity which is used to photodarken the sample.

Tanaka (9) has measured the absorption edge shift (Δ Eo) for different light intensities and found that the magnitude of the darkening produced in a sample was not linear with exposure time. The edge shift ΔEo gradually gets larger and departs from the linear curve for increased exposure time.

A photo-induced increase in refractive index has also been observed (10) in thin films of As_2S_3.

3.4 Photo-induced structural changes

X-ray diffraction measurements have shown that reversible structural changes occur at the same time as photodarkening occurs. Figure 3.6 shows the results of these X-ray diffraction measurements: the curves are for an annealed film, and for photodarkening occuring at the two temperatures 290 K and 77 K, all measurements being made at 290 K. (optical measurements were also made at the same time and these have already been shown in figure 3.4). The main feature of figure 3.6 is that photodarkening causes a decrease in the first diffraction maximum and an increase in the first minimum. This indicates that photostructural changes cause an increase in the randomness of the atomic configuration. Similar results have also been observed by Elliott (11) using neutron scattering and EXAFS techniques. Also far-infra-red absorption (12) and ESR (13) have been used to study the reversible structural changes, but again only a qualitative indication that structural randomness is increased is reported.

Changes in sample thickness after photodarkening have also been reported (5). Figure 3.7 shows the trace of a mechanical thickness monitor as it crosses the boundary between an unexposed and exposed area. It shows quite clearly that film thickness increases after photodarkening. Tanaka (9) has investigated the

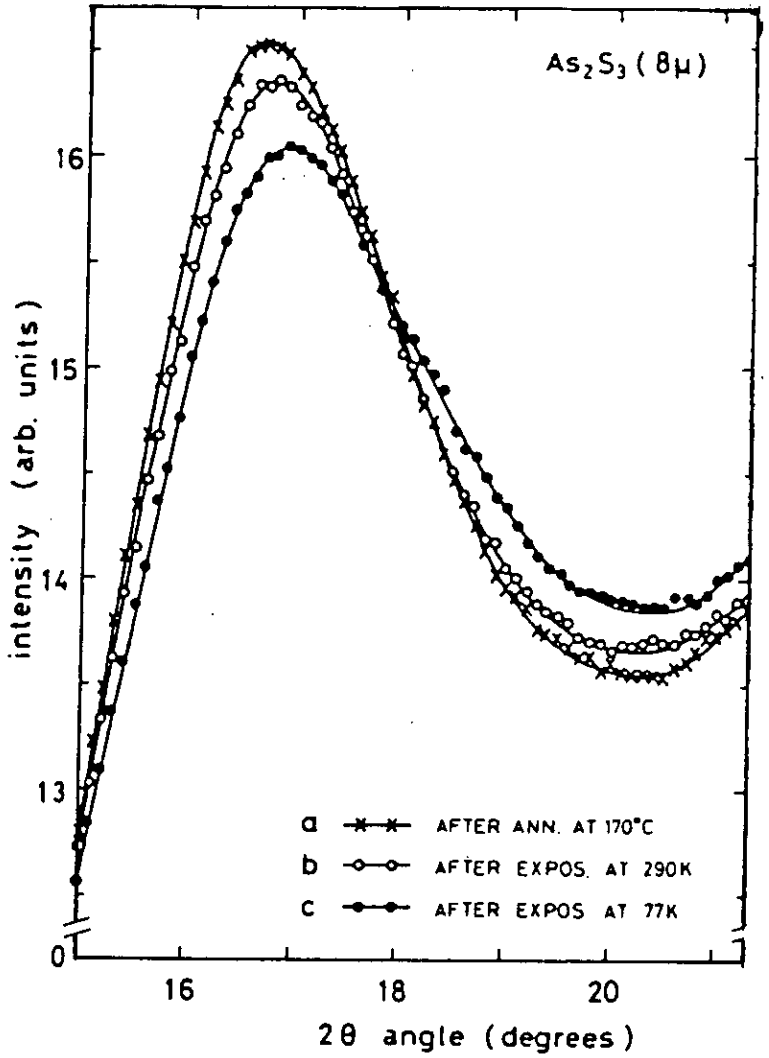

Figure 3.6 Photo-induced changes in the X-ray diffraction curve of evaporated As_2S_3 for different exposure temperatures. (Ref.8)

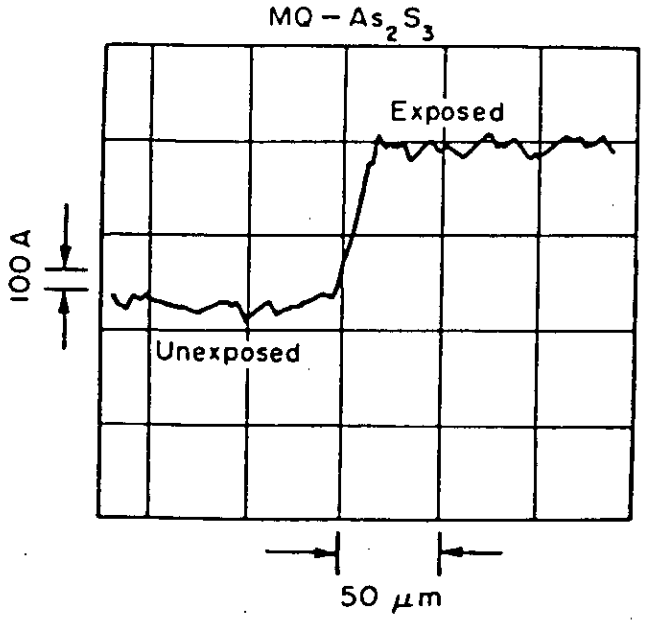

Figure 3.7 Typical trace showing the photo-induced thickness change for melt-quenched As_2S_3. (Ref.5).

relationship between the photo-induced thickness change and film thickness (d). His results show that fractional change Δd has very little dependence on d, indicating that it is most likely a volume effect. He also finds that bulk and film samples exhibit an effect of similar magnitude, and also that exposure at lower temperatures produces a larger change in thickness.

3.5 Spectral response

It was previously stated that light with energy close to the optical gap causes photodarkening. A more detailed study of the spectral response of photodarkening has been made by Tanaka (14) and the results are shown in figure 3.8. The photo-induced shift in absorption edge was measured at different photon energies, the results then being normalized to the number of absorbed photons. The response curve appears flat for energies > 2.4 eV (15) and therefore it appears that photodarkening is induced by interband optical absorption.

3.6 Mechanisms of photodarkening

3.6.1 Double well potential model

Several authors have proposed this type of model (9, 16).Consider figure 3.9 which shows a local bonding geometry that might be found in an As_2S_3 film. Positions

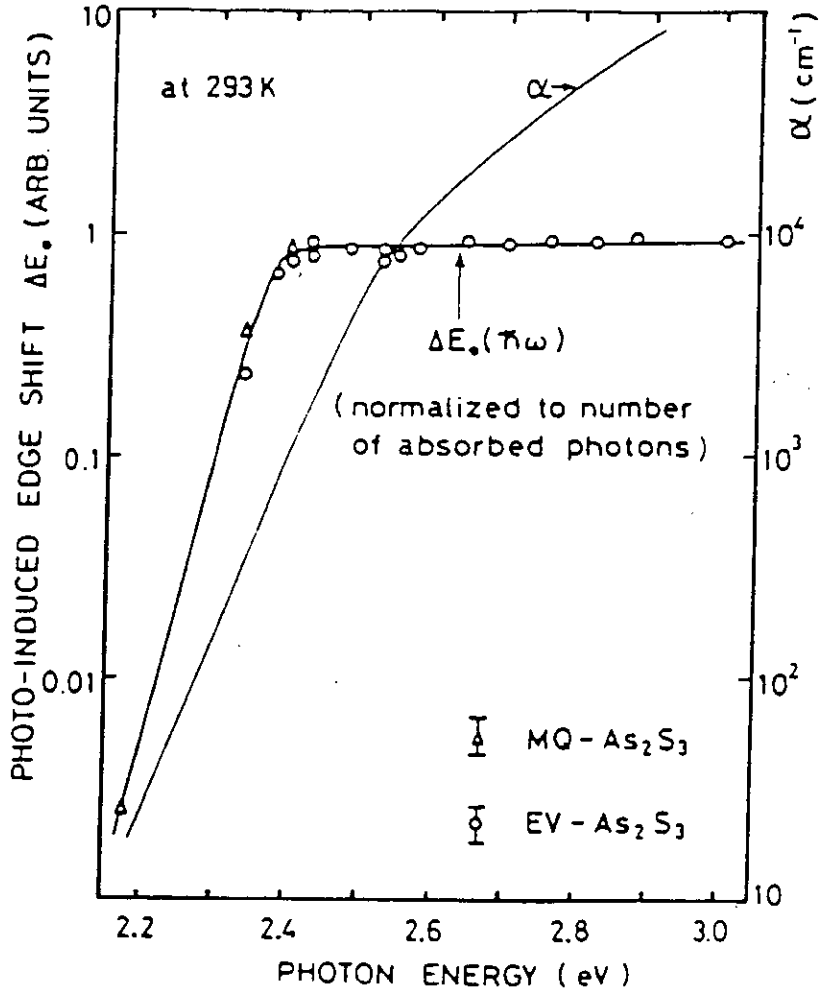

Figure 3.8 Spectral response of photodarkening in As_2S_3. The data is accurately normalized to the number of absorbed photons. (Ref.14).

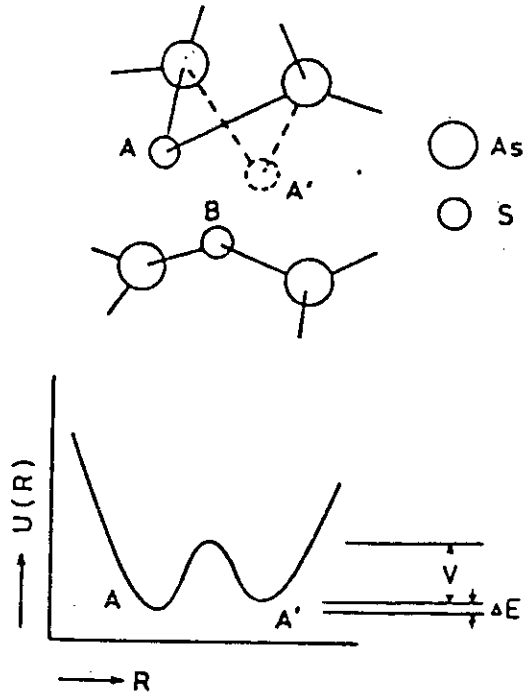

Figure 3.9 A schematic model of bistable local bonding geometries and the corresponding double well potential. (Ref.9).

A and A' represent a local bistable bonding configuration, and can be modelled by a "double well potential". The normal annealed condition of the film is state A. By irradiating with bandgap light the system gains enough energy to "flip" to state A' which is considered as the photodarkened state. The important feature of this model is that bonds are not broken. Instead there would be a change in bond length and also a change in bond angle.

3.6.2 Bond-breaking models

The first bond-breaking model was proposed by Keneman et al (17) who assumed that after the initial evaporation the As_2S_3 film consisted mainly of As_2S_2, S and As_2S_3. Annealing at Tg converts the film to homogeneous As_2S_3 by the reaction

$$As_2S_2 + 1/2\ S_2 \rightarrow As_2S_3 \qquad (3.2)$$

Once the film is in the annealed state they ascribe the reversible photodarkening effect to arsenic clustering according to the reaction

$$As_2S_3 \underset{\text{heat}}{\overset{\text{light exposure}}{\rightleftharpoons}} yAs + As_{2-y}S_3 \qquad (3.3)$$

Berkes et al (18) have also made similar suggestions.

Another bond-breaking model is the "self-trapped exciton" suggested by Street (19). The exciton is an optically excited hole-electron pair with an energy, Ex. It is assumed that the energy of a defect pair (D^+, D^-) will be much lower than Ex. The exciton is therefore unstable and will immediately form a D^+ D^- pair. According to Elliott (11), in As_2Se_3 this will cause an As-Se bond to break and a Se-Se bond to form, the result being a pair of metastable defects, Se^{3+} and As^{2-}. In terms of bond redistribution, for every As-Se bond broken, 2 Se and 1 As bond-angles are lost and 3 Se bond angles are created.

A further model suggested by Elliott (11) is one in which two As-Se bonds are broken simultaneously, and one As-As and one Se-Se bond are formed instead. This model predicts that the constituent atoms remain neutral,but that the short range order is partially destroyed.

3.6.3 Photo-polymerisation models

Grigorovici and Vancu (20) have proposed a model based on photo-induced polymerisation. For this model to be applicable it is necessary that discrete molecular units exist, even in well-annealed films. Illumination then causes these molecular units to join together in a more organized way. There are two main problems with this model. First, the annealing of the films, which erases

the photodarkening, would be connected with de-polymerisation but there is no evidence to support this. Secondly, the polymerisation model predicts densification and consequently a decrease in the thickness (volume) of the sample after illumination. This is in contradiction to the results already stated for As_2S_3 (5).

3.7 References

1. Leadbetter, A. J.,Apling, A. J. and Daniel, M. F., J. Non-Cryst. Sol., 21, 47, (1976).
2. Solin, S. A. and Papatheodorou, G. N., Phys. Rev., 15(4), 2084, (1977).
3. Kenemen, S. A., Bordogna, J. and Zemel, J. N., J. Opt. Soc. Am., 68, 32, (1978).
4. Kimura, K., Nakata, H., Murayama, K. and Minomiya, T., Solid State Commun., 40, 551, (1981).
5. Tanaka, K., Solid State Commun., 23, 63, (1977).
6. Lyubin, V. M. and Fedorov V. A., Sov. Phys. Solid State,23, 1353, (1981).
7. Hamanaka, H., Tanaka, K., Tsuji, K. and Minomura, S., J. Phys., Parais Colloq., 42, 399, (1981).
8. Tanaka, k., Appl. Phys. Letts., 26, 243, (1975).
9. Tanaka, K., J. Non-Cryst. Sol., 35&36, 1023, (1980)
10. Tanaka, K. and Ohtsuka, Y., Thin Solid Films, 57, 59, (1979)

11. Elliot, S. R., J. Non-Cryst. Solids, 59-60, p. 929, (1983)

12. Utsugi, Y., J. Appl. Phys., 49, 3470, (1978).

13. Kumeda, M., Solid State Commun., 21, 717, (1977).

14. Tanaka, K. Proc. 7th Intern. Conf. Amorphous and Liquid Semiconductors, Edinburgh, ed. by W. E. Spear, p.787, (1977).

15. Mott, N. F. and Davies, E. A., "Electronic Processes in Non-Crystalline Materials", Second Edition (Oxford: Clarendon Press), Chap. 6., (1979).

16. Averjanov, V. L., Kolobov, A. V., Kolomiets, B. T. and Lyubin, V. M., Phys. Stat. Sol.(a), 57, 81, (1980).

17. Keneman, S. A., Bordogna, J. and Zemel, J. N., J. Appl. Phys., 49(9), (1978).

18. Berkes, J. S., Ing, S. W. and Hillegas, W. J., J. Appl. Phys., 42, 4908, (1971).

19. Street, R. A., Solid State Commun., 24, 363, (1977).

20. Grigorovici, R. and Vancu, A., J. Phys., Parais Colloq., 42, 391, (1981).

CHAPTER 4

THE PHOTODISSOLUTION OF METALS IN CHALCOGENIDE GLASSES

4.1 Introduction

The photodissolution of Ag into As_2S_3 films was first observed by Kostyshin et al (1) in 1966 and since that time has been the subject of many investigations. This chapter is a review of the results and ideas of those investigations. The aim is to present our current understanding of the photodissolution process.

4.2 The optical sensitivity of photodissolution

The optical sensitivity of the photodissolution process can be defined as the rate at which the Ag film dissolves into the As-S film. As with all photo-induced effects it is important to investigate the intensity and wavelength dependence of the process.

4.2.1 Intensity dependence

Goldschmidt and Rudman (2) have made quantitative measurements on the rate of Ag dissolution using a technique which measured the change in resistance of the dissolving Ag layer. From a previously determined resistance-thickness curve they were then able to

determine the relationship between the number of dissolved Ag atoms and the number of incident photons. Their results are shown in figure 4.1. The curve can be divided into three distinct stages: Stage 1, a slow but increasing variation with exposure; Stage 2, a region of linear variation where there is a constant rate of dissolution of Ag with exposure; and finally stage 3, which begins when ~100 Å of Ag has dissolved, shows a decreasing rate of Ag dissolution with exposure. Similar shaped curves have been observed by Buroff and Baera (3), who used chemical analysis to find the amount of dissolved Ag after periods of exposure, and also by Kudoyarova et al (4) using a Ag film labelled with Ag110 radioactive nuclei.

The initial part of the curve, where the reaction is slow, has been called the induction period (2). It has also been reported that the induction period is inversely proportional to the illumination intensity and is observed independently of whether the sample is illuminated from the Ag or As-S side. It is found that if, during stage 2, the light causing the photodoping is interrupted for time periods from ~10 ms (2) to 24 hours (2, 3) then after the interruption, the photodoping continues at the previous rate. Stage 2 is thought to be due to an interface reaction (2) and stage 3 caused by the transport of Ag ions through the reaction products.

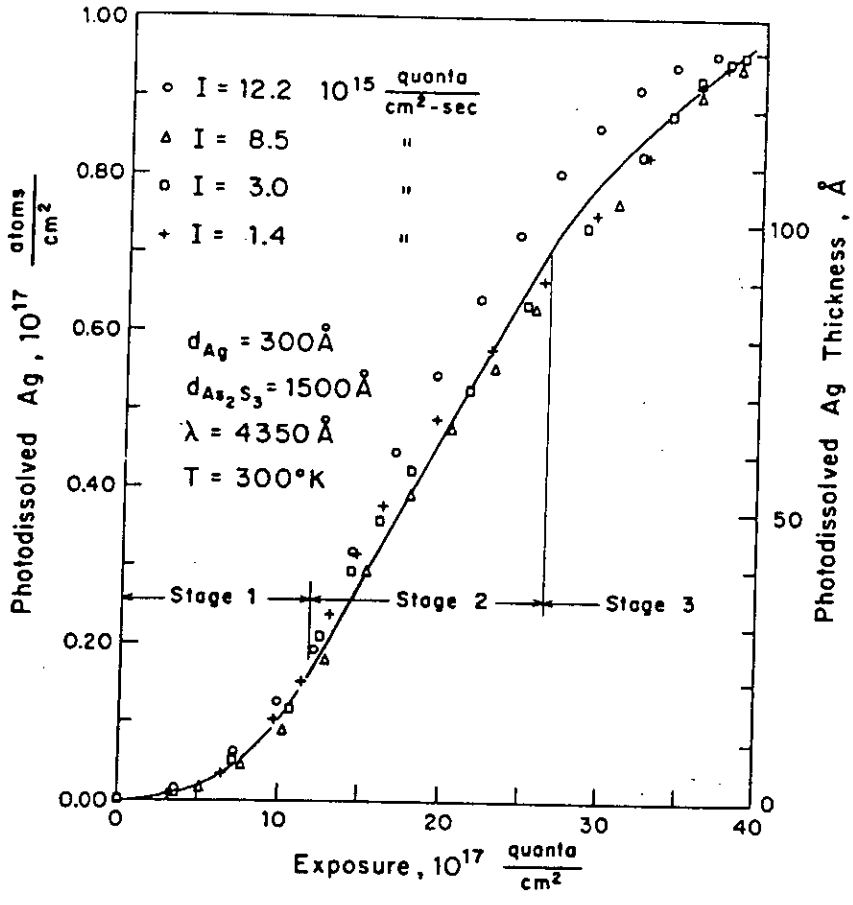

Figure 4.1 The amount of Ag photodissolved into As_2S_3 as a function of exposure time (exposure = intensity x time). (Ref.2).

4.2.2 Spectral sensitivity

Lavine et al (5) have measured the wavelength dependence of the photodissolution process using an optical wedge technique. In this method a rectangular area of light is projected onto a sample. The horizontal axis of the rectangle is linear in wavelength whereas the vertical axis is a function of intensity. After a period of exposure a pattern is formed on the surface of the sample which represents the spectral sensitivity. Two sets of Ag/As_2S_3 film structures with thicknesses of 200 nm of Ag on 300 nm of As_2S_3 and 5 nm of Ag on 50 nm of As_2S_3 were used in the experiments.

The sensitivity curves for the thinner sample are shown in figure 4.2(a). Curve A is for illumination from the As_2S_3 side of the film and indicates that the photodissolution sensitivity is independent of the As_2S_3 absorption edge. The sensitivity curve is uniform above 2.6 eV whereas the absorption coefficient (α) is increasing steeply. Furthermore the decrease in sensitivity below 2.6 eV only falls by an order of magnitude compared to more than a 3 orders of magnitude decrease in α over the same energy range. For illumination from the Ag side (curve B) the overall shape of the curve is the same, but the sensitivity is reduced by ~ 1/2.

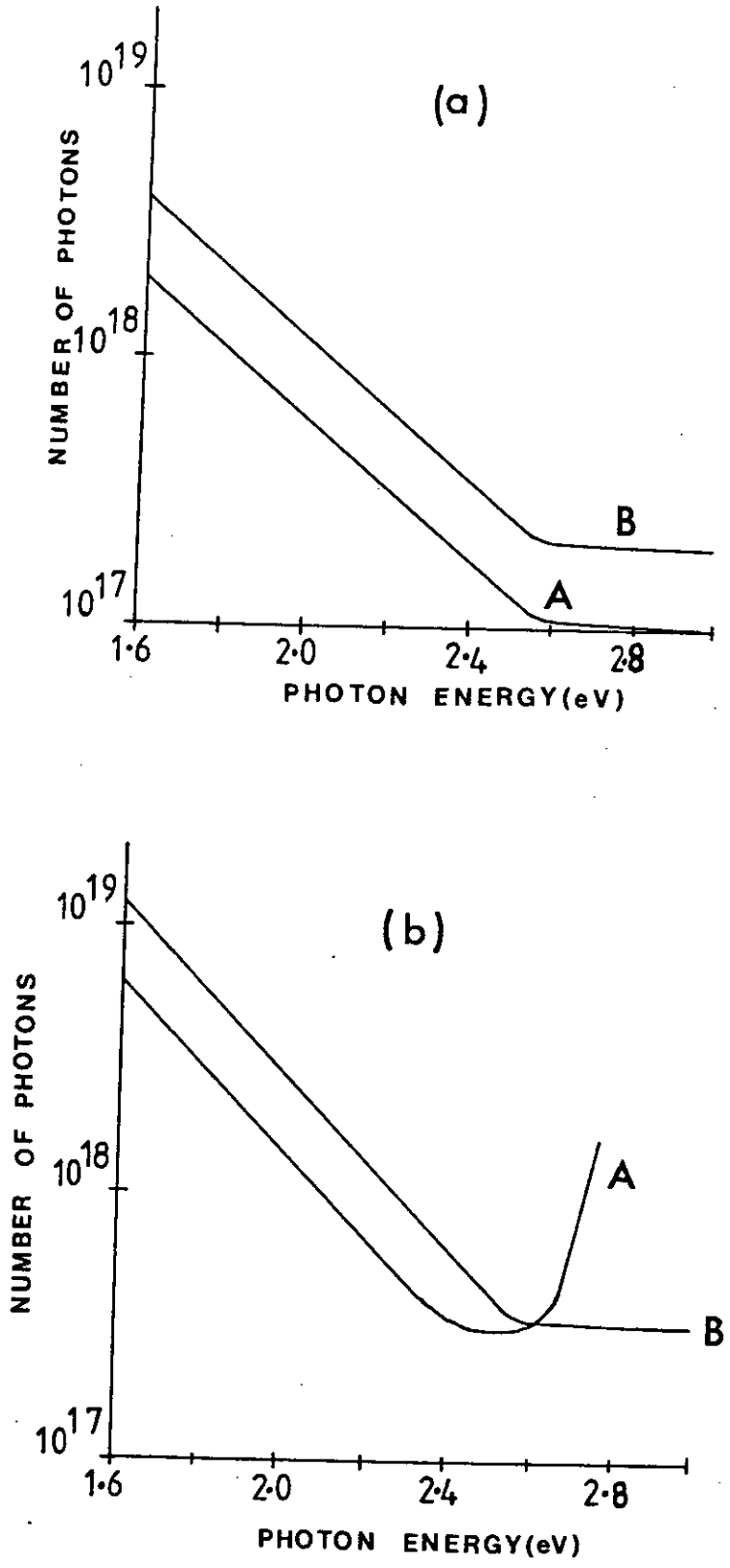

Figure 4.2 Number of photons to generate a negative relief image as a function of photon energy for illumination from the As_2S_3 side (curve A) and Ag side (curve B): (a) 5nm Ag on 50nm As_2S_3, (b) 20nm Ag on 300nm As_2S_3. (Ref.5).

The sensitivity curves for the thicker structure (200 nm Ag/ 300 nm As_2S_3) are shown in figure 4.2(b). For illumination from the As_2S_3 side (curve A) the effect of optical absorption in the As_2S_3 film at energies above ~2.6 eV is clearly seen. The As_2S_3 film is reducing the amount of light reaching the Ag/As_2S_3 contact area, which suggests that the absorption of light within the interface region is important for photodissolution to occur. Illumination from the Ag side shows a similar sensitivity to the thinner sample (curve B, Figure 4.2(a)) but there is a reduction in sensitivity due to the thicker Ag layer. It is clear from figure 4.2(a), curve A, that when illumination is from the As_2S_3 side of the film the sensitivity is limited by the absorption edge of the chalcogenide. The As_2S_3 film thickness is therefore a useful parameter to vary to determine whether the dissolution rate is controlled by light absorbed at the Ag-As_2S_3 interface or by light absorbed in the bulk of the As_2S_3.

Goldschmidt and Rudman (2) have stated that if it is caused by light absorbed at the interface between Ag and As_2S_3 then the rate of the initial part of the photodissolution could be described by the rate equation

$$\text{rate} = Io\ EXP(-\alpha d) \qquad (4.1)$$

where α is the linear absorption coefficient, Io the light intensity at the As_2S_3 surface and d is the thickness of the layer. Their results do in fact show the dependence described by equation (4.1) and suggest that light absorbed in the vicinity of the Ag-As_2S_3 interface causes photodissolution.

Goldschmidt and Rudman (2) also measured the wavelength dependence of the linear part of the dissolution rate (see figure 4.1) for two different As_2S_3 film thicknesses (110 nm and 282.5 nm) deposited on top of a 30 nm thick Ag film. The results are shown in figure 4.3 and span the energy range 2.4 eV to 2.7 eV with a single measurement made at the He-Ne laser wavelength (E=1.96 eV). Illumination was from the As_2S_3 film side and the light intensity was 10 mW/cm^2. For the thinner of the two samples the rate curve shows a steep rise from 2.4 eV to 2.7 eV, the value at 2.7 being ~6 times the value at 2.4 eV. For the thicker sample, the curve peaks at ~2.7 eV, with the maximum value ~1/2 the value of the thinner sample at the same value of photon energy. The value for the rate of photodissolution at the He-Ne laser energy was the same for both samples.

The authors conclude that the above experiments suggest that the photodissolution rate is proportional to the light absorbed in the As_2S_3 film close to the Ag/As_2S_3 interface. And also that photo-electrons ejected

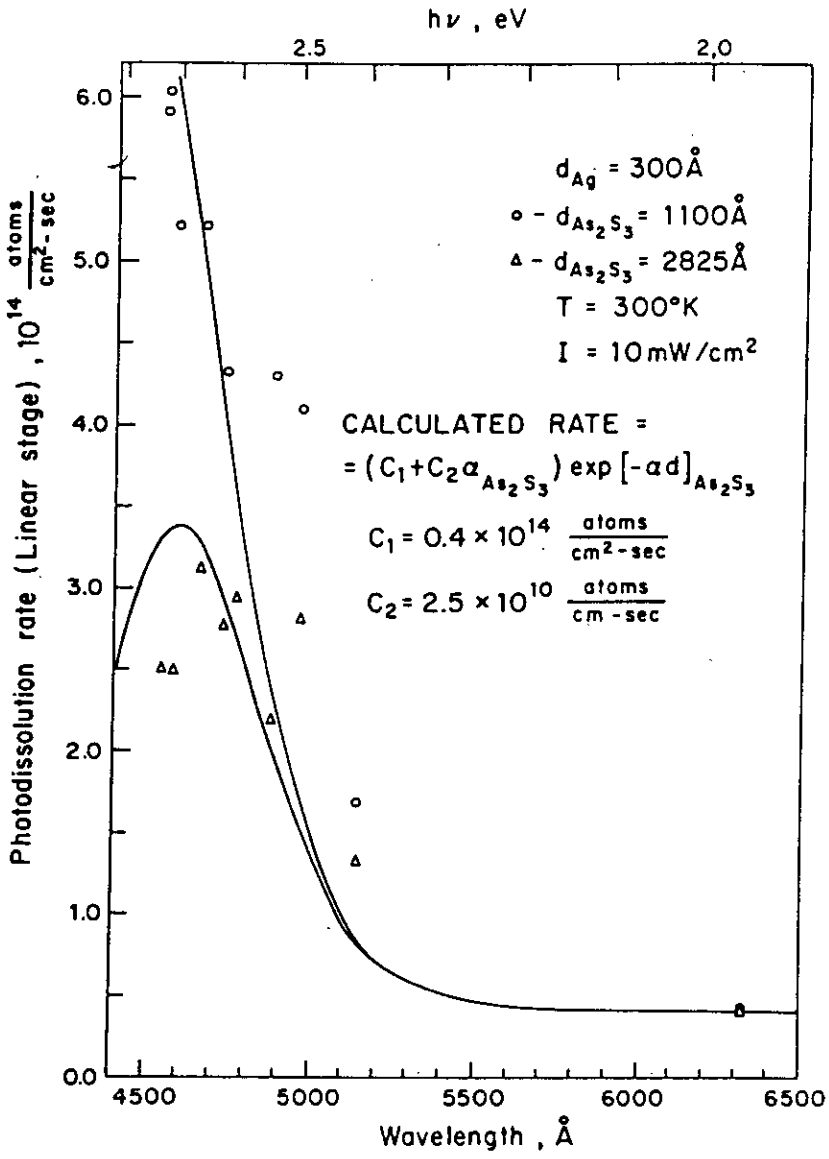

Figure 4.3 Dependence of the linear part of the photodissolution rate on wavelength. (Ref.2).

from the Ag into the As_2S_3 contribute to photodissolution. Kokado et al (6) have also measured the spectral sensitivity of the photodissolution process when illumination is from the chalcogenide film side for different film thicknesses. Samples were prepared from the Ag-As_2S_6 system and an optical wedge technique (described earlier) was used to measure the spectral sensitivity. Their results (figure 4.4) show that the short wavelength limit of the photodissolution sensitivity varied with thickness. To analyse their results they used the following expression for the interband optical absorption coefficient, α

$$\alpha = [k(hv-Eg)^2/hv] \qquad (4.2)$$

where k is a constant, hv is the photon energy and Eg is the band gap of the As_2S_6 film. They suggest that if the photodissolution efficiency is independent of the incident photon energy then the intensity (Imin) reaching the Ag-chalcogenide interface which produces the minimum detectable photodoping is given by

$$Imin = Ioexp([-k(hv^*-Eg)^2d/hv^*] \qquad (4.3)$$

where Io is the incident light intensity, d is the As_2S_6 film thickness and hv* is the short wavelength sensitivity limit. If the above suggestion is true then:

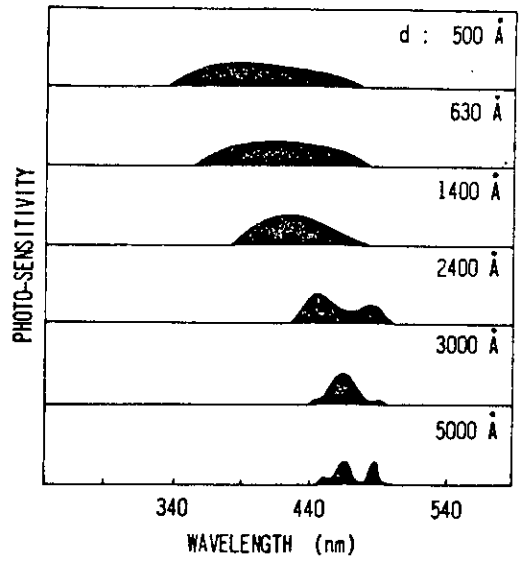

Figure 4.4 Spectral photosensitivity of the Ag-As_2S_6 photodoping system, when illuminated through As_2S_6 layers of thickness d. Multiple peaks seen in thick layers are due to interference and are not essential. (Ref.6).

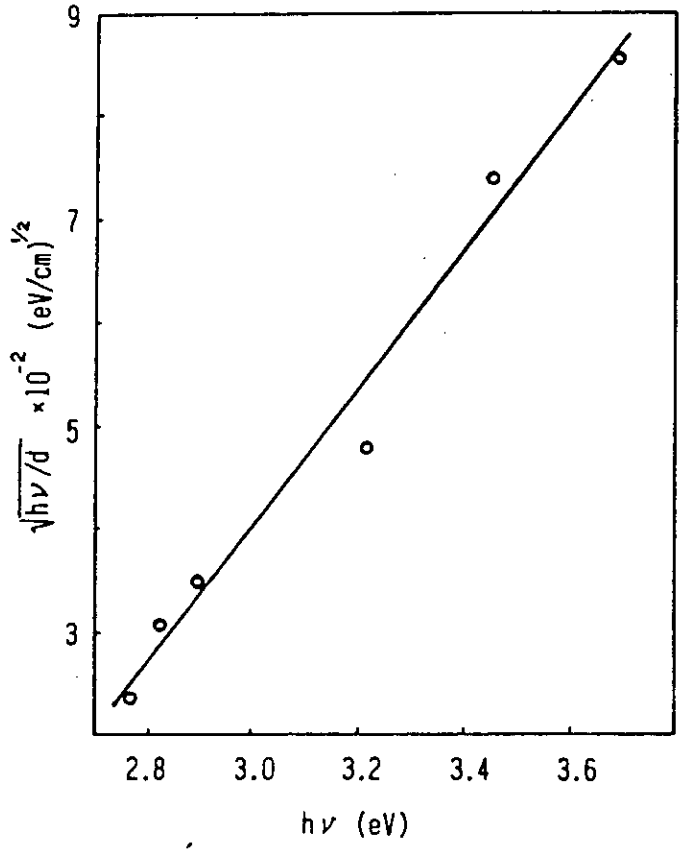

Figure 4.5 $\sqrt{(hv/d)}$ versus photon energy, at the short-wave limit of photosensitivity shown in figure 4.4. (Ref.6).

$$h\nu^* \propto (h\nu^*/d)^{1/2} \qquad (4.4)$$

and this was found to be the case (figure 4.5). Kokado also considered the possibility that as photodissolution proceeds a photodoped region is formed between the Ag and the chalcogenide and furthermore the photodoped region has an optical absorption which is shifted towards the red. They attempted to determine, using the optical wedge method, if absorption of light in the photodoped layer contributed to photodissolution. They measured the shift in the photosensitivity maximum with exposure (figure 4.6) and found it moved towards longer wavelengths. They suggest from these results that absorption in the Ag doped region contributes partly to further photodoping.

The kinetics of the photodoping process when the system Ag-As_2S_3 is exposed to He-Ne laser light (λ = 632.8 nm) has been measured by Kostyshin and Ushenin (7). They measured the change in the Ag layer thickness by measuring the optical density at 1.6 μm. In this spectral region both the As_2S_3 and the photodoped region are non-absorbing and therefore the optical density is due only to the Ag film and directly correlated with film thickness. The Ag layer thickness was 20 nm and the As_2S_3 layer was 60 nm thick. Illumination was through the As_2S_3 layer. Their results are presented as the thickness of the dissolved Ag layer as a function of the square root of illumination time. This kinetics curve has two main

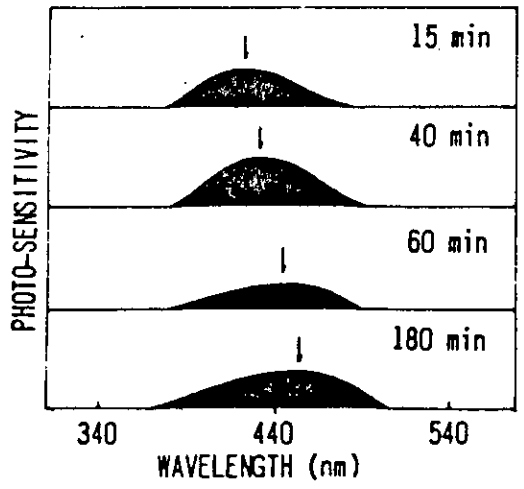

Figure 4.6 Shift of photosensitivity maximum (arrow) in the Ag-As_2S_6 system with exposure time. The sensitivity scale for the lower two spectrograms are reduced. (Ref.6).

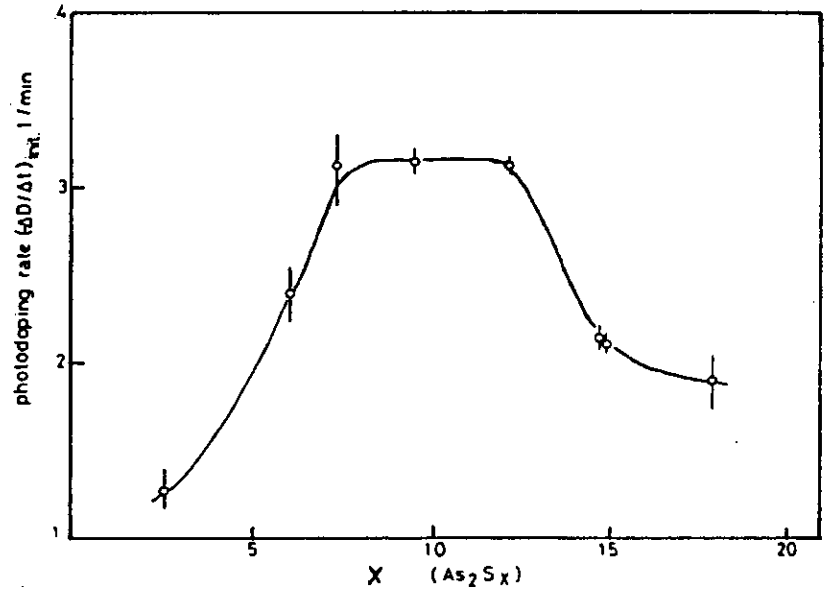

Figure 4.7 Dependence of the initial photo-doping rate on the composition of the As_2S_x system. The sensors were exposed to the mercury-line (366 nm, 1.2mW/cm^2). (Ref.8).

parts: an induction period as before but in this case followed by a region where the reaction kinetics are parabolic, implying a diffusion-controlled process. Similar results were obtained by Inoue et al (8).

4.2.3 The pre-history and composition of the As - S film

The majority of photodissolution experiments involve As-S films which are in the as-deposited state. However, the properties of the As-S films can be changed considerably by annealing or by exposure to bandgap light (see Chapter 3 - photodarkening).

Matsuda and Kikuchi (9) have stated that if the As_2S_3 film was photodarkened prior to the deposition of the Ag film then the rate of dissolution was enhanced. A more quantitative investigation has been made by Tamaki and Shoichi (10), who compared the dissolution rates when As_2S_3 film were as-evaporated, annealed and pre-exposed. The method used to measure the dissolution rates was to monitor the resistance change of a thin strip as it was photo-dissolved. They found that the largest dissolution rate occurred in pre-exposed annealed films and was three times higher than the rate for the as-deposited film. The value for the annealed film was approximately twice the value for the as-deposited film.

Lavine et al (5) have also measured the dissolution rate of Ag into pre-annealed As_2S_3 films and found an increase of approximately an order of magnitude compared to the as-deposited film.

The composition of the As-S film also affects the photodissolution process. Inoue et al (8) have measured the dependence of the initial photodissolution rate on the composition of As_2S_x system where x=3 to 18. The results (figure 4.7) show an increasing rate as x increases from 3 to 7. There is then a plateau region until x=12 after which the rate falls. The results show quite clearly that the initial part of the photodissolution process is strongly affected by the sulphur content of the As-S film.

4.2.4 Lateral dissolution on a conducting substrate and electric field enhancement

A series of experiments have been carried out by Matsuda and Kikuchi (9) in which they investigated the effect on the photodissolution process of a conducting substrate. The samples were prepared by first evaporating a film of Au on half of the surface of a glass slide. Next, a Ag strip was evaporated along the centre line of the slide and spanning both the Au and glass areas. Finally the whole surface was coated with As_2S_3. Their results (figure 4.8) show a dramatic lateral spread of

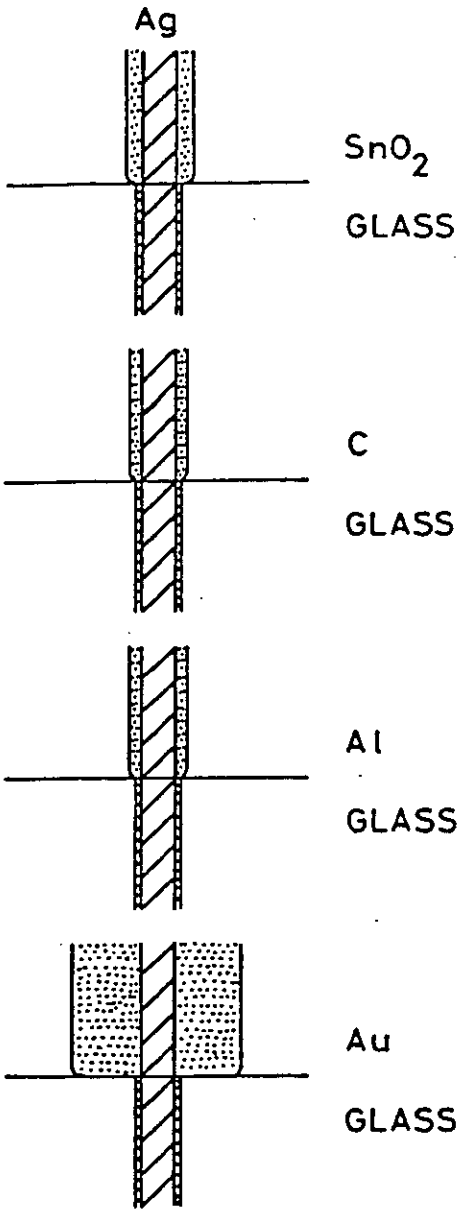

Figure 4.8 Schematic representation of the substrate dependence in transverse photodoping. (Ref.9).

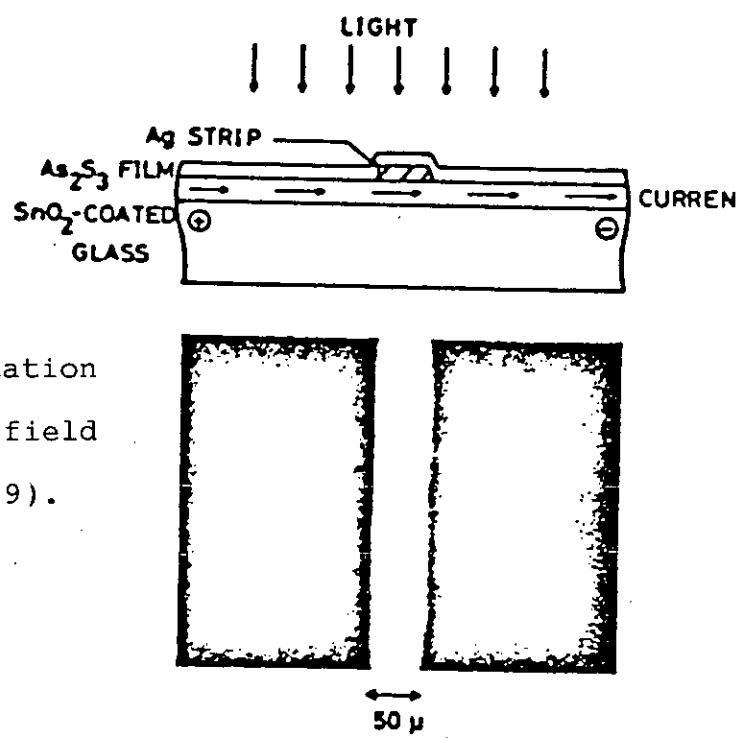

Figure 4.9 Schematic representation and photograph of electric field enhanced photodoping. (Ref.9).

the Ag photodoped region when in contact with the conducting Au part of the substrate. Results for other conducting substrates are also shown in the figure.

It was also found by Matsuda and Kikuchi that an electric field enhanced the photodissolution process. The samples studied had the film structure described above with SnO_2 used as the conducting film; the system is illustrated in figure 4.9. It was found that the lateral spread of photodissolution was markedly enhanced and that the enhancement was at the negative electrode side of the Ag strip, consistent with moving Ag^+ ions. Prior application of the electric field was also found to enhance subsequent photodissolution but the application of an electric field after photodissolution had finished produced no further effect.

4.3 Characteristics of Ag photodoped chalcogenides

4.3.1 The concentration profile of Ag dissolution

The concentration of Ag in the photodoped region of a chalcogenide is uniform in the direction of movement and then falls abruptly after a certain distance. This step-like profile of the photodissolution front has been observed in Rutherford back-scattering experiments (11, 12) and using electron microprobe techniques (8, 9).

Another characteristic of the photodoping process is that once the Ag layer has dissolved (i.e. no Ag is in contact with the As_2S_3 film) then the photodissolution front stops and a sharp step-like boundary remains between the photodoped region and the undoped region.

The maximum amount of Ag that will dissolve into an As-S film of a certain thickness depends greatly on the composition. This has been determined by Yamaguchi et al (13). For films with the formula As_2S_n the amount of photodissolved Ag appears to increase linearly with the sulphur content (figure 4.10). There is, however, a spread of values for the amount of Ag which dissolves into As_2S_3 (12, 13, 14, 15): these range from 32 atm.% to 47 atm.%.

It should be noted that the values of 32 atm.% Ag dissolution are obtained when an As_2S_3 film is deposited on to a thin Ag film, so that the As_2S_3 is very much in excess and is able to completely dissolve the Ag film. The method used to obtain the value of 47.5 atm.% was different: in this case the thickness of As_2S_3 was constant and there was an excess of Ag in order to find the maximum value of Ag that would dissolve.

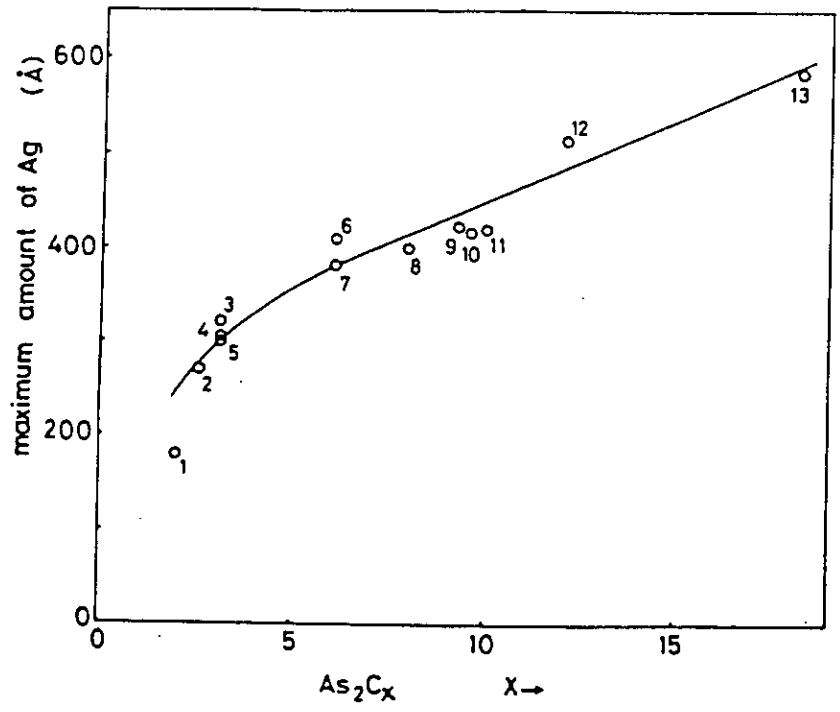

Figure 4.10 The maximum amount of silver photdissolved in to various chalcogenide films (50 nm thick).

1, $As_2Se_{1.9}Te_{0.12}$: 2, $As_2S_{2.6}$: 3, As_2Se_3 : 4, $As_2S_{2.9}Te_{0.1}$ 5, As_2S_3 : 6, As_2S_6 : 7, $As_2Se_{4.9}Te_{1.2}$: 8, As_2S_8 : 9 $As_2S_8Se_{1.3}$ 10, $As_2S_{9.6}$: 11, $As_2S_8Te_2$: 12, As_2S_{12} : 13, $As_2Se_{16}Te_2$. (Ref.13).

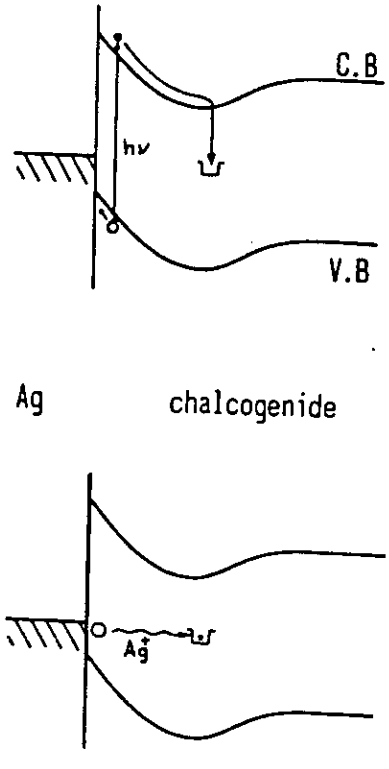

Figure 4.11 Illustration of proposed model: (a) photocarrier separation, (b) diffusion of silver ions attracted by trapped electrons. (Ref.6).

4.3.2 Chemical and structural properties

A feature of the photodissolution process which makes it of practical interest is that the photodoped material is insoluble in alkaline solutions whereas initially the As-S films are very soluble (14). It is thought that structural modifications occur in photodoped material which resist alkaline attack. The information about the structure of photodoped chalcogenides is, however, limited and contradictory.

Matsuda (9) obtained the x-ray diffraction pattern from the surface of an As_2S_3 film into which Ag was photodissolved. Precise details about experiments are not given, but it is known that the As_2S_3 film was evaporated first at a rate of 83 Å/sec. and that onto this was evaporated a film of Ag 20-100 nm thick, illumination during photodissolution being from the Ag film side. They state that the Ag film was etched off and studies of the surface made. Their results show faint traces of Ag_2S and As_2S_2 crystals.

Contrary to these results the diffraction studies reported by de Neufville (16) and Salik (17) find no crystallinity in Ag-photodoped As_2S_3 films. The samples investigated by Salik (15) were fabricated by evaporating the As_2S_3 on top of the Ag and the rate of evaporation was 2.5 nm per second.

4.3.3 Electrical properties

After the photodissolution of Ag the electrical conductivity of As_2S_3 films increases by as much as six orders of magnitude. The I-V characteristics of Ag photodoped $As_{24}S_{70}Te_6$ films have been measured by Sakuma et al (18) using surface type cells. At voltages between 20 and 100 V the samples became unstable and dendritic growth of Ag occured: it originated at the negative electrode and branched towards the positive electrode.

4.4 Models of the photodissolution process

4.4.1 The formation of a junction potential at the Ag-chalcogenide interface

It has been proposed by Kokado et al (6) that a potential barrier exists at the interface between the Ag and the chalcogenide. The potential is assumed to have a minimum in the vicinity of the interface (figure 4.11). When photons are absorbed by the chalcogenide at the interface, photocarriers are generated (holes and electrons). They suggest the holes will be captured by Ag atoms and the electrons are repelled by the junction potential into the interior of the chalcogenide to be trapped. Assuming that the electron traps are associated with loosely bound chalcogen atoms, they speculate that the coulomb attraction between a negative chalcogen ion

and a positive Ag ion is large enough for the Ag ion to be pulled into the chalcogenide. As the Ag enters the chalcogenide, a layer of a new composition rich in Ag is formed. The interface junction will move with the photodoped region and gradually form a hetero-junction.

As photodoping continues, the junction region becomes wider and they state that the rate determining step for photodoping will be the diffusion of Ag ions through the photodoped region. They have derived an equation for the rate of growth of the doped region whose depth is x, with time t as

$$dx/dt = kIabs + (k'/x)\ Iabs \qquad (4.5)$$

where Iabs is the number of absorbed photons per unit time and k, k' are constants. They state that the first term is for a photoenhanced chemical reactivity with a short range influence and the second term describes the coulomb attraction between photogenerated ions which drives the diffusion of Ag. At the beginning of photodoping (until a 6 nm thick layer of Ag is dissolved) the second term is negligible, but in the later stages the first term can be neglected and this gives the photodoped depth x a square root dependence on time

$$x = (2k'Iabs\ t)^{1/2} \qquad (4.6)$$

This was consistent with their own experiments.

4.4.2 Photodissolution: a tarnishing reaction

Malinowski and Buroff (19) suggest that photodoping is a typical tarnishing reaction and that it is similar to the tarnishing of Ag in a S atmosphere. They emphasise a particular feature of the Ag tarnishing process, namely that Ag and S continue to react despite the formation of the intermediate reaction product, Ag_2S. This is because solid Ag_2S has a large ionic and electronic conductivity. The Ag enters the Ag_2S lattice and dissociates into ions and electrons. Both of these charge carriers can move through the Ag_2S layer and thus provide a continuous supply of Ag at the S interface. Malinowski and Buroff suggest that in the photodoping process illumination produces mobile holes, which, they state, is equivalent to excess S in the As_2S_3 film, and if the photo-excitation is close enough to the Ag interface then Ag-S bonds are formed. This is, therefore, analogous to the tarnishing reaction described above; the illumination provides a supply of atoms which initially reacts at the Ag interface producing a layer of Ag_2S. However, as explained above, the Ag_2S allows the passage of both Ag ions and electrons and the Ag film will continue to react with the photogenerated holes (excess S atoms) produced in the chalcogenide until the Ag film is consumed.

In predicting the reaction kinetics of photodissution Malinowski and Buroff suggest the following sequence of events. In the initial stages of the process the first photoexcited holes (excess S atoms) reaching the Ag interface are permanently trapped by the formation of Ag-S bonds. However, further progress of the reaction is quickly blocked by the formation of a space charge due to the trapped electrons left behind. The positive charge of the holes is transferred to the Ag atoms forming Ag^+ ions. These eventually penetrate the space charge forming a gradually increasing thickness of Ag_2S. The rate of the reaction starts to increase. Eventually the conductance of the Ag_2S layer would reach a stationary value, but the increased thickness means a delay in the transport of Ag. Consequently, after a sufficiently long time the diffusion rate of Ag through the reaction products determines the rate of photodoping. The authors state that this type of parabolic law has been observed by Inoue et al (8).

4.4.3 Absorption of Light inside the Ag

Janai (20) has speculated that photodissolution occurs by light absorption in the Ag film. He states that if the photo-excitation takes place entirely within the Ag side of the junction, all the experimental observations concerning photodoping, can be explained. The fact that

photodoping stops once the Ag film is consumed is simply because no excitation can take place if there is no Ag film. The photodoped region has a phase boundary with a step-like profile because it is being pushed from behind. Janai states that there is no diffusion process; the driving force for photodissolution is in the Ag film.

These ideas are also supported by Lavine et al (5). They have shown that the spectral dependence fits qualitatively the internal photo-emission characteristic of Ag in contact with As_2S_3. From this they suggest the following model.

Incident photons are absorbed in the Ag and generate hot electrons. The mean-free-path of the hot electrons is of the order of 2-5 nm and therefore photons absorbed within the mean-free-path of the surface of the Ag will generate a hot electron which can traverse to the As_2S_3. There are many trapping sites in the As_2S_3 and the effect will be to attract Ag^+ ions into the As_2S_3. They suggest that the initial transfer of Ag^+ ions will be linear with photon flux until a gradient is established to promote diffusion.

These authors state, however, that the model does not provide an explanation of the induction period (see section 4.2.1) nor does it explain why the photodoped phase is resistant to alkaline attack.

4.5 References

1. Kostyshin, M. T., Mikhailovskaya, E. V. and Romanenko, P. F., Sov. Phys. Solid State, 8(2), 451, (1966).
2. Goldschmidt, D. and Rudman, P. S., J. Non-Crystalline Solids, 22, 229, (1976).
3. Buroff, A. and Baeva, R., Proc. 6th Int. Conf. on Amorphous and Liquid Semiconductors, Leningrad, USSR, (Kolmiets, B. T., Editor), (1975).
4. Kudoyaarova, V. Kh., Dzhafarov, T. D. and Mikhailov, M. D., Sov. Phys. Semicond., 13(10), 1191, (1979).
5. Lavine, J. M., Lis, S. A., Goldberg, G. M. and Masters, M. I., Proc. Electrochem. Soc., 82-89, 265, (1982).
6. Kokado, H., Shimizu, I. and Inoue, E., J. Non-Crystalline Solids, 20, 131, (1976).
7. Kostyshin, M. T. and Ushenin, Yu. V., Sov. Phys. Semicond. 16(1), 11, (1982).
8. Inoue, E., Kokado, H. and Shimizu, I., Proc. 5th Int. Conf. on Solid State Devices, Tokyo, (1973). Suppl. to J. Japan Soc. of Appl. Phys., 43, (1974).
9. Matsuda, A. and Kikuchi, M., Proc. 4th Conf. on Solid State Devices, Tokyo, (1972). Suppl. to J.Japan Soc. of Appl. Phys., 42, 239, (1973).
10. Tamaki, Y. and Shoichi, K., J. Appl. Phys. 52(2), 647, (1983).

11. Yamamoto, Y. and Tadatsugu, I., J. Appl. Phys., 47(8), 3603, (1973).

12. Goldschmidt, D., Bernstein, T. and Rudman, P. S., Phys. Stat. Sol. (a), 41, 283, (1977).

13. Yamaguchi, M., Shimizu, I. and Inoue, E., J. Non-Crystalline Solids, 47, 341, (1982).

14. Kolwicz, K. D. and Chang, M. S., J. Electrochem. Soc. Solid State, 127, 135, (1980).

15. Plocharski, J., Przyluski, J. and Wycislik, H., J. Non-Crystalline Solids, 56, 325, (1983).

16. De neufville, J. P., Proc. 5th Int. Conf. on Amorphous and Liquid Semiconductors, Garmisch-Parkenkirchen, Germany (Stuke, J. and Brenig, W., editors), Taylor and Francis, London, (1976).

17. Salik, J. and Nadiv, S., Phys. Stat. Sol.(a), 38, 177, (1976).

18. Sakuma, H., Shimizu, I., Kokado, H. and Inoue, E., Proc. 3rd Conf. on Solid State Devices, Tokyo, (1971).

19. Malinowski, J. and Buroff, A., Contemp. Phys., 19(2), 99, (1978).

20. Janai, M., Phys. Rev. Lett., 47(10), 726, (1981).

CHAPTER 5

EXPERIMENTAL METHODS

5.1 Sample preparation and analysis

5.1.1 Preparation of bulk glasses

Bulk As-S glasses were prepared by melting the elements arsenic and sulphur (both of 5N purity) in a 1 cm bore quartz tube.The tube typically was filled with 10 g of material and then evacuated to $< 10^{-4}$ torr and sealed. The tube was then placed in a furnace fitted with a rocking mechanism. Because of the high vapour pressure of arsenic and the serious risk of explosion, the tube was first heated to 500^{o}C and held at this temperature for about 2 hours to allow an initial reaction between the arsenic and sulphur. The furnace temperature was then raised to 850^{o}C and with the furnace rocking at about 12 oscillations a minute, it was held at this temperature for 24 hours. At the end of this time the tube was removed from the furnace and allowed to cool in air.

5.1.2 Preparation of thin bulk samples by hot pressing

The technique of hot pressing was used to produce samples of As-S glasses which had thicknesses in the range 10-50 μm. The method involved heating bulk

fragments of the As-S glass between two glass slides. The heating was carried out on a hot plate that was placed inside a glove box, through which there was a flow of dry nitrogen. When the As-S glass melted it was spread thinly and evenly between the two glass slides by applying a weight to the top slide. Usually the glass slides were removed to leave thin self-supporting samples.

5.1.3 Preparation of thin films by thermal evaporation

Thin As-S and Ag films of up to 5 μm in thickness were prepared by the thermal evaporation of bulk material. A schematic diagram of the evaporation apparatus is shown in figure 5.1. It was of conventional design and consisted essentially of a vacuum chamber and a pumping system. The chamber had at its base a molybdenum boat which was resistively heated and contained the bulk material to be evaporated. A step-down transformer (11 V, 150 A) controlled by a variac was used to produce the high currents needed to heat the boat.

Ag films were easily prepared since the bulk material evaporates well under a wide range of conditions. A small molybdenum boat (1cm dia.) was used and contained the bulk Ag. The boat was heated until the Ag melted and then the heating was increased to evaporate off the Ag. Evaporation rates, measured with a crystal thickness monitor, were kept at 5 nm/sec. It has been reported (1)

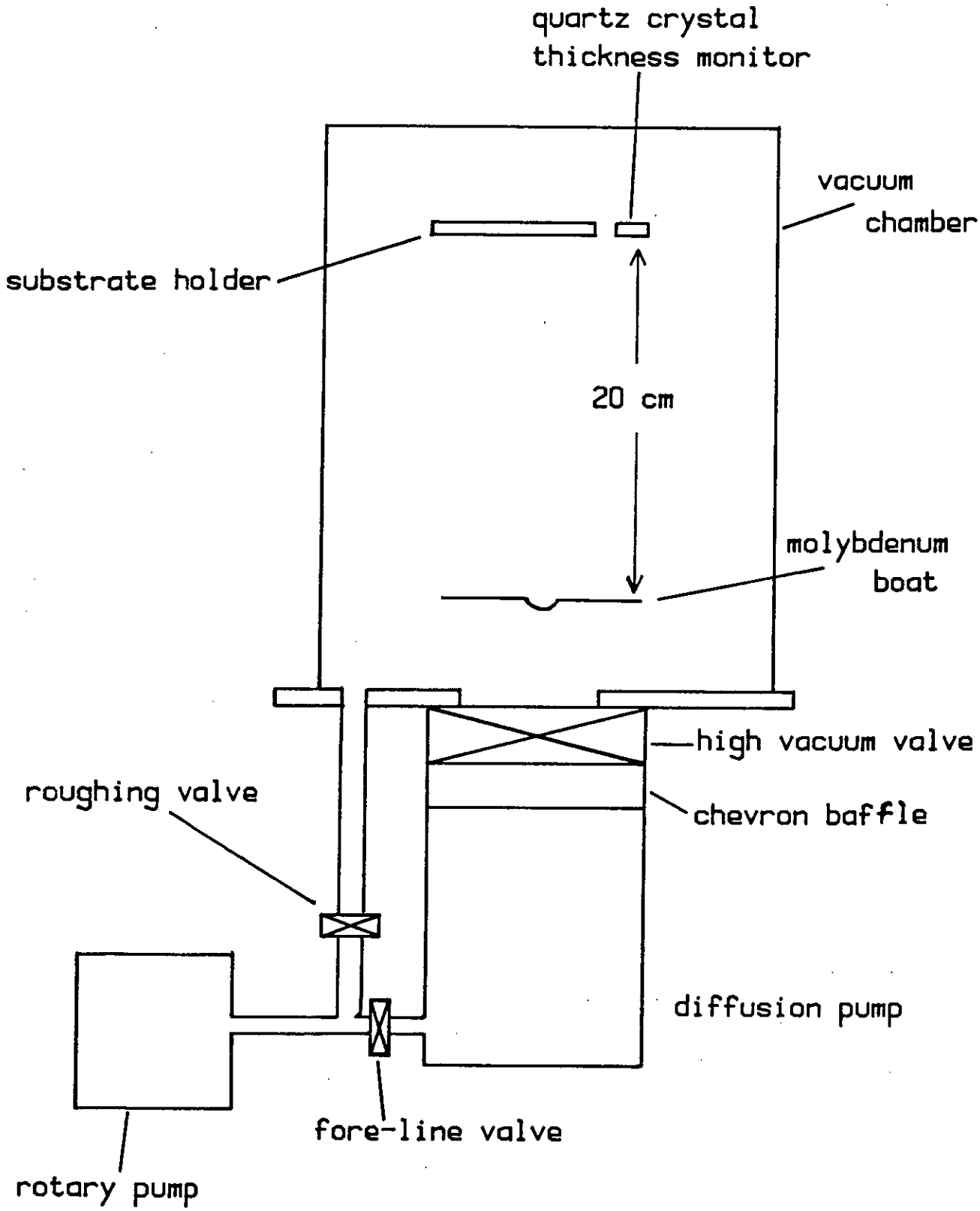

Figure 5.1 Schematic diagram of the evaporating system.

that rates of this order produce films which have a structure (for thicknesses > 15 nm) similar to bulk Ag.

The preparation of thin As-S films was complicated due to the fact that it is a two-component system. It is reported that low evaporation rates of ~5 Å/sec. produce a film stoichiometry which is close to that of the bulk starting material (2) With this in mind the following technique for evaporating As-S films with different stoichiometries was used. A T-type thermocouple (Cu-Cu/Ni) was attached to a 2 cm dia. molybdenum boat. The boat was then heated to a temperature which produced an evaporation rate of 5 Å/sec. (measured with a crystal thickness monitor). The temperature was then kept constant to produce a constant evaporation rate. Therefore, to produce particular As-S films stoichiometries the bulk starting material was always heated to a particular temperature which was then kept constant. This enabled films with reproducible stoichiometries to be formed, e.g to produce $As_{40}S_{60}$ films, bulk $As_{40}S_{60}$ was heated to 588 K.

5.1.4 Electron microprobe analysis

The actual stoichiometries of the As-S films and bulk evaporation material, used in this work, were found using the technique of electron-beam microprobe analysis (3). The analysis was performed by Mr R Hill of the Geology

Dept. Edinburgh University using a purpose built machine. Two requirements need to be satisfied when preparing samples for the analysis. Firstly, the surface of the sample needs to be optically flat and secondly the samples must be a minimum of 5 um thick, the penetration depth of the electron beam. Bulk samples were prepared by sealing with araldite a fragment of the material into a 3 mm dia. brass tube. After the araldite had set the end of the tube was polished until the surface of the sample was optically flat. Film samples were prepared by evaporating the material onto glass slides coated with a layer of Al. The Al layer was needed to test that the As-S layer was of sufficent thickness (> 5 um). The analyser could be set to detect Al so that if the As-S film were too thin the electron beam would penetrate through to the Al beneath and a reading would be registered. The results of the analysis are shown in table 5.1.

5.1.5 Film thickness measurements

5.1.5.1 Quartz crystal oscillators

A film thickness monitor, based on a quartz oscillator, was used to make measurements during the evaporation of films and enabled films of a desired thickness to be easily fabricated. The quartz crystals used in the monitor were AT cut and were operated at series mode resonance. The crystals were thin discs, 14

Source material	Film composition ±0.5 at. %
$As_{40}S_{60}$	$As_{41}S_{59}$
$As_{37}S_{63}$	$As_{38}S_{62}$
$As_{28.6}S_{71.4}$	$As_{30}S_{70}$
$As_{25}S_{75}$	$As_{30}S_{70}$
$As_{15}S_{85}$	$As_{20}S_{80}$

Table 5.1 As-S film compositions analysed by electron probe microanalysis

mm in diameter, with thin film Au electrodes on each face. When installed in the vacuum chamber a mask was used so that the evaporated material only fell on a 8 mm diameter region at the centre of one crystal face. The back electrode was only 6 mm in diameter and therefore the evaporated material completely covered the oscillating part of the crystal. As a film of a given material is deposited on the crystal the resonant frequency changes to a lower value. It will change from its initial value, Fq, to a new value, Fc, for a given film thickness, Lf. An equation which relates the film thickness (in cms) to the frequency change is:-

$$Lf=(1/CPf)(F/FqFc) \qquad (5.1)$$

where Pf is the film density (in g/cm^3) and F=Fq-Fc. C is a constant which has a theorectical value of $2.26\times10^{-6} g cm^{-2} Hz$ but was found experimentally to be 2.21×10^{-6} $g cm^{-2} Hz$ (see section 5.1.5.3). Lu and Lewis (4) show that for Ag films the equation is valid for frequency shifts of more than 10% of Fq. No experimental verification was available for As-S films, but mechanical stylus measurements (section 5.1.5.3) showed that the constant C in equation (5.1) was similar to that obtained for Ag. Equation (5.1) was therefore used to determine the thickness of deposited As-s films.

The crystals used had a fundamental resonance

frequency of 6 MHz. They were obtained from Megatech Ltd and had the electrode geometry shown in figure 5.2(a). A small holder was made which exposed the circular deposition area (figure 5.2(b)) and also made electrical contact to the front and back faces of the crystal. A novel feature of the apparatus was that the oscillator circuit (figure 5.3) was placed inside the vacuum chamber very close to the crystal. This ensured that the crystal oscillator continued to function for large frequency shifts. normally, the crystal is connected to the outside of the vacuum chamber via a co-axial lead. parasitic capacitance problems cause the oscillator to fail to oscillate for frequency shifts of < 1% of Fq. The oscillator was protected inside the vacuum chamber by resin encapsulation. The oscillator output was fed to a frequency counter which displayed the frequency as a 7 digit number, thus giving 1Hz accuracy.

A computer program was written, based on equation (5.1) to determine the correspondence between frequency and thickness. For a particular start frequency (usually 6 MHz) the end frequency was calculated for a particular film density and required film thickness. The program was written in BASIC and is given in Appendix I.

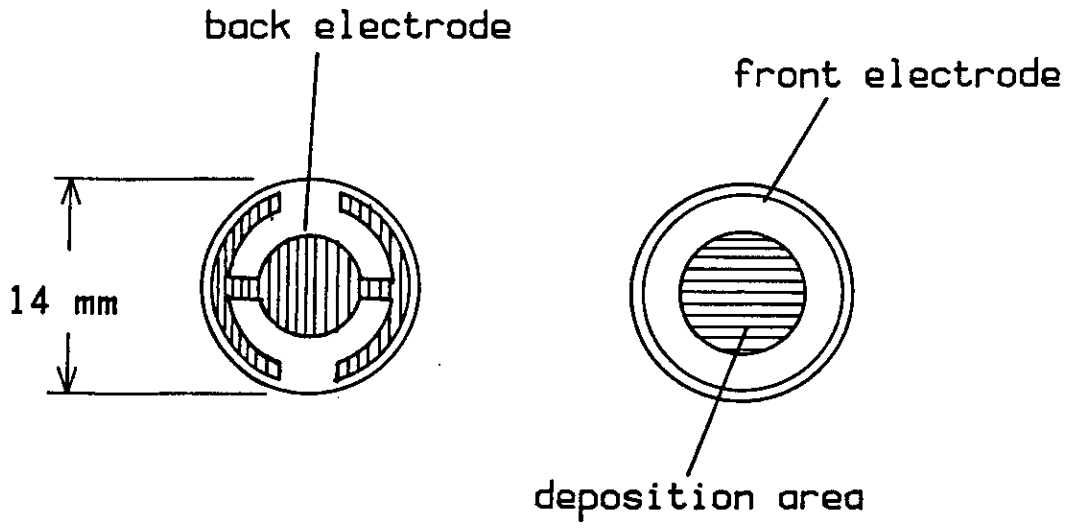

(a)

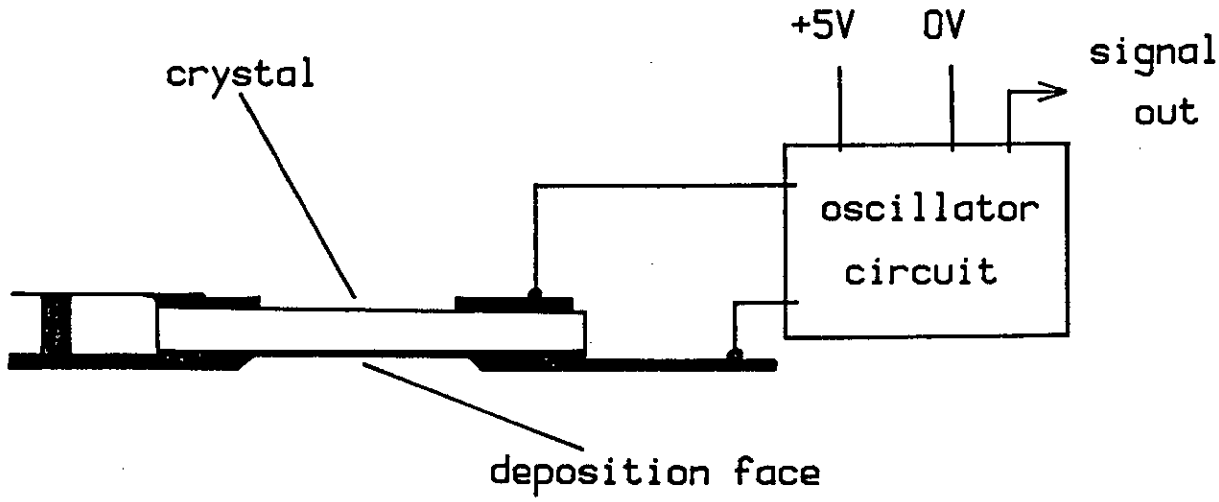

(b)

Figure 5.2 The quartz-crystal thickness monitor:
(a) quartz-crystal electrode geometry,
(b) details of crystal holder.

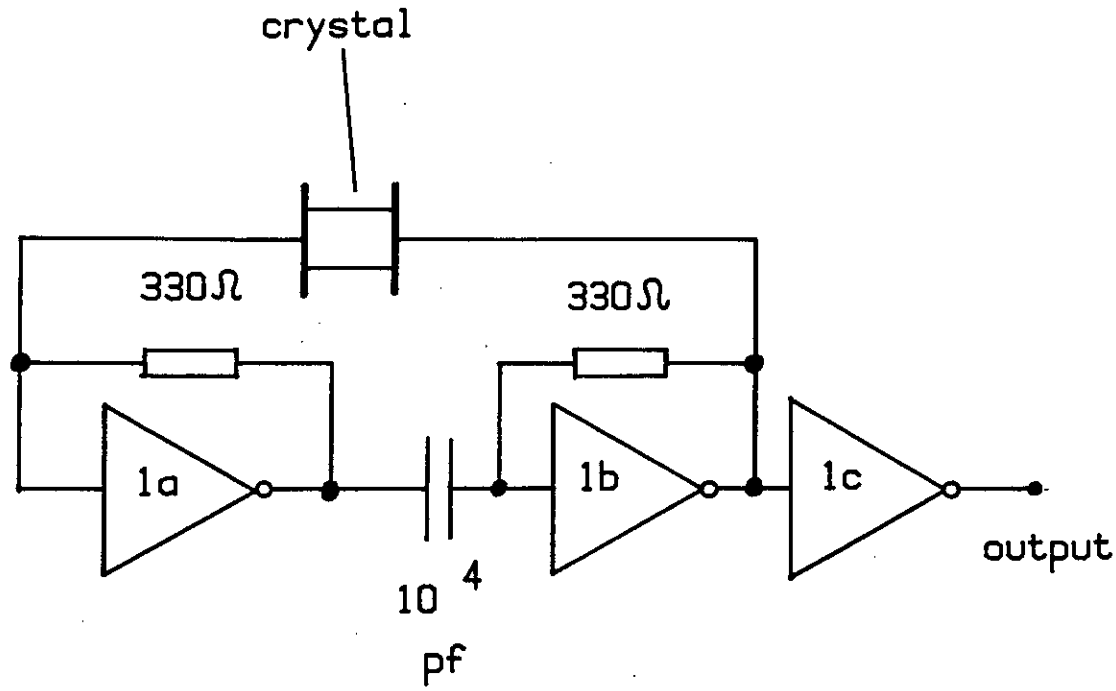

IC1a - LS7404

+5V pin 14

0V pin 7

output pin 6

Figure 5.3 Circuit diagram of crystal oscillator.

5.1.5.2 Optical monitoring

A schematic diagram of the optical monitoring system is shown in figure 5.4. The beam from a He-Ne laser passed through an optical window situated in the base of the vacuum chamber. It was then reflected from the surface of a glass slide, which was the substrate for the film, onto a Si photo-diode placed at the base of the chamber. When a high reflectivity Ag film is deposited on the glass slide the reflectivity curve goes from a low to a high value very quickly and saturates for film thicknesses > 50 nm. As-S films, however, are high refractive index dielectrics and therefore the reflectivity of highly monochromatic laser light (λ=632.8 nm) will go through alternating maxima and minima, producing a sinusoidal variation as a function of film thickness. In the present case these variations were monitored on a chart recorder and were then used to obtain the film thickness or refractive index. The film thickness, d, is given by the equation;

$$d=(P\lambda)/(2n) \qquad (5.2)$$

where λ is the He-Ne laser wave length (632.8 nm), n is the refractive index and P is the order no. of the interference, P being integer for minima and half-integer for minima.

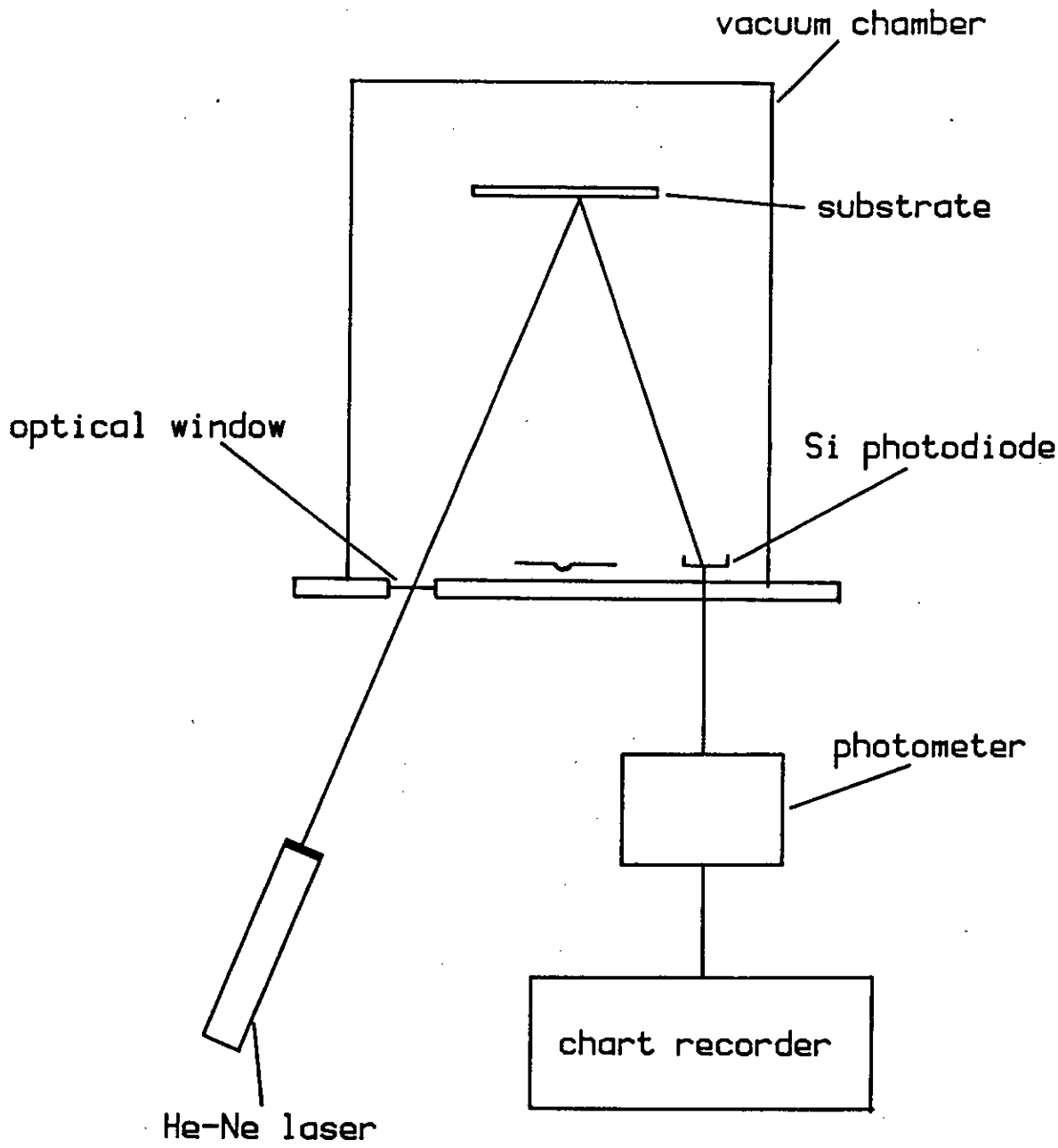

Figure 5.4 Schematic diagram of optical monitoring system.

5.1.5.3 Mechanical stylus

A mechanical stylus instrument (Taylor Hobson Talysurf 4) was used to measure the thickness of deposited films and was useful as a calibration check for the quartz thickness monitor. The full scale sensitivity on the most sensitive measuring range was 500 nm and therefore for calibration purposes, As-S and Ag films of 490 nm thickness were prepared.

These films were deposited onto glass slides half of which was covered with a mask with a straight edge. This produced a well-defined step in the film thickness suitable for the mechanical stylus to profile and therefore give an accurate measure of the film thickness. This enabled the constant C in equation (5.1) to be obtained for both As-S and Ag films.

5.2 Raman scattering experiments

5.2.1 Apparatus

A schematic diagram of the Raman scattering apparatus is shown in figure 5.5. The basic elements of the system consisted of a laser, a sample illuminator, a spectrometer, a detection system and a control system. A brief description of each of these elements now follows.

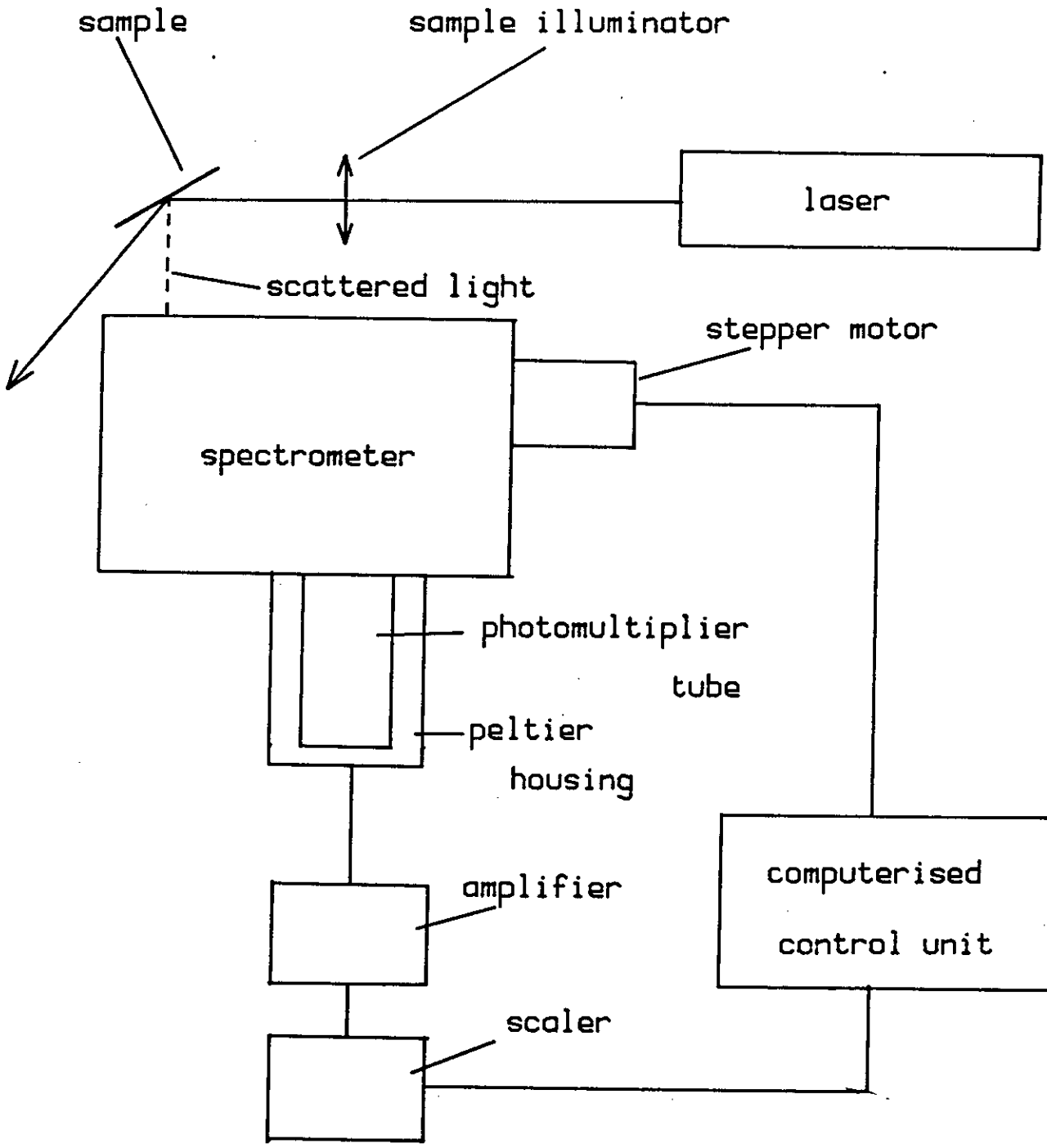

Figure 5.5 Schematic diagram of Raman scattering apparatus.

(a) Laser

A Kr-ion laser (Spectra Physics 165) was mainly used as the excitation source. Two wavelengths of this laser were used, 647.1 nm and 676.4 nm. The beam power available at 647.1 nm was in excess of 500 mW (but to avoid sample damage 200 mW or less was normally used). The power available at 676.4 nm was 50 mW.

In some photodarkening experiments an Ar-ion laser (Spectra Physics 164) was employed. The lasing wavelengths at 514.5 nm and 488 nm were used as light at these wavelengths induced photostructural changes and allowed the recording of a Raman spectrum at the same time.

(b) Sample illuminator

This consisted of a sample holder and a condensing lens to focus the laser light onto the sample. A lens was also used to focus the scattered light from the sample onto the entrance slits of the spectrometer. In addition there was a mechanism for introducing neutral density filters into the path of the laser beam before it reached the sample. This was particually important when the position of the spectrometer coincided with the position of the exciting line (laser wavelength). The intensity of light produced at the exciting line (due to Rayleigh scattering) was about six orders of magnitude greater than that of the light produced by Raman scattering. The

detection system would be damaged by such an intensity and therefore the neutral density filters were needed to attenuate the laser beam as the spectrometer was scanned across the exciting line.

(c) Spectrometer

The spectrometer was a Coderg T800 triple grating instrument and allowed Raman bands close to the exciting line to be observed. As the transmission of light through a grating spectrometer is polarisation dependent a polarisation scrambler was placed in front of the spectrometers entrance slit to compensate for this. The spectrometer was scanned in frequency by a stepper motor controlled by a microcomputer.

(d) The detection system

The detection system consisted of a specially constructed photomultiplier which produced a current pulse each time a photon was detected. The current pulses were amplified, shaped, passed through a noise discriminator, and then fed into a counting scaler which displayed the mumber of counts (photons/sec.) and outputted the information digitally to the computer. The photomultiplier was contained in a Peltier-cooled housing which lowered the temperature to 223 K, thereby reducing the dark count (noise pulses) considerably. Typically the dark count was 3-4 counts/sec.

(e) The control system

A microcomputer (Hewlett Packard-HP85) was used to control the spectrometer and also as a data aquisition system. Connected to the microcomputer was a Hewlett Packard multiprogrammer (model 6942A). This housed several control cards including a timer-pacer, for sending step pulses to the stepping motor system, and a counter-totaliser for receiving the photon counts from the photomultiplier. The sequence of events in a single step-count operation was as follows; The step pulses are initiated by the HP85 controller, and the timer-pacer is triggered when the step is complete. While the output from the timer-pacer is held high, the counter-totaliser is enabled and counts photons. The data, from the recording of a Raman spectrum, was stored as a file on flexible discs, but for detailed analysis of the data it was transferred to a main frame computer (ICL 2970/80), operated by the Edinburgh Regional Computing Centre.

5.2.2 Experimental methods

5.2.2.1 Obtaining a Raman spectrum

The Raman spectra of thin film and bulk samples were obtained mainly by reflecting the laser beam off the surface of the sample. In the case of film samples deposited onto glass slides, an intermediate metal layer (usually aluminium) was deposited between the glass

substrate and the film to form a reflecting surface. This also ensured a clean baseline for the Raman spectrum since metals produce no measurable Raman signal. Surface Raman scattering was also used to obtain the Raman spectra of bulk samples, in which case the surface of the sample had to be optically polished. The scattered light from the specimen was focused onto the entrance slit of the spectrometer, a process which required careful adjustment to produce a good spectra.

It is usual in Raman spectroscopy to assign the exciting line as zero wavenumber (where wavenumber is reciprocal wavelength and is given in cm^{-1}). All spectra were recorded from -10 to 520 cm^{-1} (the Stokes spectrum) and the step size was either 0.5 or 1 cm^{-1}. The reproducibilty of the Raman system was inherently very good. Each time a Raman spectrum was recorded the spectrometer scanned across the exciting line, thus fixing the 0 cm^{-1} position. Quantitatively, the error in the measured frequency was estimated to be ~1 cm^{-1}.

5.2.2.2 Plasma lines

In addition to coherent light at the lasing frequency, the laser produces relatively weak incoherent light at other frequencies. The incoherent light arises from non-lasing transitions within the plasma and gives rise to what are called "plasma lines". It was essential

to remove the plasma lines from the Raman spectra otherwise they could easily be mistaken for genuine Raman features. In the present work a prism filter was used to purify the beam: this used a combination of prisms to separate out by refraction most of the non-lasing light and then mask this component. In very weak Raman spectra, however, plasma lines might appear. In this situation the spectrum must be compared with the positions of known plasma lines for the laser used.

5.2.2.3 Data handling

All data handling and graph plotting were performed on the Edinburgh-multi-access-system (EMAS) which is a facility provided by the Edinburgh regional computing centre. A comprehensive library of programs was available which made data analysis a straightforward procedure. The basic operations that could be carried out are as follows;

1. Removal of noise spikes.
2. Smoothing of data.
3. Normalisation of spectra.
4. Peak finding.
5. Multiple graphing.
6. Addition and division of spectra

After processing, spectra were plotted using a Tektronix plotter (4662) connected to the EMAS system

5.3 Optical transmissivity measurements

Optical transmissivity measurements were made using a Varian DMS 80 uv-visible spectrophotometer which had a wavelength range of 190-900 nm. This was a dual beam instrument and therefore measurement was simply a matter of putting the film to be measured in to the sample compartment of the instrument. A reference substrate could also be placed in the reference chamber of the instrument if necessary. The results were obtained as transmissivity versus wavelength.

5.4 Photodarkening experiments

5.4.1 Photodarkening by Ar-ion laser

A schematic diagram of the apparatus used in these experiments is shown in figure 5.6. It consisted of an Ar-ion laser set at the wavelength 514.5 nm, a shutter to control the exposure of the sample and a Si photodiode connected to a photometer monitored the light signal. A chart recorder was used to record the data.

Two types of experiment were performed. In the first type an As-S film was placed in the path of the laser beam, the shutter was opened and the decrease in transmissivity was monitored as the sample photodarkened. The shutter was then closed and re-opened periodically to

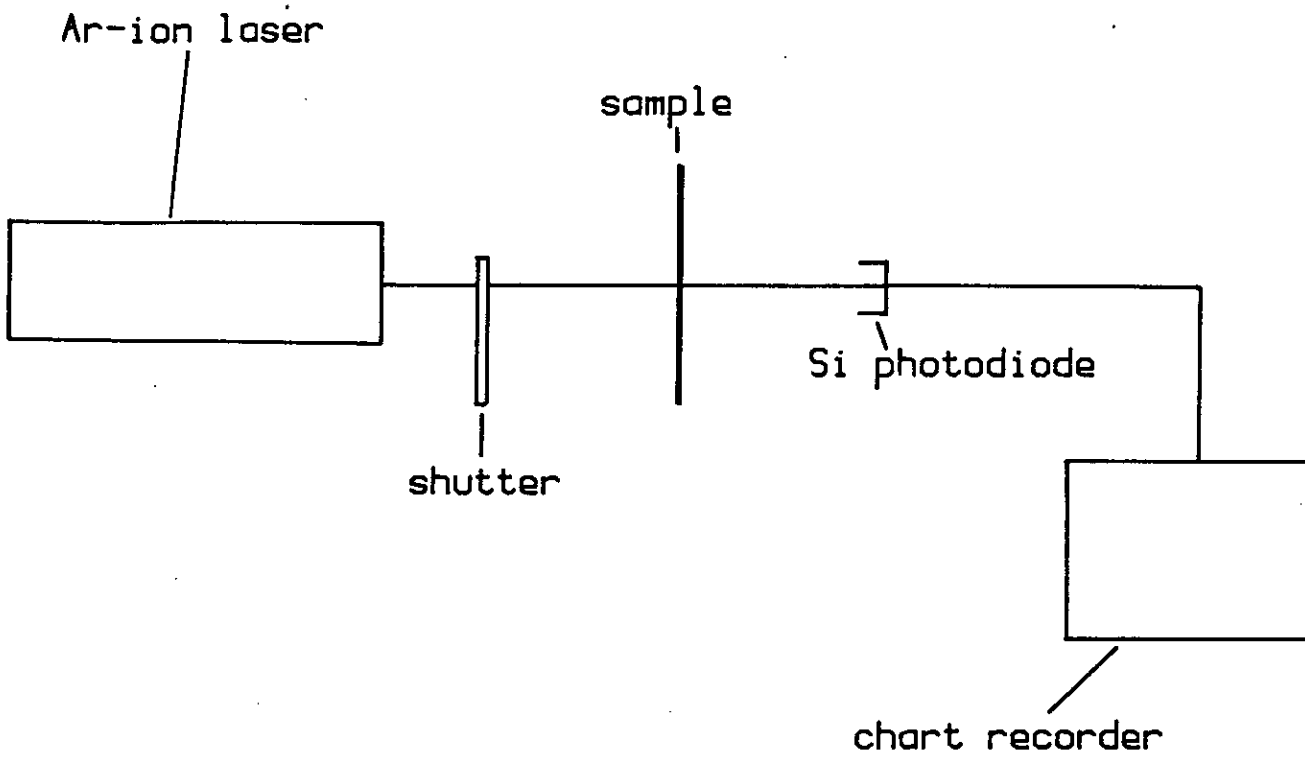

Figure 5.6 Diagram of photodarkening experiments using an Ar-ion laser.

see, for example, how permanent the light-induced changes were. In the second type, a sample was again placed in the path of the laser beam but in this case the photodarkening was allowed to saturate. A constant transmission reading was then obtained on the chart recorder. The effect on the transmission value of increasing and decreasing the laser power was then investigated.

5.4.2 Temperature dependence of optical transmissivity

A schematic diagram of the experimental set up used to measure the temperature dependence of optical transmissivity is shown in figure 5.7. It consisted of a Varian single beam spectrophotometer and a cryostat. The cryostat fitted into the sample compartment of the spectrophotometer and had optical windows to enable light to pass through the cryostat and the film sample that it contained. Measurements were made as follows; firstly the transmissivity value, without the sample in place, was adjusted to give a full scale reading on the chart recorder. The sample was installed in the cryostat, the wavelength set to a particular value, and the transmissivity measured as a function of temperature. The temperature range covered was 130 to 443 K and the wavelength positions at which measurements were made were 500, 510, 520 and 530 nm.

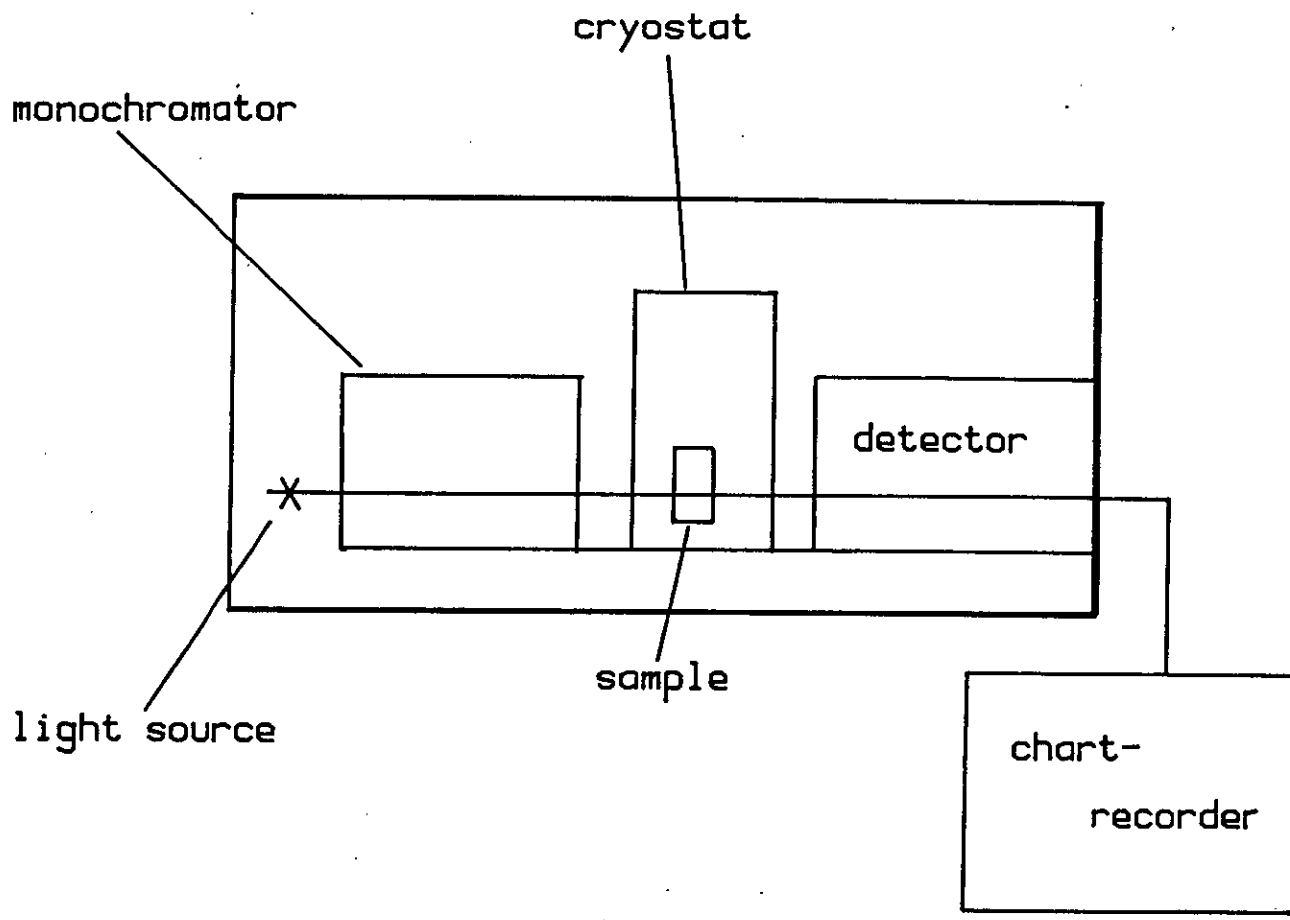

Figure 5.7 Apparatus used to measure the temperature dependence of photodarkening.

5.5 Photodissolution experiments

5.5.1 Intensity dependence measurements

A schematic diagram of the apparatus used to determine the dependence of the photodissolution rate on incident light intensity is shown in figure 5.8. It consisted of a dye laser (tuned to 571.5 nm) with a beam diameter broadened, by a lens, to 1 cm. The output power of the laser could be varied between 0 and 50 mW and it was used to photodope a Ag film 80 nm thick in to an $As_{30}S_{70}$ film 260 nm thick. To measure the dissolution rate of the Ag film a second light source with a wavelength of 710 nm and a beam diameter of 2 mm was used. This source had a very low intensity and since the As-S film was transparent to 710 nm light, it was suitable for measuring the change in transmissivity of the Ag film as photodissolution proceeded. There was a point in the transmissivity-time curve (measured on a chart recorder) at which the rate of dissolution was a maximum. This always corresponded to the same thickness of Ag left on the slide and was used as a way of fixing the end point of the experiment. To make determination of the end point easier, especially at low power levels, the transmissivity signal was differentiated and would therefore go through a maximum at the end point.

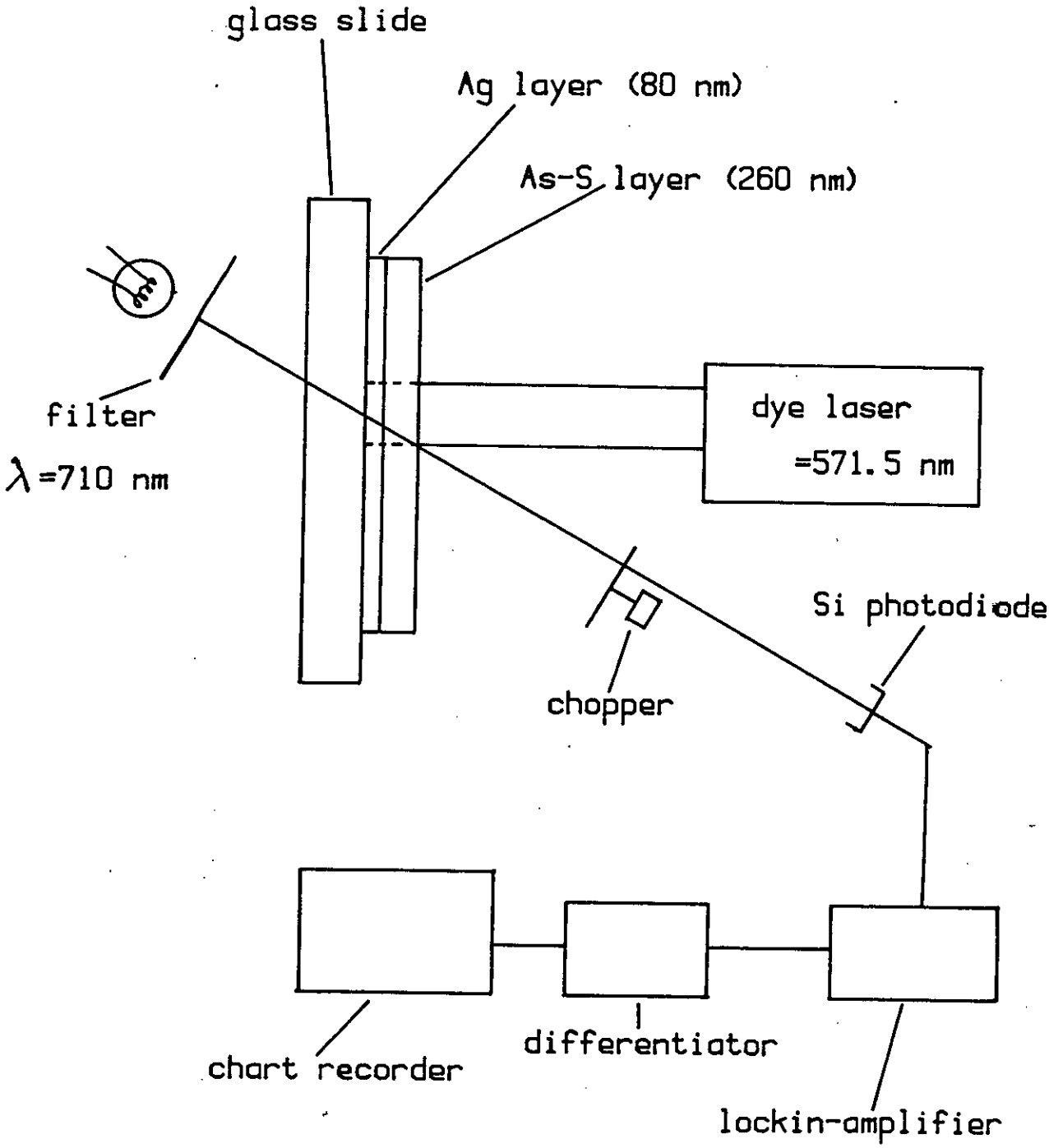

Figure 5.8 Apparatus used to measure the intensity dependence of the photodissolution process.

5.5.2 Electric field measurements

The dissolution process and its dependence on electric fields could be monitored using a resistance measurement technique. For these experiments thin film samples were fabricated with the geometry shown in figure 5.9(a). The first layer of the structure consisted of Ag strips 2 mm wide and 70 nm thick. On top of this was deposited an As-S film, 250 nm thick, which was narrower than the slide to allow electrical contact to be made to each end of the Ag strips. The top layer of the structure was a thin transparent film of Au. This was narrower than the As-S layer to prevent shorting of the Ag strips. The cross-section through the sample under illumination is shown in figure 5.9(b). The resistance of the Ag strips was measured by an AC method. A 1 volt sinusoidal signal (500 Hz) was applied as shown in figure 5.9(a). The resistance of the Ag strip was about 5 Ω and therefore a 1 MΩ resistor was used to limit the current passing through the Ag strip to 1 μA. This was necessary to prevent heating effects. The voltage across the sample was proportional to its resistance and was was measured by a lockin amplifier previously calibrated with a standard resistance. The sample was placed under a microscope through which a light source was focused and the centre part of the Ag strip was illuminated (see figure 5.9(a)). As photodissolution occurred the Ag strip thinned and the resistance measurement allowed the

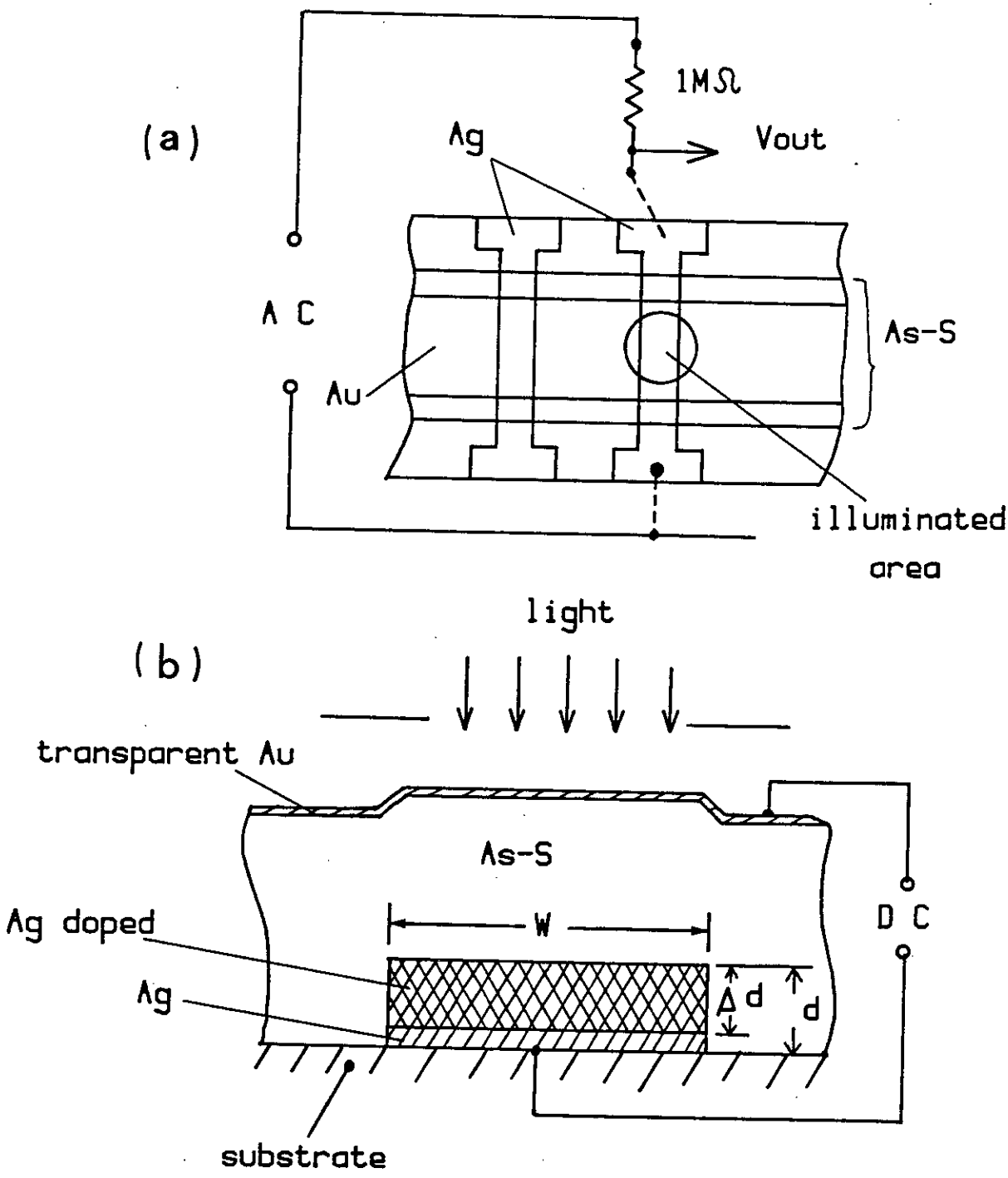

Figure 5.9 Sample geometry for electric field measurements: (a) plan view, (b) cross-sectional view.

dissolution to be monitored. A DC potential could also be applied between the top Au layer and the bottom Ag strip so that the effect of making the Au layer positive or negative with respect to the Ag strip could be observed.

5.5.3 Transverse photodissolution experiments

Samples used to study transverse photodissolution consisted of a Ag/As_2S_5 combination deposited on to a microscope slide (75 mm X 25 mm). The first layer was a Ag film, 300 nm thick, and the upper layer an As_2S_5 film 700 nm thick. The samples were kept in complete darkness until they were used.

The experimental arrangement is shown in figure 5.10. The sample was illuminated with an Ar-ion laser (λ =488 nm, E=2.541 eV) from the As_2S_5 side of the film. The laser beam was expanded using a spatial filter (a X20 objective and a 12.5 μm pin hole) and then collimated with an appropriate lens to produce a 1 cm^2 diameter light beam. The power reaching the sample was measured using a thermopile (Laser Instruments model 17S), and was typically between 10 and 50 mW/cm^2.

To monitor the photodoping rate a low powered He-Ne laser was used (Spectra Physics model 167). The He-Ne laser was reflected off the surface of the sample at the centre of the 1 cm^2 irradiated area. The angle of

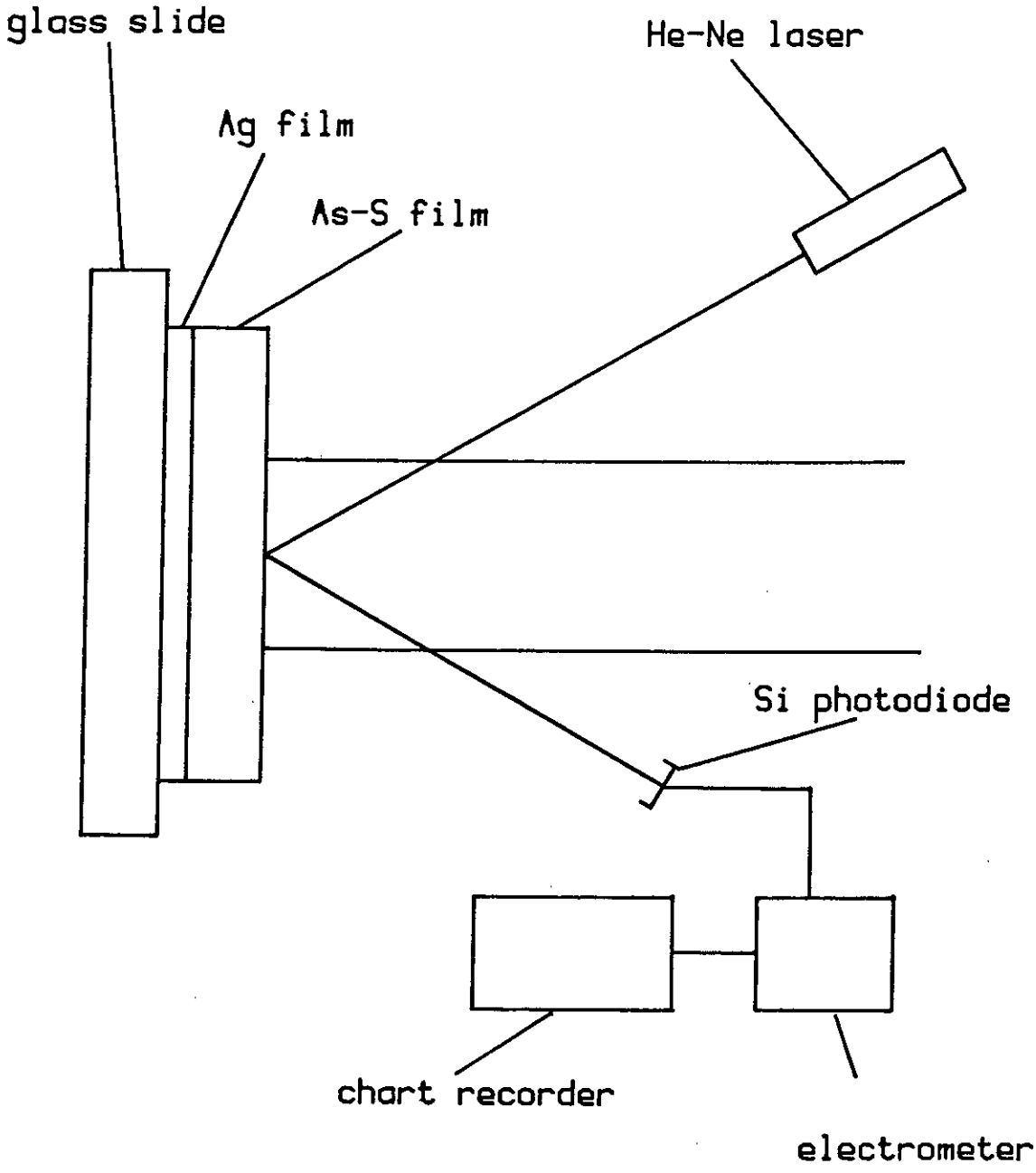

Figure 5.10 Apparatus used for transverse photodissolution experiments.

incidence was 10° and the laser (λ =632.8 nm) had its power further reduced from 0.85 mW to 10 μW by a neutral density filter. The signal from the He-Ne laser was detected by a Si photodiode connected to a Keithly 602 electrometer operating as a current-to-voltage converter. A chart recorder was connected to the electrometer and the reflectance changes that occurred during the photodoping was recorded.

After positioning the He-Ne probe beam in the correct place on the surface of the sample the photodoping by the Ar-ion laser was initiated using an electromechanical shutter.

5.5.4 Lateral photodissolution experiments

Samples for the lateral photodissolution experiments were fabricated with the geometry shown in figure 5.11(a). Microscope slides (25 mm X 75 mm) were used as substrates. The first stage in fabrication was to coat half the area of the slide with a Au film. This film was sufficiently thick (100 nm) to be homogeneous and a good electrical conductor. Next a Ag film was deposited as a strip 5 mm wide and 600 nm thick. The strip was parallel to the longest side and ran down the centre of the slide. Finally a film of As-S (30 nm thick) was evaporated to cover the whole of the slide.

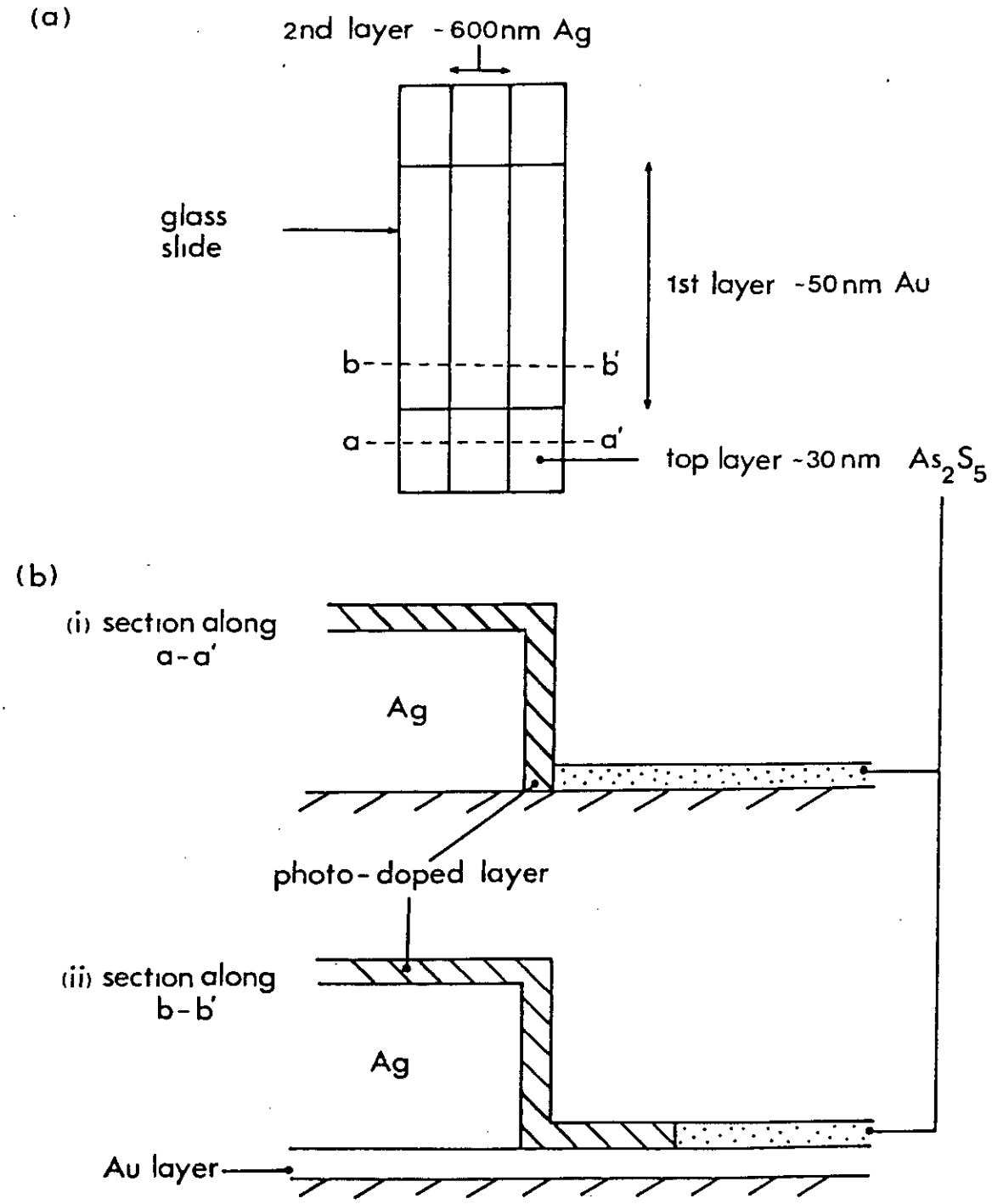

Figure 5.11 The sample geometry used in the lateral photodissolution experiments: (a) plan view, (b) cross-sections at indicated regions.

Figure 5.11(b) shows a cross-section through the structure and illustrates the large difference in dimensions between the thickness of the Ag strip and the As-S film. The structure was fabricated in this way so that the quantity of Ag available to photodope the surrounding As-S film was very much in excess and therefore providing a reservoir of Ag for lateral photodoping along the surface of the slide.

The reason for coating half the slide with a Au film was to investigate the effect on the lateral photodissolution of an electrically conducting substrate.

Sample illumination and measurement were carried out using a standard microscope fitted with incident illumination. The light source was a 50 W quartz-halogen lamp operated from a 12 V DC power supply. The infra-red part of the spectrum (>1 μm) was removed with a distilled water filter (5). The intensity of the light projected through the microscope on to the sample was controlled by an iris but also depended on the magnification of the objective used. The microscope was always focused on to the surface of the sample and therefore the disc of light projected on to the sample was sharp and always the same size for a given objective. A X40 objective was normally used. The microscope was fitted with a vernier eyepiece which had been calibrated against a graitical and this enabled lateral dissolution distances to be measured.

5.6 References

1. Heavens, O. S., "Optical Properties of Thin Solid Films", (London: Butterworth Scientific Publications), p.167, (1955).
2. Goldschmidt, D. and Rudman, P. S., J. Non-Cryst. Solids, 22, 229, (1976).
3. Hawkes, P. W., "Electron Optics and Electron Microscopy", (Taylor and Francis Ltd), p.182-189, (1972).
4. Lu, C. and Lewis, O., J. Appl. Phys., 43, 4385, (1972).
5. Oriel Corporation, catalog of optical systems and components, p.D49, (1977).

CHAPTER 6

PHOTODARKENING IN THE As-S SYSTEM

RESULTS AND DISCUSSION

6.1 Introduction

This chapter is concerned with the investigation of the optical and structural properties of the photodarkening effect. As-S samples in the form of thin films, thin bulk glasses and glassy powders were used.

6.2 Thin As-S films

6.2.1 Results

6.2.1.1 Stoichiometric films

The optical transmissivity of thin films of As_2S_3 was influenced by the intensity and wavelength of illumination, the ambient temperature and the thermal history of the film. Typical results are shown in figs. 6.1 to 6.4. Curve (i) in fig. 6.1 (a) shows the transmissivity as a function of wavelength for an as-deposited, vacuum-evaporated thin film of As_2S_3; curve (ii) is for an annealed film (473 K, 1 hour) and curve (iii) is for a film after illumination (tungsten lamp, 1 hour); all curves were measured at room temperature.

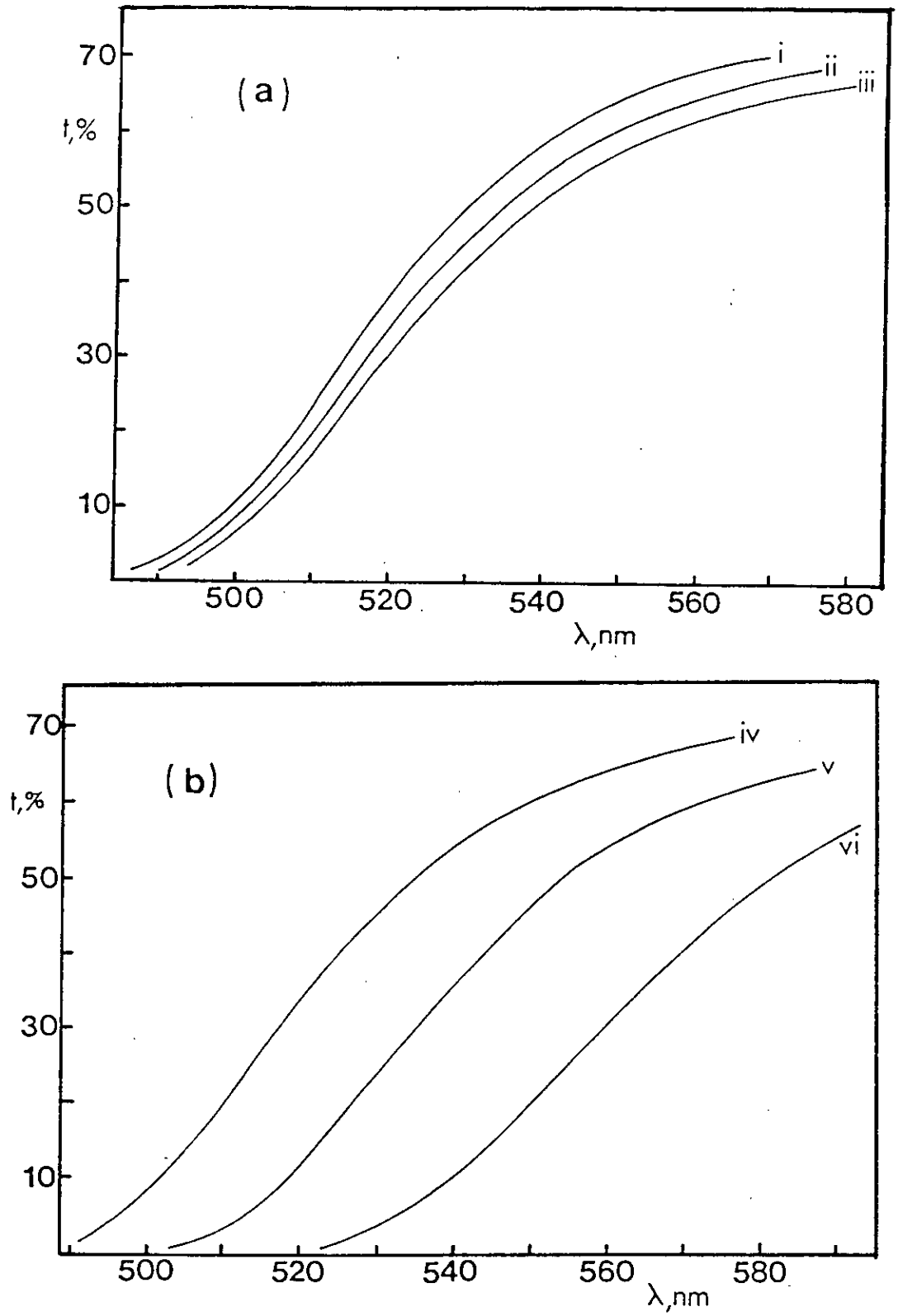

Figure 6.1 The spectral dependence of transmissivity of As_2S_3 films: (a) curve (i) as-evaporated film, curve (ii) annealed film, curve (iii) annealed film exposed to tungsten lamp for 1 hour. (b) annealed film measured at (i) 300 K, (ii) 405 K, (iii) 501 K.

The sequence of measurements could be (i) -> (ii) -> (iii) -> (ii) -> (iii) and so on, or (i) -> (iii) -> (ii) -> (iii) and so on. In fig.1 (b) the curves (iv), (v) and (vi) are for an annealed film measured at 300, 405, and 501 K, respectively; these results simply correspond, of course, to the decrease in optical energy gap with increasing temperature and illumination.

Figure 6.2 illustrates in more detail the effect of temperature (and heat treatment) on transmissivity at four different wavelengths. Again, these results could be obtained in a variety of ways. For example, curve (c) (λ = 510 nm) could be traced out by starting at point 1, corresponding to an annealed film at about room temperature. Illumination would cause the transmissivity to decrease down a vertical line to point (2). On raising the temperature the transmissivity decreases still further (as in fig. 6.1 (b)), and at a high temperature (in this case about 433 K) the sample is at least partially "annealed". In the particular experiment illustrated the temperature was then decreased continuously to about 103 K the film was illuminated and the transmissivity decreased down the vertical line. On reheating the transmissivity decreased further, along the lower line, and the loop could be retraced. It would also be possible, of course, to stop at any intermediate temperature to carry out the photodarkening process, for example, as indicated by the dashed vertical line at

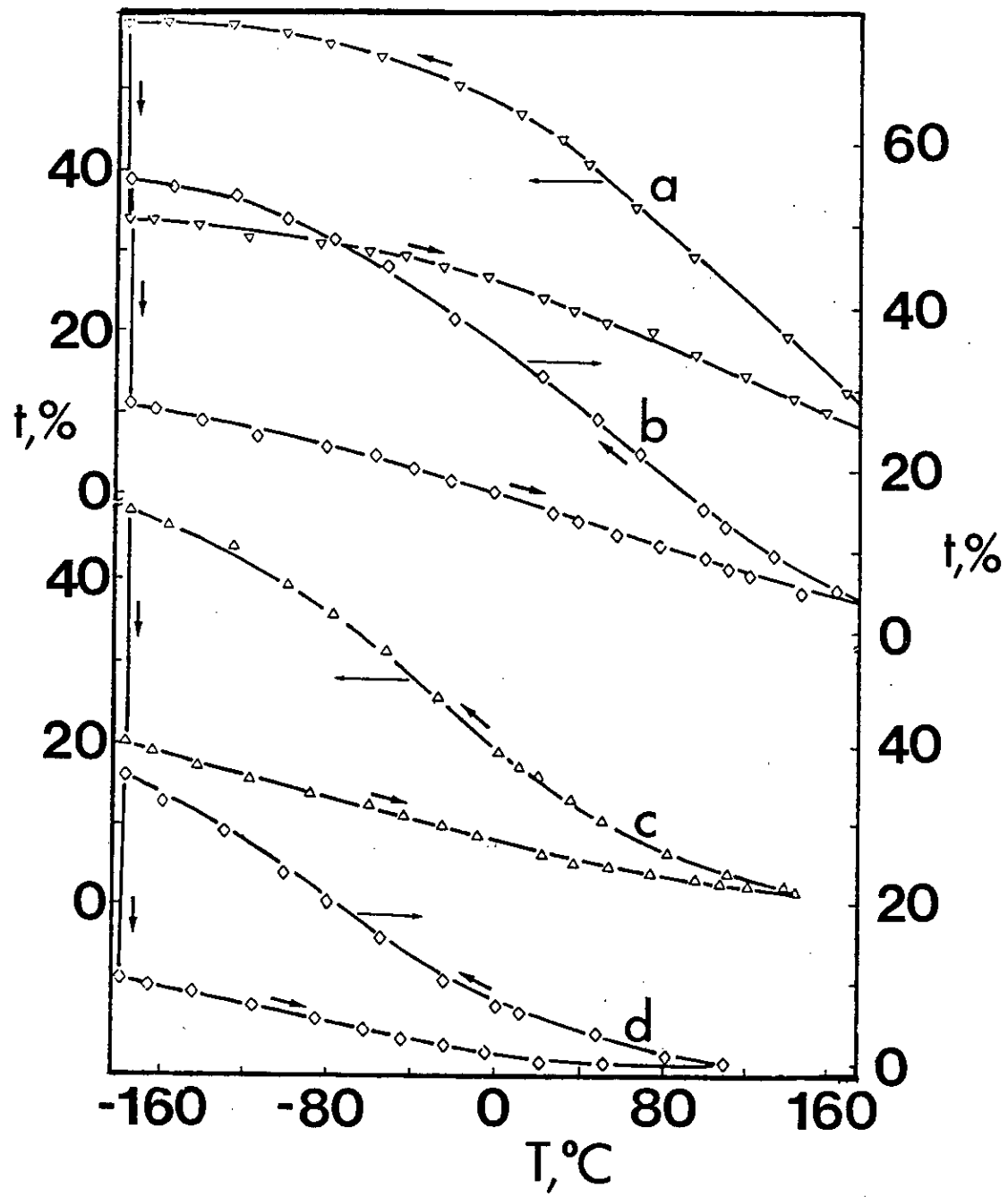

Figure 6.2 The temperature dependence of the transmissivity of As_2S_3 thin films measured at the following wavelengths: (a) 530 nm, (b) 520 nm, (c) 510 nm and (d) 500 nm. The vertical lines correspond to the change in transmissivity produced by illumination by a tungsten lamp for 1 hour.

about 173 K. Note, however, that the temperature cycling of the upper part of the loop could be followed in either direction, but the vertical transitions (photodarkening) can occur only in the downward direction.

Figure 6.3 illustrates the development of the photodarkening effect at room temperature as a function of time, but with the illumination turned off and on at arbitrary intervals; during the on-periods the intensity of illumination remained constant. A similar experiment is recorded in fig. 6.4, but here the illumination was subjected to several arbitrary decreases or increases in intensity at different times. The following points should be noted from figs. 6.3 and 6.4.

1. A small annealing effect is observed, even at room temperature.

2. On illumination there is an initial rapid decrease in optical transmissivity (photodarkening), but on interrupting the illumination the transmissivity increases (annealing) and then decreases again on further illumination. (fig. 6.3).

3. On decreasing the intensity of illumination, photobleaching is observed (fig. 6.4), whereas on increasing the intensity further photodarkening occurs.

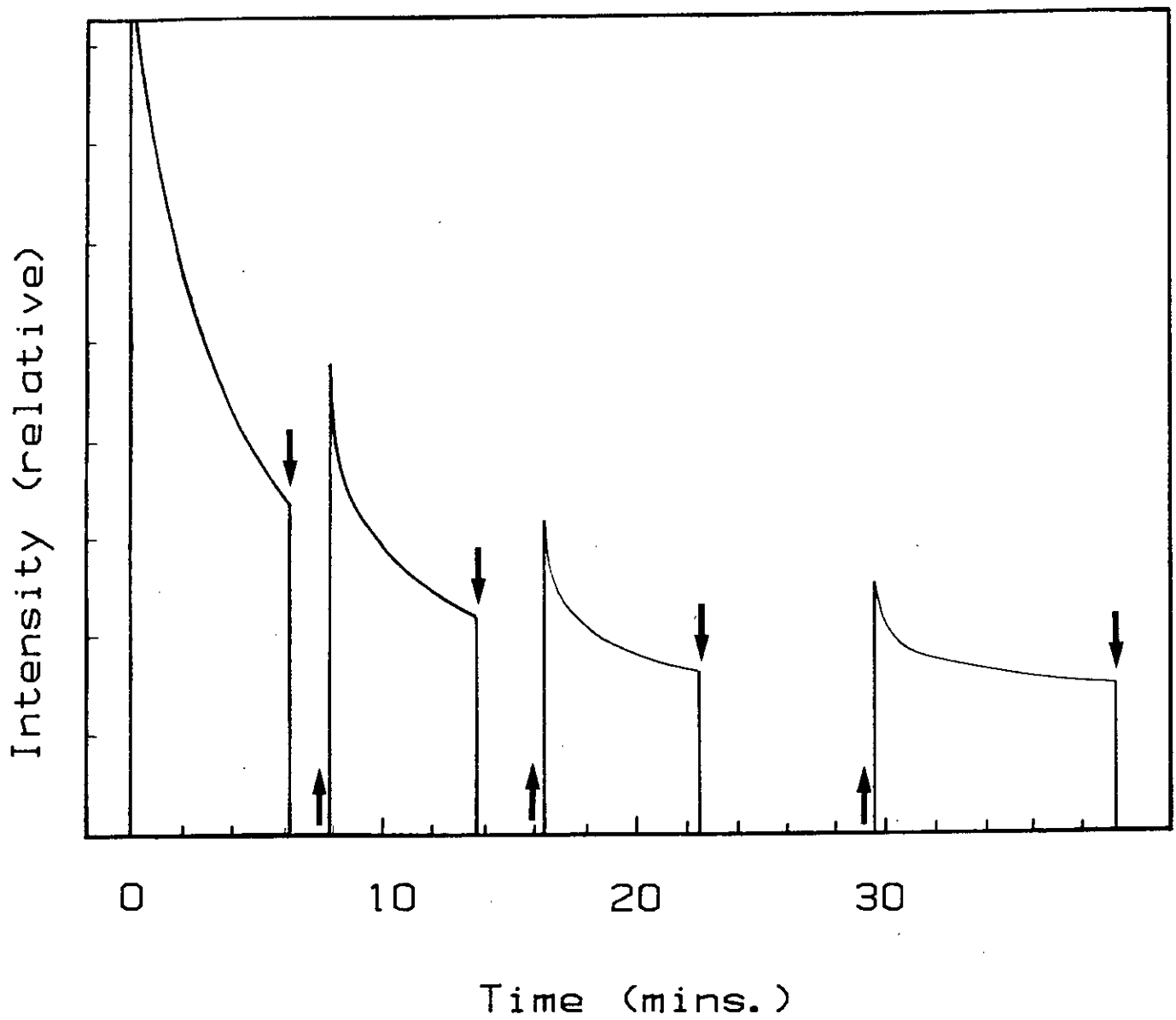

Figure 6.3 The change in transmissivity of annealed As_2S_3 thin films during illumination at a constant intensity by 514.5 nm laser light. The vertical arrows correspond to the closing (↓) and opening (↑) of a shutter. The measurements were made at room temperature.

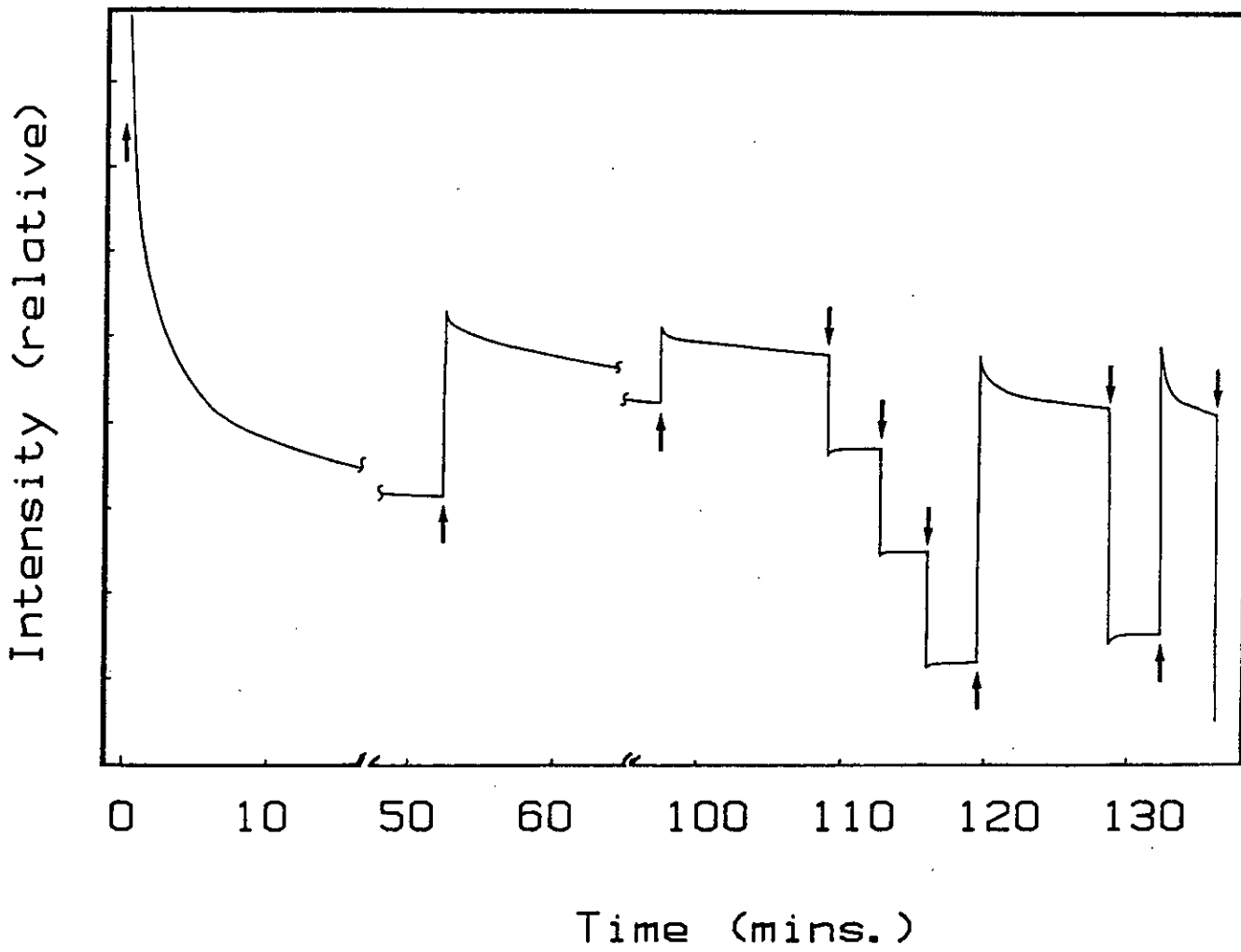

Figure 6.4 The change in transmissivity of annealed As_2S_3 thin films when illuminated by 514.5 nm laser light. The vertical arrows correspond to increasing (↑) and decreasing (↓) incident laser intensity. The measurements were made at room temperature.

4. The rates of photodarkening and bleaching are not the same (fig. 6.4). This asymmetry implies that the changes in transmissivity cannot be caused by thermal effects (that is, by the small changes in sample temperature during and after illumination).

5. After prolonged exposure at a particular intensity the optical transmissivity decreased to a saturation value. In the saturated state the photodarkening is determined, at a given temperature, by the wavelength and intensity of illumination. This implies, that for a given intensity, the cycles of changes traced out in fig. 6.2 are unique provided the photodarkening (that is, the lower part of the cycle) has reached its saturation value.

The total change in transmissivity for the reversible part of the photostructural change was greater than 90% of its initial value at a wavelength of 514.5 nm. The upper level of the intensity of illumination which can be applied is limited by irreversible processes which would lead to melting and disintegration of the sample.

The Raman spectra of evaporated As_2S_3 films are shown in figure 6.5. Curve (a) shows the as-deposited film. The characteristic sharp features in the 100-250 cm^{-1} have been assigned to molecular units such as As_4S_4, S_n and As_4 (1, 2, 3). After annealing the film curve (b)

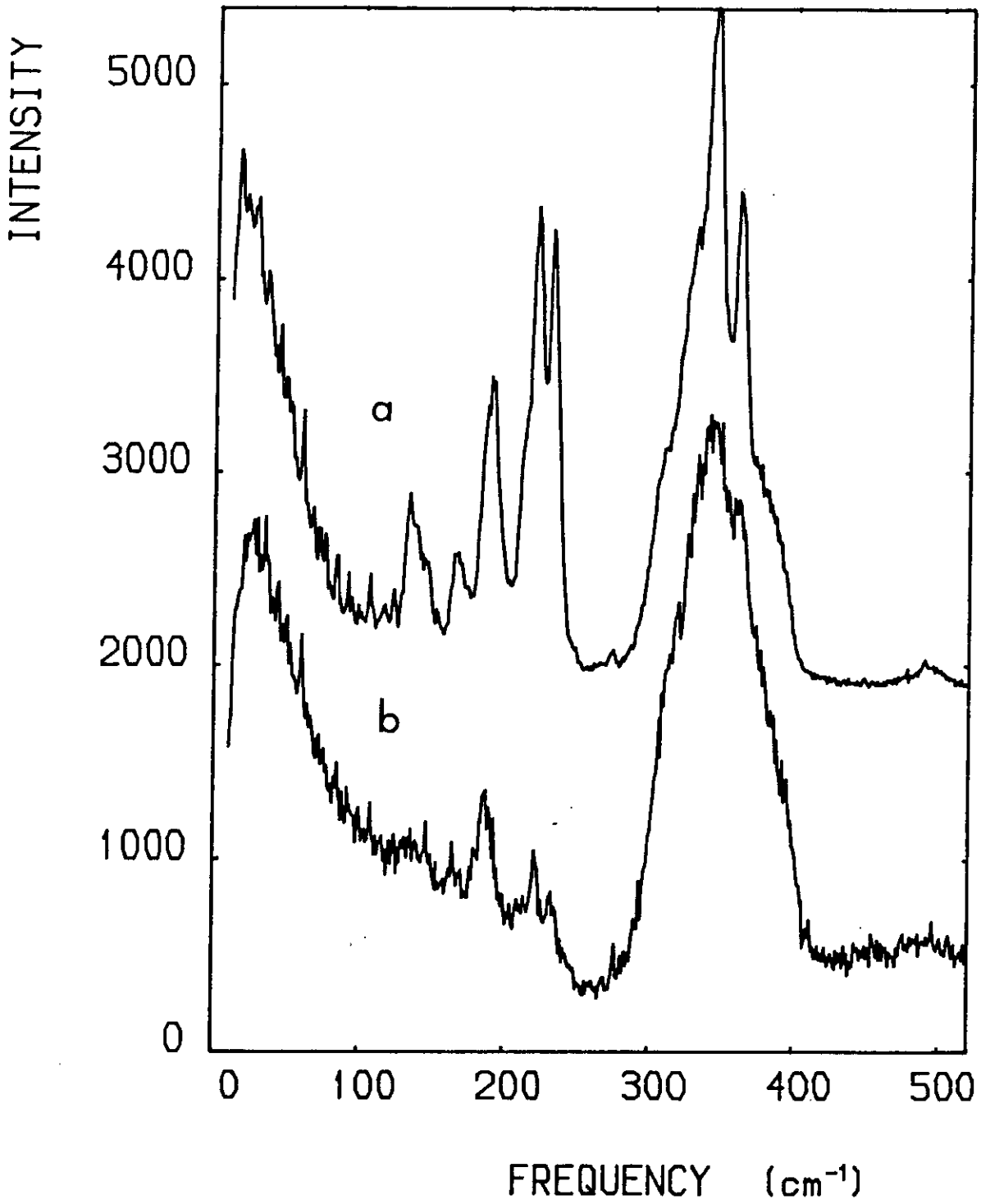

Figure 6.5 Raman spectra of (a) an as-evaporated and (b) an annealed As_2S_3 thin film.

was obtained. The sharp features are considerably reduced, but relatively broad features with maxima at 187 and 231 cm^{-1} remain. Similar results were observed by Nemanich et al. (2) and were taken as evidence that some "wrong" bonds of the type As-As and S-S exist even in well-annealed As_2S_3 films.

Figure 6.6 shows the effect of illumination on the Raman spectra of As_2S_3 films. It can be seen that the bands with maxima at 187 and 231 cm^{-1} are clearly affected by the illumination (curve a to b). The intensity of the band at 231 cm^{-1} is increased, while the intensity of the band at 187 cm^{-1} is decreased. Similar results were obtained by Ewen (1) on bulk As_2S_3 glasses. Ewen observed a general decrease in the intensity of the Raman spectrum during illumination, but the relative intensity of the band at 231 cm^{-1} increased. The results are also in agreement with those of Bertoluzza et al (4) who found that illumination of As_2S_x glasses with $x < 3$ changed the Raman spectra. The Raman band near 231 cm^{-1} was enhanced, and the intensity of the band at 187 cm^{-1} reduced.

Curve (c) in fig. 6.6 was obtained after annealing the film a second time. It is clearly similar to curve (a), showing that the observed reversible photodarkening is connected with reversible changes in structure. Curve (d) was obtained after the sample was illuminated again. The enhanced 231 cm^{-1} band and the reduced 187 cm^{-1} Raman

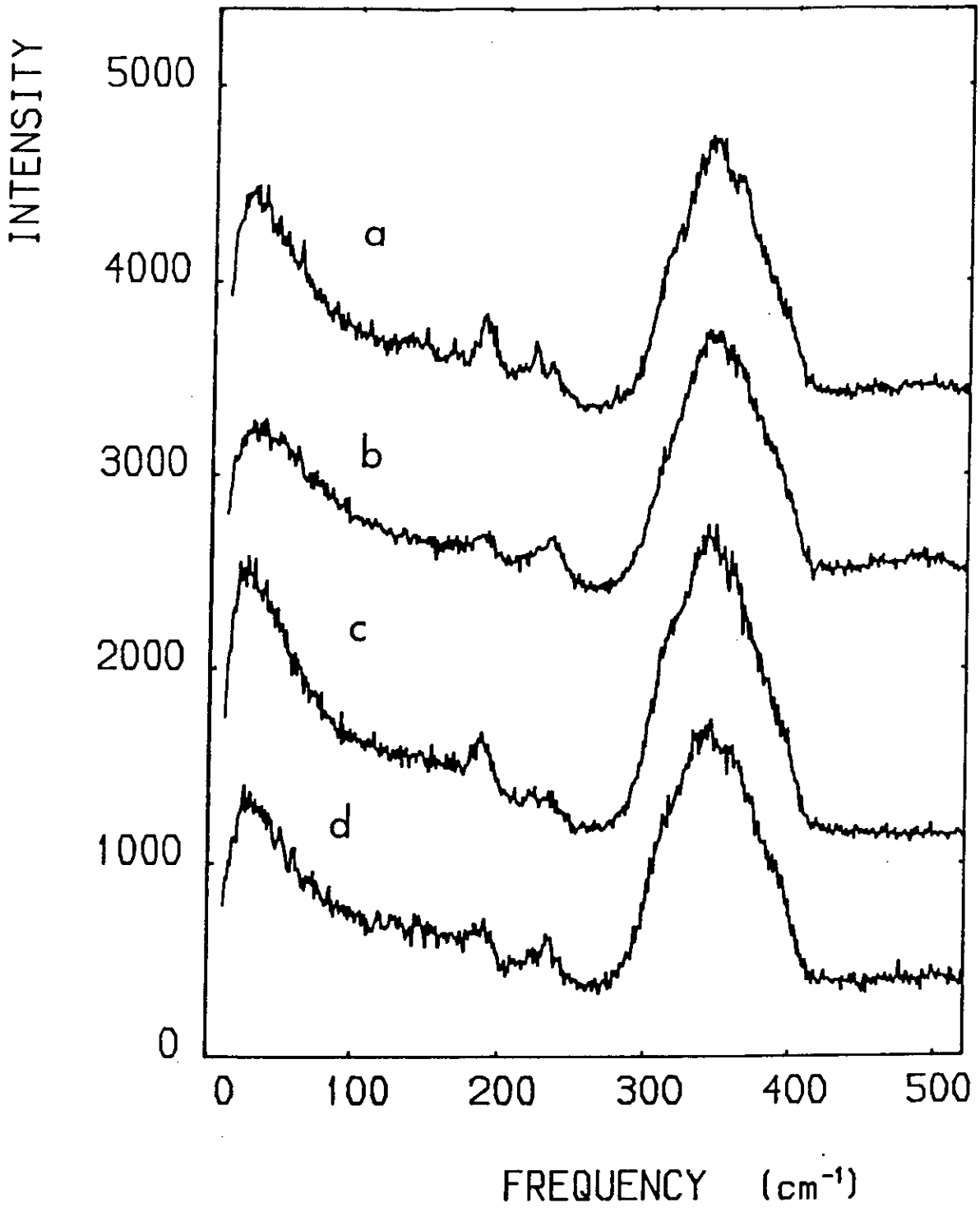

Figure 6.6 The Raman spectra of a typical As_2S_3 film illustrating reversible photodarkening: (a) the first annealed state, (b) the photodarkened state produced by Ar-ion laser illumination, (c) the second annealed state and (d) the second photodarkened state produced by Ar-ion laser illumination. All spectra were recorded using the 647.1 nm wavelength, and were normalized to the height of the 240 cm^{-1} Raman band.

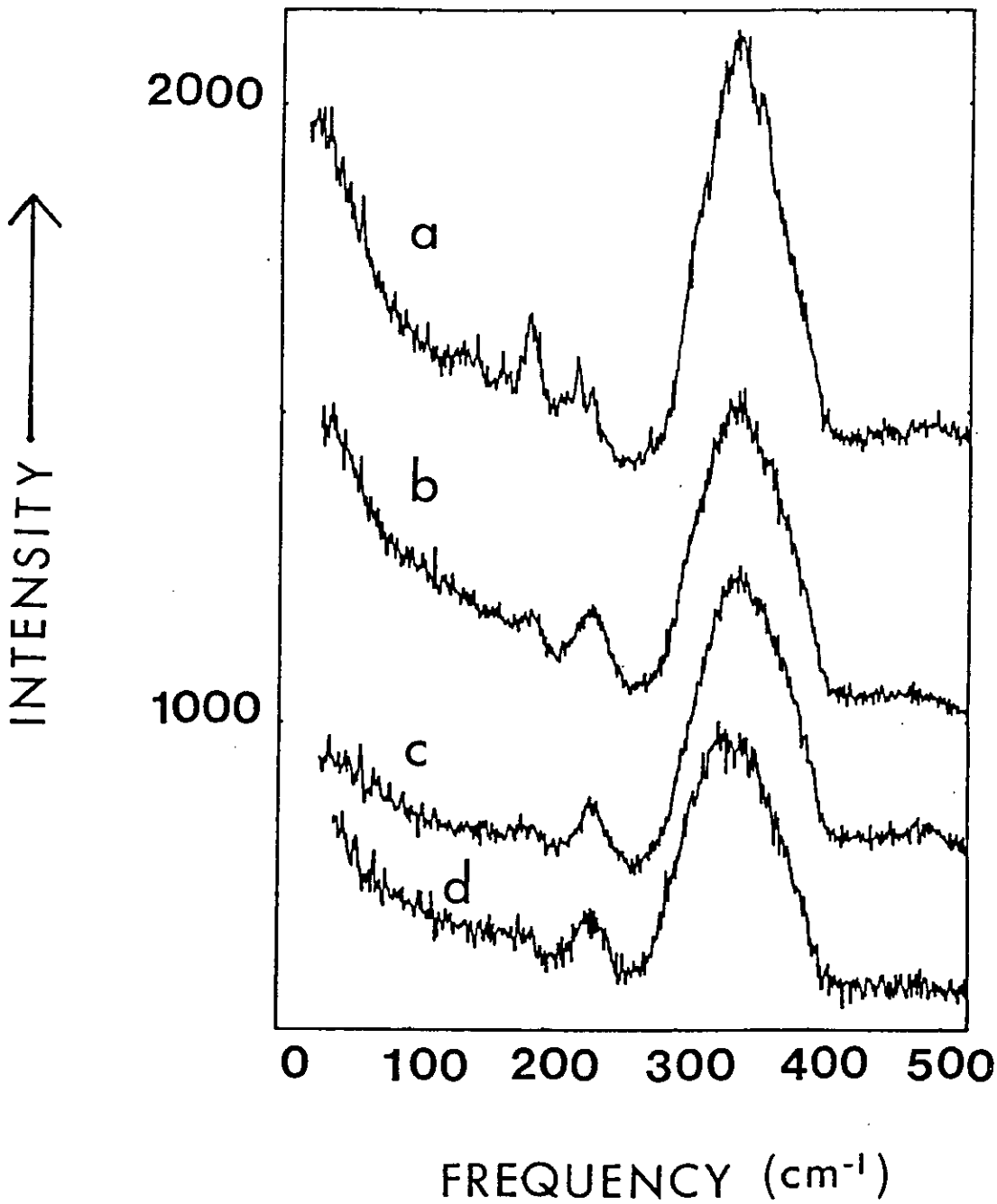

Figure 6.7 Raman spectra of As-S thin films: (a) an annealed film (excitation wavelength, 647.1 nm), (b), (c), and (d), the films were photodarkened and excited using the wavelengths 568.2, 530.9 and 488.0 nm respectively.

band are again seen. The cycling between the well-annealed and photodarkened state was repeated many times with reproducible results.

Figure 6.7 shows the Raman spectra of As_2S_3 films which were photodarkened using the exciting wavelength. The Raman spectra were recorded after the photodarkening had saturated. Curve (b), (c) and (d) were recorded using wavelengths of 568.2, 530.9 and 488.0 nm, respectively, and they reveal a further enhancement of the 231 cm^{-1} Raman band compared with the photodarkening state shown in figure 6.6. Curve (a) shows the Raman spectrum of a well-annealed film for comparison (λ exc = 647.1 nm). Changes in the Raman spectra (fig.6.7) and transmissivity were reversible, and after annealing the original state (figure 6.7, curve (a)) was restored. The reversibility was demonstrated several times. Since the results are similar over a broad range of wavelengths (568.2 - 488 nm) this indicated that the observed enhancement of the 231 cm^{-1} band does not result from a resonance effect.

The sharp Raman band at 231 cm^{-1} in the Raman spectra of As_2S_x glasses has been assigned to the vibrations of As-As bonds, as reported by Ewen (1), Nemanich et al. (2) and Kosek et al (5). In these papers the increase in the intensity of the Raman band at 231 cm^{-1} was correlated with an increase in the As-As bond density. Moreover, the Raman spectrum of amorphous arsenic has a broad band

between 170 and 310 cm^{-1}, the centre being at approximately 225 cm^{-1} (6, 7). Lucovsky and Knights (8) studied the infrared absorption spectra of amorphous As and found a strong absorption band centred at 230 cm^{-1} which they connected with the vibrations of As_4 pyramids.

6.2.1.2 Non-stoichiometric films

The Raman spectra of the As-rich films that were studied (of composition $As_{42.5}S_{57.5}$) are shown in figure 6.8 The as-evaporated film (curve A) exhibits many sharp features which are connected with the molecular structure of the film (2, 3). The Raman band with its maximum near 231 cm^{-1}, corresponding to As-As vibrations (1, 8), was relatively intense compared with the 231 cm^{-1} band in the stoichiometric As_2S_3 films, so that the density of As-As bonds in as-evaporated films was high. The spectrum of the annealed film (curve B) suggests that annealing produced polymerisation of the molecular species, as indicated by the disappearance of many of the sharp features in the Raman spectra. Only the Raman bands at 187, 222 and 231 cm^{-1}, which are associated with molecular features, remained after annealing.The intensity of the 231 cm^{-1} band was reduced after annealing, which indicates that the As-As bond density had decreased.

Illumination of the As-rich films by an Ar-ion laser

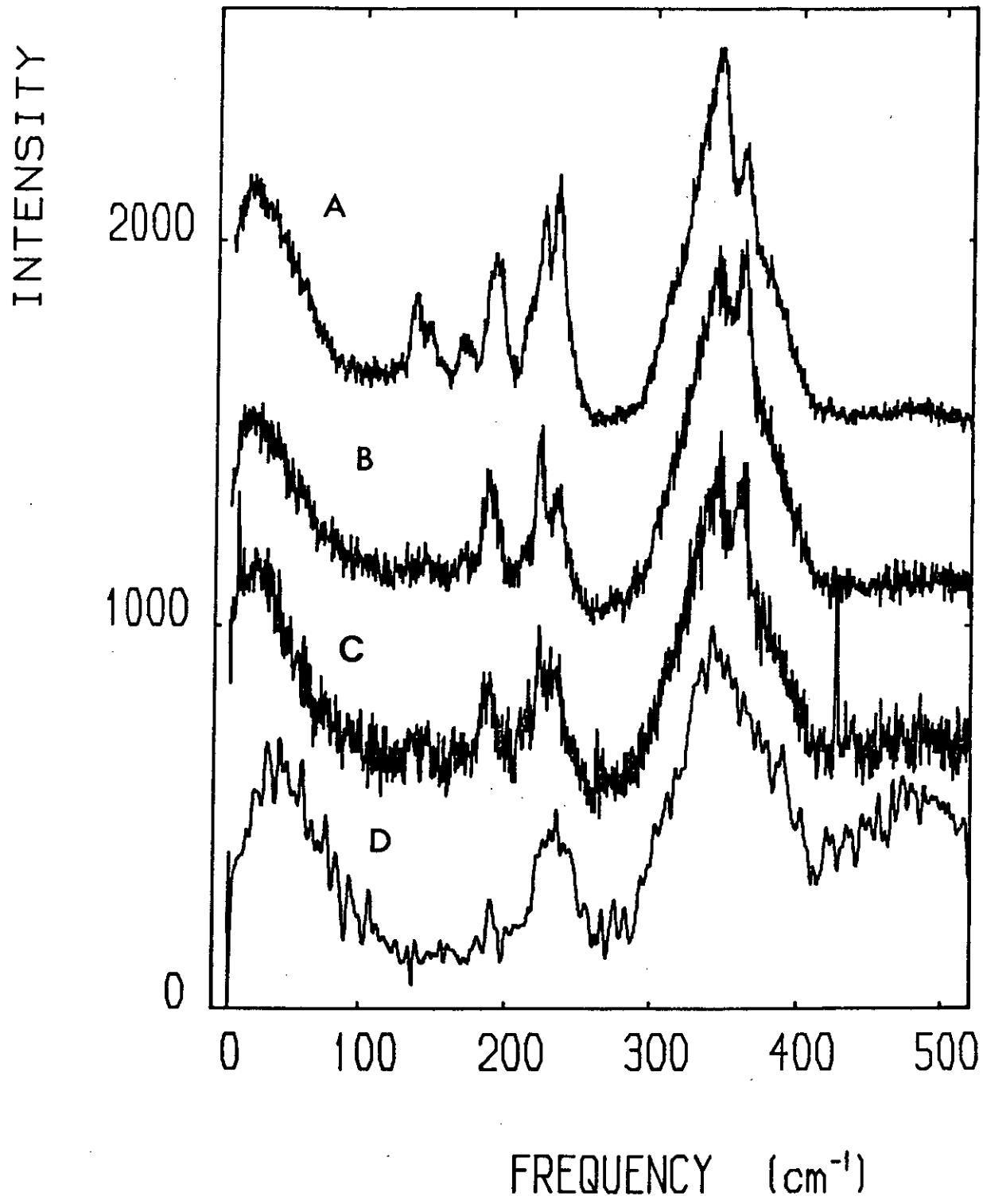

Figure 6.8 Raman spectra of As-S thin films of composition $As_{42.5}S_{47.5}$. Curve A - as-evaporated, B - annealed, C - after illumination (W lamp, 30 mins.) and D - further illumination (W lamp, 1 hour).

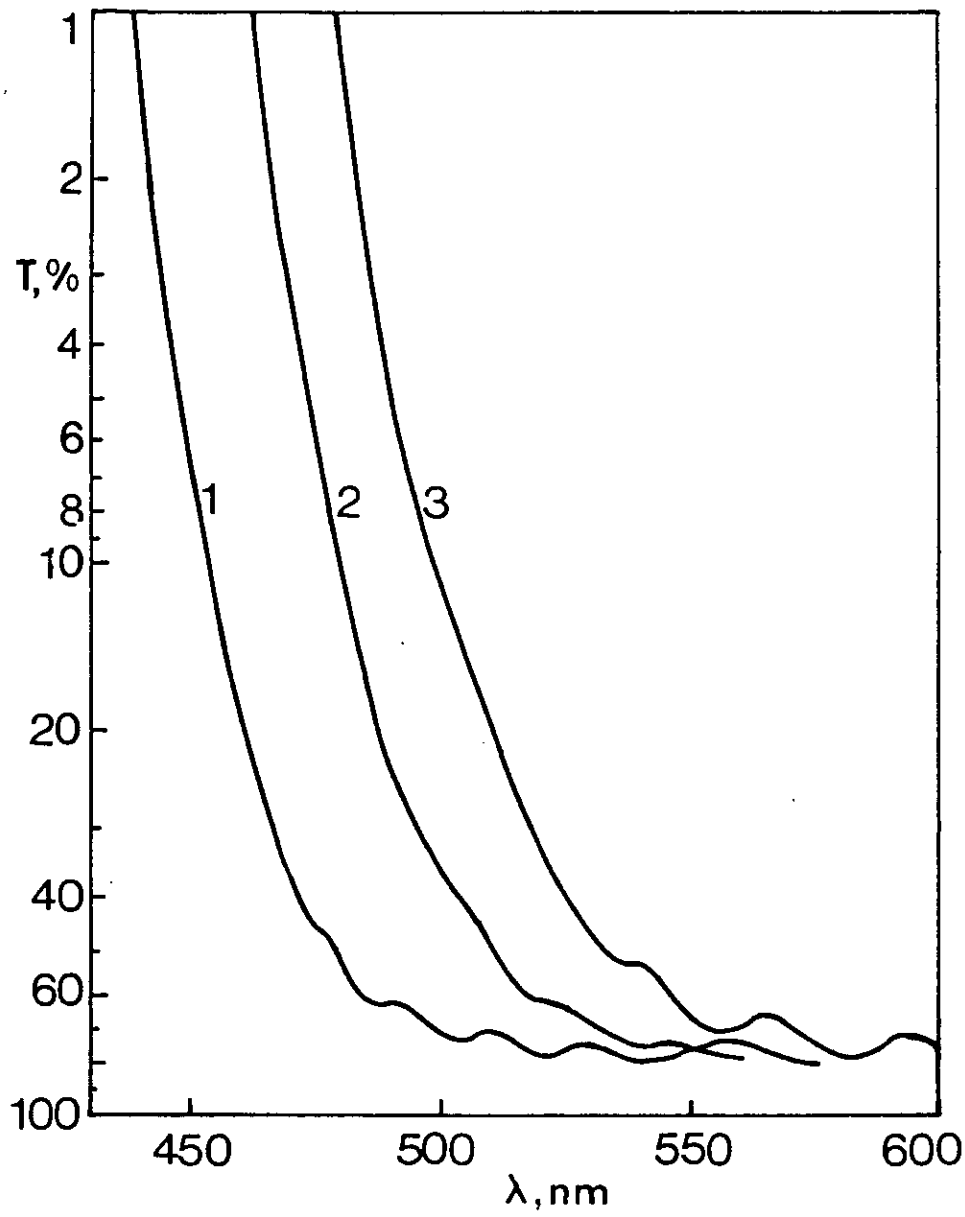

Figure 6.9 Optical transmissivity of As_xS_{1-x} films. Curve 1 - x=0.29, as-evaporated, curve 2 - x=0.425, annealed and curve 3 - x=0.425, after illumination (W lamp, 1 hour).

(λ = 514.5 nm) changed their transmissivity (figure 6.9). Spectra C and D of figure 6.8 show that it also enhanced the relative intensity of the 231 cm^{-1} band, compared with that for the annealed state of the film. After annealing the original values of the 231 cm^{-1} Raman band intensity and the optical transmissivity were fully restored so that , as with stoichiometric films, the photodarkening process was completely reversible and cycling between the photodarkened and annealed states was carried out many times.

Sulphur-rich films of composition $As_{30}S_{70}$, were also illuminated by intense laser light (λ =514.5 nm and power 60 mW/cm^2) for two hours. But no detectable optical change in transmissivity was observed (figure 6.9, curve 1). There was also no observable change in the Raman spectra of $As_{30}S_{70}$ films after illumination.

6.2.2 Discussion

From the results it is deduced that the enhanced 231 cm^{-1} band in the Raman spectra of As_2S_3 thin films is caused by an increase in the density of As-As bonds in photodarkened films. The band is not as broad as the band at 231 cm^{-1} found in amorphous As (6, 7) which may be a result of the more molecular nature and the weaker coupling of As-As atoms into the amorphous network in photodarkened films. Since it was found that the

intensity of the Raman band at 231 cm^{-1} is increased with photodarkening and decreased with annealing, this suggests that the reversible part of the photodarkening effect is associated with a redistribution of chemical bonds in As_2S_3 films which involves an increase in the density of As-As bonds under illumination.

In well-annealed films of As_2S_3, the hetero-type bonds of As-S are preferred, and the reversible structural change connected with photodarkening can be described by

$$2\ [As\text{-}S] \rightarrow [As\text{-}As] + [S\text{-}S] \qquad (6.1)$$

Equation (6.1) shows that the bond statistics of As_2S_3 films are shifted by strong illumination from a state which is close to the chemical ordered model towards a state described by the random network model. The randomness of the chemical bond distribution is therefore increased. In a chemical approach the photodarkening process can be described as a photolytic reaction,

$$As_2S_3 \underset{A(T),\ h\nu_2,\ I_2}{\overset{h\nu_1,\ I_1}{\rightleftharpoons}} As_2S_{3-x} + xS \qquad (6.2)$$

where I_i is the incident light intensity ($I_1 > I_2$), $h\nu_i$ is the incident light energy ($h\nu_2 > h\nu_1$; $h\nu_1$=Eg of the glass). A(T) indicates thermal annealing at a temperature T. Similar suggestions have already been made by several

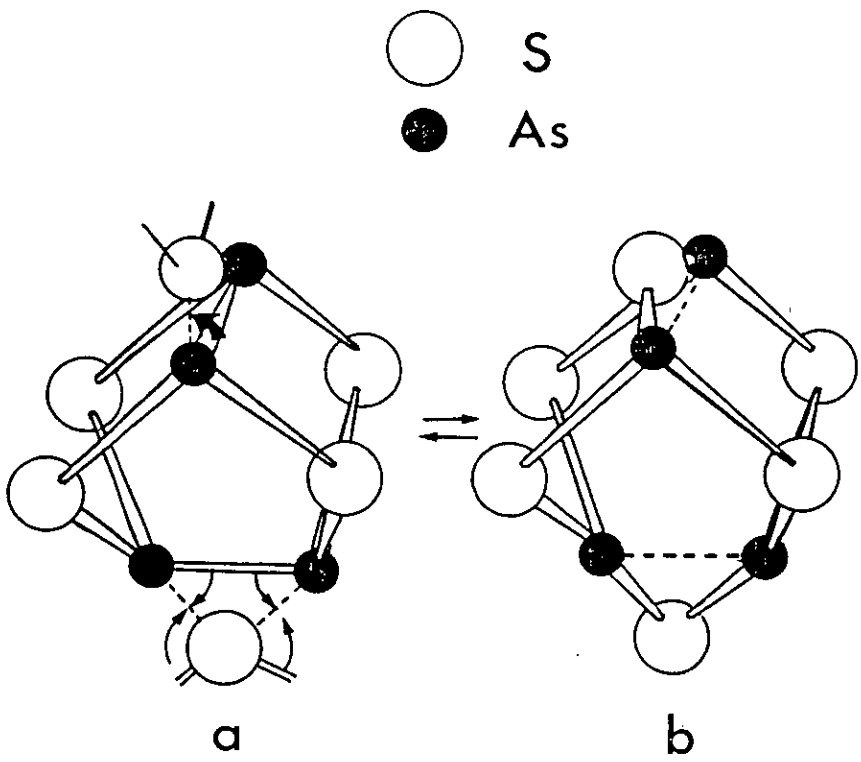

Figure 6.10 A simplified model illustrating the structural units in (a) photodarkened and (b) annealed As_2S_3 films. The formation of As_n clusters n>2 will be a further stage in the process.

authors, but mostly without the support of direct evidence.

The formation of homo-type bonds (As-As and S-S) from hetero-type bonds in As-S layers is possible without large structural rearrangement; a proposed mechanism is illustrated in figure 6.10. The final products of this reaction are probably As_n ($n > 2$) clusters. The formation of relatively stable homo-type bonds in compound chalcogenides (for example, As-As bonds in As_2S_3), which corresponds to a decrease in the formal valence state of "metallic" atoms, is possibly the factor which enables the formation of two metastable states in these compounds. Photo-structural effects have been found in chalcogenide systems containing As, Sb and Ge, and each of these elements can form lower-valence chalcogenides and relatively strong homo-type bonds.

The chemical reactions described by equations (6.1) and (6.2) are thermodynamically unfavourable (ΔG is positive). The As-As bonds or As clusters formed by photodarkening can be spontaneously "dissolved" and converted back to As-S bonds. The rate of this process is slower at low temperatures, and only in the vicinity of Tg, where the atoms are relatively mobile, can thermal bleaching "dissolve" all types of As_n clusters ($n > 2$) and completely reverse the photodarkening process. At lower temperatures, where only partial photobleaching

occurs, the smaller As_n clusters (n=2) represented by single As-As bonds can probably be dissolved, and larger As clusters - for example, As_4 pyramids- may be relatively stable and form the steady-state part of the photodarkening effect. As the formation of As clusters involves the absorption of several photons, the density of As-As bonds, which are directly related to changes in optical density, will be influenced by changing the intensity of the incident light or by the temperature of the layer (see figures 6.2 - 6.4)

The photodarkening effect is thus a dynamic process, and some photobleaching of films can be observed even at room temperature (see figures 6.3 and 6.4). The observed intensity of the 231 cm^{-1} Raman band is lower in samples measured several hours after photodarkening (figure 6.6) than in samples photodarkened to saturation by the exciting wavelength used to record the Raman spectra. The amorphous state contains many defects of local structure,and the energy of individual bonds has no sharp value. Thus, as we found, even illumination of As_2S_3 films with $h\nu < E_g$ can produce the photodarkening effect, but the change in transmissivity is lower than the change produced by bandgap illumimation. This result is also in accordance with the data obtained by Tanaka (9).

In crystalline As_4S_n (n=3, 4), and probably in the amorphous As-S systems, As-As bonds are longer than As-S

bonds (for example, in As_4S_4 As-As = 2.59 Å, and in As_4S_3 As-As=2.45 Å and As-S=2.21 Å (11). In this model the photodarkening is connected with the breaking of some As-As bonds. Instead of shorter As-S bonds, longer As-As bonds are formed. The reported increase in the thickness of As_2S_3 layers after illumination (11, 12) which was confirmed in this work, can be accounted for if it is assumed that a small fraction of the As-S bonds contribute to the change in thickness. Only changes in bond length perpendicular to the substrate plane contribute to the thickness change ΔX;

$$\Delta X = \Delta b \sin \psi \qquad (6.3)$$

where the change in bond length per bond, Δb, is given by

$$\Delta b = (b_{As-As} + b_{S-S}) - b_{As-S} \qquad (6.4)$$

and ψ is the angle between a given bond direction and the substrate plane. Thus, the mean value of ΔX is

$$\overline{\Delta X} = (\Delta b/\pi) \int_0^{\pi} \sin\psi \, d\psi = 2\Delta b/\pi \qquad (6.5)$$

A similar expression can be obtained for the average thickness Xo of the original As-S bonds;

$$\overline{Xo} = 2b_{As-S}/\pi$$

and hence

$$\overline{\Delta X}/Xo = \Delta b/b_{As-S} \qquad (6.6)$$

For the bond lengths quoted above, and with b_{S-S} = 2.2 Å, these equations give $\overline{\Delta X}/Xo$ = 0.068.

According to Hamaka et al. (12), the relative change in thickness determined experimentally is 0.004, and hence the fraction of As-S bonds involved in the photostructural change is 0.004/0.068 = 0.059, approximately 6% of the total.

In S-rich films As atoms are at a greater mean distance from each other since they are separated by $[S-S]_n$ bonds. Consequently the probability that two or more As atoms will be in adjacent positions is lower, and therefore the photodarkening sensitivity is considerably reduced. This is in accordance with the result that photodarkening was not observed in films with the composition $As_{29}S_{71}$. In contrast, As-As bonds are always present in As-rich films, even in well-annealed samples and the probability that As atoms will be in neighbouring positions increases with As content. This can explain the increased photodarkening sensitivity of As-rich films.

6.3 Bulk As-S samples

6.3.1 Results

6.3.1.1 Stoichiometric glasses

The Raman spectra of thin bulk As_2S_3 glasses are shown in figure 6.11. There were no observable differences in the Raman spectrum after illumination at room temperature (spectrum a) and also no change in the optical transmissivity during Ar-ion laser illumination. However, photodarkening was observed at low temperature. Curve b is the Raman spectrum obtained at 36 K and shows an enhancement of the 231 cm^{-1} band. The photodarkening was produced during the recording of the Raman spectra and increasing the incident laser power further enhanced the 231 cm^{-1} band (curve c).

It was found that when the bulk samples were ground to a fine powder the photodarkening effect was considerably more pronounced. In fact photodarkening was observed at room temperature when the samples were powders. Curve d (figure 6.11) shows the Raman spectra of a powder in which photodarkening was produced by the exciting wavelength (λ =530.9 nm). The enhancement of the 231 cm^{-1} Raman band can be seen to be larger compared with the spectra of the thin bulk samples shown in figure 6.11.

Figure 6.11 Raman spectra of bulk As_2S_3 samples. Curves (a), (b) and (c) are for thin bulk samples and curves (d) and (e) are for powdered samples. Curves (a), (b) and (c) were recorded using the exciting wavelength of 568.2 nm, (a) being recorded at 300 K, (b) and (c) at 36 K. Spectra (d) and (e) were recorded at 300 K using the exciting wavelength of 530.9 nm. Incident laser power was 10 mW for all spectra except curve (c) which was 50 mW.

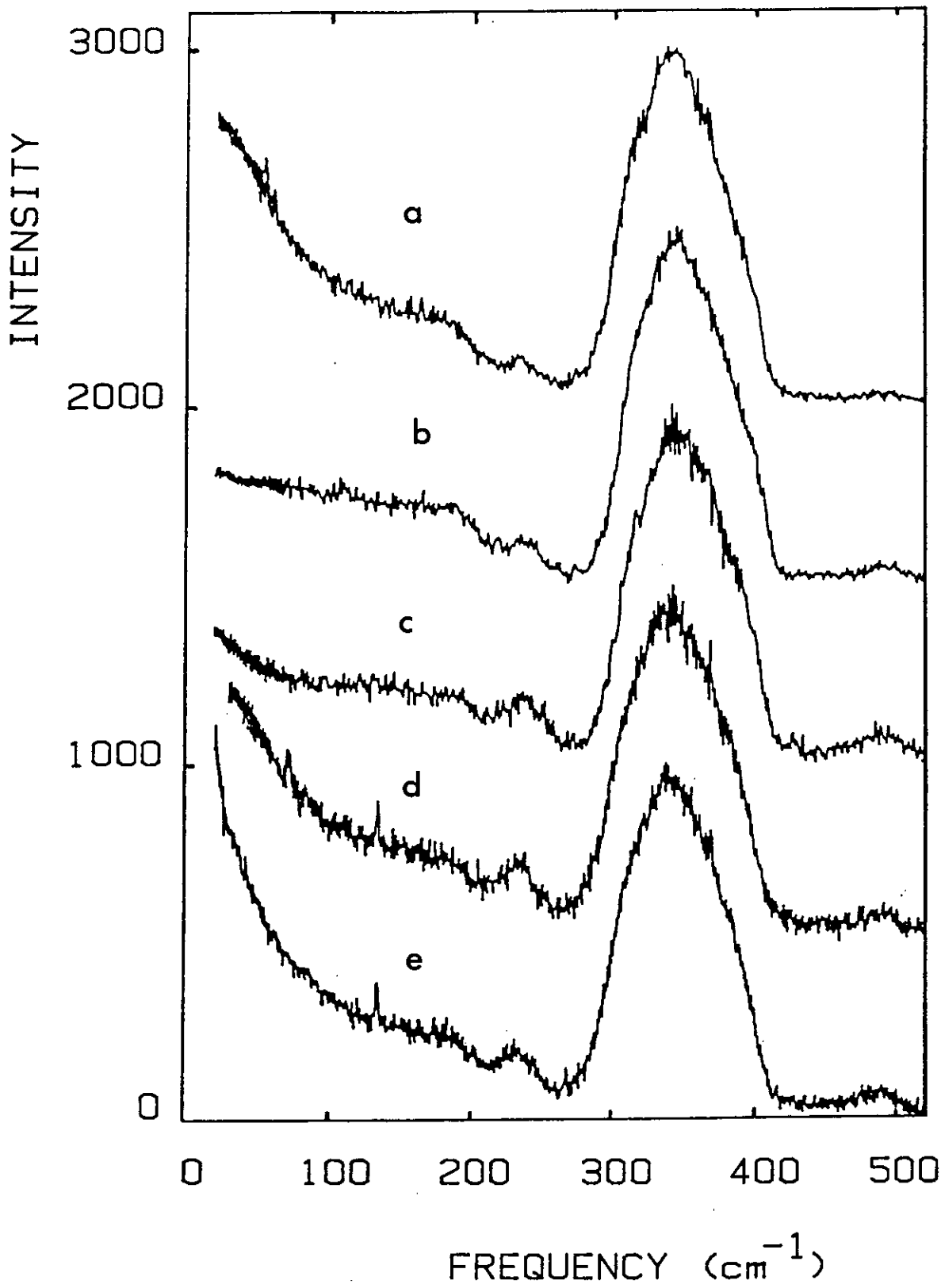
3000
2000
1000
0
INTENSITY
a
b
c
d
e
0
100
200
300
400
500
FREQUENCY (cm^{-1})

Figure 6.12 also illustrates the photodarkening produced in glassy powders. Curve a is the spectrum of an undarkened sample recorded at room temperature and is clearly similar to the spectrum of a thin bulk sample (curve a, figure 6.11). Illumination at low temperatures produced a large photodarkening effect. This is shown by the curves b and c (figure 6.12) where the samples were photodarkened by the exciting lines 568.2 and 530.9 nm respectively. It is clear from these last two curves that both the 231 cm^{-1} and 490 cm^{-1} Raman bands are enhanced after the samples were photodarkened.

The diffuse reflectivity spectra were also measured for powdered As_2S_3 samples. The results are shown in figure 6.13. A shift towards longer wavelengths was found (curve a -> curve b) after photodarkening. These results are similar to the shift in absorption edge to longer wavelengths observed in thin film samples.

6.3.1.2 Non-stoichiometric samples

Arsenic-rich samples of composition $As_{42.5}S_{57.5}$ exhibited a higher photodarkening sensitivity than the stoichiometric composition and both the thin bulk and powdered samples could be photodarkened at room temperature. The Raman spectra of the As-rich samples are shown in figure 6.14. Curve a is the spectrum of an

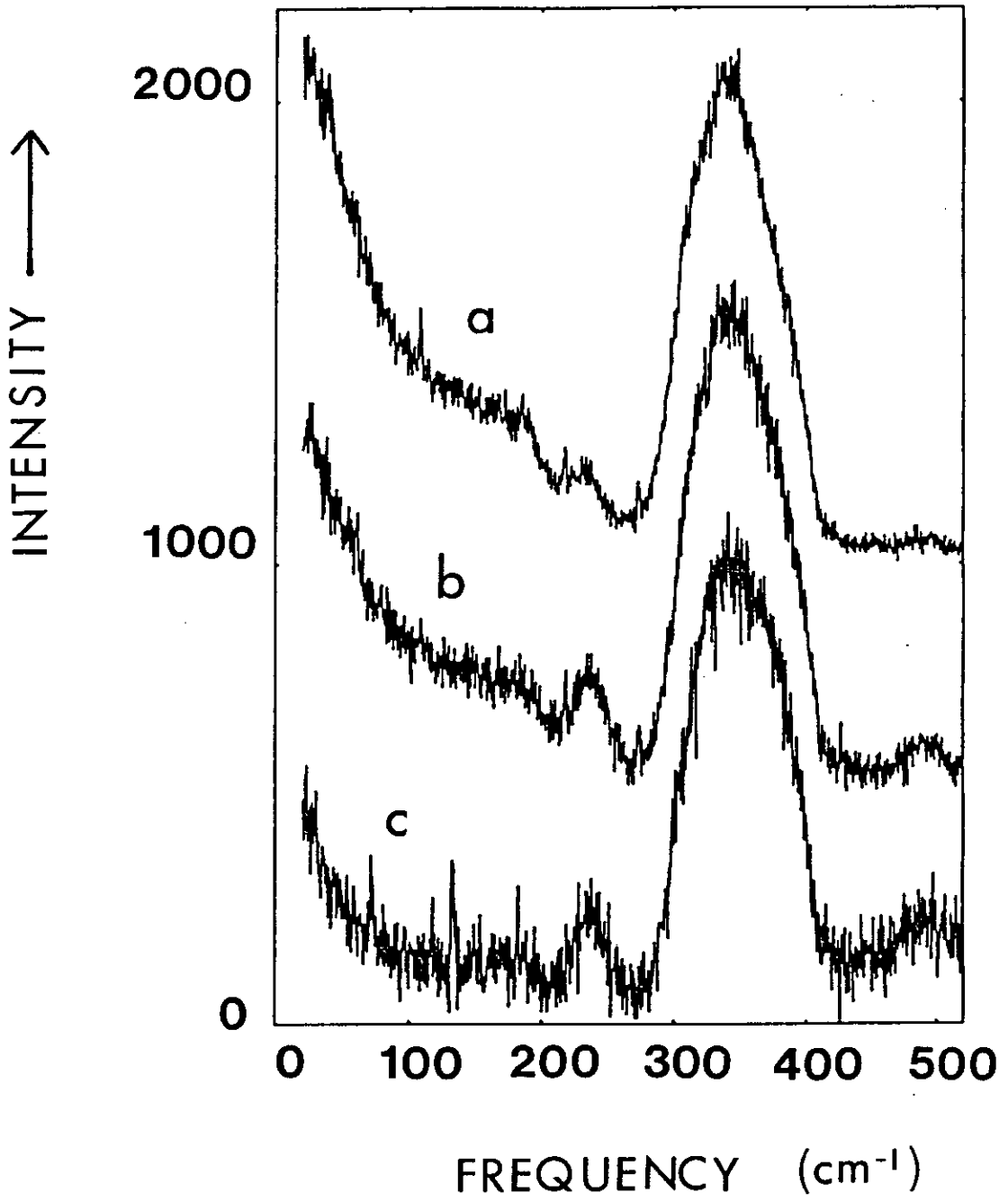

Figure 6.12 Raman spectra of glassy As_2S_3 powders:

(a) T=300 K, exciting line 568.2 nm.

(b) T=75 K, exciting line 568.2 nm.

(c) T=75 K, exciting line 530.9 nm.

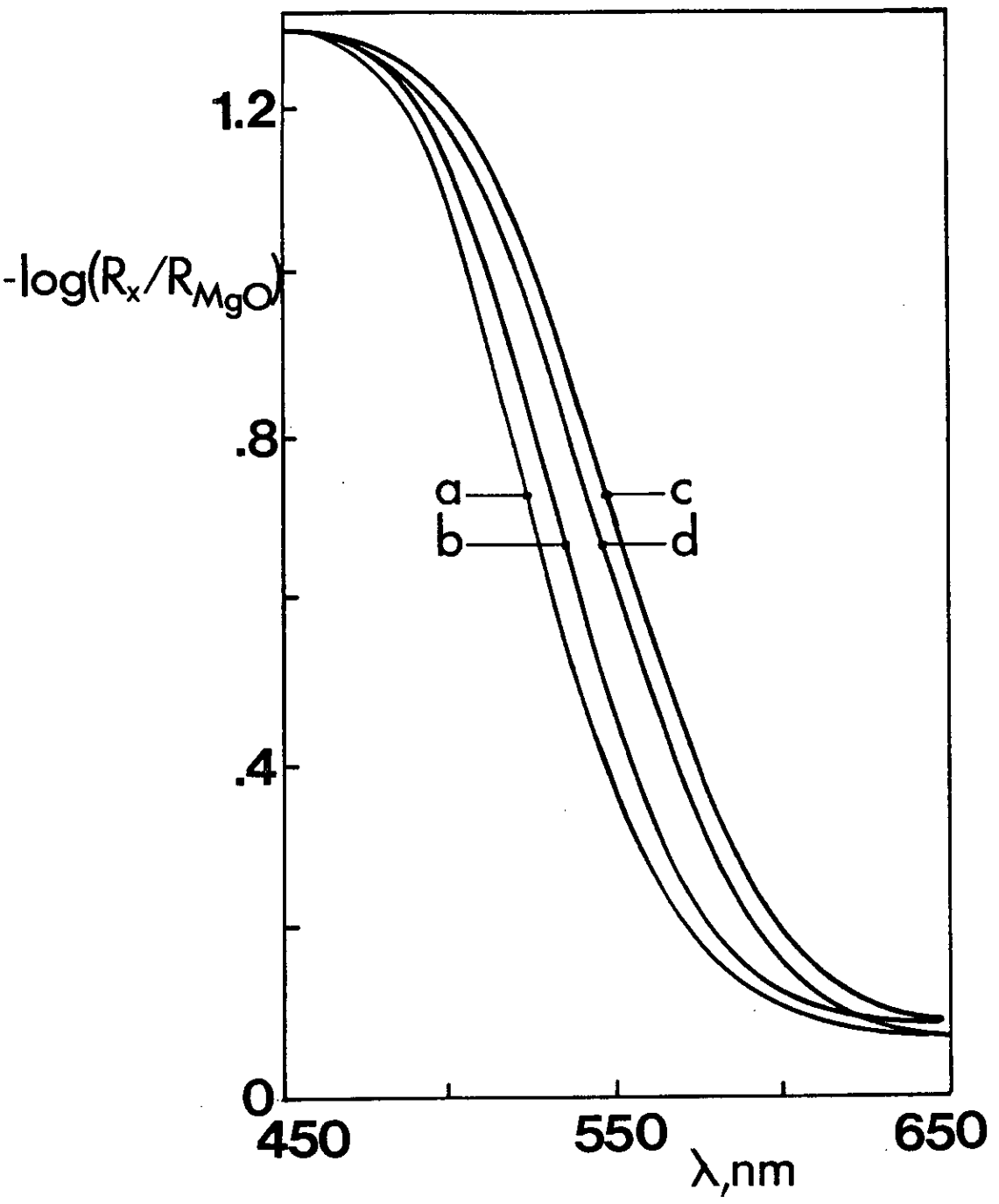

Figure 6.13 Diffuse reflectivity of glassy As-S powders: Curves (a) and (b) are the unexposed and exposed state respectively for As_2S_3, and curves (c) and (d) are the respective unexposed and exposed state for the composition $As_{42.5}S_{57.5}$.

Figure 6.14 Raman spectra of thin bulk As-S samples of composition $As_{42.5}S_{57.5}$. All curves are for thin bulk samples except curve (g) which is for a powdered sample. Curves (a), (b) and (c) were recorded at 300 K, curve (a) being the undarkened state (exciting wavelength, 647.1 nm) and curves (b) and (c) were recorded using the wavelengths 568.2 and 514.5 nm repectively. Curves (d), (e), (f) and (g) were recorded at 36 K using the exciting wavelength 568.2 nm, and the incident power for the respective curves was 30, 50, 80, and 10 mW.

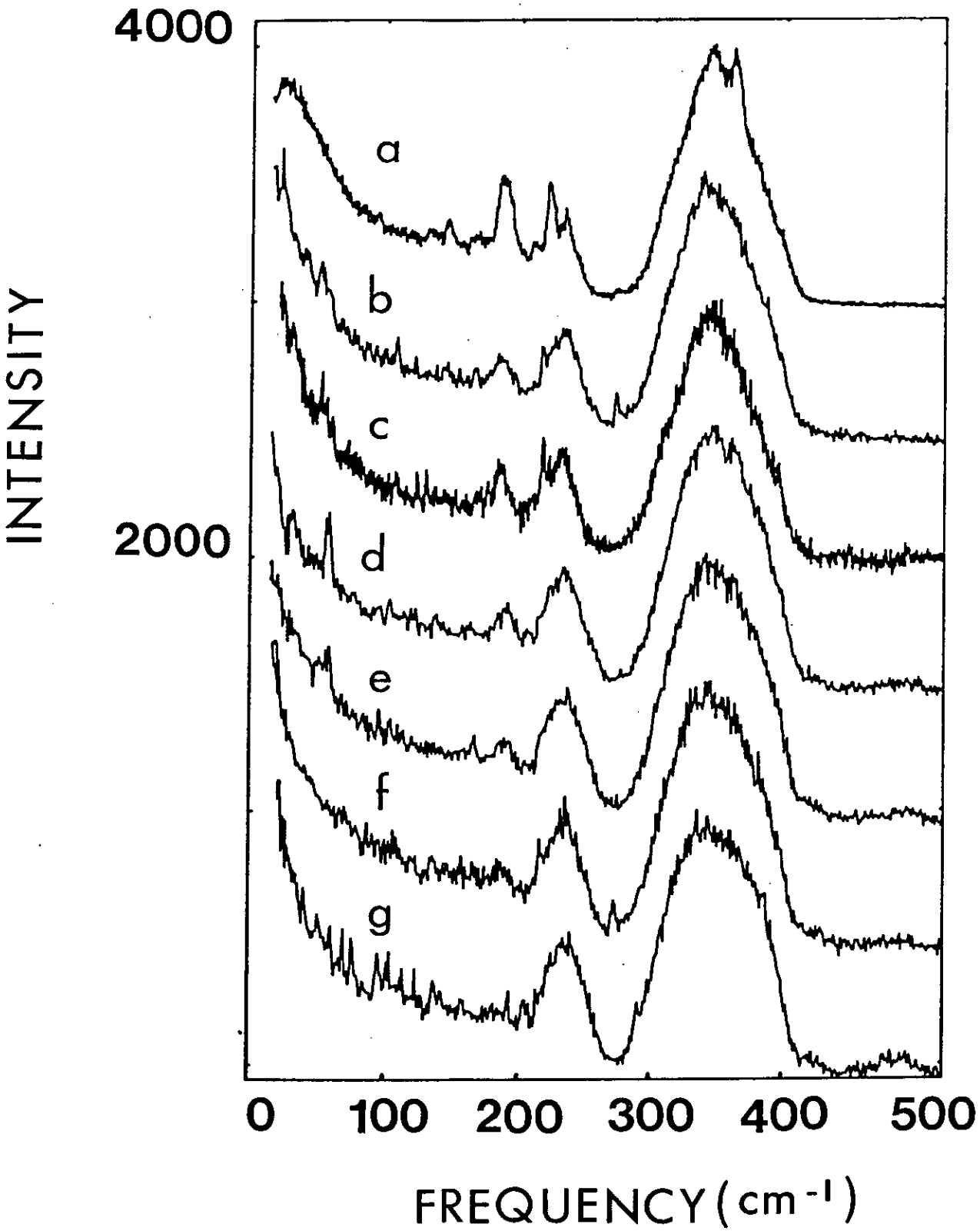
4000
2000
INTENSITY
a
b
c
d
e
f
g
0
100
200
300
400
500
FREQUENCY (cm⁻¹)

undarkened bulk sample recorded at room temperature. The sharp bands in the spectra are due to As_4S_4 molecular vibrations (2). Curves b and c show the effects of illumination at room temperature. A broad band at 231 cm^{-1} is formed whilst the sharp feature at 187 cm^{-1} is depressed. At low temperatures the enhancement of the 231 cm^{-1} band is greater and the 187 cm^{-1} band is further depressed (curves d, e, f and g).

Curves d, e and f are the Raman spectra of thin film samples recorded at 36 K and show how the 231 cm^{-1} band is further enhanced by increasing the power of the exciting line. Curve g is the Raman spectrum of a powdered As-rich sample. It again shows that powdered samples are more sensitive to photodarkening than bulk samples. It also exhibits an enhancement of the spectral region around 490 cm^{-1}.

The diffuse reflectivity of powdered As-rich samples is shown in figure 6.13. The spectral curve shifts to longer wavelengths (curve d -> c) after photodarkening.

It should be noted that the photodarkening effects that were observed in the As-rich thin bulk and powdered samples were completely reversible. The original undarkened state was obtained by annealing at the glass transformation temperature.

6.3.2 Discussion

The experiments have shown that reversible photodarkening in thin bulk and powdered As-S glasses is comparable to that observed in thin amorphous films. The extent of photodarkening increases with the As content of the glass and also, for samples of a fixed composition, the sensitivity of powdered samples is higher.

At low temperatures the photodarkening in both types of samples is more pronounced. Also, as well as the 231 cm^{-1} Raman band being enhanced, there is an indication that the Raman band at 490 cm^{-1}, associated with S-S bonds, is also enhanced as a result of photodarkening.

It was proposed in section 6.2.2 that reversible photodarkening in thin films can be explained in terms of the re-distribution of chemical bonds, and described by equation (6.2). These ideas will now be applied to the interpretation of photodarkening in bulk glasses. The Raman data clearly shows an enhancement of As-As bond vibrations in photodarkened samples. However the way in which the As-As bonds are incorporated into the amorphous network is not clear. It is possible that As_4S_4 structural units are formed or alternatively As atoms may form As_n clusters ($n > 3$). The formation of As_4S_4 units seem unlikely since other features in the Raman spectra corresponding to As_4S_4 molecular vibrations are lowered

during photodarkening. Furthermore, As_4S_4 crystals (realger) are unstable when exposed to light and would not be a product after intense illumination.

The formation of As_n clusters appears to be more probable since the band at 231 cm^{-1}, which is enhanced in photodarkened samples, is similar to the Raman band found in amorphous As. The Raman band in the photodarkened samples is sharper than the band in a-As but this is probably because the As-As bonds that form clusters are of a molecular nature. The As_n clusters are not phase separated as we judge from the following points:-

(a) The Raman bands are sharp.

(b) The change of photodarkening under different illumination conditions is relatively fast and reproducible.

(c) A mixture of powdered amorphous As (2-5wt.%) and a-As_7S_3 powder is a brown-yellow colour whereas photodarkened a-As_2S_3 powder is a deep red.

(d) The Raman scattering intensity of a-As is low and phase-separated As would not cause such a large change in the 231 cm^{-1} band as is found experimentally in photodarkened samples.

Since As-As bonds are longer than As-S bonds (10) they are probably more easily formed near voids or other types of defects involving free volume within the amorphous network. This could explain the higher photodarkening sensitivity of bulk samples of the same composition since during the grinding of the powders many defects will be formed inside the glassy particles. This would make the formation of As-As bonds in thin bulk samples much more unlikely since there would be a large internal tension opposing the increase in volume which must occur when longer As-As bonds are formed. In terms of equation (6.2) an increase in pressure shifts the equilibrium position back towards the left hand side and the photodarkened centres are immediately redissolved. The mechanism just described may be similar to the effect of applying external pressure during the photodarkening of samples. Kolobov et al (13) found that the compression of thin films of As_2Se_3 lowered their photodarkening sensitivity. And as As_2Se_3 is chemically and structurally close to As_2S_3, a similar effect would probably occur in the As-S system. At room temperature the rate of thermal annealing is relatively high, and since there are small numbers of voids and defects in bulk glasses, the photodarkening effect will be negligible in bulk samples at room temperature. At low temperatures thermal annealing is very much reduced and a larger number of stable As_n clusters coupled to the amorphous network will be formed. This would explain why

photodarkening in bulk samples is only observed at low temperatures.

6.4 References

1. Ewen, P. J. S., Ph. D. Thesis, Edinburgh University, (1978).
2. Nemanich, R. J., Connell, A. N., Hayes, T. M. and Street, R. A., Phys. Rev. B, 18, 6900, (1978).
3. Solin, S. A. and Papatheodorou, G. N., Phys. Rev. B, 15, 2084, (1977).
4. Bertoluzza, A., Fagnano, C. and Monti, P., "Molecular Spectroscopy of Dense Phases", edited by M. Grosman et al (New York: Elsevier), p. 405, (1979).
5. Koseck, F., Cimpl, Z., Matyas, M. and Pisarcik, M., Czech. J. Phys. B, 32, 719, (1982).
6. Lannin, J. S., Phys. Rev. B, 15, 3836, (1977).
7. Davies, E. A., J. Phys., Paris Colloq., 42, 855, (1981).
8. Lucovsky, G. and Knights, J. S., Phys. Rev. B, 10, 4324, (1974).
9. Tanaka, K., Solid State Commun., 34, 201, (1980).

10. Porter, E. J. and Sheldrick, G. M., J. Chem. Soc., Dalton Trans., p. 1347, (1972).

11. Tanaka, k., "Structure and Excitation of Amorphous Solids", edited by G. Lucovsky and F. L. Galeener, A. I. P. Conf. Proc. No. 31 (New York: American Institute of Physics), p. 148, (1976).

12. Hamaka, H., Tanaka, K. and Iizima, S., Solid State Commun., 23, 63, (1977).

13. Kolobov, A. V., Lyubin, V. M. and Taguyrdzhanov, M. A., Solid State Commun., 41, 453, (1982).

CHAPTER 7

PHOTODISSOLUTION - COMPOSITIONAL AND STRUCTURAL ASPECTS

7.1 Introduction

During the photodissolution process an As-S film goes from an initial state via a complex reaction mechanism to a final photodoped state. The first part of this chapter describes a Raman investigation into the structure of As-S films before and after the photodissolution process. The second part of the chapter describes the effects of the photodissolution of Ag on the optical properties of As-S films.

7.2 Structural properties of Ag photodoped As-S films - a Raman study

7.2.1 Results

In figure 7.1, curves A and B are the spectra of As-S films of composition $As_{41}S_{59}$ and $As_{38}S_{62}$, respectively. The sharp features of these spectra are attributed to molecular units of As_4S_4, and the features at 491 cm^{-1} to the symmetric stretching mode of S-S bonds (1). Spectra C and D in figure 7.1 are of the Ag photodoped films corresponding again to the original compositions $As_{41}S_{59}$ and $As_{38}S_{62}$ respectively (ie. as in curves A and B).

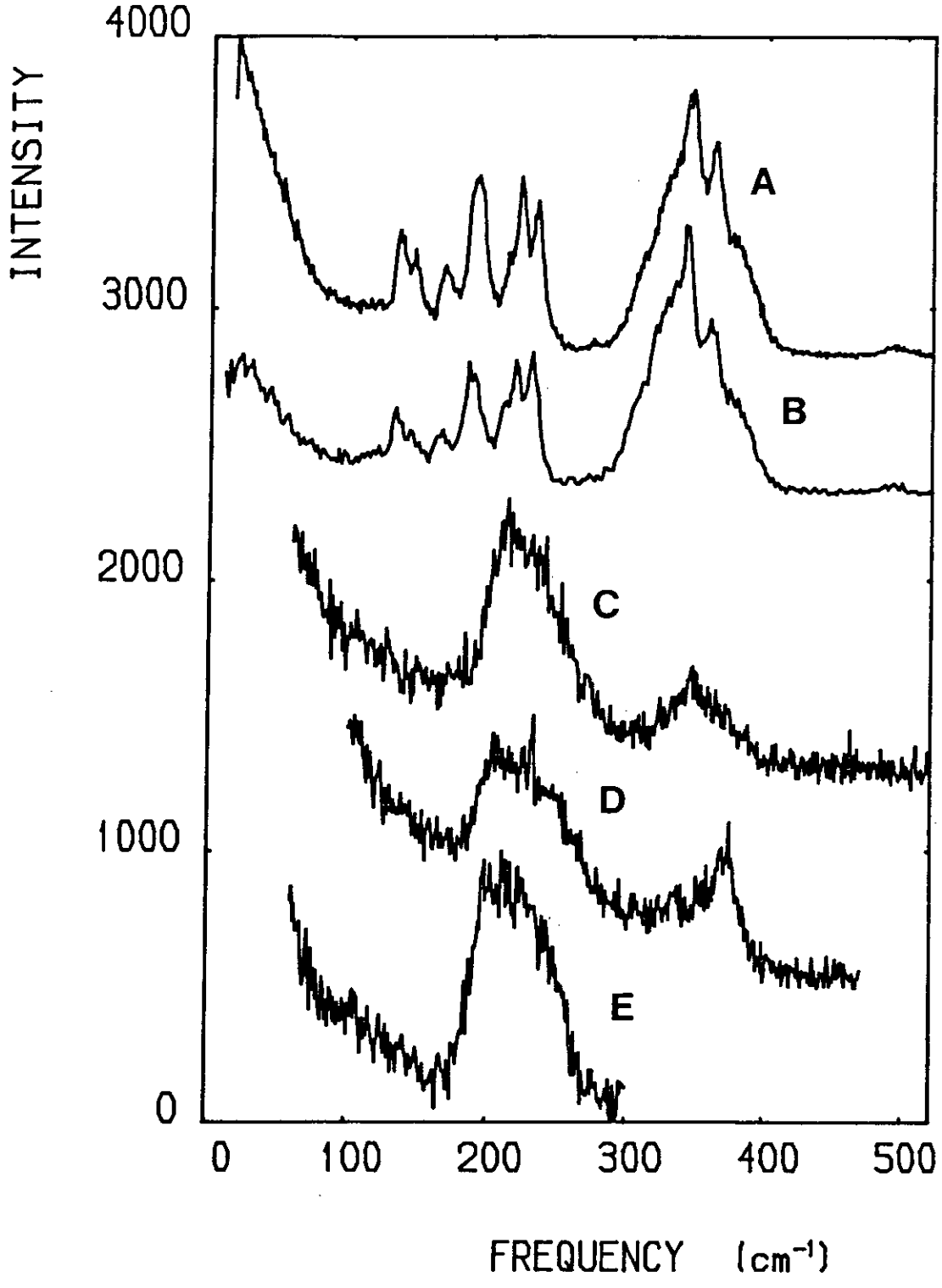

Figure 7.1 Raman spectra of films of composition $As_{41}S_{59}$ (curve A) and $As_{38}S_{62}$ (curve B). Curves C and D are the spectra for Ag photodoped $As_{41}S_{59}$ and $As_{38}S_{62}$ respectively. Curve E is the Raman spectrum of amorphous As.

These two spectra are similar, each having two broad Raman bands in the regions 150-300 cm^{-1} and 300-400 cm^{-1}. Curve E in figure 7.1 is the Raman spectrum of amorphous As and this closely matches the band in the 150-300 cm^{-1} region in spectra C and D. The other band, in the region 300-400 cm^{-1} in curves C and D, is probably due to amorphous Ag-As-S phases, as it is known that bulk glasses in the Ag-As-S system have strong Raman bands in this spectral region,(2).

Curve A in figure 7.2 is the Raman spectrum for a film of composition $As_{30}S_{70}$, which agrees well with that of a bulk glass of the same composition (3). The features in the region 425-525 cm^{-1} are attributed to S in S_8 rings and S-S bonds in linear As-S_n-As linkages. Curve B is the Raman spectra of the Ag photodoped material. It has a broad spectrum and comparison with the spectrum of a bulk glass of composition $Ag_{30}As_{22}S_{48}$, shown in curve C, suggests that the photodoped film has the same structure. In figure 7.3, curve A is the Raman spectrum of a film of composition $As_{20}S_{80}$, and again this is very similar to the spectrum of a bulk glass of the same composition (3). The sharp features are due to the vibrations of distorted S_8 rings. The Raman spectrum of the Ag photodoped film (curve B) has a very broad band in the region 100-300 cm^{-1} and a relatively sharp feature at 350-400 cm^{-1}. The other spectrum (curve C) was obtained from a film of Ag_2S formed by reacting S vapour with a Ag film which was

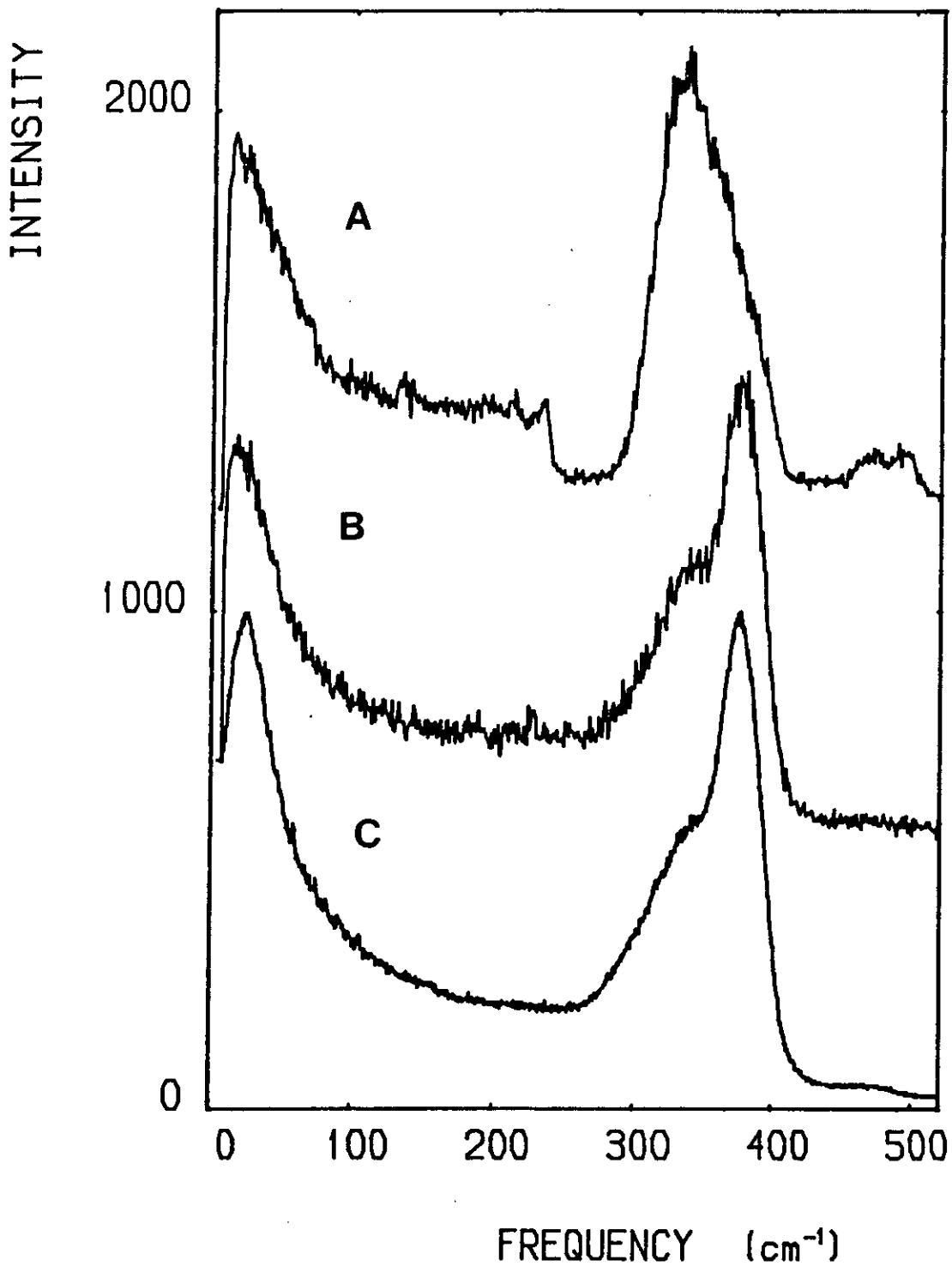

Figure 7.2 Raman spectra of films of composition $As_{30}S_{70}$ (curve A). Curve B is the spectrum of Ag photodoped $As_{30}S_{70}$. Curve C is the spectrum of a bulk Ag-As-S glass of composition $Ag_{30}As_{22}S_{48}$.

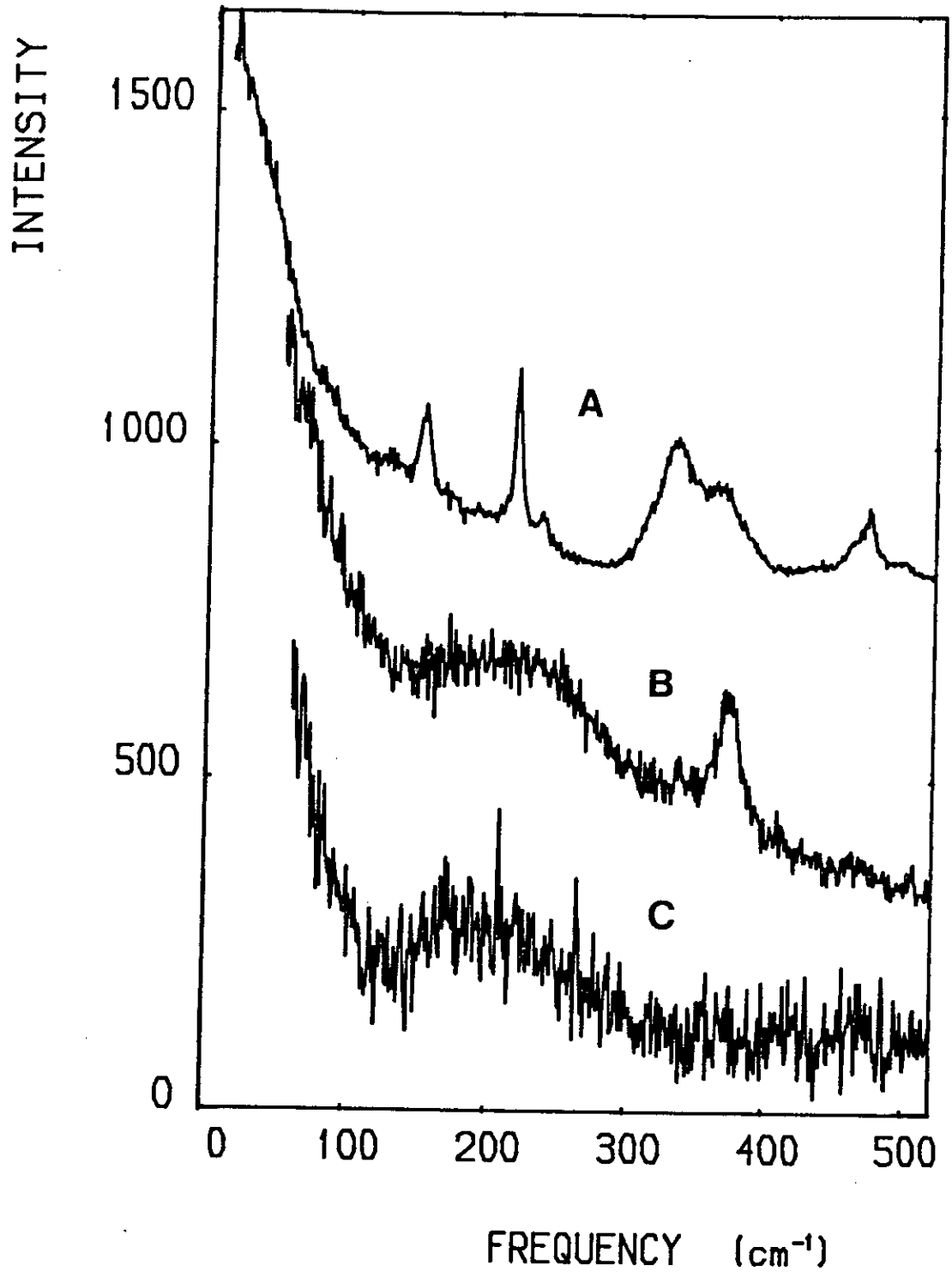

Figure 7.3 Raman spectra of films of composition $As_{20}S_{80}$ (curve A). Curve B is the spectrum of Ag photodoped $As_{20}S_{80}$. Curve C is the spectrum of a Ag_2S film formed by reacting S vapour with a Ag film.

about 0.5 μm thick. A comparison of spectra B and C suggests that Ag_2S is present in the photodoped As-S film, which was originally $As_{20}S_{80}$. The band between 350-400 cm^{-1} , formed during the course of the experiment, probably arises from the formation of a Ag-As-S glassy phase.

7.2.2 Discussion

Figure 7.4 illustrates the phase diagram for the Ag-As-S system and it shows the principal crystalline compounds as well as the glass-forming regions determined by Kawamoto et al (4). Also drawn on the diagram are tie-lines joining elemental Ag with four As-S compositions studied in this work. (N.B. The composition $As_{41}S_{59}$ is taken to be approximately As_2S_3). As the photodoping proceeds the resulting overall composition must move along these tie-lines. Of those four lines, only the one joining the Ag with $As_{30}S_{70}$ intersects the central glass-forming region. This is in accord with Raman results which show that Ag photodoped $As_{30}S_{70}$ has a structure very similar to that of bulk glass within the central region of glass formation and close, in composition, to the Ag-$As_{30}S_{70}$ tie-line (2) . It is possible therefore that in this case the Ag photodoped film remains a homogeneous, uniform phase.

The tie-lines joining Ag with $As_{41}S_{59}$ (As_2S_3) and

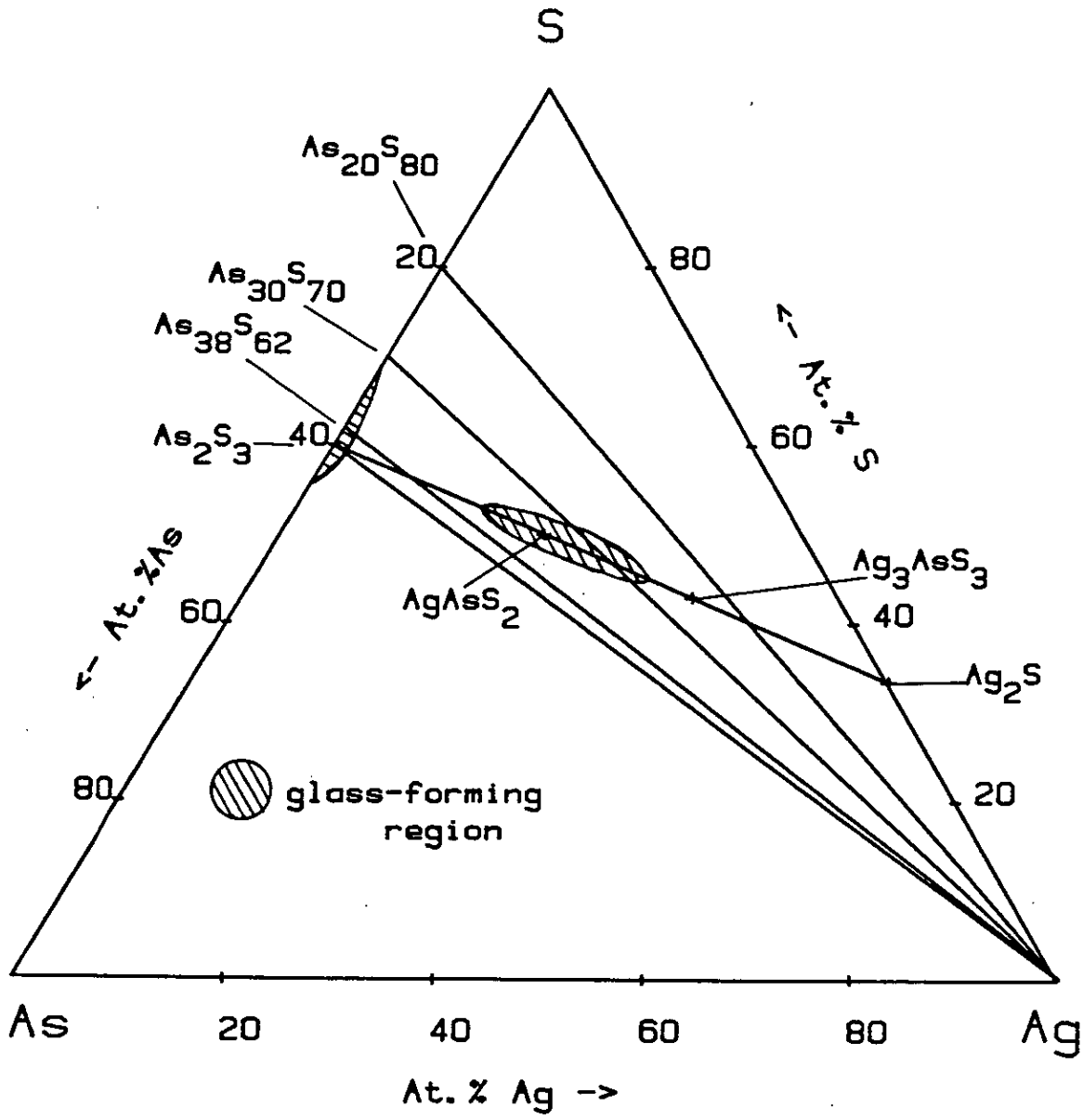

Figure 7.4 Compositional diagram of the Ag-As-S system showing the compositions of the films investigated by Raman spectroscopy. Also shown are some of the known ternary compounds.

$As_{38}S_{62}$ are on the As-rich side of the central glass-forming region but they do not intersect it. The Raman results indicate that amorphous As and an Ag-As-S phase, corresponding in structure to a composition within the glass-forming region, are present in the photodoped material. This implies that when the overall photodoped composition lies outside the glass-forming region, the photodoping also involves a process of phase separation. The evidence is that the Ag-As-S component which is formed is within the glass-forming region and that excess As is precipitated, probably in an amorphous form.

For the system Ag-$As_{20}S_{80}$ the tie-line also does not intersect the central glass-forming region. In this case, the Raman results suggest that initially, Ag_2S is formed (although it is by no means certain that it is stoichiometric Ag_2S), and only after prolonged exposure is there a further photoinduced effect towards the formation of a glassy Ag-As-S phase.

It is premature to extrapolate the latter observation (ie. Ag_2S formation) to the whole system but in general the results of this work do suggest that the photodoping process is a two-stage solid-state reaction. The initial reaction may be between Ag and S in As-S films and it should be noted here that even in stoichiometric glassy As_2S_3, S-S bonds are present (3). It is imagined that these homopolar S-S bonds are involved in the initial

reaction. The second reaction is between Ag_2S and the remaining As-S matrix. This reaction will proceed only if the reaction products are more stable than the reactants. It is likely that this will be so if the reaction products are within, or close to, the central glass-forming region. The structure of Ag-As-S glasses is based on AsS_3 pyramids joined by S-As-S linkages (4), (2), so that very little structural rearrangement is required in the second reaction.

7.3 The optical properties of As-S films before and after the photodissolution of Ag

7.3.1 As-S films

The optical transmissivity curve of a thin $As_{32}S_{68}$ film of thickness 712 nm is shown in figure 7.5. It can be seen that large interference effects occur in the part of the curve where optical absorption is small. As the optical absorption increases towards shorter wavelengths the transmission curve falls steeply towards zero.

A method, outlined by Goldschmidt (5), was used to obtain the optical absorption coefficient and refractive index as a function of wavelength from the transmission data. The method involves optically modelling a thin absorbing film on a thick transparent substrate.

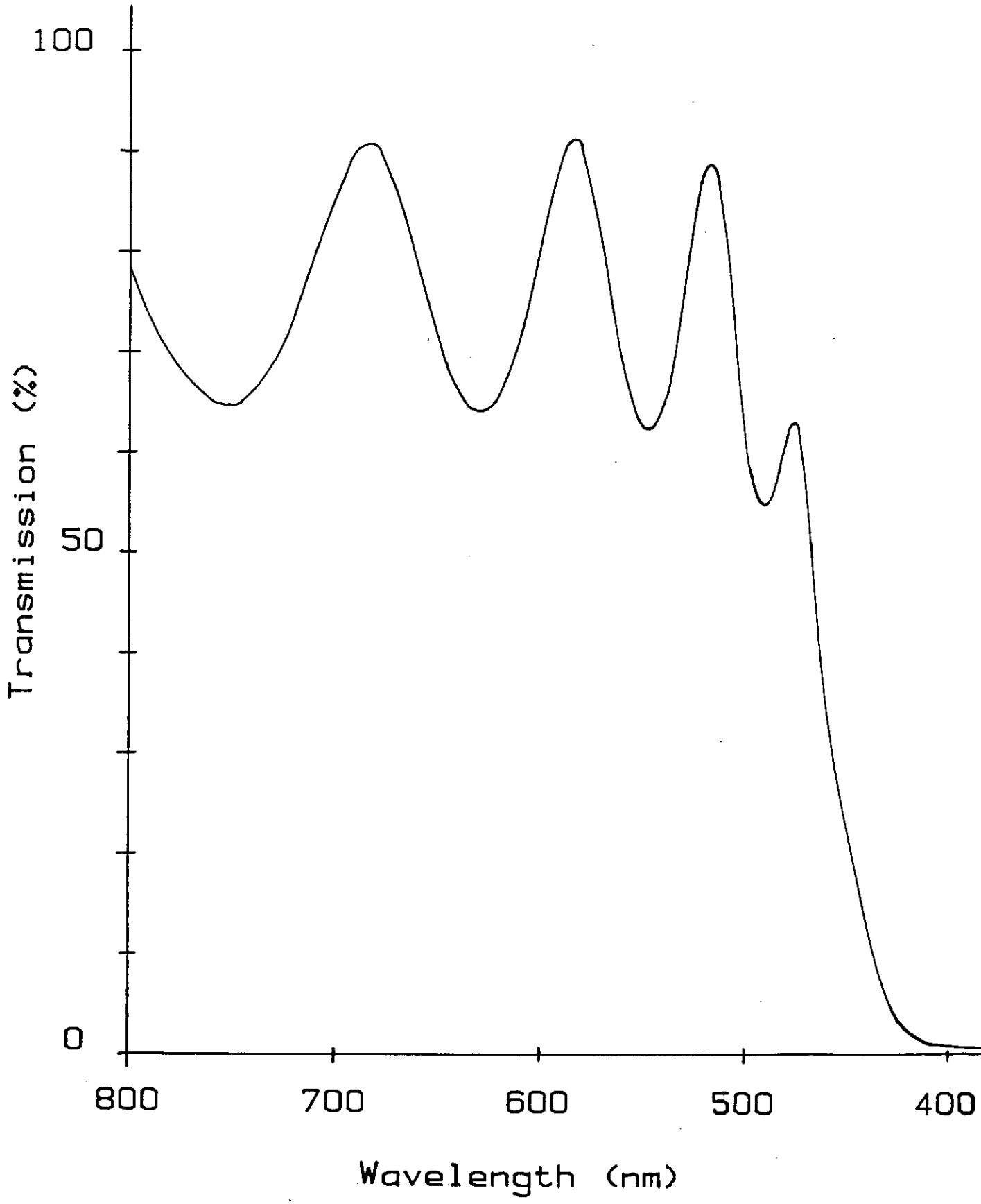

Figure 7.5 Transmissivity curve of a film of composition $As_{32}S_{68}$ and of thickness 712 nm.

The equation for the transmission, T, of light through a thin absorbing film on a transparent substrate is given by Goldschmidt as;

$$T = \frac{A}{(B-C+D)} \qquad (7.1)$$

where $A = (1-R01)(1-R12)(1-R20)e^{-\alpha d}$, $B=(1-R12.R20)$,

$C = 2(R01.R20)(1-R20)e^{-\alpha d}.COS(2Kd)$, and

$D = R01(R12-R20)e^{-2\alpha d}$

The parameters are defined as follows. Air is considered as medium 0, the film as medium 1 and the glass substrate as medium 2. The interfacial reflection coefficients between the mediums 0 and 1, 1 and 2, and between 2 and 0 are R01, R12 and R20 respectively. These are found in the usual way from the refractive index of the mediums on either side of the interface ie.

$$R01 = \frac{(n0 - n1)}{(n0 + n1)} \qquad (7.2)$$

where n0 is the refractive index of medium 0 and n1 is the refractive index of medium 1. R12 and R20 are found in a similar way. The other parameters used in equation (7.1) are the thickness of the film, d, the absorption coefficient, α and the wave number, w. The wavenumber is related to the wavelength, λ and the refractive index, n by

$$w = 2\pi n/\lambda \qquad (7.3)$$

For equation (7.1) to be valid it has been assumed that the extinction coefficient, k (which is related to the absorption coefficient α by $k = \alpha\lambda/4\pi$) is much less than the refractive index of the film, nf (ie. nf >> kf). To use equation (7.1) the refractive index of film and substrate over the required spectral region is needed.

The refractive index of the substrate, ns, was found by measuring the transmissivity of the glass slide over the required spectral region. For a parallel sided glass slide the transmission, T, is given by (6) as;

$$T = 1 - \frac{(2r)}{(1+r)} \qquad (7.4)$$

where r is the interfacial reflection and is given by;

$$r = \frac{(ns-1)}{(ns+1)} \qquad (7.5)$$

from (7.4) and (7.5)

$$ns = \frac{(C+1)}{(1-C)}$$

$$\text{where } C = \frac{(R)}{(2-R)} \qquad \text{and} \quad R = 1-T$$

The curve of ns vs. λ obtained using this method is shown in figure 7.6.

For the interference effects which are shown in figure 7.5 the refractive index of the film, nf, satisfies the relationship

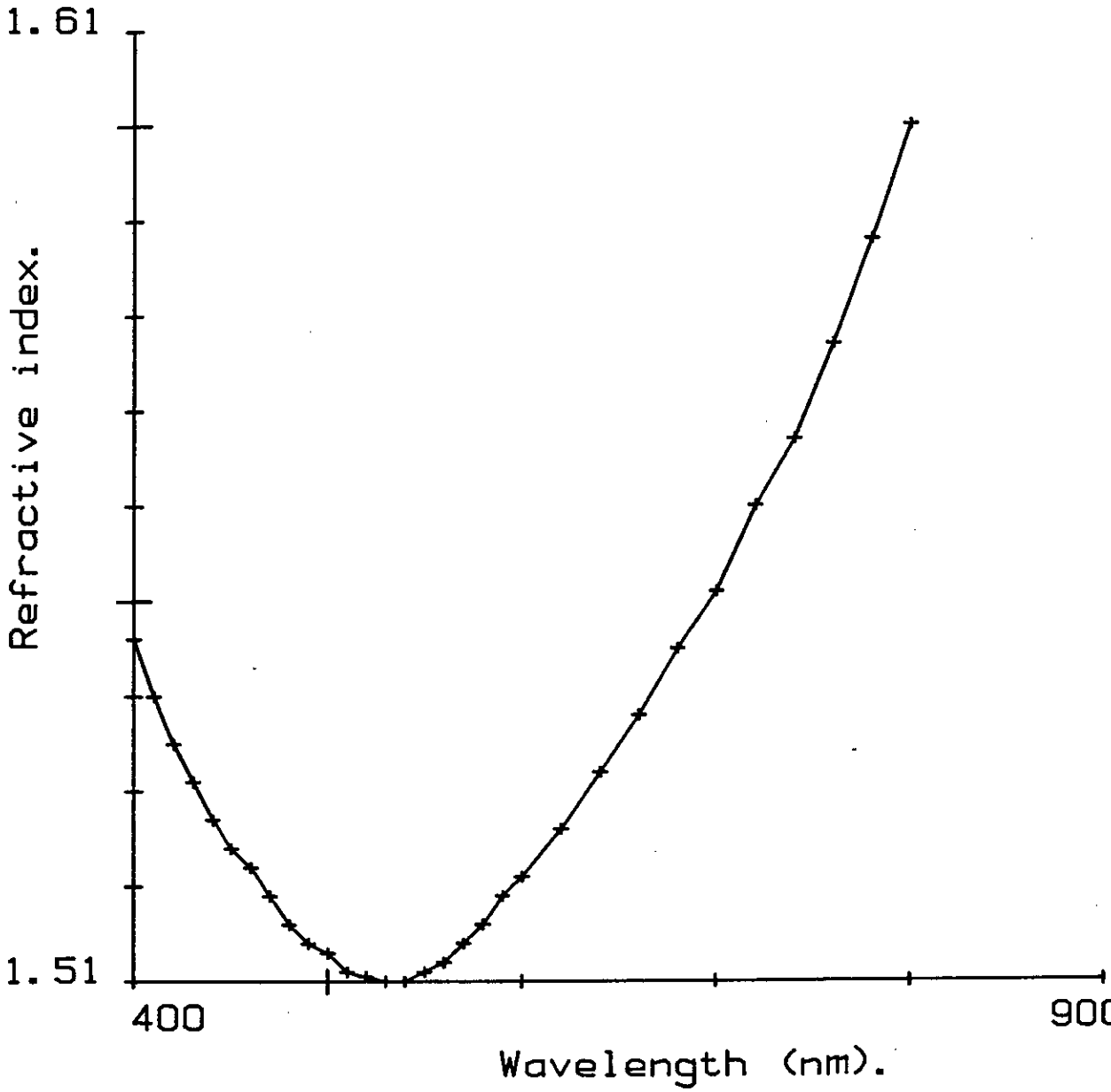

Figure 7.6 The dispersion curve of a glass microscope slide. Slides of this type were used as substrates for optical measurements.

$$nf = P\lambda/2d \qquad (7.6)$$

when the transmissivity values go through a minimum or maximum; P is an integer for maxima and a half-integer for minima. At the wavelength of 630 nm the transmission was a minimum with a value of 64%. Equation (7.1) was then used to find a value of nf which gave a transmission value of 64%. The value of d was obtained from equation (7.6) which can be rearranged as;

$d = P\lambda/2nf$ where P is a multiple of a 1/2.

The values which satisfied these conditions were nf = 2.4337, P = 5.5 and d = 712 nm. With the value of nf at 630 nM fixed, nf at other turning points was found from equation (7.6) with the value of P increasing by a 1/2 after each turning point. To find the values of nf at shorter wavelengths where no interference exists the single oscillator dispersion equation was used;

$$n = \left[1 + \frac{A\lambda}{\lambda^2 - \lambda_c^2}\right]^{1/2} \qquad (7.7)$$

Values of n were known at the turning points mentioned above, and therefore simultaneous equations were formed using equation (7.7) and the values of A and λ_c obtained. The equation for nf can then be expressed as;

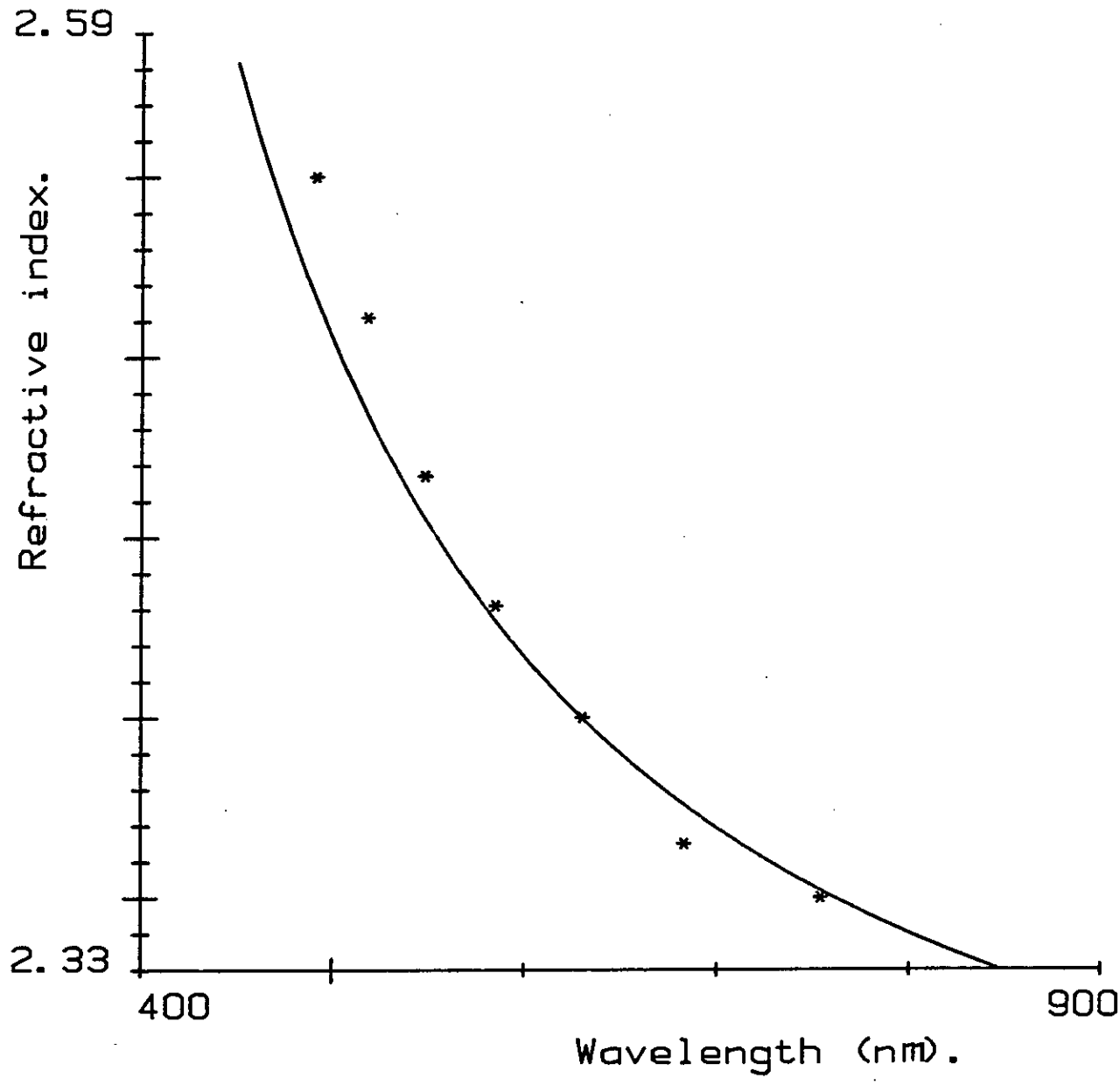

Figure 7.7 Dispersion curve of a film of composition $As_{32}S_{68}$.

$$nf = \left[1 + \frac{4.08\,\lambda^2}{\lambda^2 - (238)^2} \right]^{1/2} \qquad (7.8)$$

Figure 7.7 shows the dispersion curve for the film obtained using equation (7.8) ;the crosses are the values of nf obtained from equation (7.6) and it can be seen that good agreement is obtained. Having derived the dispersion curves for the film and substrate, equation (7.1) was then used to find the values of the optical absorption coefficient which satisfy the transmission values given in Figure 7.5. The results are shown in Figure 7.8. The values of the absorption coefficient are given in cm^{-1} and are plotted as a function of photon energy. The curve has a similar shape to the curve given in the literature for amorphous As_2S_3 (7), but is displaced towards higher photon energy.

7.3.2 Photodoped Films

The photodissolution of Ag into $As_{30}S_{70}$ films causes the light yellow colour of the As-S film to change to a deep red, which indicates that there is a large change in the optical absorption after photodissolution. It was found that two types of Ag-photodoped films could be formed, depending on the experimental conditions. Figure 7.9 (a) shows the situation where a thin As-S film was deposited on to a glass slide and a thick film of Ag evaporated on top of it. The thickness of the Ag was

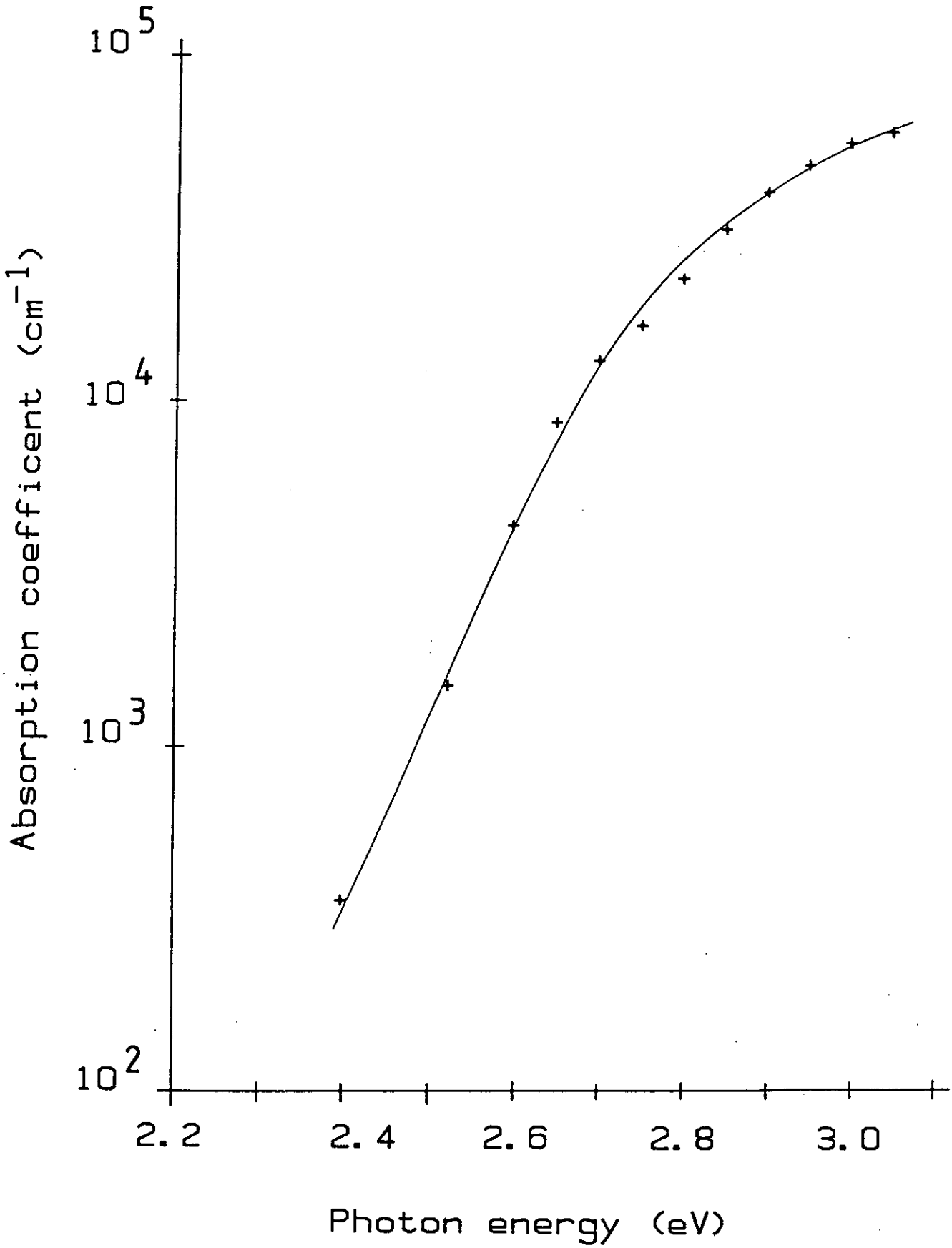

Figure 7.8 Optical absorption curve for a film of composition $As_{32}S_{68}$.

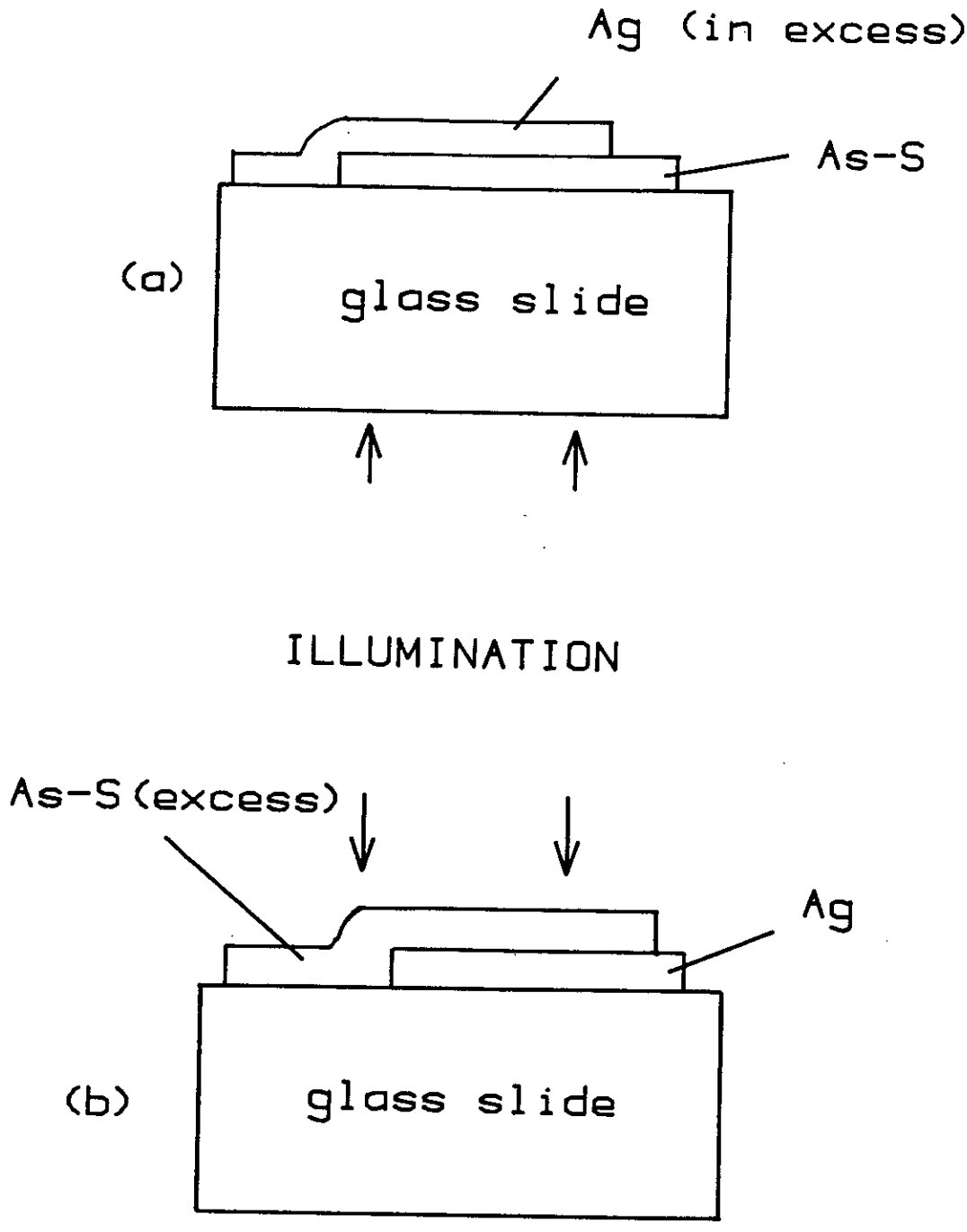

Figure 7.9 Diagram illustrating how photodoped As-S films were prepared: (a) excess Ag source, and (b) excess As-S source.

sufficient to fully photodope the As-S film when illuminated through the substrate. The excess Ag was removed with a suitable solvent to leave a photodoped film which had an excess of Ag present.

The other type of photodoped sample is shown in Figure 7.9 (b): the Ag film was deposited first followed by a thick As-S layer. In this case the As-S was in excess and completely dissolved the Ag layer. Excess As-S was removed with a suitable solvent to leave a photodoped film obtained from an As-S rich source. The sample prepared from the Ag rich source was a deep red colour when viewed in white light, whereas the sample prepared from the As-S rich source was an orange colour. Figures 7.10 and 7.11 show the optical transmissivity curves of photodoped films for the two types of sample prepared with excess As-S and excess Ag present respectively.

First consider the sample prepared with excess As-S present and its transmissivity curve, figure 7.10. Interference effects are clearly seen in the transmissivity curve but there is optical absorption, even at long wavelengths, and this reduces the maximum transmissivity values to less than the bare substrate transmissivity.

Equation (7.1) cannot be used alone to find the film refractive index at a specific minimum, as before. In

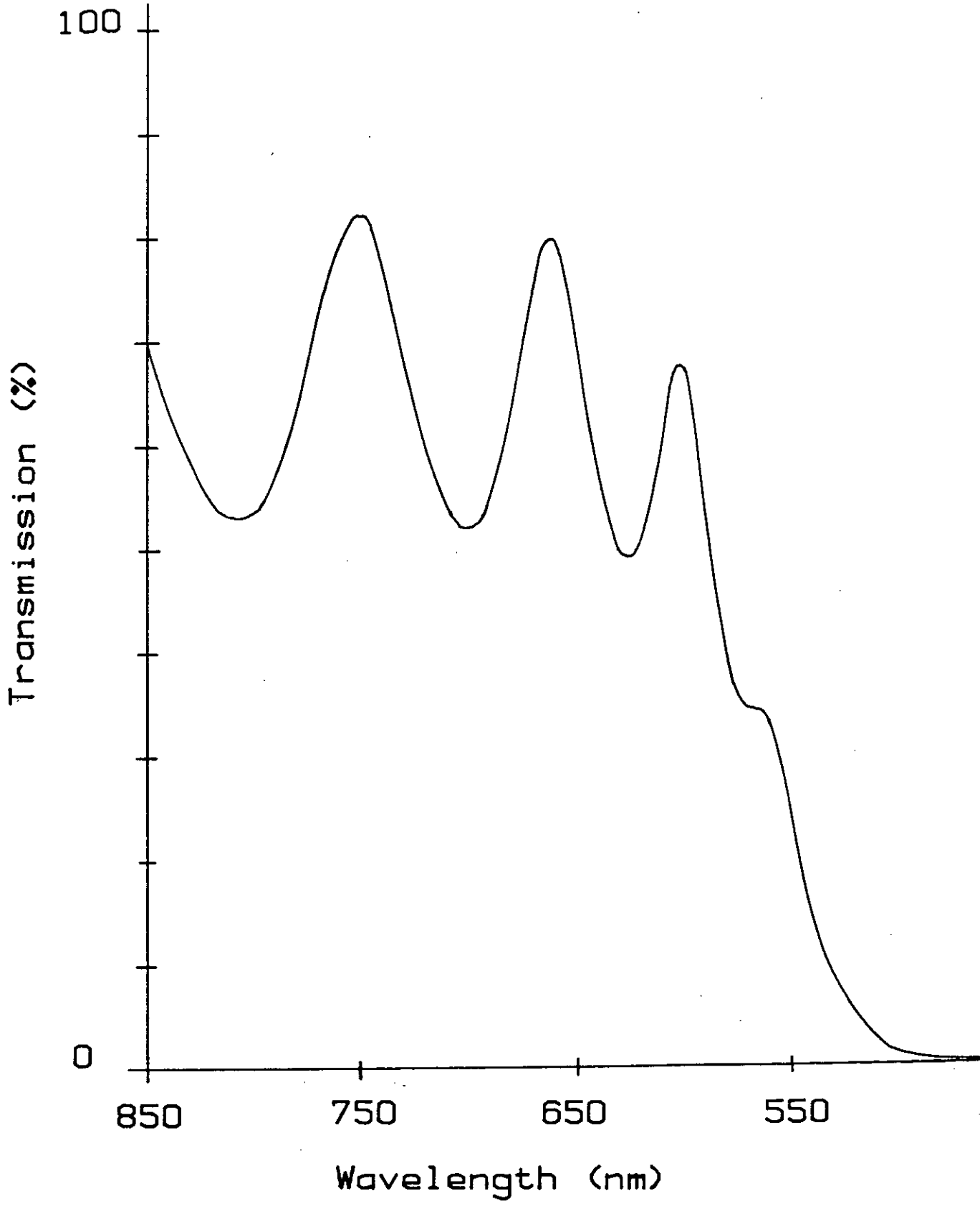

Figure 7.10 Transmissivity curve of a Ag photodoped As-S film prepared with an excess of As-S (see figure 7.9(b)).

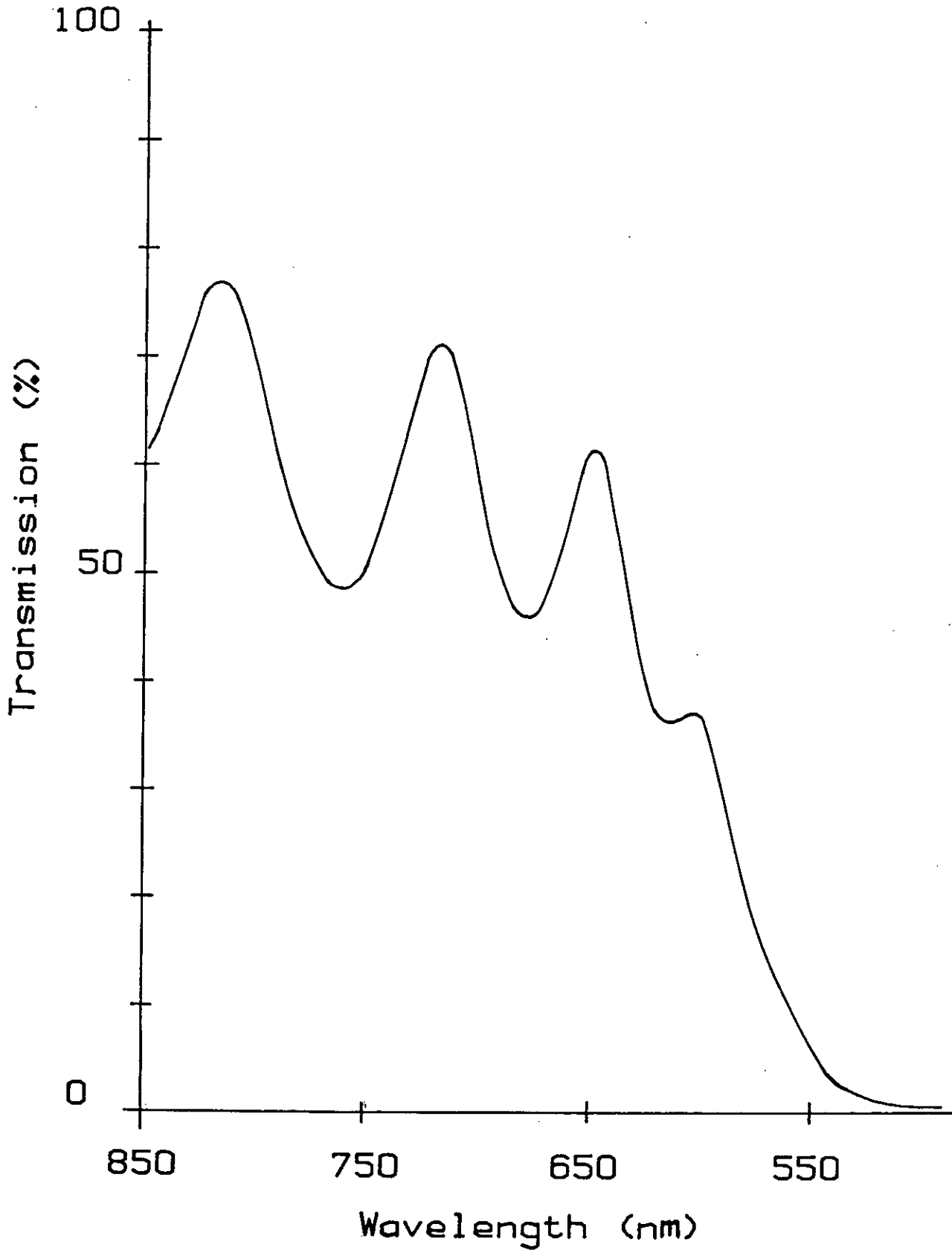

Figure 7.11 Transmissivity curve of a Ag photodoped As-S film prepared with an excess of Ag (see figure 7.9(b)).

this case the film thickness was measured separately using a mechanical stylus. Equation (7.6) was used and a value of P was found which gave a reasonable answer for nf. As before the values of nf obtained from the interference conditions were well-fitted by the single oscillator dispersion equation and the following result was obtained;

$$nf = \left[1 + \frac{4.84\,\lambda^2}{\lambda^2 - (308)^2}\right]^{\frac{1}{2}} \qquad (7.9)$$

Equation (7.9) is plotted in figure 7.12 and together with equation (7.1) was then used, as described previously, to find the values of the optical absorption coefficient which fit the transmissivity data of figure 7.11. Figure 7.13 (curve A) is the result and shows optical absorption plotted as a function of photon energy. A similar procedure was followed to obtain the absorption curve for the photodoped layer which was obtained when the Ag layer was present in excess. The curve for this sample is shown in figure 7.13 (curve B).

It is quite clear from figure 7.12 that the sample prepared from an excess Ag layer is much more optically dense than that prepared from an excess As-S layer. Both samples show considerable tailing of the absorption edge which suggests absorption due to inhomogeneities or impurities. The tailing starts at 0.6 μm, and if

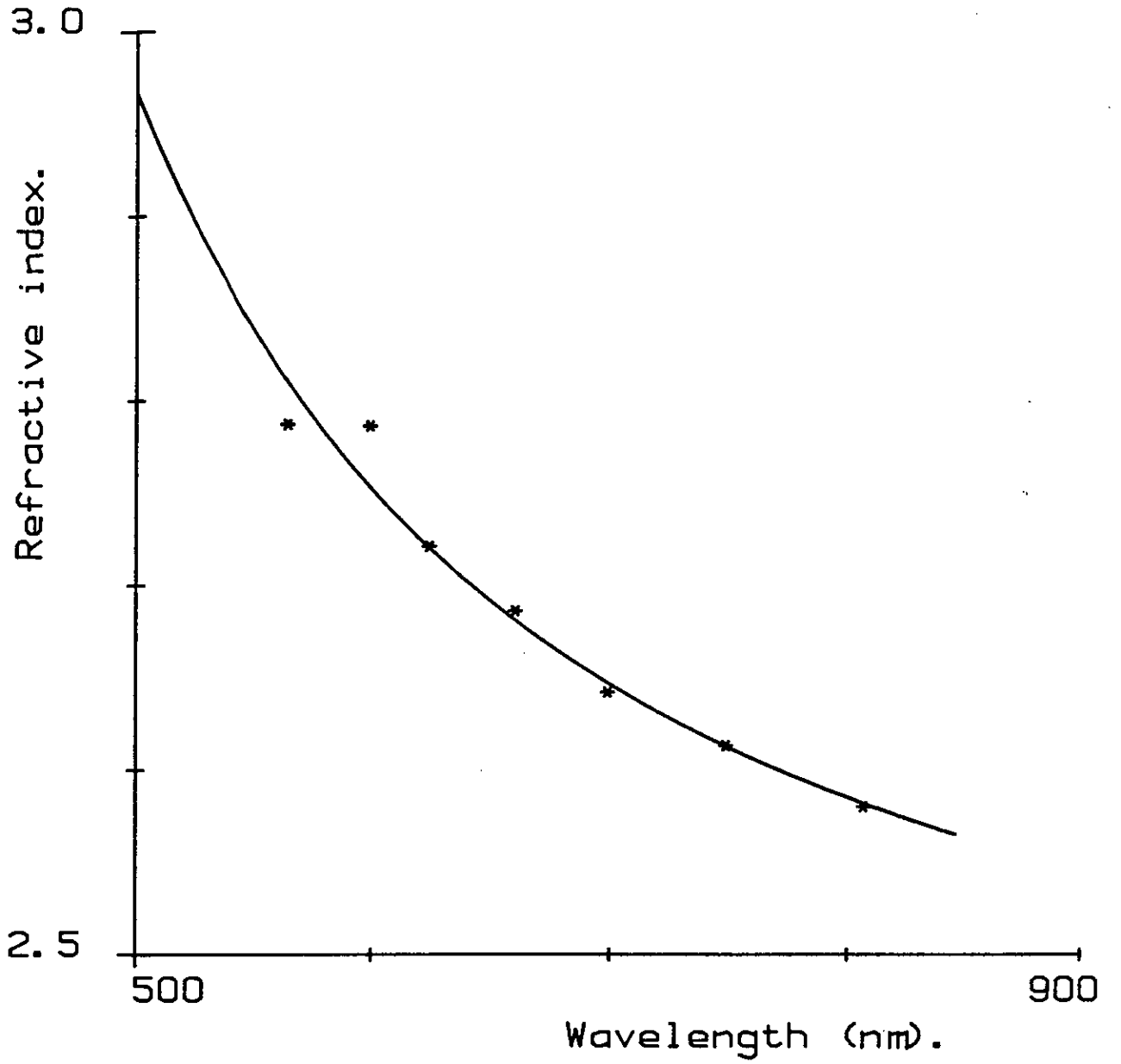

Figure 7.12 The dispersion curve of a Ag photodoped As-S film prepared with an excess of Ag present.

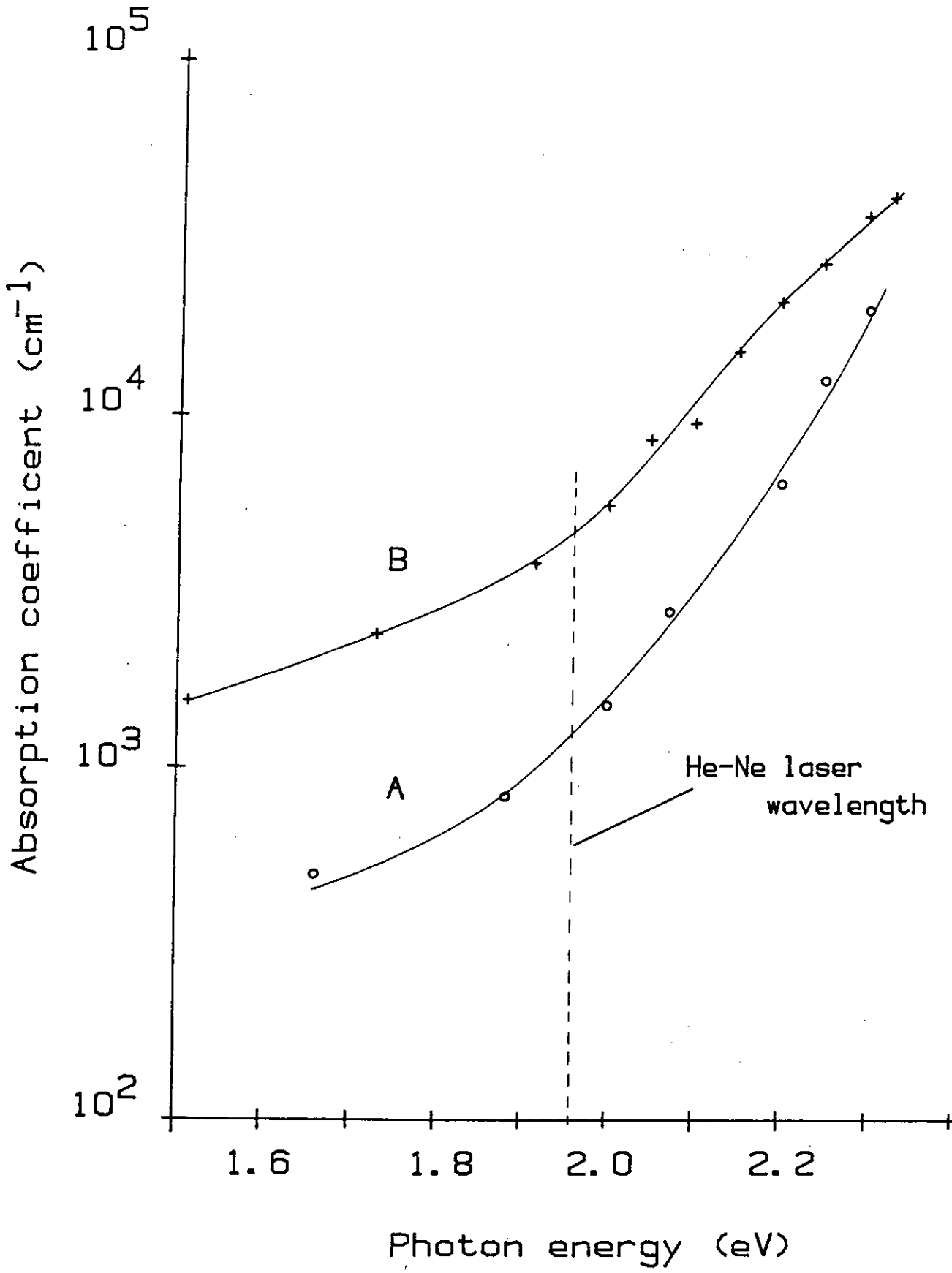

Figure 7.13 Optical absorption curves of Ag photodoped As-S films. Curve A is for a film prepared with excess As-S present and curve B with excess Ag present.

inhomogeneities are responsible this would be their approximate size. As the samples were found to be completely homogenous and amorphous, inhomogeneities cannot be responsible for the tailing and therefore impurity absorption, probably due to Ag atoms (or ions), is the likely cause.

In the preparation of films from an excess Ag layer it was always found that the films peeled off the substrate when dipped in the Ag etching solution. It was found necessary to stop photodoping just prior to the last of the As-S film dissappearing. This would give some error in the thickness of the film and consequently the absorption curve B of figure 7.13 should be moved up to higher values.

7.4 References

1. Nemanich, R. J., Connell, G. A. N., Haynes, T. M. and Street, R. A., Phys. Rev. B, 18, 6900, (1978).
2. Firth, A. P., Owen, A. E. and Ewen, P. J. S., J. Phys., Paris Colloq., 42, 903, (1981).
3. Ewen, P. J. S., Ph. D. Thesis, University of Edinburgh, pp. 143-145, (1978).
4. Kawamoto, Y., Agata, M. and Tsuchihashi, S., J. Ceram. Assoc. Jap., 82, 502, (1974).
5. Goldschmidt, D., J. Opt. Soc. Am. A., 1, (3), 275, (1984).

6. Vasicek, A.,"Optics of Thin Films", (North-Holland Publishing Comp.), p.58, (1965).

7. Mott, N. F. and Davis, E. A., "Electronic Processes in Non-Crystalline Materials", Second Edition, (Oxford: Clarendon Press), p.498, (1979).

CHAPTER 8

PHOTODISSOLUTION - STUDIES OF Ag DISSOLUTION RATES

8.1 Effect of light intensity

Using the technique described in section 5.5.1 the intensity dependence of the photodissolution rate for Ag-$As_{30}S_{70}$ samples was found. The samples were fabricated by first evaporating a Ag film 56 nm thick onto a glass slide. An As-S film of composition $As_{30}S_{70}$, with a thickness of 210 nm, was evaporated onto the Ag. The wavelength of the light used was 571.5 nm, with an intensity ranging from 4 - 50 mW.

The results are shown in figure 8.1 and are plotted as the logarithm of reciprocal time (which represents speed) versus the logarithm of incident light power. By analysing the results of chemical kinetics it was possible to find the rate of photodissolution and its dependence on the concentrations of the reactants. In general the rate of a chemical reaction is proportional to the a^{th} power of the concentration of one reactant and the b^{th} power of the second, if two reacting species are involved, that is:

$$\text{Rate} = K\, C_A^a\, C_B^b \qquad (8.1)$$

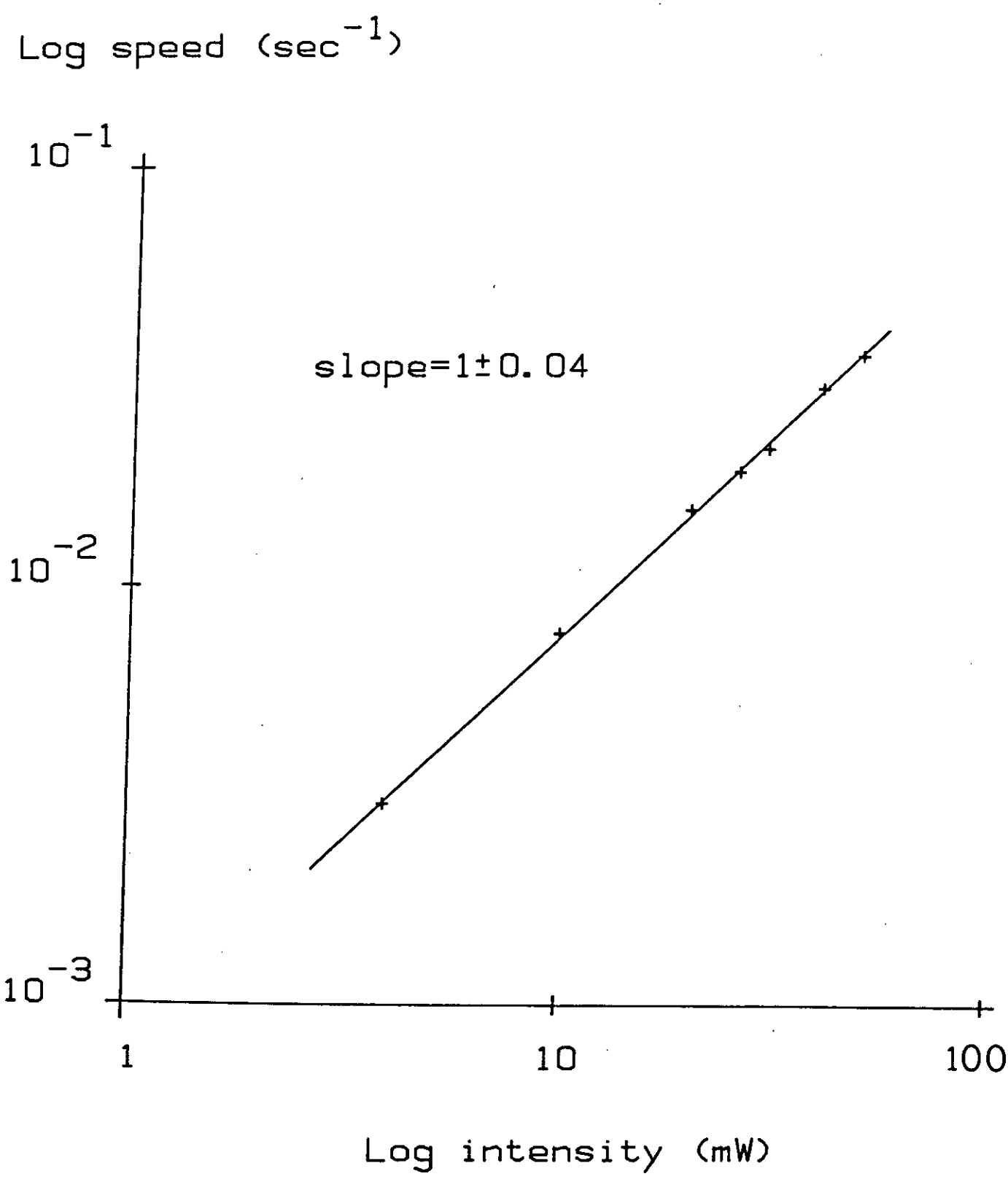

Figure 8.1 The rate of photodissolution of Ag in to $As_{30}S_{70}$ films as a function of incident light intensity plotted on a log-log scale.

where K is a constant, C_A is the concentration of reactant A and C_B is the concentration of reactant B. The overall order of the reaction, n, is simply

$$n = a + b \qquad (8.2)$$

If the rate of the reaction depends only on the concentration of reactant A and a = 1 then the reaction is first order (i.e. n = 1). To find the order of the photodissolution process from figure 8.1 it was assumed that the speed of the dissolution process (v) depended on the concentration of a species, Cs, and could be written as

$$v = K\ Cs^n \qquad (8.3)$$

where n is the order of the reaction. In logarithmic form this becomes,

$$\log v = \log K + n \log Cs \qquad (8.4)$$

and plotting log v versus log Cs would give a graph of slope n. It was also assumed that the concentration of the reacting species, Cs, depended on the incident light power, P : log Cs was taken as being proportional to log P. It can be seen from figure 8.1 that the slope of the graph, n, is very close to unity and hence indicates a first order reaction. Therefore the speed of the photodissolution process appears to depend on the

concentration of one species, which might possibly be Ag atoms (or ions).

8.2 Electric field enhancement

Samples with the configuration shown in section 5.5.2 were used to investigate the effect of an applied DC electric field on the Ag layer dissolution rate. The rate of dissolution was measured by monitoring the resistance change of a thin Ag strip as proposed by Goldschmidt (1). The DC electric field was applied by using a transparent top Au electrode.

The results of these experiments are shown in figure 8.2 and are plotted in terms of Ro/R, where Ro is the initial resistance of the Ag strip and R is the value of the resistance measured at a particular time during the photodissolution of the Ag strip. In terms of resistivity and film thickness Ro/R can be expressed as:

$$Ro/R = (\rho_o/do).(d/\rho) \qquad (8.5)$$

where ρ_o and do are the initial values of resistivity and thickness respectively and ρ and d are values measured at a particular time during the photodissolution. For a Ag strip thickness > 30 nm ρ can be considered constant but rises very steeply below 20 nm (1).

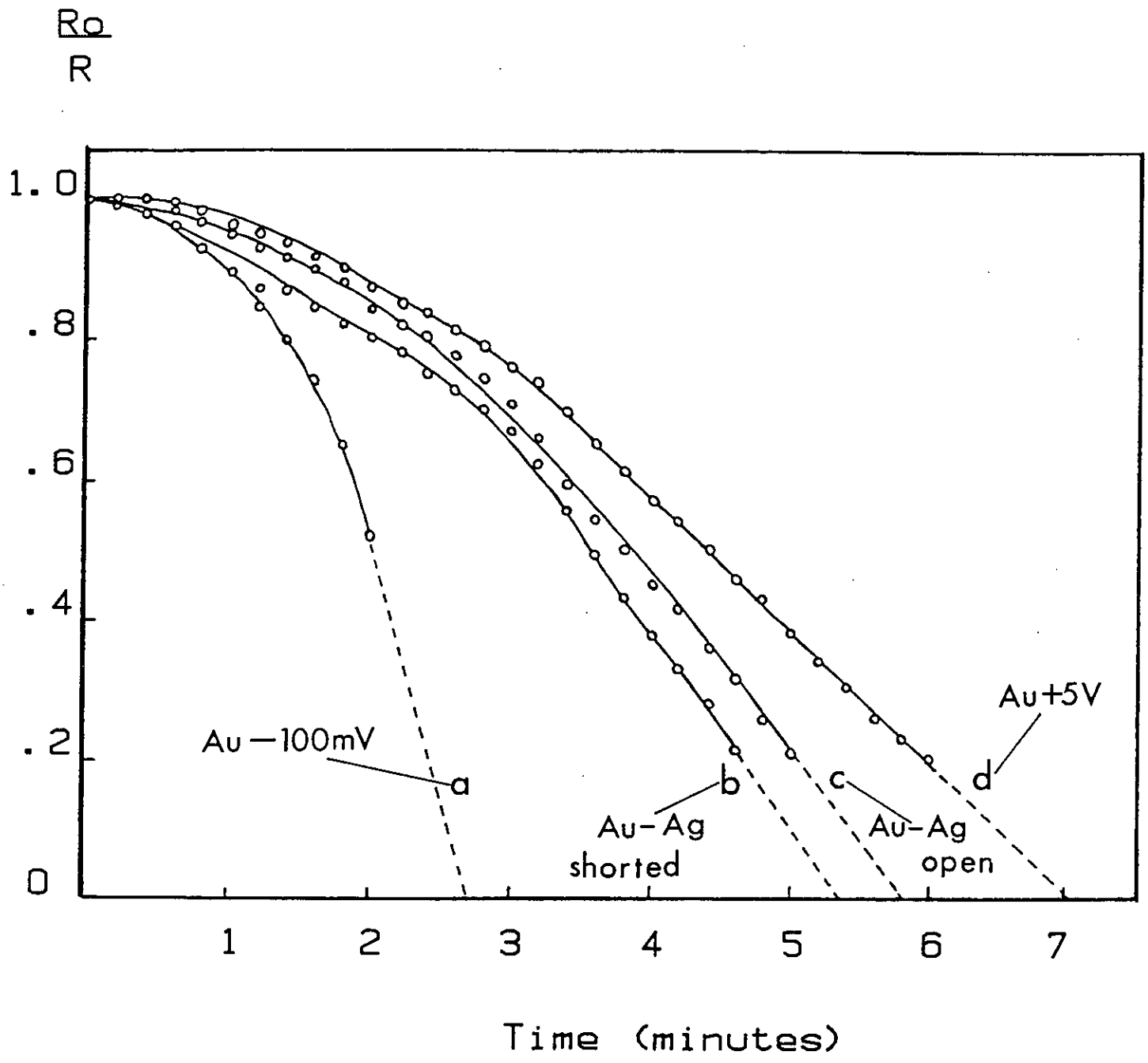

Figure 8.2 The resistance change of thin Ag strips during their photodissolution in to As-S films. And the effect of an external electric field on dissolution times.

Measuring Ro/R to determine the rate of the Ag layer dissolution is therefore only valid for d > 30 nm. To find the values of Ro/R for d < 30 nm the curves of figure 8.2 were extrapolated and are shown as dotted lines.

For the situation where no field was applied (curve c) the time to completely dissolve the Ag strip was 5.8 minutes. When a voltage of +5V was applied to the top Au electrode the process was slowed down and 7 minutes were needed to dissolve the Ag strip. Applying a negative voltage of only -100 mV speeded up the dissolution rate considerably (curve a) and a dissolution time of 2.7 minutes was recorded. It was also found that shorting the top Au electrode to the bottom Ag layer increased the speed of dissolution (curve b). The time to dissolve the Ag strip decreased by 7.5% compared with the open circuit measurement.

The results are consistent with the contention that Ag^+ ions are mobile in photodoped films and play an important role in the photodissolution process.When the top Au electrode is positive the field opposes the Ag^+ ions and slows down the process whereas a negative potential applied to the top Au electrode would attract the positive ions and enhance the dissolution. The increased dissolution rate when the sample was short circuited could be explained if the supply of electrons,

which would be kept constant by the short circuit, is also important in the process.

8.3 Lateral dissolution

The sample configuration that was used in these experiments has been described in section 5.5.4. Illumination of the area above the Ag strip caused photodissolution and the thin As-S layer on top of the Ag was quickly consumed. If the illumination was on the part of the sample where no Au film covered the glass slide then nothing further happened. However on the part of the sample where a Au film was present, the illumination caused further photodissolution. The dissolution front moved through the As-S layer parallel to the substrate and away from the Ag strip. This result has already been illustrated (see figure 5.11) and it should be noted that photodissolution only occurred in the illuminated area.

It was possible to observe the illuminated area through the microscope and by adjusting an iris in front of the light source it was easy to pin point particular areas for illumination. It was found that only the contact area between the photodoped and undoped As-S film need be illuminated to produce photodissolution and by moving the illuminated area in a straight line away from

the Ag strip a finger-shaped area of photodoped material could be produced. This result is shown in figure 8.3. Figure 8.3(a) illustrates schematically how the illuminated area was moved and how a finger shaped area was produced while Figure 8.3 (b) is a photograph, taken through the microscope, of what was actually observed. The speed at which the tip of the finger,(i.e. the dissolution front) moved is shown in figure 8.4 and is presented as the dissolution distance versus illumination time. It can be seen that a linear plot was obtained indicating a constant speed of dissolution. The rate, obtained from the slope of the graph, was 1 um per minute. The results of similar experiments to this indicated that the photodissolution could be continued indefinitely by moving the illuminating area in the way described. The process stopped, however, if the source of Ag was consumed. The speed of dissolution depended little on illumination intensity: above a moderate level of illumination a further increase in the intensity had no effect. At low illumination levels the photodissolution did not stop but it was noticed that the layer close to the Au photodoped first so that the photodissolution proceeded as a wedge. This is illustrated in figure 8.5 and was observed through the microscope as a light-red coloured area appearing first and gradually changing to a deeper red. The fact that illumination of the contact area between photodoped and undoped As-S produced further dissolution indicates quite

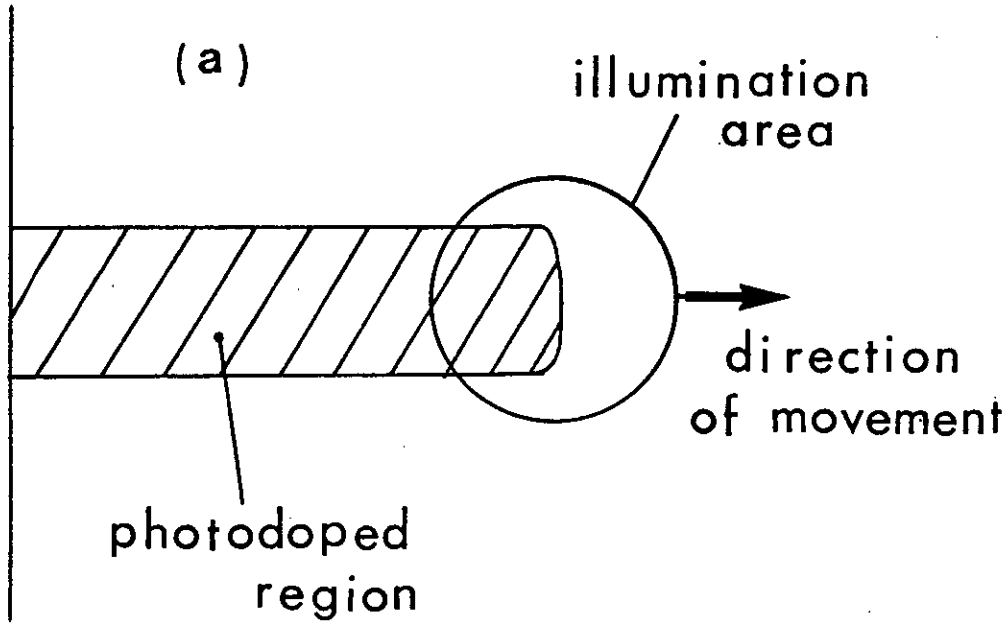

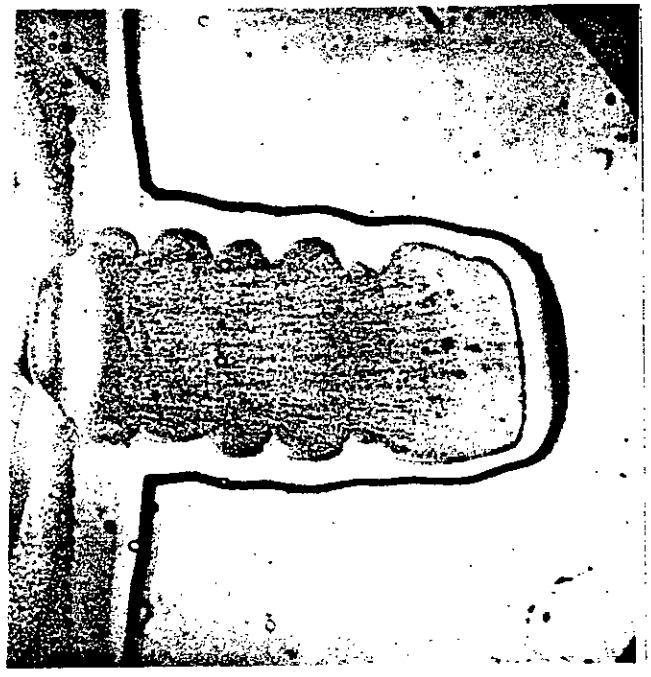

(b)

Figure 8.3 The movement of a photodoped finger-shaped area drawn out in an As-S film above a gold layer. (a) schematic representation and (b) the strip photographed through a microscope.

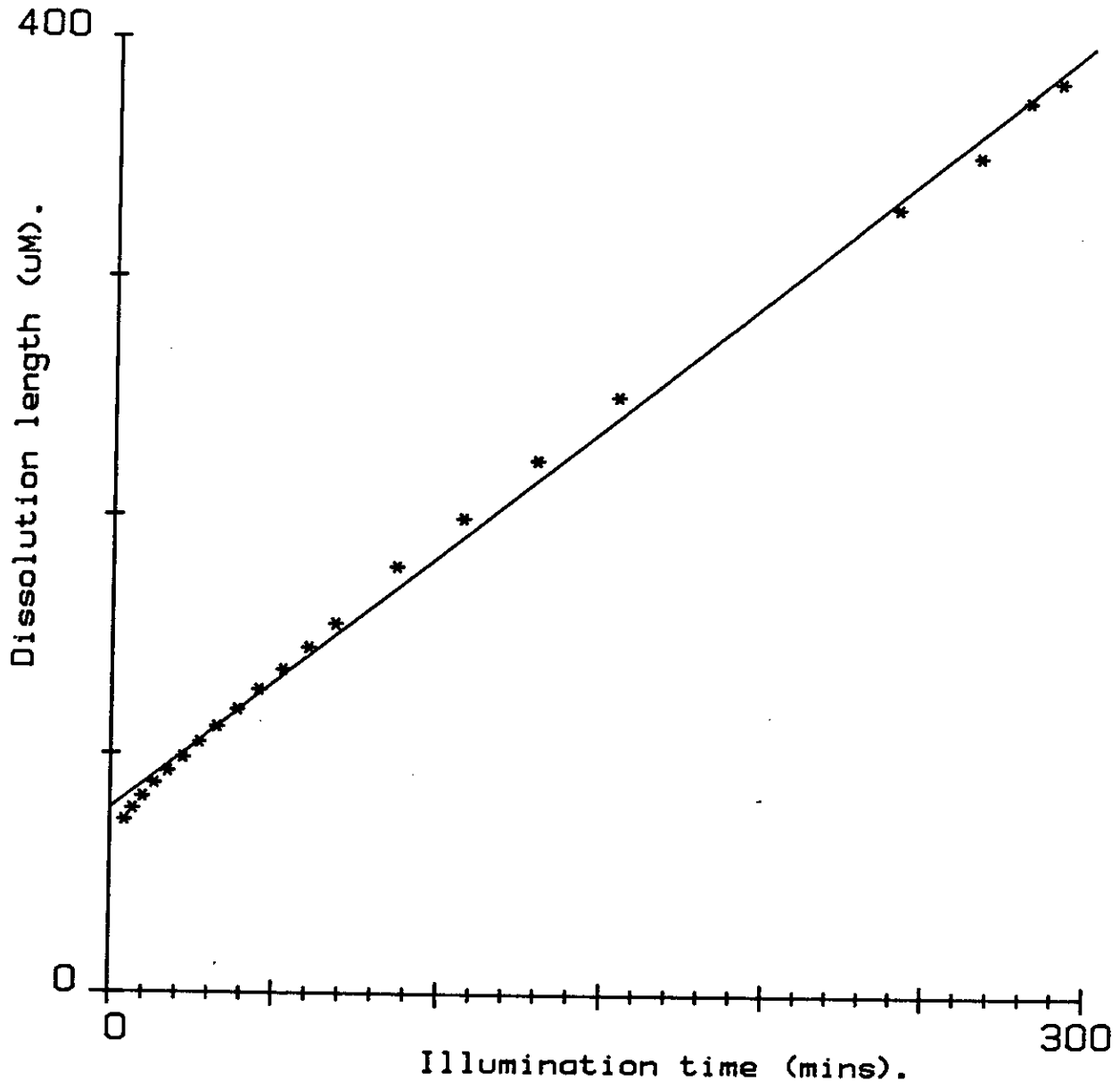

Figure 8.4 Distance travelled by the photodissolution front (dissolution length) against time. The straight line is a linear fit to the data points and has a gradient of ~ 1 um per minute.

clearly that it is light absorbed in this region that causes photodissolution. The Ag need not be illuminated for photodissolution to occur. Also, although the Au film plays a role in increasing the speed of dissolution next to its surface, photodissolution normal to the film (figure 8.5) is not influenced by the Au layer.

8.4 Transverse photodissolution

8.4.1 Introduction

Transverse photodissolution refers to the situation where an As-S film is deposited onto a Ag film and Ag dissolves into the As-S film under illumination.

Goldschmidt and Rudman (1) have stated that if the illumination is with collimated light, then the Ag layer dissolves in a planar and uniform way. Also, the Raman results, presented in section 7.2, showed that the photodoped product was a single phase homogenous material for As-S compositions near $As_{30}S_{70}$. This suggests that during the photodissolution process the As-S layer, the photodoped layer and the Ag layer remain as distinct homogenous layers. If this hypothesis is correct it would be possible to model the photodissolution process using the theory of thin film optics. And measuring changes in the optical constants of the photodoped film might be a useful technique for determining transverse

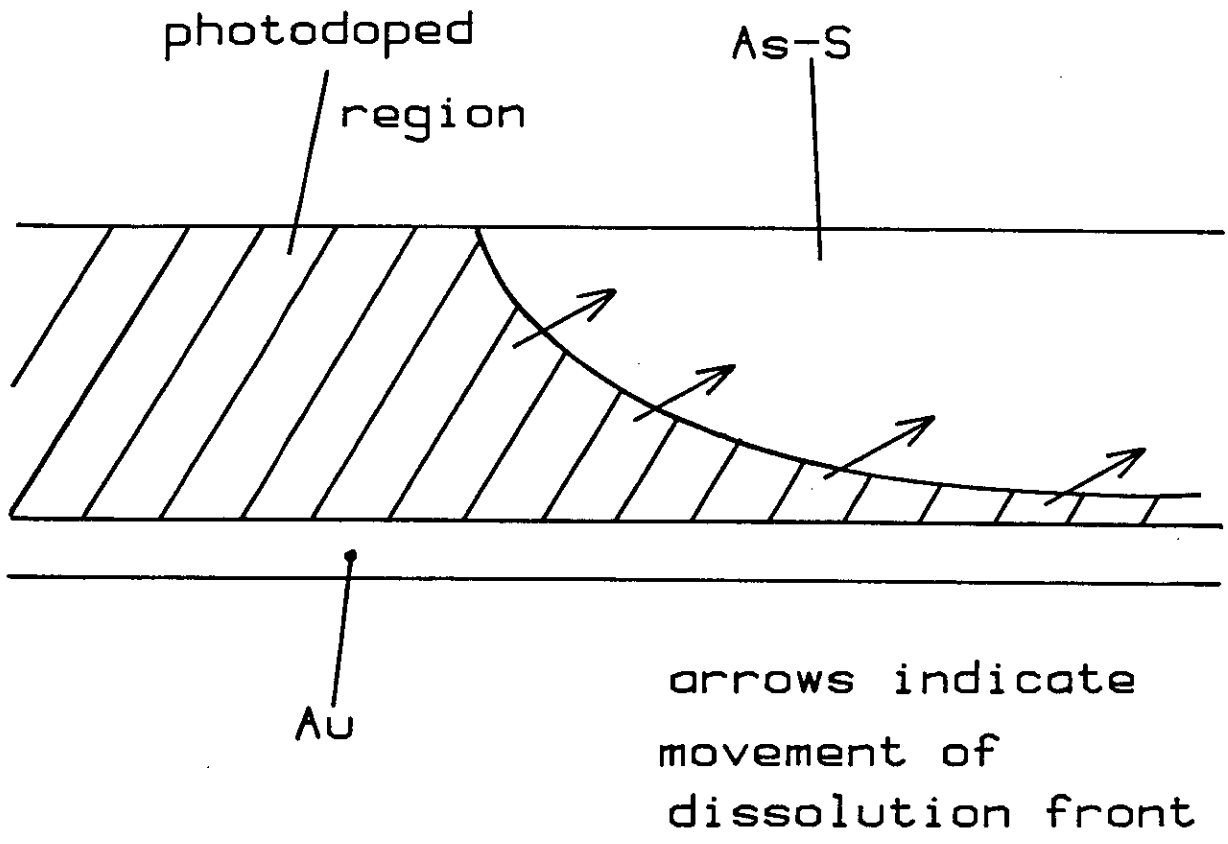

Figure 8.5 Schematic representation of the movement of the photodissolution front on a Au substrate.

dissolution rates.

In the next section the optical characteristics of the photodissolution process are modelled and the predicted optical reflectivity of the photodoped film is found as a function of increasing photodoped thickness. The section following the optical model presents experimentally determined reflectance curves and in the final section the optical model is compared with experimental results.

8.4.2 Optical model

Consider a Ag film in contact with an As-S film of composition $As_{30}S_{70}$. After illumination with a collimated light source a cross-section through the layers will be similar to that shown in figure 8.6. The system consists of three thin layers on a glass slide and as the photodissolution process proceeds the thickness of the various layers will change. It is assumed that the layers remain distinct and homogenous, so that it should be possible to model the optical characteristics of the system and predict its reflectivity, for a particular wavelength, during photodissolution.

The situation was simplified by considering the Ag layer to be very thick compared to the thickness of the As-S layer so that the Ag is in excess. This system now

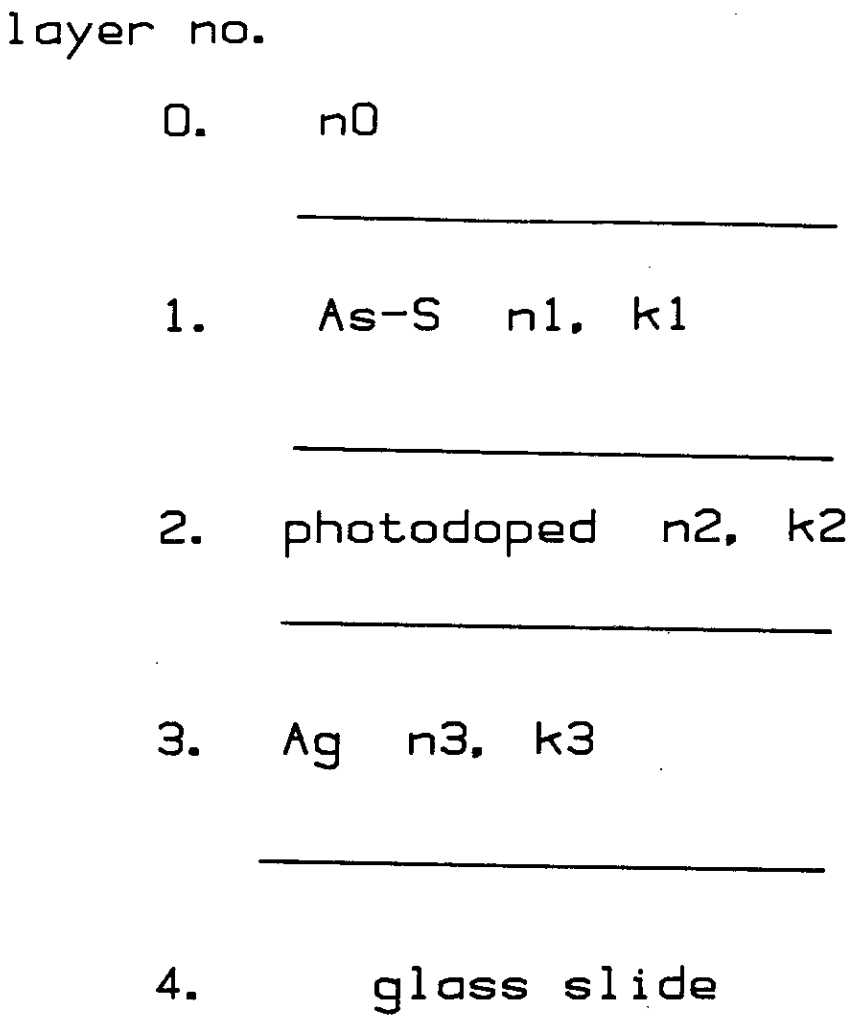

Figure 8.6 A proposed layer structure used in optically modelling the photodissolution process.

corresponds to a two-layer system of an As-S and a photodoped layer on a Ag film substrate. The equations needed to predict the reflectivity for this situation (shown in figures 8.6) have been given by Heavens (2). There are two important aspects to the optical modelling procedure: firstly, determining the way in which the layers change with time and secondly finding realistic optical constants for the individual layers.

Consider first the problem of modelling the changes in layer thickness during photodissolution. If a Ag film of thickness d_{Ag} dissolves into an As-S film of thickness d_{As-s}, then a photodoped layer of thickness d_{PD} is formed. This is illustrated in figure 8.7 and as shown it is assumed that;

$$d_{PD} = d_{Ag} + d_{As-S} \qquad (8.6)$$

This was in fact confirmed experimentally by traversing with a mechanical stylus the boundary between an illuminated and non-illuminated area : no difference in height between the two areas was observed. It is also necessary to know the ratio d_{As-S} / d_{Ag}, which specifies what thicknes of As-S dissolves a particular thickness of Ag. This was found experimentally, as described below.

Ten strips of Ag were evaporated onto a glass slide, the strips ranging in thickness from 10-100 nm in steps of

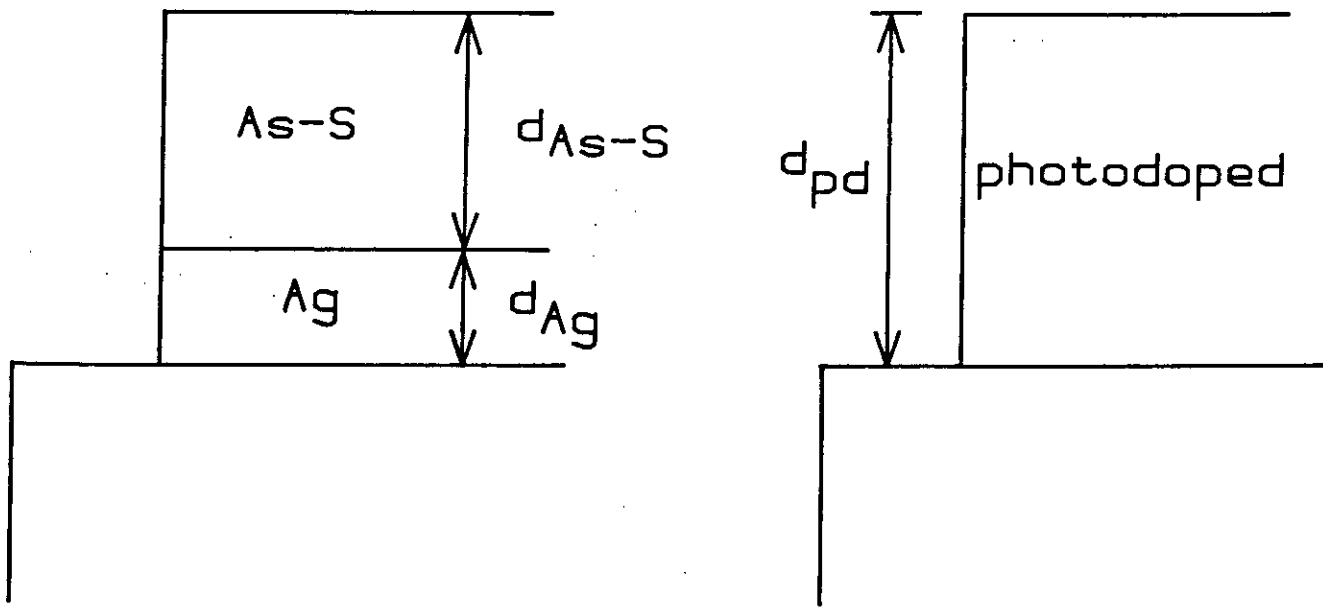

Figure 8.7 A schematic representation of the resulting photodoped thickness formed from the initial As-S and Ag film thicknesses.

10 nm. Half the slide was then flood illuminated for a suitable time, after which the thickness of Ag that completely dissolved into the As-S film was found. From this method the ratio of d_{As-S}/d_{Ag} was found to be 2 ± 0.1. Thus during the photodissolution process, as the As-S film thickness changes from d_{As-S} to zero, the thickness of the photodoped layer goes from zero to $(d_{As-S} + d_{As-S})$.

The problem of finding the optical constants for the Ag film, the photodoped film and the As-S film must now be considered. Since the optical model was to be tested experimentally using the He-Ne laser wavelength (λ = 632.8 nm) the optical constants at this wavelength were needed.

The optical constants of As-S film of composition $As_{30}S_{70}$, at the He-Ne wavelength of 632.8 nm, have already been given (Section 7.3.1) and are n1 = 2.4, k1 = 0. Similarly the optical constants of the photodoped layer, for the situation in which the layer was photodoped from a Ag rich source, have been given (Section 7.3.2): these are n2 = 2.75 and k2 = 0.025.

The optical constants of the Ag film were found by measuring the reflectivity curve, at the He-Ne wavelength during the deposition of $As_{30}S_{70}$ onto a previously evaporated Ag film. The reflectivity curve obtained is

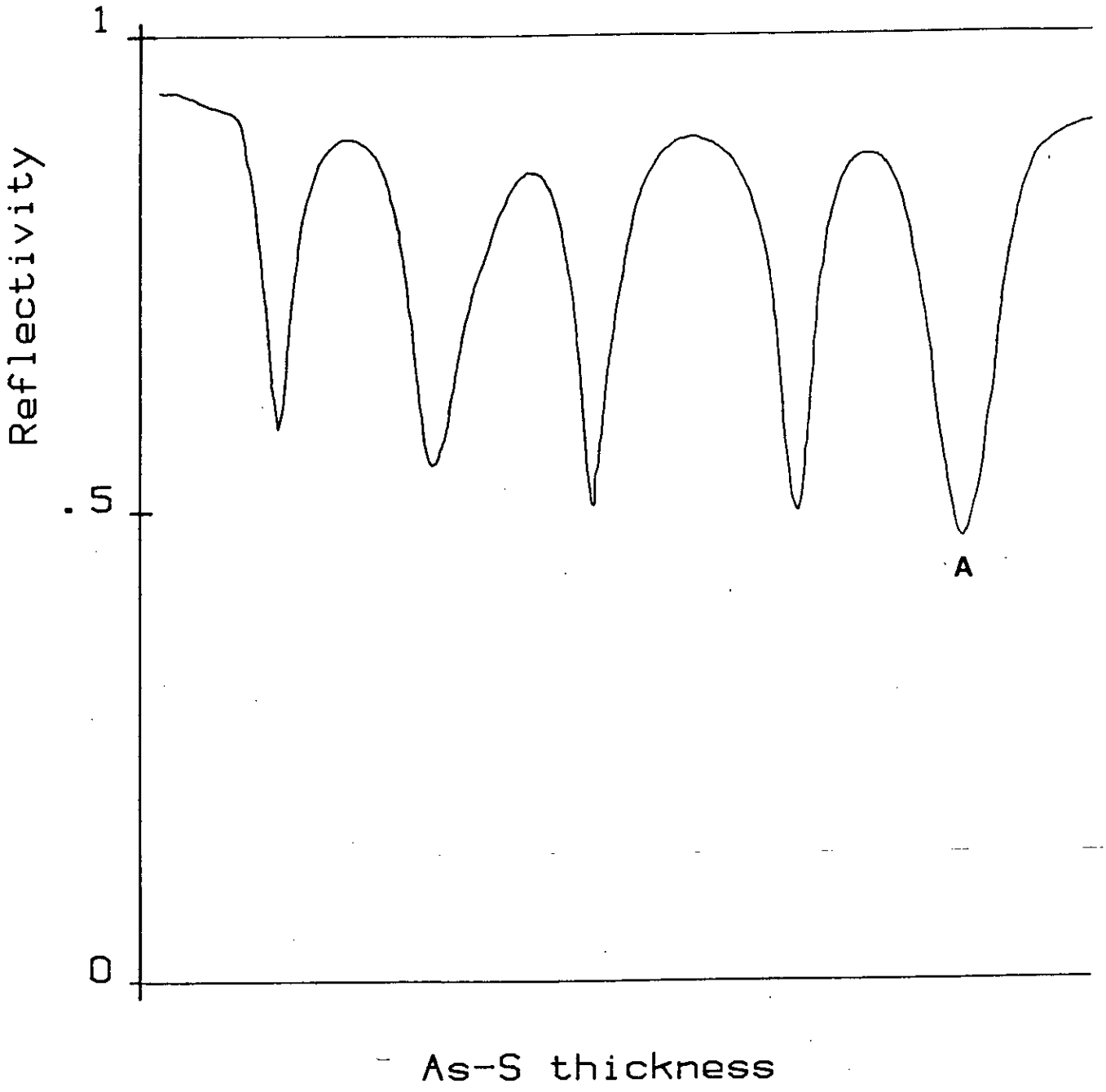

Figure 8.8 The measured in situ reflectivity (for He-Ne laser light) of an As-S film during its deposition on to a glass slide coated with a thin film of Ag. Position A indicates an As-S film thickness where reflectivity is a minimum.

shown in figure 8.8. By modelling the reflectivity of a single absorbing film or an absorbing substrate the optical constants of the substrate can be found in the following way. The reflectivity of a single film on an absorbing substrate can be calculated using the equations given by Heavens (2). Based on these equations a computer program was written to calculate the reflectivity as a function of film thickness. A listing of the program is given in Appendix III. The program requires as input the optical constants of both the substrate and the film. The film constants are known (i.e. n = 2.40, k = 0), therefore the program was used to find values for the optical constants of the substrate that produced a reflectivity curve which fitted the experimentally determined curve. The values found were n = 0.5 and k = 3. The computed curve is shown in figure 8.9.

A computer program was also written based on the equations given by Heavens (2) for two absorbing layers on an absorbing substrate. A complete listing of the program is given in Appendix III. The computed reflectivity (using the thickness relationship, equation (8.6),and the optical constants for the layers given above) for an As-S film of thickness 700 nm on a Ag substrate is shown in figure 8.10. Before further comments are made about the computer-generated curves, the experimentally found curves will first be presented.

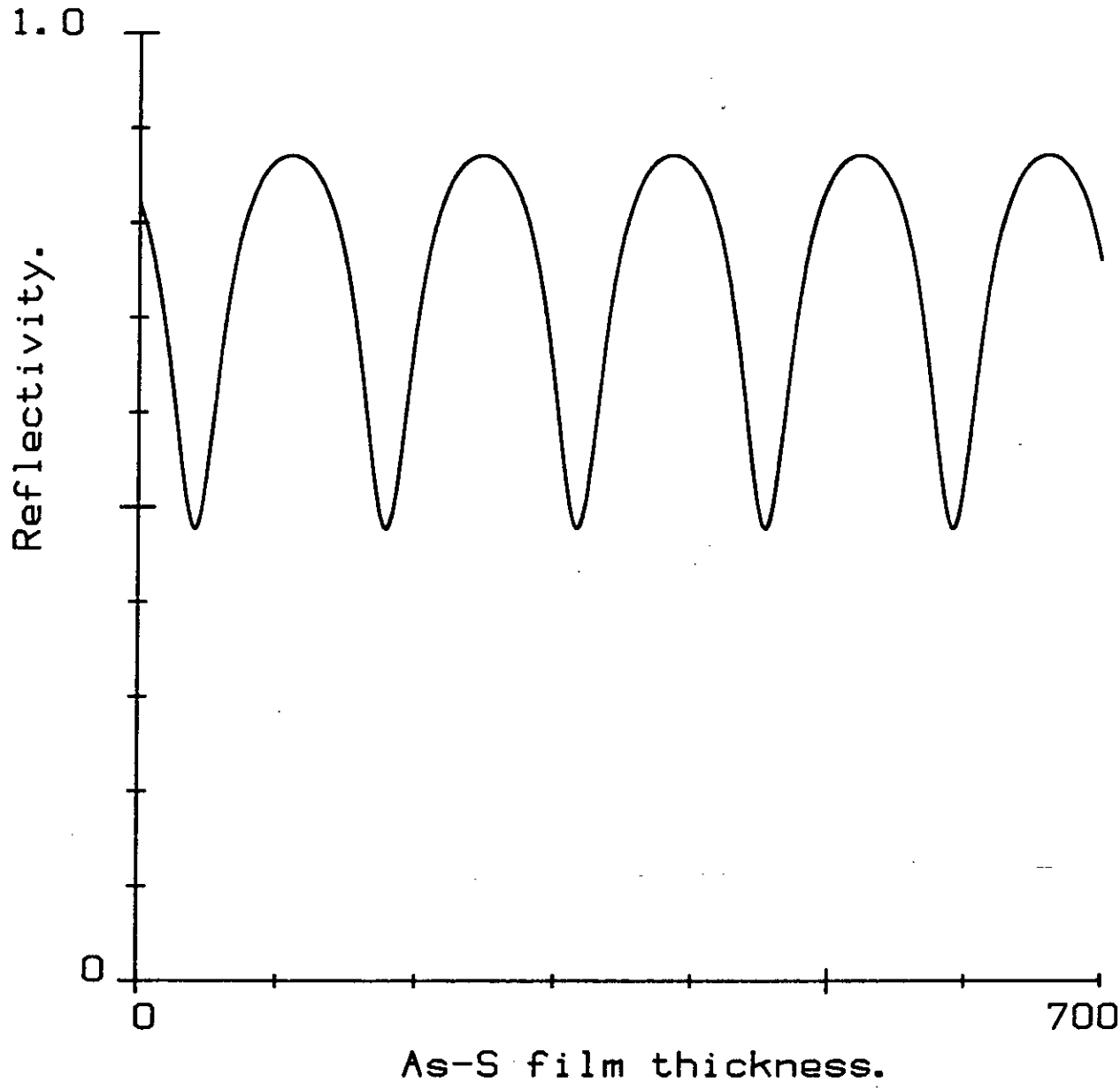

Figure 8.9 The computer generated reflectivity (for He-Ne laser light, 632.8 nm) for the build up in thickness of an As-S film on a Ag film substrate. The optical constants used in the simulation are discussed in the text.

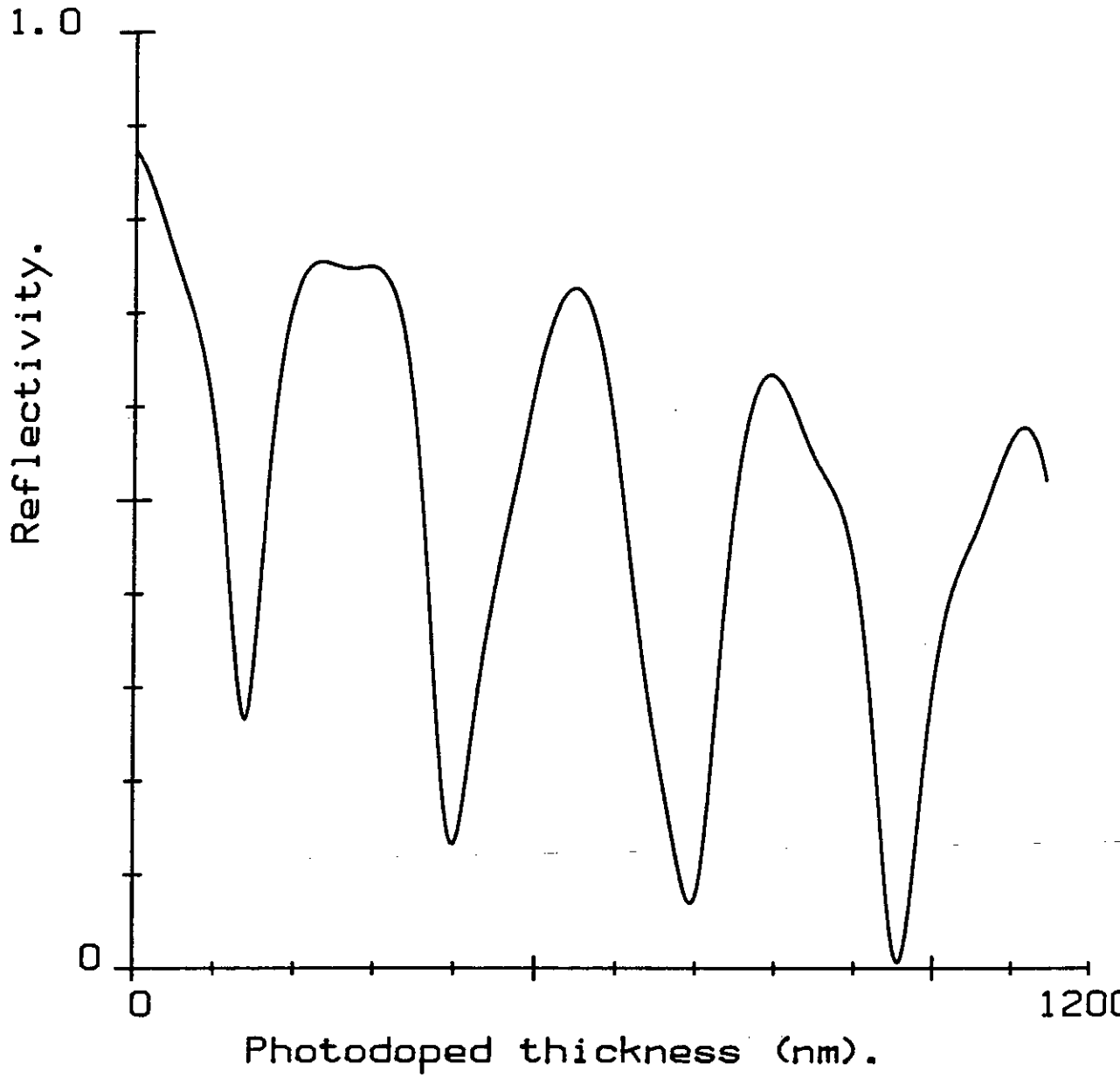

Figure 8.10 A computer generated reflectivity curve (for He-Ne laser light, 632.8 nm) simulating the dissolution of Ag in to As-S films. The optical constants used in the simulation are discussed in the text.

8.4.3 Results

Figure 8.11 shows a typical result, and is the reflectance curve that was recorded during the photodissolution of 297 nm of Ag into 742 nm of $As_{30}S_{70}$. As can be seen, symmetrical sinusoidal oscillations are observed indicating strong interference effects. All samples were fabricated using optical thickness monitoring. A typical reflectance curve versus thickness has already been given (figure 8.8) for an As-S layer deposited onto a Ag film. The evaporation process can be stopped at any time to give a maximum or minimum in the reflectance value. The initial reflectance value measured during the transverse photodissolution will be the same as the final value that was measured during the optical thickness monitoring, since both methods use the same optical arrangement. The reflectance curve produced during photodissolution for a sample fabricated to give a minimum initial reflectance (i.e. deposition stopped at point A in figure 8.8) is shown in figure 8.12. Again strong sinusoidal oscillations are observed starting from the initial low value. This suggests that the disappearing As-S layer is responsible for the sinusoidal variations. If true then the peak-peak distances represent a constant thickness of As-S. In fact a peak-peak, or trough -trough, distance, d is given by

$$d = \lambda/2n \qquad (8.7)$$

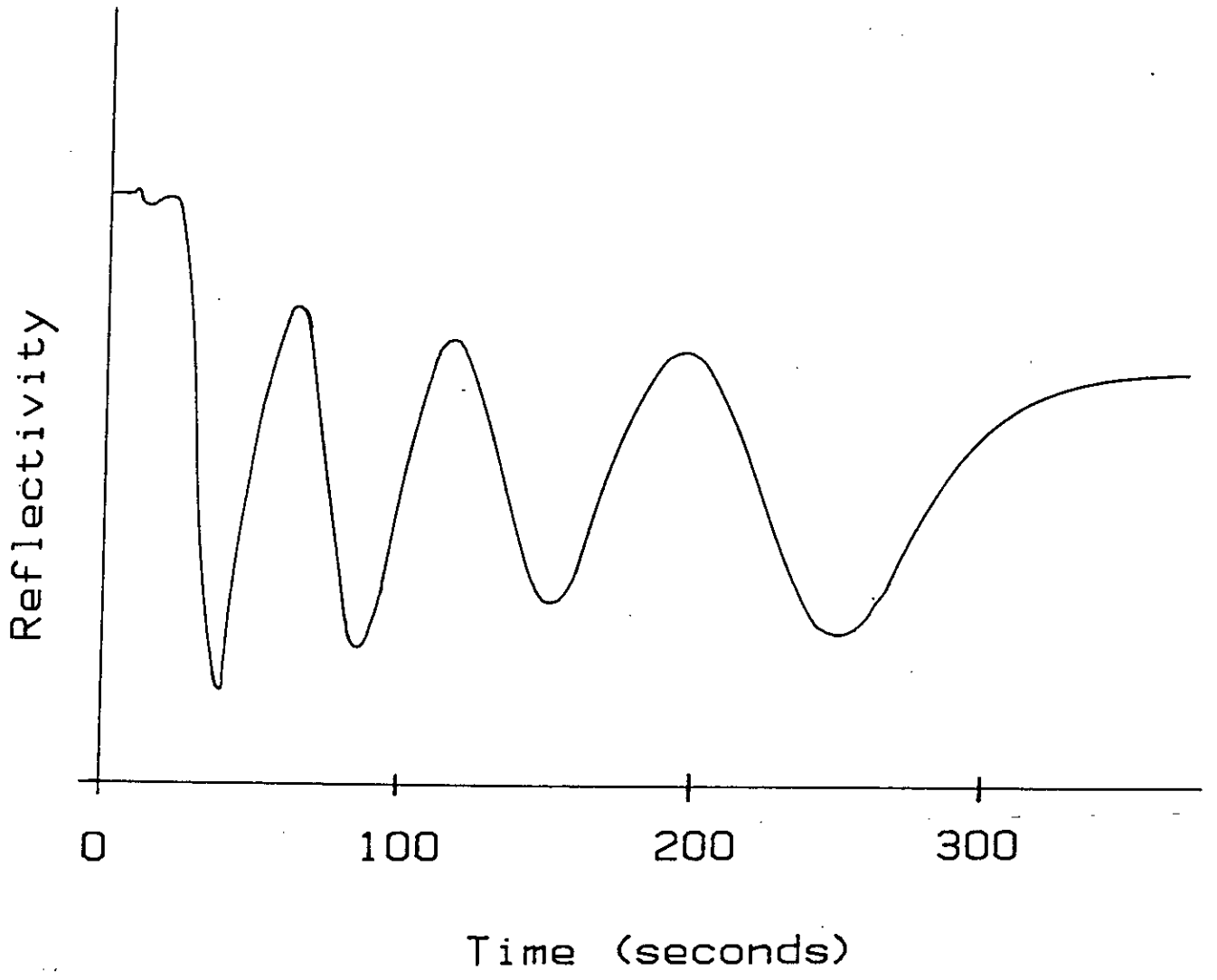

Figure 8.11 Experimentally measured reflectivity curves (for He-Ne laser light) during the photodissolution of Ag in to As-S films.

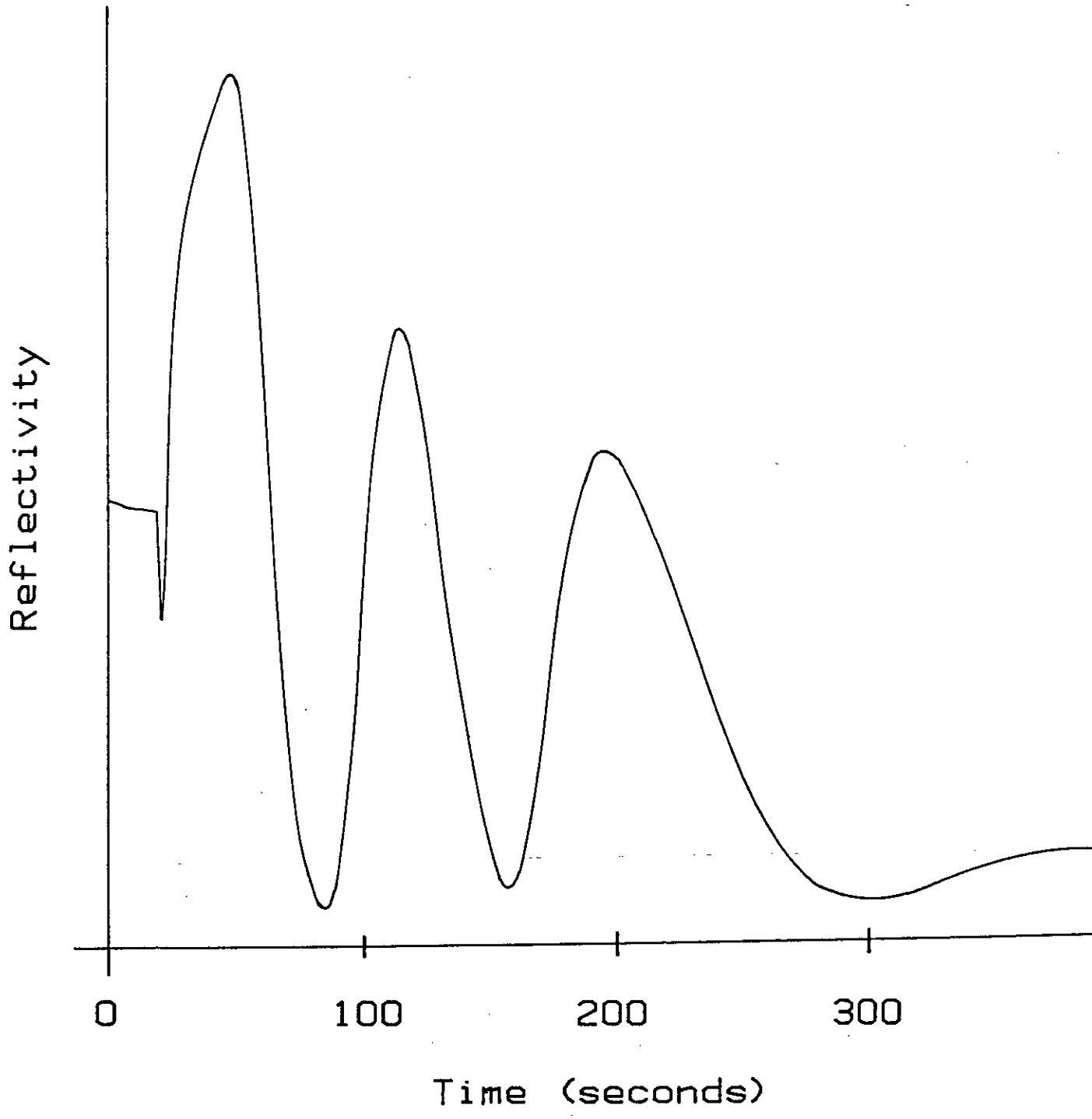

Figure 8.12 Experimentally measured reflectivity curves (for He-Ne laser light) during the photodissolution of Ag in to As-S films. The initial As-S film thickness was tailored to produce an initial minimum in reflectivity (position A, figure 8.8).

where $\lambda = 632.8$ nm and $n = 2.4$.

$$d = 132 \text{ nm}.$$

It is therefore possible to obtain the peak positions from figure 8.11, assume they represent a constant As-S thickness, and thus obtain the rate of disappearance of the As-S layer. The results are shown in figure 8.13, and are in fact plotted as disappearing As-S thickness versus the square root of time. A straight line plot is obtained with a slope of 3.4×10^{-6} cm.sec^{-1} . A $t^{1/2}$ plot is a strong indication that a diffusion process is occurring and therefore the motion of the interface between the As-S and photodoped layer is probably limited by a diffusion process.

8.4.4 Comparison of the experimental results with the optical model

Comparing the experimentally obtained curve (figure 8.11) with the computer curve (figure 8.10) shows that the latter exhibits a more complicated interference behaviour; the experimental curves show a near sinusoidal variation with thickness. This suggests that the optical constants used in the computer model need adjusting. The values used for the As-S layer are known quite accurately and are unlikely to be at fault. It is more likely to be the optical constants of the photodoped layer that need

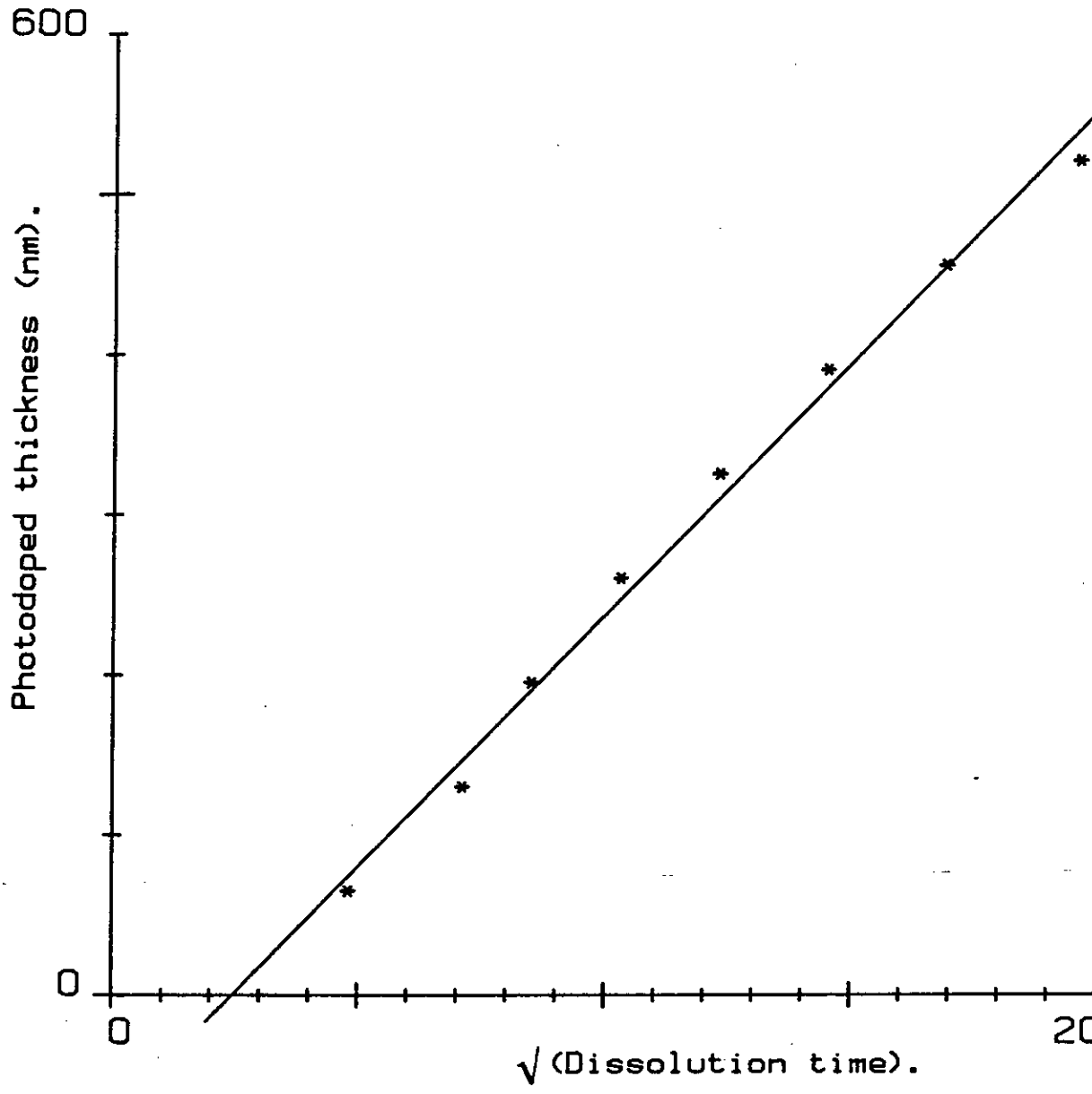

Figure 8.13 A plot of the disappearing As-S film thickness (derived from the interference effects shown in figure 8.11) as a function of the square root of time. The sraight line is a linear fit to the data points.

adjusting. It was shown in figure 7.13 that the absorption edge of the photodoped layer depends strongly on how the photodoped layer is formed. When it is formed from a Ag-rich source (i.e. when a Ag layer is always in contact with the photodoped layers) the optical absorption is much stronger. However, to fit the computer model to the experimental curves a value of k2 which is higher than the value found experimentally is needed. Figure 8.14 shows the computed curve generated using the same values for the optical constants as before, but with k2 changed to 0.7 ($\alpha = 1.4 \times 10^5$ cm^{-1}). It is now in agreement with the experimental curve (figure 8.11).

An explanation is needed as to why the predicted value of k2 is much higher than the value found experimentally. One reason might be sample preparation, for it was always found that when a photodoped layer was formed from a Ag-rich source, the etching process to remove Ag damaged the sample. To produce complete films it was necessary to stop the photodissolution before the As-S film was completely saturated with Ag. However, this would probably only alter the value by a factor of 2, and the actual difference is a factor of 30. Another reason might be that a thin Ag layer is formed at the As-S/photodoped interface. This would also have the effect of increasing the k value. To resolve the question, however, a more complex computer program would be needed since it becomes a three-layer problem.

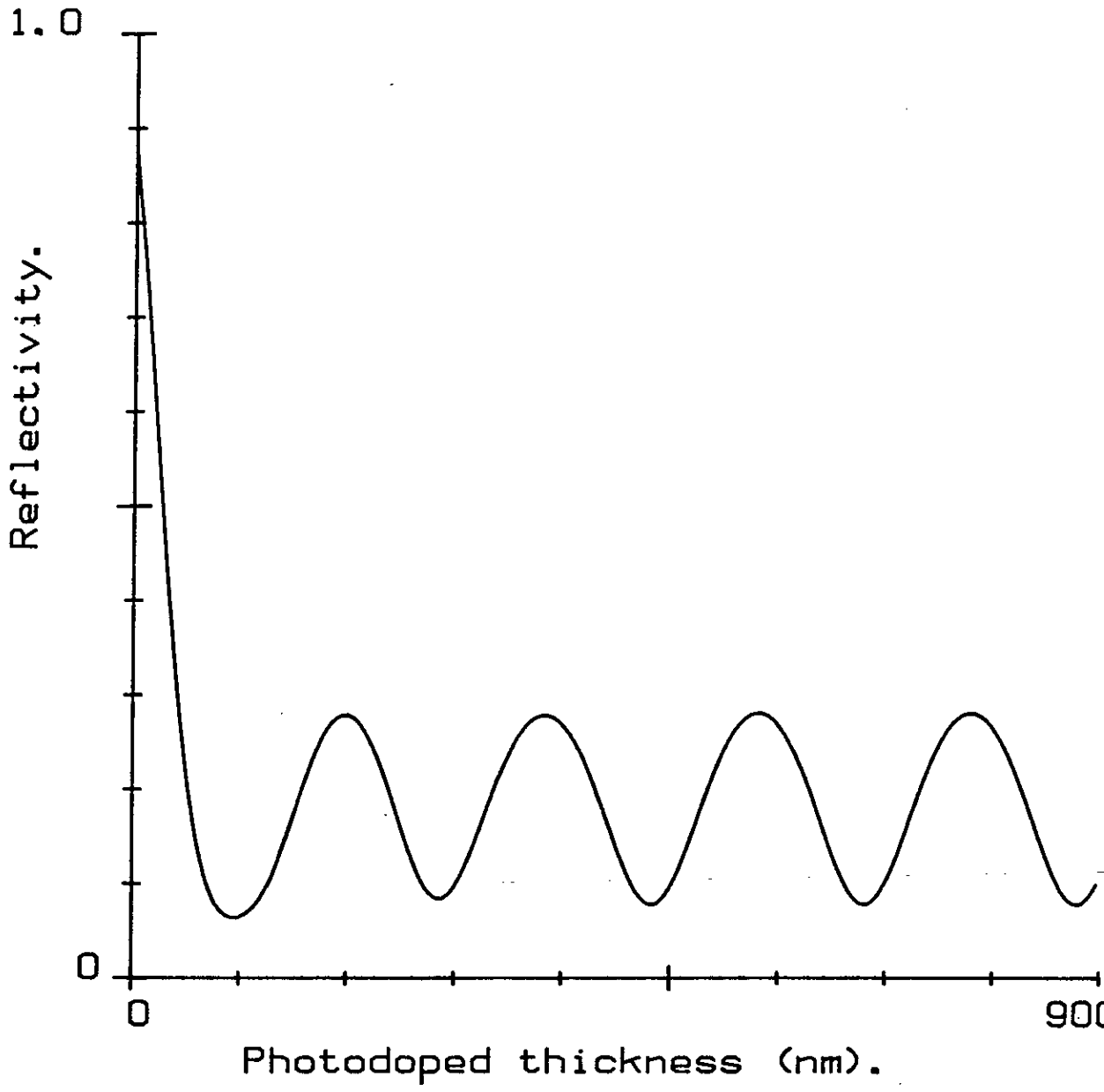

Figure 8.14 A computer generated reflectivity curve (for He-Ne laser light, 632.8 nm) simulating the dissolution of Ag in to As-S films. The optical constants used in the simulation are discussed in the text.

8.5 References

1. Goldschmidt, D. and Rudman, P. S., J. Non-Cryst. Solids, 22, 229, (1976).
2. Heavens, O. S., "Optical Properties of Thin Solid Films", (London: Butterworth Scientific Publications), chpt. 4, (1955).

CHAPTER 9

PHOTODISSOLUTION - A POSSIBLE MECHANISM

9.1 Summary of experimental results

1. After the photodissolution of Ag into an As-S film of composition $As_{30}S_{40}$ a homogenous compound was formed with a structure similar to a bulk Ag-As-S glass (section 7.2).

2. The transmissivity results (section 7.3.1) showed that if the As-S film were photodoped when Ag was in excess the resulting photodoped film was optically much more absorbing than one formed when As-S was in excess.

3. An analysis of the intensity dependence of the rate of photodissolution (section 8.1) in terms of chemical kinetics suggests that the process can be considered as a 1^{st} order chemical reaction. This implies that the photodissolution process is dependent on the concentration of only one photo-excited species.

4. The photodissolution rate was found to be enhanced by an external electric field (section 8.2) and the direction of the field was consistent with the fact that Ag ions form the mobile species that is responding to the light.

5. Lateral dissolution experiments (section 8.3) have shown that photodissolution occurs when light is absorbed at the interface between the photodoped and undoped regions. The interface between the Ag and the As-S layer need not be excited with light. Also, lateral dissolution only occurs on a conducting substrate indicating that the supply of electrons is an important factor in the photodissolution process.

6. From the transverse photodissolution studies (section 8.4) it was found that the (photodoped / As-S) interface moved with a $t^{1/2}$ relationship, which suggests a diffusion limited process.

9.2 Discussion

It was clear from the discussion of the Raman results in chapter 7 that $As_{30}S_{70}$ formed an homogeneous Ag-As-S compound after the photodissolution of Ag. This strongly suggests that the photodissolution process is a photochemical reaction in which Ag reacts with the $As_{30}S_{70}$ film to form a glassy Ag-As-S compound as a product of the reaction. There is a problem, however, with this simple picture in that once the Ag layer has reacted with the As-S layer they will at once be separated from each other by the product of the reaction, so that further reaction will be prevented from taking

place. However if the photodissolution process were similar to the tarnishing reaction of Ag by S, forming Ag_2S, then the continuing progress of the reaction could be explained. The tarnishing reaction between Ag and S is illustrated in figure 9.1 and the mechanism has been fully explained by Wagner (1).

The reaction concerns the formation of a compact layer of material, Mex, between the two reacting species (figure 9.1). The question arises: does the reaction proceed by the migration of X through MeX and react with Me at the interface AB, or does Me migrate through MeX and react with X at the interface CD. Firstly, since Me and X can only migrate in an ionic crystal as ions, either process requires the transport of electrons as well as ions. Tarnishing will not occur if the reaction product MeX has no electronic conductivity. However, the interface which the reaction is most likely to occur at depends more on the relative mobilities of the cations (+ve). In general cations move more easily than anions (see table 2, page 31 ref.1) and therefore reaction at interface CD is more probable than reaction at AB.

This is in fact observed for the system Ag-S and was proven in the following way by Wagner (1). Liquid S is separated from a cylindrical slab of Ag by two slabs of Ag_2S (α -Ag_2S) as shown in figure 9.2. After the reaction had proceeded for one hour at $220^{o}C$, the

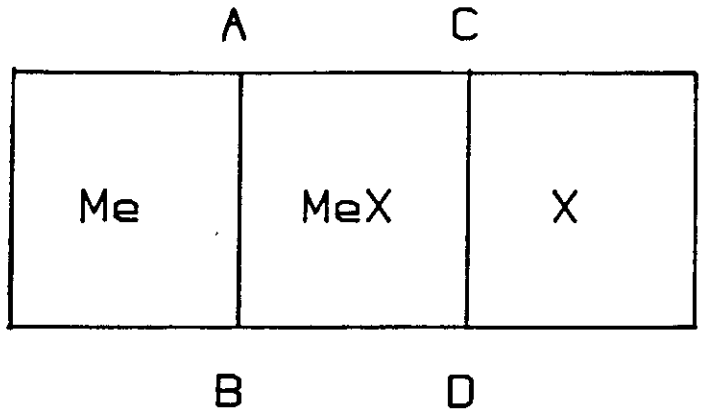

Figure 9.1 The formation of a compact layer of oxide or salt, MeX, between two reacting species.

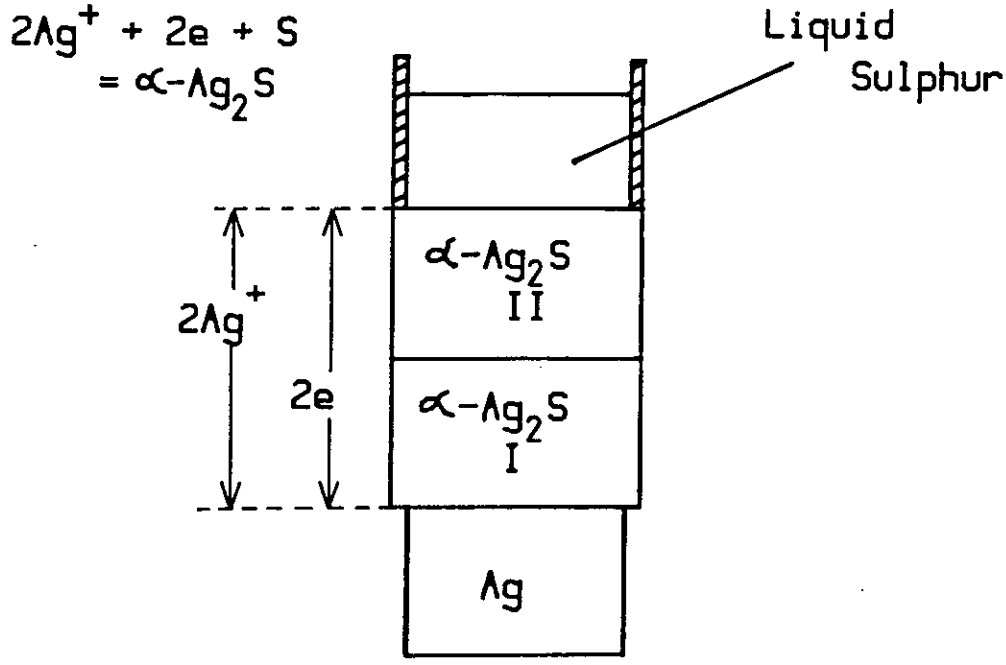

Figure 9.2 The experimental system used by Wagner (1) in determining the Ag-S tarnishing mechanism.

upper slab (II) had increased in weight but the weight of the lower slab (I) was unaltered. Furthermore, the weight increase in slab (II) was paralleled by a chemically equivalent weight decrease in the Ag slab. This proves that Ag diffuses through the sulphide and that the reaction takes place entirely at the Ag_2S-S interface. Since α-Ag_2S is essentially an electronic conductor (above 176°C), electrons pass easily through it and the rate determining process is the diffusion of Ag ions.

The photodissolution process appears to be very similar to the tarnishing process. In the case of $As_{30}S_{70}$ the structure of the photodoped material was found to be similar to that of a bulk Ag-As-S glass (section 7.2) and Kawamoto and Nishida (2) have found these glasses to be Ag-ion conductors. They also concluded that the structural concept of α-Ag_2S can be applied to the glasses. It was also found in this work (section 8.2) that Ag^+ ions were mobile and could be influenced by an externally applied electric field.

Although it is confirmed that the photodoped material is a Ag-ion conductor, its electronic conductivity is not certain and, as explained above, for the tarnishing model to be valid electronic conductivity must exist. Koebel et al (3) have measured the mixed conductivity (ionic and electronic) of Ag_2S at room temperature. Using electrodes of aqueous Ag ions to measure the conductivity of the

Ag_2S sample, they found purely ionic conduction: there was no electronic conduction. However, when one of the electrodes was a bulk Ag contact the same ionic conductivity was found but a considerable electronic conductivity was also observed. It is thought that the bulk Ag contact acts as an electronic donor since the Ag_2S is in equilibrium with excess Ag.

Figure 9.3 illustrates the normal photodissolution process showing the Ag layer separated from the As-S layer by the photodoped material. The resemblance to the tarnishing process can be clearly seen and since the Ag layer is in contact with the photodoped layer, it can be expected, as explained above, that the photodoped layer will be a mixed conductor and allow Ag ions and electrons to flow in opposite directions.

In the tarnishing process described earlier the reaction occurs when Ag ions diffuse through the reaction products and react with S at the interface CD (figure 9.1). This is also the case in the photodissolution process. The lateral dissolution experiments show that photodissolution occurs when light is absorbed at the interface CD (figure 9.3(b)), which is the interface between the photodoped material and the As-S film. From the results of the transverse photodissolution experiments the interface between the photodoped layer and the As-S layer was found to move at a rate governed

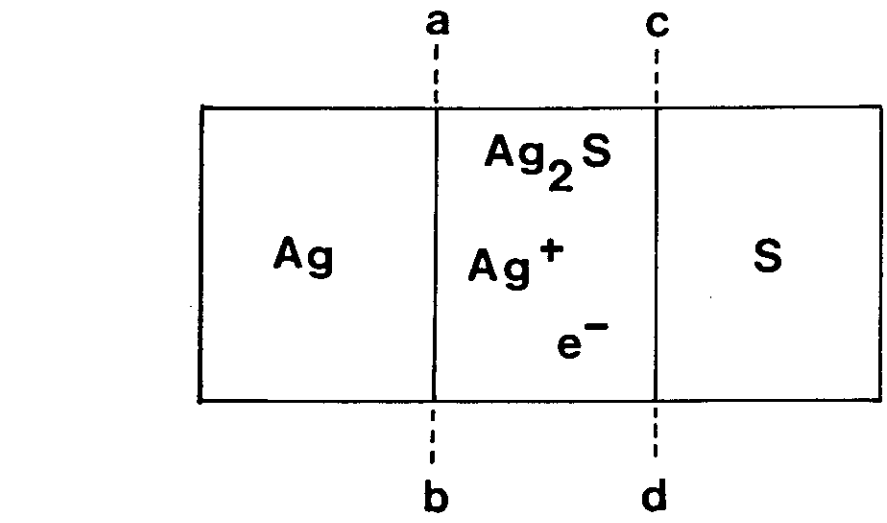

(a)

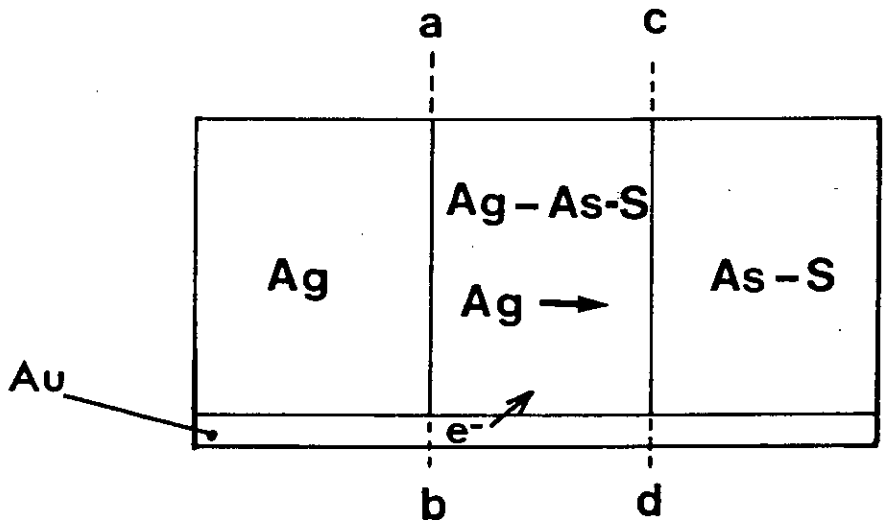

(b)

Figure 9.3 Schematic illustrations comparing the tarnishing and photodissolution processes: (a) the tarnishing of Ag by S and (b) the photodissolution process.

by diffusion of either Ag^+ ions or electrons through the photodoped layer. In the lateral dissolution experiments the interface moved at a much faster rate, and this process is more likely to be limited by the Ag^+ ion mobility since there was an effectively infinite supply of electrons provided by the Au layer. Therefore, in transverse photodissolution, the diffusion limited process is probably due to electrons. The concept of tarnishing, when applied to the photodissolution process, explains how the Ag can be transported as ions through the photodoped layer to the As-S interface, where a photochemical reaction occurs. It does not explain, however, how the illumination, at the interface, causes the photodissolution. A possible mechanism for this is discussed below.

The optical absorption results (section 7.3.2) indicated that a photodoped layer which was formed whilst in contact with an excess Ag layer was optically more absorbing than a layer formed in the case where the Ag film was completely consumed by an excess As-S layer. Also there was considerable tailing of the absorption edge for the more absorbing film. These results can be explained if excess Ag is considered to be present in a photodoped film, with the excess level being maintained by an intimate contact with a Ag layer. Consider again figure 9.3(a), which illustrates a stage during the photodissolution process. It will be assumed that the

photodoped layer has reached the point where it contained the maximum excess of Ag. The glass forming region of the Ag-As-S system (section 2.3.2) is an island region centred around the composition $Ag_{25}As_{25}S_{50}$ and therefore it might be expected that beyond a certain concentration of Ag the photodoped film would become unstable and possibly precipitate Ag. Furthermore the instability might be enhanced by the action of light for it has been reported (4) that bulk glasses of composition $Ag_{45}As_{15}S_{40}$ exhibit an effect termed "Ag photo-deposition" in which a silvery deposit (identified as metallic Ag) is formed on the surface under illumination. Similar effects are reported to occur on the surface of proustite (Ag_3AsS_3) crystals (5) after strong illumination.

It is proposed, therefore, that photodissolution occurs as a result of the photo-deposition of Ag at the interface between the photodoped and undoped regions. The production of Ag at the interface will, however, be limited by the supply of electrons and can be represented by the equation

$$Ag^+ + e^- \rightarrow Ag$$

In As-S compounds the electronic properties are dominated by hole transport. In fact electron transport is not observed in transit measurements (6). It seems that free electrons are immediately trapped at defects, which in

the case of S-rich films are likely to be 3-fold co-ordinated S atoms (referred to as C^{3+} centres). Therefore it is also likely that as soon as a +ve Ag ion combines with an electron at a C^{3+} centre to form metallic Ag, it will spontaneously react with the S atom to form a Ag-S bond. Further reaction would probably then take place resulting in the formation of an homogenous Ag-As-S compound.

This mechanism can, in fact, explain the observed wavelength dependence of the photodissolution process (see section 4.2.2) at wavelengths longer than the absorption edge of the As-S film. The strength of Ag-S bonds is likely to be weaker than that of As-S bonds and therefore lower energy photons are required to break Ag-S bonds. In other words photodissolution is caused by photons interacting with the photodoped layer and not the As-S film. However, the generation of holes and electrons in the As-S film by photoconductivity might play some role in the photodissolution process.

9.3 References

1. Wagner, C., Z. Phys. Chem., 21b, 25, (1933).
2. Kawamoto, Y. and Nishida, M., J. Non-Cryst. Solids, 20, 393, (1976).
3. Koebel, M., Ibl, N. and Frei, A. M., Electrochimica Acta, 19, 287, (1973).

4. Maruno, S. and Kawaguchi, T., J. Appl. Phys., 46, 5312, (1975).

5. "Encyclopedia of Minerals and Gemstones", edited by M. O'Donoghue, (Orbis Publishing London), p.170, (1976).

6. Ing, Jr, S. W., Neyhart, J. H. and Schmidlin, F., J. Appl. Phys., 42, (1971).

CHAPTER 10

CONCLUSIONS AND SUGGESTIONS FOR FURTHER WORK

10.1 Conclusions

10.1.1 Photodarkening in As-S compounds

It has been found that the reversible part of the photodarkening effect observed in As-S films, thin bulk samples and glassy powders is accompanied by an increase in the Raman band with its maximum at 231 cm^{-1}. This was interpreted as an increase in the As-As bond density as a result of illumination. This experimental evidence supports previous speculative suggestions about bond redistribution or a photolytic chemical reaction connected with photodarkening. The actual state of chemical bond redistribution depends on the intensity and wavelength of illumination and also on the temperature of the film. Photodarkening is a dynamic process which has an equilibrium position which can be shifted by changes of temperature and conditions of illumination. This interpretation gives a structural meaning to the double-well model. It also predicts the increase in volume of illuminated films.

10.1.2 Photodissolution of Ag into As-S compounds

Raman results suggest that photodoped as-evaporated films of As_2S_3, $As_{38}S_{62}$ and $As_{20}S_{80}$ are phase separated whereas photodoped $As_{30}S_{70}$ films are homogeneous and have a structure similar to that of a bulk glass within the central region of glass formation and close to the Ag-$As_{30}S_{70}$ tie line. Therefore compositions in the approximate range $As_{36}S_{64}$ to $As_{28}S_{72}$ would be expected to form a homogeneous Ag photodoped phase since their tie lines pass through the central region of glass formation.

Kinetic experiments have shown that the photodissolution process is a 1st order chemical process and that the mobile species are Ag^+ ions. Also, results which concern the migration of Ag atoms which occurs when photodissolution is carried out on a conducting substrate, indicate that the actinic radiation is absorbed in the photodoped layer, close to the interface between the doped and undoped regions. A mechanism based on the tarnishing process has been found to be appropriate in explaining the photodissolution process.

10.2 Further work

Raman scattering was found to be a useful technique for investigating the photodarkening effect. Further experiments could therefore be carried out on other chalcogenide systems which exhibit photodarkening. It could be applied to the As-Se, Ge-Se and Ge-S systems and also pure Se.

Similar remarks apply to metal photodissolution. Raman spectroscopy proved useful in identifying the products that are formed after photodoping and the technique could therefore be used to look at metal photodoping in other chalcogenide systems.

A particular problem with Raman scattering from thin films is the weak Raman signal due to the small analysing volume that is used. A possible way to improve the situation and increase the Raman signal is to use a prism-coupling technique, such as is commonly used in the field of integrated optics.

More photodissolution kinetics experiments could be performed, in particular the temperature dependence of the photodissolution rate could be investigated. Both the lateral and transverse photodissolution arrangements could be used. It would be important however to separate out the different stages of dissolution so that, for

example, an activation energy for the latter diffusion process could be found.

Further experiments might include investigating the effect of pre-heating (annealing) and pre-illumination of the As-S or the Ag/As-S combination prior to photodissolution. Again the lateral and transverse experimental geometries could be used.

Finally, ways of improving the photodissolution sensitivity could be investigated. This is of particular importance when applying the photodissolution process to industrial applications, such as photoresist technology in microlithography. Ways of doing this might include modifying the chalcogenide. For example, if ionic conductivity of the photodoped region is important, adding small amounts of iodine would enhance the ionic conductivity and possibly enhance photodoping sensitivity. Another might involve using a more reactive metal such as Cu or, to tailor sensitivity, a Cu/Ag alloy.

APPENDIX I

This appendix lists a computer program that was used to calculate film thickness based on the frequency change of an oscillating quartz crystal. Equation (5.1) descibes the relationship for obtaining film thickness as a function of frequency shift. It can also be rearanged to give the frequency shift for a required film thickness and this was also incorporated in to the program.

```
10   MODE 7
20   CLS
30   G=6E6:REM For 6 MHz crystals
40   PRINT:PRINT
50   INPUTTAB(0,3)"Present frequency  "F
70   INPUT ' "Density (g/cm3)    "P
80   C=2.21*1E-6
90   U=(1/F)-(1/G):X=U/(C*P)
100  L=X*1E8
110  W=L
120  PRINT ' "Frequecy change or thickness"
130  A$=GET$
140  IF A$="T" THEN 200
150  INPUT ' "Thickness (anstroms)   "T
160  L=L+T:L=L*1E-8
170  S=1/((C*P*L)+(1/G))
175  PRINTTAB(0,12)
180  PRINT "End Frequency (Hz)  "S
```

```
190  GOTO 250
200  INPUT ' "End Frequency  (Hz)   "Z
210  U=(1/Z)-(1/G):X=U/(C*P)
220  Y=X*1E8
230  Y=Y-W
235  PRINTTAB(0,12)
240  PRINT ' "Thickness (anstroms) ";Y
250  PRINT TAB(10,20) "Again (Y/N)"
260  A$=GET$
270  IF A$="Y" THEN 20
280  END
```

APPENDIX II

In this appendix a computer program is listed which was used to obtain the absorption coefficient of a thin film from measurements of its transmissivity. The program is based on a method outlined by Dan Goldschmidt, J. Opt. Soc. Am. A., Vol 1, No. 3, (1984). The Optical constants used in the program are discussed in section 7.3.

```
 10  n0=1 : REM Refractive index of air
 20  INPUT"wavelength (nM)   "W
 30  INPUT"Film index  "n1
 40  INPUT"Film thickness  "d
 50  INPUT "Substrate index "n2
 60  W=W*1E-7 : d=d*1E-7
 80  INPUT"absorption coefficient (cm-1) a "a
 90  R01=((n0-n1)/(n0+n1))^2
100  R12=((n1-n2)/(n1+n2))^2
110  R20=((n2-n0)/(n2+n0))^2
130  A=(1-R01)*(1-R12)*(1-R20)*EXP(-a*d)
140  B=(1-R12*R20):K=(2*PI*n1)/W
150  C=2*SQR(R01*R12)*(1-R20)*EXP(-a*d)*COS(2*K*d)
160  D=R01*(R12-R20)*EXP(-2*a*d)
190  T=A/(B-C+D)
200  PRINT ' "d ";d
210  PRINT ' "transmissivity is ";T '
220  GOTO80  : REM  try  another  "a"  value  if
          transmissivity not equal to measured value.
```

APPENDIX III

This appendix lists the computer program that was used to calculate the reflectivity of two absorbing film layers on an absorbing substrate. It represents an optical model of the photodissolution of Ag in to As-S films. The optical constants used in the program are discussed in section 8.4.2.

```
 10  DIM X(500),Y(500)
 20  @%=131594
 30  j=0
 40  MODE4
 50  n0=1
 60  PRINT:PRINT
 70  dAg=500      :REM Ag film thickness
 80  d1=700:st=10:REM As-S film thickness and step size
 90  dd=d1
100  n1=2.4:k1=0       :REM As-S film
110  n2=2.75:k2=0.025 :REM Photodoped film
120  n3=0.5:k3=3       :REM Ag film substrate
130  w=0.6328E-4       :REM wavelength of He-Ne laser
140  ra=2
150  CLG
155  REM VDU display routine
160  DRAW 0,1023:DRAW 1279,1023:DRAW 1279,0:DRAW 0,0
170  ST=st+(st/ra)
180  D1=(d1+(d1/ra))
```

```
190  F=1279/D1
210  FOR d2=0 TO D1 STEP ST
220  IF d2 >= (dAg+ra*dAg) THEN 380
240  d1=d1*1E-7:d2=d2*1E-7
250:
260  PROCfilm1
270  PROCfilm2
280:
285  PRINT TAB(0,1),k2
290  d1=d1*1E7:d2=d2*1E7
300  j=j+1
310  X(j)=d2:Y(j)=R2
320  X=F*d2:Y=R2*1023
330  DRAW X,Y
340  d1=d1-st
350  NEXT d2
360  REM : routine for saving data on disc
380  PRINT"Do you want to create a file?"
390  A$=GET$
400  IFA$="N" THEN END
410  INPUT"File name "A$
420  F=OPENOUT(A$)
430  FOR J=1 TO j
440  PRINT £F,X(J),Y(J)
450  NEXT J
460  CLOSE£F
475  PRINT "d1= ",dd
477  PRINT"no  of points= ",j : END
```

```
520  DEF PROCfilm1
530  C=(n0+n1)^2+k1^2
540  g1=(n0^2-n1^2-k1^2)/C
550  h1=(2*n0*k1)/C
560  C=(n1+n2)^2+(k1+k2)^2
570  g2=(n1^2-n2^2+k1^2-k2^2)/C
580  h2=(2*(n1*k2-n2*k1))/C
590  C=(2*PI*d1)/w
600  a1=C*k1:y1=C*n1
610  p2=EXP(a1)*COS(y1)
620  q2=EXP(a1)*SIN(y1)
630  t2=EXP(-a1)*(g2*COS(y1)+h2*SIN(y1))
640  u2=EXP(-a1)*(h2*COS(y1)-g2*SIN(y1))
650  p12=p2+g1*t2-h1*u2
660  q12=q2+h1*t2+g1*u2
670  t12=t2+g1*p2-h1*q2
680  u12=u2+h1*p2+g1*q2
690  R1=(t12^2+u12^2)/(p12^2+q12^2)
700  ENDPROC
```

```
760  DEF PROCfilm2
770  C=(n2+n3)^2+(k2+k3)^2
780  g3=(n2^2-n3^2+k2^2-k3^2)/C
790  h3=(2*(n2*k3-n3*k2))/C
800  C=(2*PI*d2)/w
810  a2=C*k2:y2=C*n2
820  p3=EXP(a2)*COS(y2):q3=EXP(a2)*SIN(y2)
830  t3=EXP(-a2)*(g3*COS(y2)+h3*SIN(y2))
840  u3=EXP(-a2)*(h3*COS(y2)-g3*SIN(y2))
850  r2=EXP(a1)*(g2*COS(y1)-h2*SIN(y1))
860  s2=EXP(a1)*(h2*COS(y1)+g2*SIN(y1))
870  v2=EXP(-a1)*COS(y1)
880  w2=-EXP(-a1)*SIN(y1)
890  r12=r2+g1*v2-h1*w2
900  s12=s2+h1*v2+g1*w2
910  v12=v2+g1*r2-h1*s2
920  w12=w2+h1*r2+g1*s2
930  p13=p12*p3-q12*q3+r12*t3-s12*u3
940  q13=q12*p3+p12*q3+s12*t3+r12*u3
950  t13=t12*p3-u12*q3+v12*t3-w12*u3
960  u13=u12*p3+t12*q3+w12*t3+v12*u3
970  R2=(t13^2+u13^2)/(p13^2+q13^2)
980  ENDPROC
```

APPENDIX IV

PUBLISHED WORK

1. "Structural changes in amorphous arsenic sulphide films on photodoping with silver studied by Raman spectroscopy", "The Structure of Non-Crystalline Materials, 1982", edited by P. H. Gaskell, J. M. Parker and E. A. Davies (London: Taylor and Francis), p.286, (1983).

2. "A model for photostructural changes in the As-S system", J. Non-Crystalline Solids, 59&60, 921, (1983).

3. "Reversible photodarkening and structural changes in As_2S_3 thin films", Phil. Mag. B, 50, 463, (1984).

STRUCTURAL CHANGES IN AMORPHOUS ARSENIC SULPHIDE FILMS ON PHOTODOPING WITH SILVER STUDIED BY RAMAN SPECTROSCOPY

A.P. Firth, P.S. Ewen* and A.E. Owen

Department of Electrical Engineering, University of Edinburgh, King's Buildings, Edinburgh EH9 3JL, UK

**Department of Physics, University of Edinburgh, James Clerk Maxwell Building, Edinburgh EH9 3JL, UK*

ABSTRACT

Raman spectroscopy has been used to study the structural changes occurring in films of As-S glasses of compositions $As_{41}S_{59}$, $As_{38}S_{62}$, $As_{30}S_{70}$ and $As_{20}S_{80}$, after photodoping with Ag. Only the photodoped film of composition $As_{30}S_{70}$ produced a single-phase homogenous material. In the other photodoped compositions there is evidence of phase separation. An explanation of these observations is given.

1. INTRODUCTION

The phenomenon known as metal photodoping is one of a variety of photostructural effects which are known to occur in chalcogenide glasses, and although widely studied there is no complete physical model for the photodoping mechanism. In recent years interest in metal photodoping has increased considerably because of its potentially important applications in submicron photolithography (Janai 1981). This paper reports on an investigation, based on Raman spectroscopy, of the photodoping of films of As-S glasses with silver.

2. EXPERIMENTAL

Films of As-S glasses, of thickness up to 5 μm and with stoichiometries ranging from As_2S_3 to As_2S_8, were prepared by vacuum evaporation. The compositions of the deposited films were determined by electron probe microanalysis, and the compositions quoted are accurate to within ±0·5 atom per cent.

The photodoping experiments were carried out as follows. Half the area of a glass slide was first coated with a layer of Al. The whole area was then coated with an evaporated layer of Ag, 0·5-1·0 μm thick, followed by the As-S glass layer, 5-8 μm thick. The purpose of the Al film was to provide a reflective layer with low Raman scattering. Samples were then exposed to a 500 W projector lamp which was cooled by a fan to prevent heat reaching the sample. As the slide was only half covered with Al it was possible to see when all the Ag had dissolved into the chalcogenide film. When the photodoping was complete the film was etched in alkaline solution to remove the undoped As-S layer. The final thickness of the (Ag-doped) As-S film was in the range 1·5-3·5 μm. Conventional back-reflection scattering was used to obtain the Raman spectra with the 6764 Å line from a Kr ion laser (Firth *et al.* 1981).

3. RESULTS

In Figure 1, curves A and B are the spectra of As-S film of composition $As_{41}S_{59}$ and $As_{38}S_{62}$, respectively. The sharp features of these spectra are attributed to molecular units of As_4S_4, and the feature at 491 cm^{-1} to the symmetric stretching mode of S-S bonds (Nemanich *et al.* 1978). Spectra C and D in Figure 1 are of the Ag photodoped films corresponding again to the original compositions $As_{41}S_{59}$ and $As_{38}S_{62}$, respectively (i.e., as in curves A and B). These two spectra are similar, each having two broad Raman bands in the regions 150-300 cm^{-1} and 300-400 cm^{-1}. Curve E in Figure 1 is the Raman spectrum of amorphous As, and this closely matches the band in the 150-300 cm^{-1} region in spectra C and D. The other band, in the region 300-400 cm^{-1} in curves C and D, is probably due to amorphous Ag-As-S phases, as it

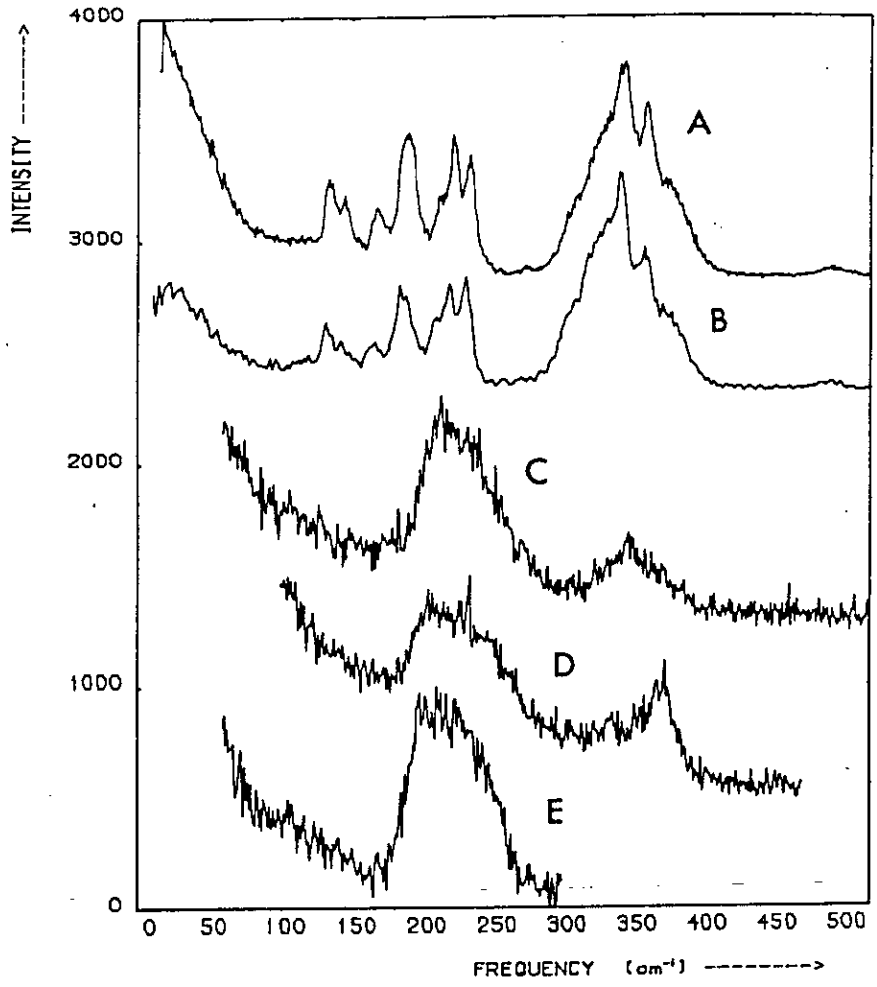

Figure 1. Raman spectra of films of composition $As_{41}S_{59}$ (curve A) and $As_{38}S_{62}$ (curve B). Curves C and D are the spectra for Ag photodoped $As_{41}S_{59}$ and $As_{38}S_{62}$, respectively. Curve E is the Raman spectrum of amorphous As.

is known that bulk glasses in the Ag-As-S system have strong Raman bands in the same spectral region (Firth *et al.* 1981).

Curve A in Figure 2 is the Raman spectrum for a film of composition $As_{30}S_{70}$, which agrees well with that of a bulk glass of the same composition (Ewen 1978). The features in the region 425-525 cm^{-1} are attributed to S in S_8 rings and S-S bonds in linear As-S_n-As linkages. Curve B is the Raman spectra of the Ag photodoped material.

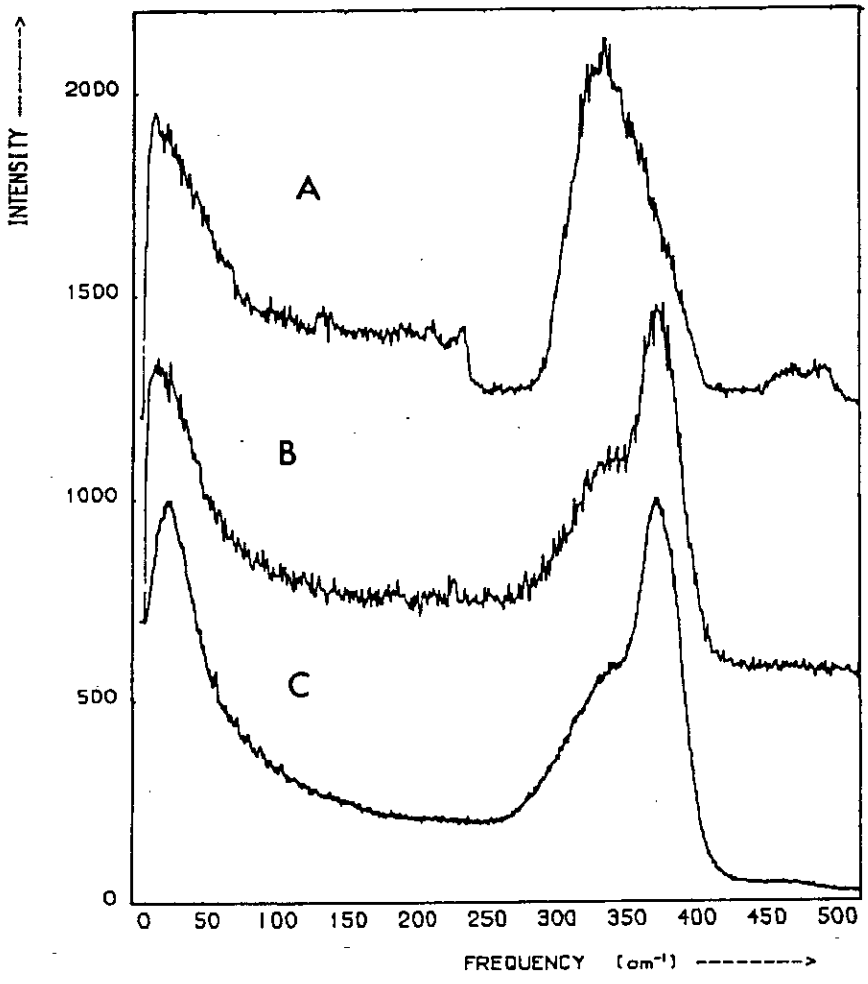

Figure 2. Raman spectra of films of composition $As_{30}S_{70}$ (Curve A). Curve B is the spectrum of Ag photodoped $As_{30}S_{70}$. Curve C is the spectrum of a bulk Ag-As-S glass of composition $Ag_{30}As_{22}S_{48}$.

It has a broad spectrum and comparison with the spectrum of a bulk glass of composition $Ag_{30}As_{22}S_{48}$, shown in curve C, suggests that the photodoped film has the same structure.

In Figure 3, curve A is the Raman spectrum of a film of composition $As_{20}S_{80}$, and again this is very similar to the spectrum of a bulk glass of the same composition (Ewen 1978). The sharp features are due to the vibrations of distorted S_8 rings. The Raman spectrum of the Ag photodoped film (curve B) has a very broad band in the region

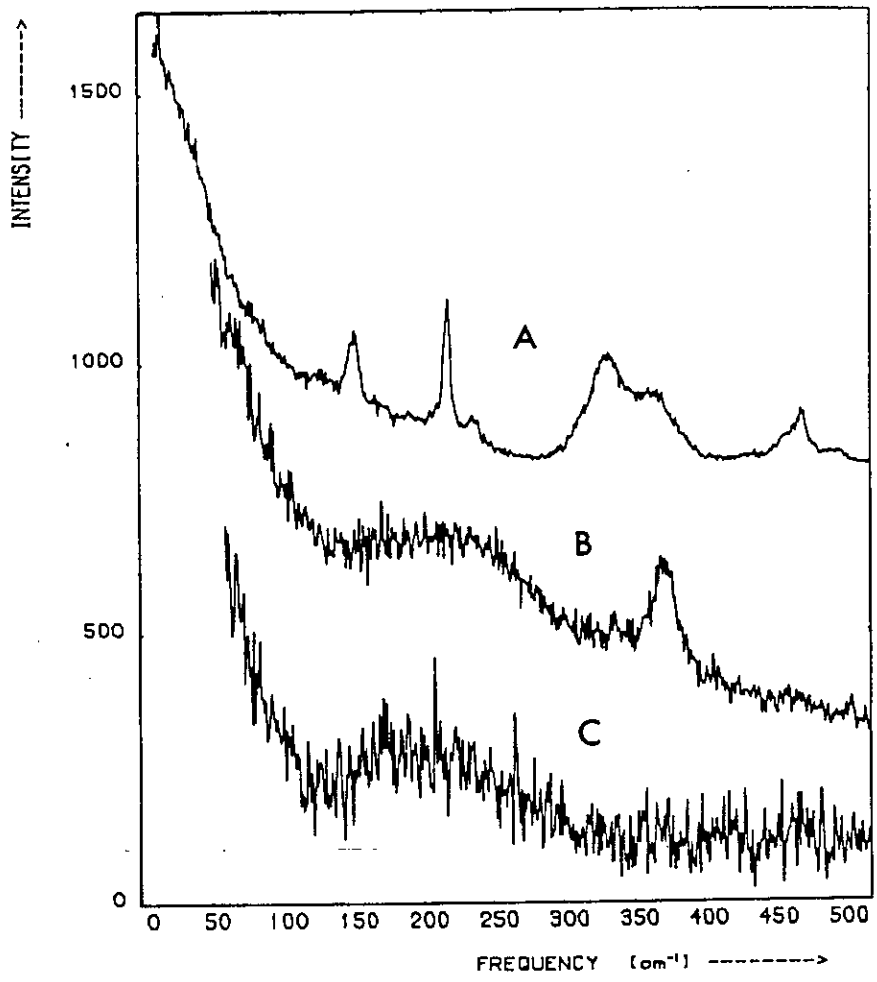

Figure 3. Raman spectra of films of composition $As_{20}S_{80}$ (curve A). Curve B is the spectrum for Ag photodoped $As_{20}S_{80}$. Curve C is the spectrum of a Ag_2S film formed by reacting S vapour with a Ag film.

100-300 cm^{-1} and a relatively sharp feature at 350-400 cm^{-1}. The other spectrum (curve C) was obtained from a film of Ag_2S formed by reacting S vapour with a Ag film which was about 0·5 μm thick. A comparison of spectra B and C suggests that Ag_2S is present in the photodoped As-S film, which was originally $As_{20}S_{80}$. The band between

350-400 cm^{-1}, formed during the course of the experiment, probably arises from the formation of a Ag-As-S glassy phase.

4. DISCUSSION

Figure 4 illustrates the phase diagram for the Ag-As-S system and it shows the principal crystalline compounds as well as the glass-forming regions determined by Kawamoto *et al.* (1974). Also drawn

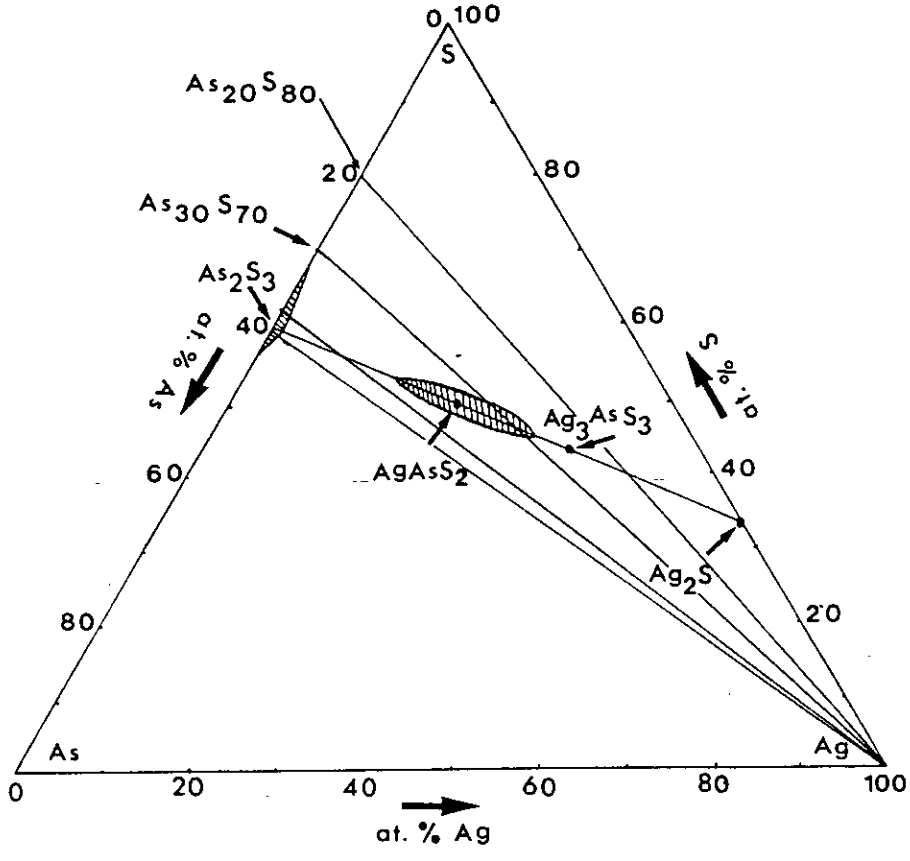

Figure 4. Phase diagram of the Ag-As-S system showing the compositions investigated in this paper and some of the knonw ternary compounds. Cross-hatching indicates glass-forming regions.

on the diagram are tie lines joining elemental Ag with four As-S compositions studied in this work (the composition $As_{41}S_{59}$ is taken to be approximately As_2S_3). As the photodoping proceeds the resulting overall composition must move along these tie lines. Of those four lines, only the one joining Ag with $As_{30}S_{70}$ intersects the central glass-forming region. This is in accord with Raman results which show that Ag photodoped $As_{30}S_{70}$ has a structure very similar to that of a bulk glass within the central region of glass formation and close, in composition, to the Ag-$As_{30}S_{70}$ tie line (Firth *et al.* 1981). It is possible therefore that in this case the Ag photodoped film remains a homogeneous, uniform phase.

The tie lines joining Ag with $As_{41}S_{59}$ (As_2S_3) and $As_{38}S_{62}$ are on the As-rich side of the central glass-forming region but they do not intersect it. The Raman results indicate that amorphous As and an amorphous Ag-As-S phase, corresponding in structure to a composition within the glass-forming region, are present in the photodoped material. This implies that when the overall photodoped composition lies outside the glass-forming region, the photodoping also involves a process of phase separation. The evidence is that the Ag-As-S component which is formed is actually within the glass-forming region and that excess As is precipitated, probably in an amorphous form.

For the system Ag-$As_{20}S_{80}$ the tie line also does not intersect the central glass-forming region. In this case, the Raman results suggest that initially, Ag_2S is formed (although it is by no means certain that it is stoichiometric Ag_2S), and only after prolonged exposure is there a further photoinduced effect towards the formation of a glassy Ag-As-S phase.

It is premature to extrapolate the latter observation (i.e., Ag_2S formation) to the whole system, but in general the results of this work do suggest that the photodoping process is a two-stage solid-state reaction. The initial reaction may be between Ag and S in As-S films and it should be noted here that even in stoichiometric glassy As_2S_3, -S-S- bonds are present (Ewen 1978). It is imagined that these homopolar -S-S- bonds are involved in the initial reaction. The second reaction is between Ag_2S and the remaining As-S matrix.

This reaction will proceed only if the reaction products are more stable than the reactants. It is likely that this will be so if the reaction products are within, or close to, the central glass-forming region. The structure of Ag-As-S glasses is based on AsS_3 pyramids joined by -S-Ag-S- linkages (Kawamote *et al.* 1974; Firth *et al.* 1981), so that very little structural rearrangement is required in the second reaction.

ACKNOWLEDGMENTS

The authors gratefully acknowledge the help of research grants from the Science and Engineering Research Council, and the co-operation of Dr. W. Taylor of the Physics Department of Edinburgh University in making available the experimental facilities for Raman spectroscopy.

REFERENCES

EWEN, P.J.S., 1978, *The Raman Spectra and Structure of Glasses in the Arsenic-Sulphur and Arsenic-Selenium Systems* (Ph.D. Thesis, University of Edinburgh), pp. 143-175.

FIRTH, A.P., OWEN, A.E. & EWEN, P.J.S., 1981, *Journal de Physique*, 42, Colloque C4, Suppl. No. 10, 903-906.

JANAI, M., 1981, *Journal de Physique*, 42, Colloque C4, Suppl. No.10, 1105-1113.

KAWAMOTO, Y., AGATA, M. & TSUCHIHASHI, S., 1974, *Journal of the Ceramics Association of Japan*, 82, 502-507.

NEMANICH, R.J., CONNELL, G.A.N., HAYES, T.M. & STREET, R.A., 1978, *Physical Review B*, 18, 6900-6918.

Journal of Non-Crystalline Solids 59 & 60 (1983) 921-924
North-Holland Publishing Company

A MODEL FOR PHOTOSTRUCTURAL CHANGES IN THE AMORPHOUS As-S SYSTEM

M. FRUMAR*, A.P. FIRTH and A.E. OWEN

Department of Electrical Engineering, University of Edinburgh, King's Buildings, Edinburgh EH9 3JL, Scotland, U.K.
* On leave from University of Chemical Technology, 53210 Pardubice, Czechoslovakia.

The photodarkening effect was studied in thin film, bulk glasses and powdered glasses of composition $As_{29}S_{71}$, $As_{40}S_{60}$ and $As_{42.5}S_{57.5}$. The amount of photodarkening produced in a sample depended strongly on the samples state and composition as well as temperature, incident light intensity and wavelength. Using Raman spectroscopy, vibrational bands at 231 and 491 cm^{-1} (assigned to As-As and S-S bond vibrations) were found to be enhanced in photodarkened samples. We present a model in which photodarkening is due to the formation of As_n clusters ($n \geq 2$) which are loosely coupled to the amorphous network.

1. INTRODUCTION

Reversible photostructural changes are of current interest because they still require fundamental understanding. They also have technological applications in high density optical storage devices and in micro-photolithography.

In this paper photodarkening was studied in stoichiometric (As_2S_3) and non-stoichiometric As-S samples. The form of the samples were thin films, bulk glassy solids and glassy powders.

2. EXPERIMENTAL

The composition of the samples studied, in each form were $As_{40}S_{60}$, $As_{42.5}S_{57.5}$ (referred to as As rich) and $As_{29}S_{71}$ (referred to as S rich). The thin films were prepared by conventional vacuum evaporation, the details of which are given in references 1 to 3; further information on the preparation of the bulk samples and powders is given in reference 3. The samples were photodarkened by a 500 W tungsten lamp, an Ar ion laser (λ = 514.5 nm) or a Kr ion laser (λ = 488.0, 530.9 or 568.2 nm). Details of the illumination conditions and Raman experiments are also given in references 1 to 3.

3. RESULTS AND DISCUSSION

For a given sample, the change of optical properties during illumination depended on temperature, incident light intensity and wavelength. As illustrated in figures 1 and 2, changing the conditions of illumination also changed the optical density of the sample. Increasing the intensity of

0022-3093/83/0000–0000/$03.00

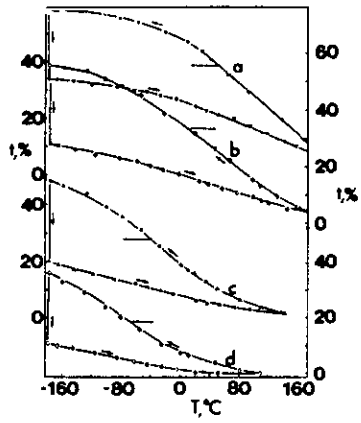

FIGURE 1
Temperature dependence of transmissivity of As_2S_3 films (measured at λ = 530 nm (a), 520 nm (b), 510 nm (c), 500 nm (d). Vertical lines describe the change produced by illumination (W lamp, 1 hour)

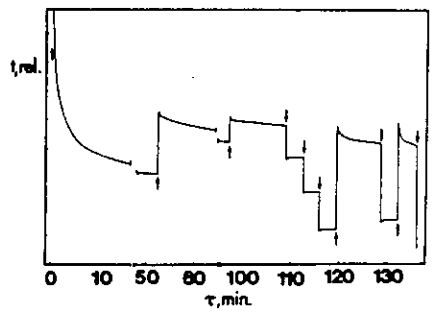

FIGURE 2
Change of transmissivity of As_2S_3 films under illumination by Ar laser (514.5 nm). Vertical lines correspond to the change of intensity of laser light.

incident light produced further photodarkening and its decrease caused some bleaching (figure 2). The optically induced changes in transmissivity were generally larger at lower temperatures (figure 1).

The reversible photodarkening effect in As-S thin films and bulk glasses was accompanied by changes in the intensities of selective Raman bands, indicating changes of local structure. An example is given in figures 3 and 4. It is clear that the photodarkening has enhanced the 231 cm^{-1} and 491 cm^{-1} Raman bands. The 231 cm^{-1} band has been assigned to As-As vibrations[4,5,6]. The Raman spectrum of a-As[4] has a broad Raman band with its maximum near 231 cm^{-1} and is attributed to As_4 pyramid vibrations[7]. The 491 cm^{-1} band corresponds to S-S vibrations and its intensity in bulk As-S samples increases with S content[4]. On annealing (210°C, $\tau \geq 2$ hrs.), the original (unilluminated) state of the photodarkened samples was restored. All annealed samples had identical optical properties to their previous unilluminated state.

Photodarkening enhances both As-As and S-S vibrational bands and we assume that this corresponds to an increase in As-As and S-S bond densities respectively. Thus illumination can change the densities of chemical bonds in amorphous As-S samples. An equation describing this process is of the form:

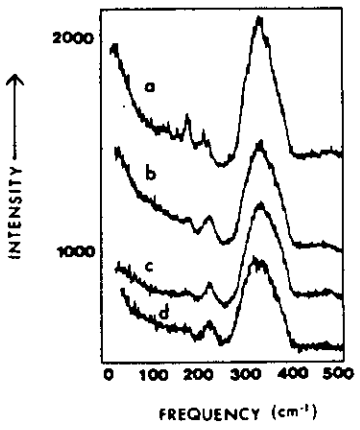

FIGURE 3
Raman spectra of As_2S_3 films photodarkening and excitation of Raman spectra by 568.2 nm (b), 530.9 nm (c), 488 nm (d), (a) annealed sample (λ_{exc} = 647.1 nm).

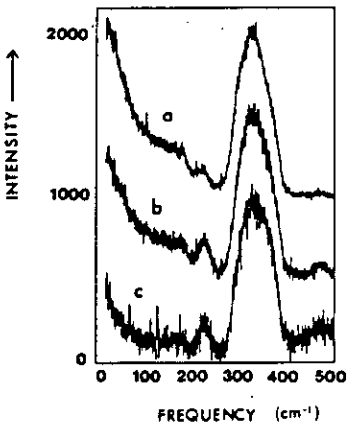

FIGURE 4
Raman spectra of glassy As_2S_3 powders (a) T = 300 K, exciting line 568.2 nm, (b) T = 75 K, exciting line 568.2 nm, (c) T = 75 K, exciting line 530.9 nm.

$$2\ [\text{As-S}] \underset{I_2,h\nu_2,A(T)}{\overset{I_1,h\nu_1}{\rightleftharpoons}} [\text{As-As}] + [\text{S-S}] \qquad (1)$$

where I_i is the incident light intensity ($I_1 > I_2$), $h\nu_i$ is the incident light energy ($h\nu_2 \geq h\nu_1$; $h\nu_1$ = energy gap), A(T) indicates thermal annealing at a temperature T, driving the system back towards its original state which is closer to thermodynamic equilibrium. The rate of annealing (bleaching) is considerably reduced at lower temperatures, but increases rapidly with temperature. The largest change of optical transmissivity and of Raman band intensities (231 and 491 cm^{-1}) were therefore obtained by illuminating at low temperatures. At temperatures near Tg no optical change could be produced and photodarkened samples were completely bleached. In samples in which the photodarkened state had saturated, the actual densities of [As-As], [S-S] and [As-S] bonds are determined by temperature, condition of illumination (I,$h\nu$), chemical composition and state of the sample (bulk glass, thin films or powders).

We suggest that photodarkening is due to the photoinduced increase in the density of [As-As] bonds. The As atoms probably form clusters (As_n; $n \geq 2$) which are loosely coupled to the amorphous network. Since As-As bonds are longer than As-S bonds photodarkening is expected to produce an increase in

thickness (volume) of thin films, and this has been observed experimentally. Furthermore, in bulk samples the formation of As_n clusters takes place under the constraint of the surrounding amorphous network, and consequently it is more difficult to photodarken bulk samples (particularly at room temperature, where thermal annealing is high). However we suppose that the formation of As_n clusters is more favourable near to voids or defects where there is free volume and no large surrounding constraint. There are a larger number of defects and voids in evaporated films and powdered glasses and the photodarkening is very much larger than in the corresponding bulk samples of the same composition. Photodarkening sensitivity also increases with As content of the samples and therefore we conclude that two conditions are necessary for an appreciable photodarkening effect to be observed. Firstly, several As atoms must be in neighbouring positions and secondly there must be volume defects in their vicinity.

When both conditions are satisfied the light induced redistribution of electron densities is stabilized by the formation of relatively stable As_n clusters. We believe that similar mechanisms can be used to describe the photodarkening effects in amorphous As selenides.

Further aspects of this paper are described and discussed in more detail elsewhere[1,2,3].

ACKNOWLEDGEMENTS

The authors gratefully acknowledge the help of research grants from the Science and Engineering Research Council, and the co-operation of Dr. W. Taylor of the Physics Department of Edinburgh University in making available the experimental facilities for Raman spectroscopy.

REFERENCES

1) M. Frumar, A.P. Firth and A.E. Owen, Phil. Mag. (submitted).

2) A.P. Firth, M. Frumar and A.E. Owen, Solid State Commun. (submitted).

3) M. Frumar, A.P. Firth and A.E. Owen, J. Non-Cryst. Solids (submitted).

4) P. Ewen, Ph.D. Thesis, Edinburgh University (1978).

5) F. Kosek et al., Czech. J. Phys. B32, (1982), 719.

6) R.J. Nemamich et al., Phys. Rev. B18, 12, (1978), 6900.

7) G. Lucovsky, J.S. Knights, Phys. Rev. B10, 10, (1974), 4324.

PHILOSOPHICAL MAGAZINE B, 1984, VOL. 50, NO. 4, 463–475

Reversible photodarkening and structural changes in As_2S_3 thin films

By M. FRUMAR†, A. P. FIRTH and A. E. OWEN
Department of Electrical Engineering, University of Edinburgh, King's Buildings, Edinburgh EH9 3JL, Scotland

[Received 29 July 1983 and accepted 1 May 1984]

ABSTRACT

The photodarkening effect in evaporated As_2S_3 films has been studied. Optical transmissivity was measured and its dependence on intensity, wavelength, temperature and previous thermal history was found. A structural investigation was also made using Raman spectroscopy. A feature at 231 cm^{-1} in the Raman spectra, which is associated with homopolar As–As bonds, is enhanced after photodarkening. A model based on the redistribution of chemical bonds under illumination is used to explain the results.

§ 1. INTRODUCTION

The strong illumination of many amorphous chalcogenides by light whose energy is near that of the optical gap may cause changes in optical transmissivity, refractive index, microhardness, density and other physical and chemical properties (see, for example, Tanaka and Ohtsuka 1978, Grigorovici and Vancu 1981, Averjanov, Kolobov, Kolomiets and Lyibin 1980). These so-called photostructural effects have a variety of potential applications in optical and optoelectronic devices, and in recent years they have been the subject of considerable research.

Many materials have been investigated, among them thin films in the amorphous As–S system and in particular the composition As_2S_3. The compound As_2S_3 is favoured because of its relative structural simplicity; it is easily prepared and amorphous thin films are stable with a low tendency to crystallize. During evaporation the vapour phase of As_2S_3 dissociates into molecular-like particles such as As_2S_2, As_3S_4, As_4 and S_n, and these molecular units can be found in the as-evaporated films condensed onto cold substrates (Nemanich, Connell, Hayes and Street 1978, Solin and Papatheodorou 1977, Keneman, Bordogna and Zemel 1978 a). The films can be 'polymerized', either by annealing near the glass transformation temperature T_g or by strong illumination with photons of energy close to that of the optical gap, E_g. The 'polymerization' is accompanied by an irreversible change in structure and other physical properties of the films. The final structure of well-annealed thin films is similar to that of bulk glasses of As_2S_3 (Solin and Papatheodorou 1977, Nemanich *et al.* 1978). The illumination of well-annealed

† Present address: University of Chemical Technology, 53210 Pardubice, Czechoslovakia.

samples by light with an energy near that of the band gap produces further changes in optical transmissivity, and other properties, which are reversible. The original state can be fully restored by annealing near T_g, or partly restored by illumination with light of energy lower than E_g.

Several models have been suggested to explain the reversible photostructural changes. Unfortunately they are mostly speculative, without directly supporting evidence, and cannot explain all the experimental observations. Berkes, Ing and Hillegas (1971), Keneman *et al.* (1978 a, b) and Tanaka and Kikuchi (1972) have all proposed that illumination of the films changes the distribution of chemical bonds in the material, and that products of photolysis such as sulphur and arsenic are formed. It is suggested that arsenic oxide is also formed when illumination is carried out in air (Berkes *et al.* 1971).

Another model of photo-induced reversible changes in chalcogenide layers assumes that there occurs photo-induced polymerization of the layers (see, for example, Grigorovici and Vancu 1981). As already mentioned, however, annealing of samples at temperatures near T_g 'erases' the photo-induced changes; if this model were correct the annealing process would be connected with depolymerization, but there is no experimental evidence to support this. Moreover, the polymerization model predicts densification and a consequent decrease in the thickness (volume) of the sample after illumination, in contradiction to the experimental results for As_2S_3 (Tanaka 1976, Hamaka, Tanaka and Iizima 1977).

A third approach to the explanation of reversible photostructural changes in chalcogenide films is essentially phenomenological (see, for example, Tanaka 1980, Krasnov and Remesnik 1980, Averjanov *et al.* 1980). It is proposed that at least two metastable states connected with a rearrangement of chemical bonds and atomic positions occur in amorphous chalcogenide films. Bandgap illumination is supposed to change the electron densities, and consequently the positions of some of the atoms are also changed. This stabilizes the new state and the previous optical properties are changed.

In this paper we report results on the optical transmissivity and its temperature and spectral dependence, as well as new results of a Raman study of photostructural changes in As_2S_3 films. Both annealed and photodarkened states have been studied, as well as the behaviour of amorphous As_2S_3 during illumination at different wavelengths and light intensities. The aim of the work is to provide new data on the reversible part of the photostructural changes in thin films of amorphous As_2S_3.

§ 2. Experimental

Thin films of amorphous As_2S_3 were deposited by vacuum evaporation onto microscope slides or slides of Corning 7059 glass, using as the source material small fragments of bulk As_2S_3 glass of 99·999% purity. The vacuum was less than 10^{-5} Torr, and the substrate was at room temperature. For some of the Raman experiments the substrate was first covered with a thin evaporated layer of Al. During deposition the thickness of the amorphous As_2S_3 films was measured with a quartz thickness monitor. Films of total thickness ranging from 1 to 5 μm were prepared, at a deposition rate of

2–5 nm s^{-1}. The As_2S_3 layers were annealed at 200–210°C for at least 1 hours; the heating and cooling took between 2 and 4 hours. To avoid oxidation of the As_2S_3, the samples were subsequently both annealed and illuminated in an atmosphere of dry N_2.

Raman spectra were measured using conventional back-reflection scattering. The samples were excited mainly with red light of wavelengths 676·4 and 647·1 nm from a Kr-ion laser. Green lines at 568·2 and 530·9 nm and the blue line at 488·0 nm were also used. A Coderg computer-controlled T800 triple spectrometer with a cooled RCA-C3 1034A photomultiplier operating in the photo-counting mode were used for detection. All spectra were measured at room temperature with a spectral slit width of $\sim 3\ cm^{-1}$. The laser was only slightly focused, and the power was kept below 50 mW. Plasma lines were removed by a prism filter.

Samples were photodarkned with a 500 W tungsten lamp at a distance of 20 cm. A solution of 1M $CuSO_4 . 5H_2O$, 2 cm thick, was used as an infrared filter. Samples were also illuminated by an Ar-ion laser fitted with a spatial filter and a beam-expanding system. Intensities up to 200 mW cm^{-2} at wavelengths of 488·0 and 514·5 nm were used. In some cases samples were actually photodarkned during the recording of the Raman spectra using the exciting wavelengths of 568·2, 530·9 and 488·0 nm. The optical transmissivity of the films was also measured during the recording of the Raman spectra.

§ 3. Results

The optical transmissivity of thin films of As_2S_3 is influenced strongly by the intensity and wavelength of illumination, the ambient temperature and

Fig. 1

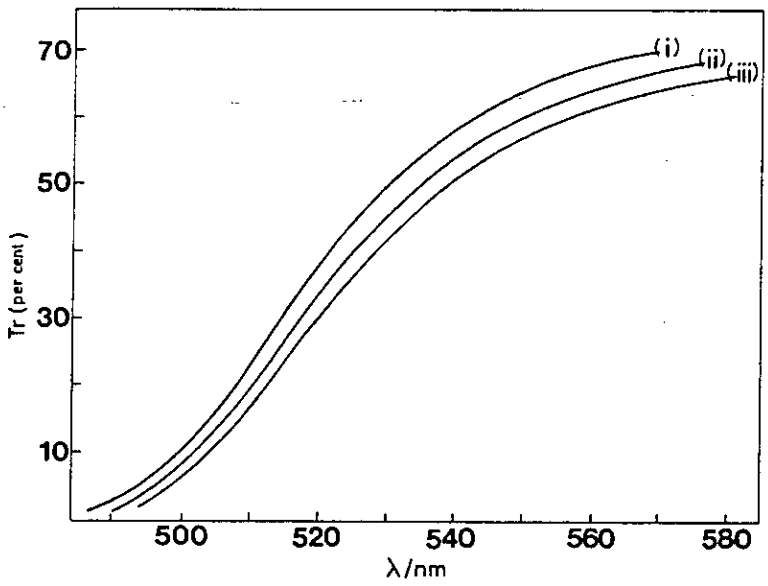

(*a*)

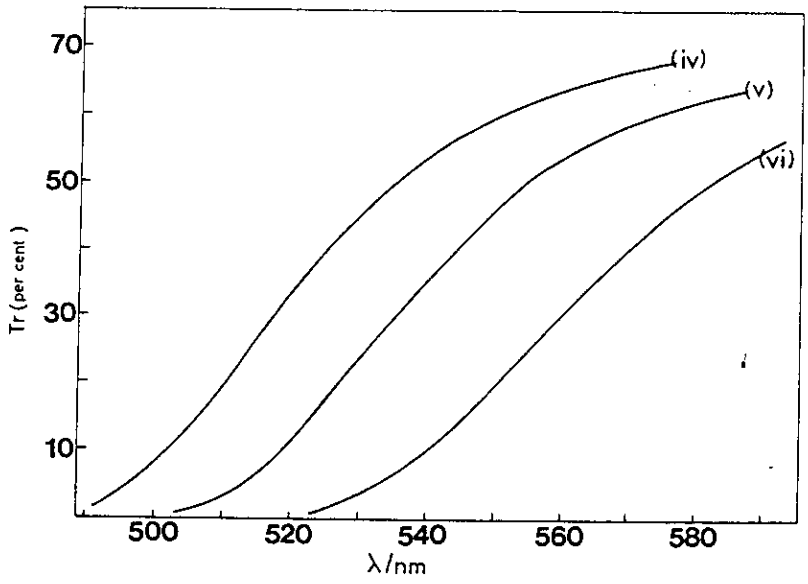

(*b*)

The spectral dependence of the transmissivity of As_2S_3 thin films. (*a*) Curve (i) as-evaporated film, curve (ii) annealed film, curve (iii) annealed film exposed to tungsten lamp for 1 hour. (*b*) Annealed film measured at (i) 300 K, (ii) 405 K, (iii) 501 K.

the thermal history of the film. Typical results are shown in figs. 1 to 4. Curve (i) in fig. 1 (*a*) shows the transmissivity as a function of wavelength for an as-deposited, vacuum-evaporated thin film of As_2S_3; curve (ii) is for an annealed film (200°C, 1 hour) and curve (iii) for a film after illumination (tungsten lamp, 1 hour); all curves were measured at room temperature. The sequence of measurements could be (i)→(ii)→(iii)→(ii)→(iii) and so on, or (i)→(iii)→(ii)→(iii) and so on. In fig. 1 (*b*) the curves (iv), (v) and (vi) are for an annealed film measured at 300, 405 and 501 K, respectively; these results simply correspond, of course, to the decrease in optical energy gap with increasing temperature and illumination.

Figure 2 illustrates in more detail the effect of temperature (and heat treatment) on transmissivity at four different wavelengths. Again, these results could be obtained in a variety of ways. For example, curve (*c*) (λ = 510 nm) could be traced out by starting at point 1, corresponding to an annealed film at about room temperature. Illumination would cause the transmissivity to decrease down a vertical line to point (2). On raising the temperature the transmissivity decreases still further (as in fig. 1 (*b*)), and at a high enough temperature (in this case about 160°C) the sample is at least partially ' annealed '. In the particular experiment illustrated the temperature was then decreased continuously to about −170°C and the upper curve, corresponding to an annealed sample, was traced out. At −170°C the film was illuminated and the transmissivity decreased down the vertical line. On reheating the transmissivity decreased further, along the lower line, and the

Fig. 2

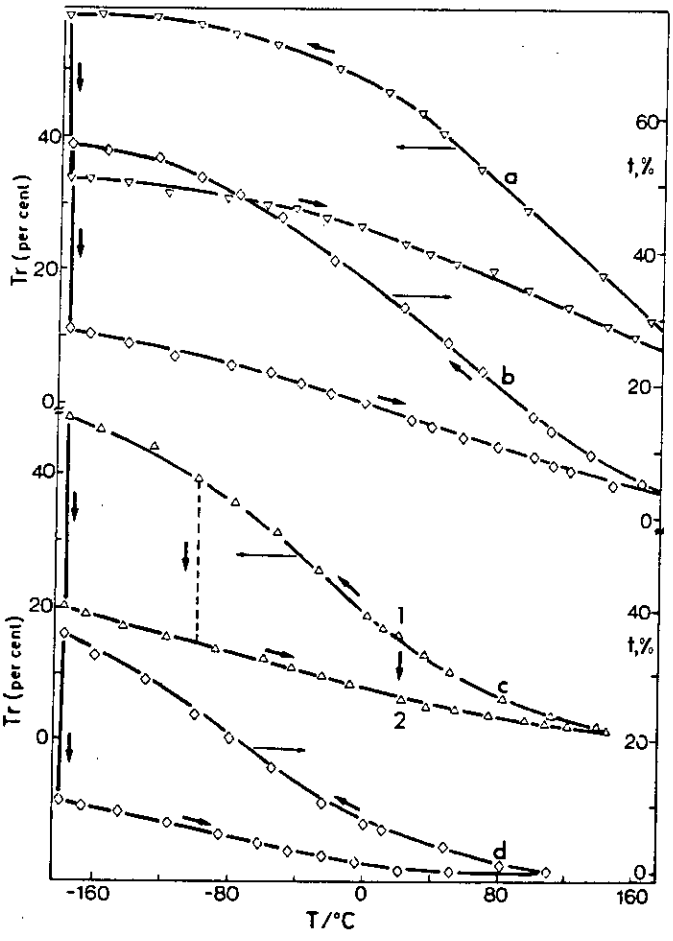

The temperature dependence of the transmissivity of As_2S_3 thin films measured at (*a*) $\lambda = 530$ nm, (*b*) $\lambda = 520$ nm, (*c*) $\lambda = 510$ nm and (*d*) $\lambda = 500$ nm. The vertical lines correspond to the change in transmissivity produced by illumination by a tungsten lamp for 1 hour.

loop could be retraced. It would also be possible, of course, to stop at any intermediate temperature to carry out the photodarkening process, for example, as indicated by the dashed vertical line at about -100°C. Note, however, that the temperature cycling of the upper part of the loop could be followed in either direction, but the vertical transitions (photodarknening) can occur only in the downward direction.

Figure 3 illustrates the development of the photodarkening effect at room temperature as a function of time, but with the illumination turned off and on at arbitrary intervals ; during the on-periods the intensity of illumination remained constant. A similar experiment is recorded in fig. 4, but here the illumination was subjected to several arbitrary decreases or increases in

Fig. 3

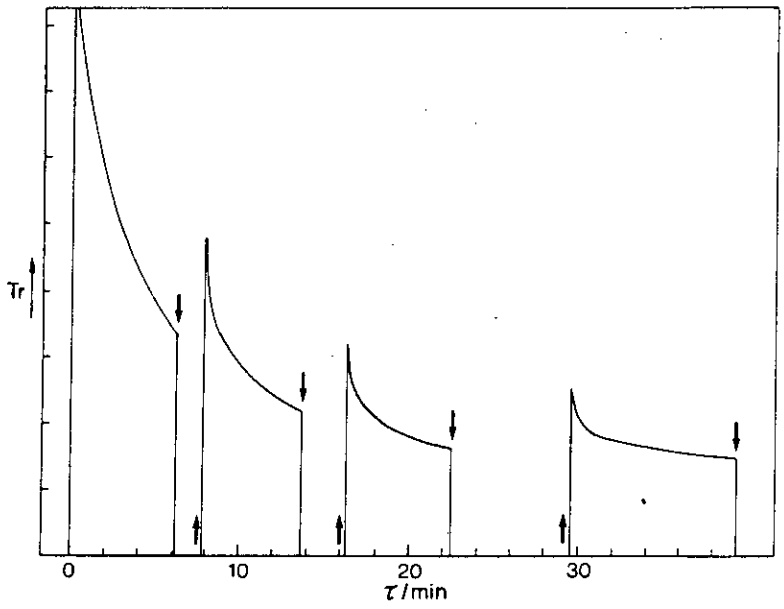

The change in the transmissivity of annealed As_2S_3 thin films during illumination at a constant intensity by 514·5 nm laser light. The vertical arrows correspond to the closing (↓) and opening (↑) of a shutter. The measurements were made at room temperature.

intensity at different times. The following points should be noted from figs. 3 and 4.

(1) A small annealing effect is observed, even at room temperature.
(2) On illumination there is an initial rapid decrease in optical transmissivity (photodarkening), but on interrupting the illumination the transmissivity increases (annealing) and then decreases again on further illumination (fig. 3).
(3) On decreasing the intensity of illumination, photobleaching is observed (fig. 4), whereas on increasing the intensity further photo-darkening occurs.
(4) The rates of photodarkening and bleaching are not the same (fig. 4). This asymmetry implies that the changes in transmissivity cannot be caused by thermal effects (that is, by the small changes in sample temperature during and after illumination).
(5) After prolonged exposure at a particular intensity the optical transmissivity decreased to a saturation value. In the saturated state the photodarkening is determined, at a given temperature, by the wavelength and intensity of illumination. This implies, that for a given intensity, the cycles of changes traced out in fig. 2 are unique provided the photodarkening (that is, the lower part of the cycle) has reached its saturation value.

Fig. 4

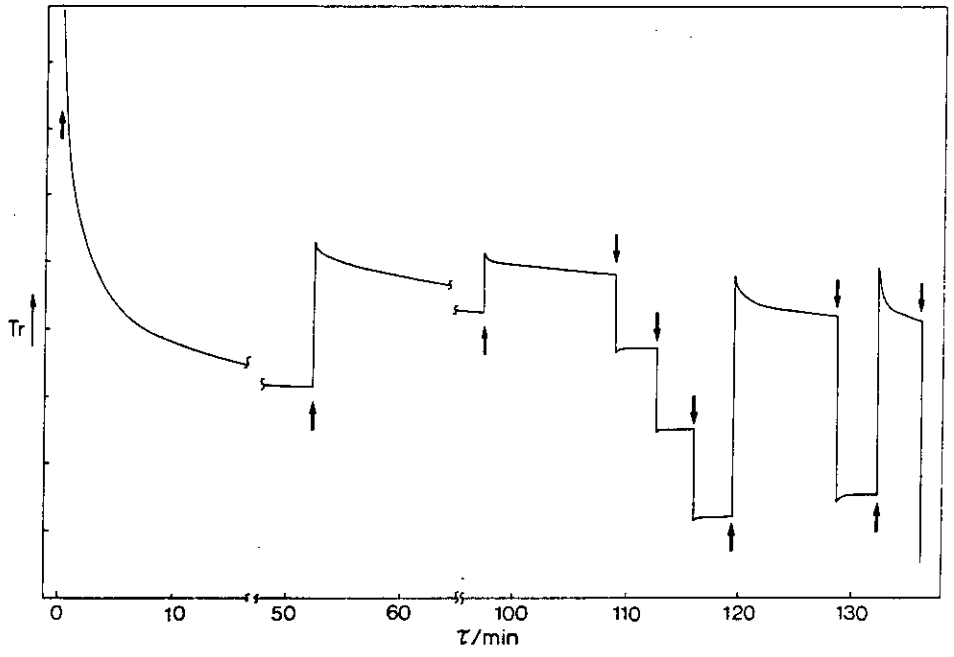

The change in the transmissivity of As_2S_3 thin films when illuminated by 514·5 nm laser light. The vertical arrows correspond to increasing (↑) and decreasing (↓) incident laser intensity. The curves were measured at room temperature.

The total change in transmissivity for the reversible part of the photostructural change was greater than 90% of its initial value at a wavelength of 514·5 nm. The upper level of the intensity of illumination which can be applied is limited by irreversible processes which would lead to melting and disintegration of the sample.

The Raman spectra of evaporated As_2S_3 films are shown in fig. 5. Curve (*a*) shows the as-deposited film. The characteristic sharp features in the region 100–250 cm^{-1} have been assigned to molecular units such as As_4S_4, S_n and As_4 (Ewen 1978, Nemanich *et al.* 1978, Solin and Papatheodorou 1977). After annealing the film curve (*b*) was obtained. The sharp features are considerably reduced, but relatively broad features with maxima at 187 and 231 cm^{-1} remain. Similar results were observed by Nemanich *et al.* (1978) and were taken as evidence that some ' wrong ' bonds of the type As–As and S–S exist even in well-annealed As_2S_3 films.

Figure 6 shows the effect of illumination on the Raman spectra of As_2S_3 layers. It can be seen that the bands with maxima at 187 and 231 cm^{-1} are clearly affected by the illumination. The intensity of the band at 231 cm^{-1} is increased, while the intensity of the band at 187 cm^{-1} is decreased. Similar results were obtained by Ewen (1978) on bulk As_2S_3 glasses. Ewen observed a general decrease in the intensity of the Raman spectrum during illumination, but the relative intensity of the band at 231 cm^{-1} increased. The results are

Fig. 5

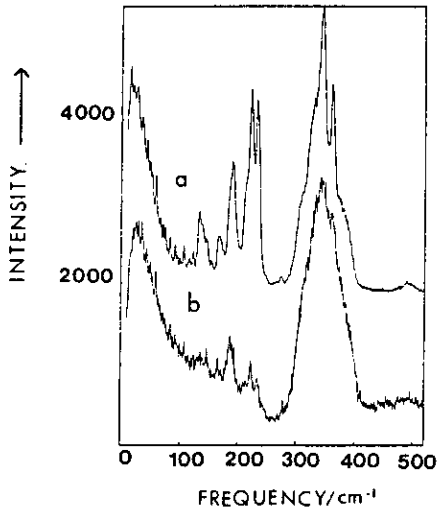

Raman spectra of (*a*) an as-evaporated and (*b*) an annealed As_2S_3 thin film.

Fig. 6

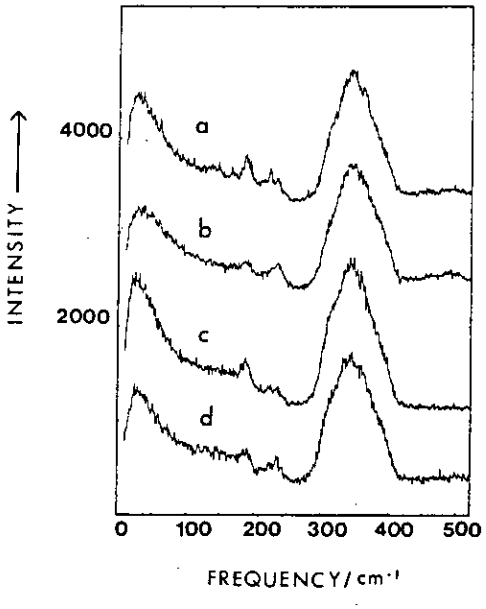

The Raman spectra of a typical As_2S_3 film illustrating reversible photodarkening. (*a*) The first annealed state, (*b*) the photodarkened state produced by Ar-ion laser illumination, (*c*) the second annealed state and (*d*) the second photodarkened state produced by Ar-ion laser illumination. All the spectra were recorded using the 647·1 mm wavelength, and were normalized to the height of the 340 cm^{-1} Raman band.

also in agreement with those of Bertoluzza, Fagnano and Monti (1979) who found that illumination of As_2S_x glasses with $x \leqslant 3$ changed the Raman spectra. The Raman band near 231 cm^{-1} was enhanced, and the intensity of the band at 187 cm^{-1} reduced.

Curve (*c*) in fig. 6 was obtained after annealing the film a second time. It is clearly similar to curve (*a*), showing that the observed reversible photodarkening is connected with reversible changes in structure. Curve (*d*) was obtained after the sample was illuminated again. The enhanced 231 cm^{-1} band and the reduced 187 cm^{-1} Raman band are again seen. The cycling between the well-annealed and photodarkened state was repeated many times with reproducible results.

Figure 7 shows the Raman spectra of As_2S_3 films which were photodarkened using the exciting wavelength. The Raman spectra were recorded after the photodarkening had saturated. Curve (*b*), (*c*) and (*d*) were recorded using wavelengths of 568·2, 530·9 and 488·0 nm, respectively, and they reveal a further enhancement of the 231 cm^{-1} Raman band compared with the photodarkening state shown in fig. 6. Curve (*a*) shows the Raman spectrum of a well-annealed film for comparison ($\lambda_{exc} = 647{\cdot}1$ nm). Changes in the Raman spectra (fig. 7) and transmissivity were reversible, and after annealing the original state (fig. 7, curve (*a*)) was restored. The reversibility was demonstrated several times.

Since the results are similar over a broad range of wavelengths (568·2–488·0 nm) this indicates that the observed enhancement of the 231 cm^{-1} band does not result from a resonance effect.

Fig. 7

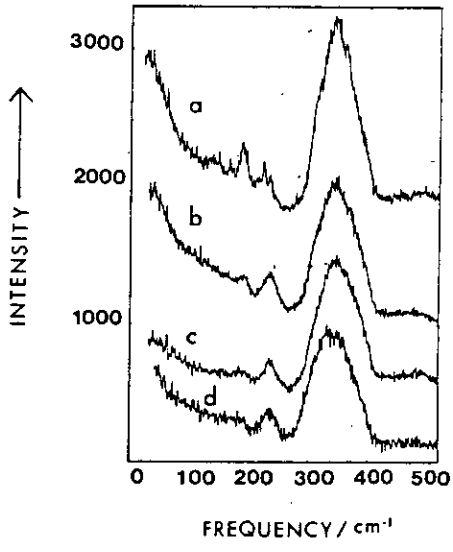

Raman spectra of As_2S_3 thin films. (*a*) An annealed film ($\lambda_{exc} = 647{\cdot}1$ nm). (*b*, *c*, *d*) The spectra of films that were photodarkened and excited using the wavelengths 568·2, 530·9 and 488·0 nm, respectively.

The sharp Raman band at 231 cm^{-1} in the Raman spectra of As_2S_x glasses has been assigned to the vibrations of As–As bonds, as reported by Ewen (1978), Nemanich *et al.* (1978), and Kosek, Cimpl, Matyas and Pisarcik (1982). In these papers the increase in the intensity of the Raman band at 231 cm^{-1} was correlated with an increase in the As content of the glass, and was thus related to an increase in the As–As bond density. Moreover, the Raman spectrum of amorphous arsenic has a broad band between 170 and 310 cm^{-1}, the centre being at $\sim$225 cm^{-1} (Lannin 1977, Davis 1981). Lucovsky and Knights (1974) studied the infrared absorption spectra of amorphous As and found a strong absorption band centred at 230 cm^{-1} which they connected with the vibrations of As_4 pyramids.

§ 4. Discussion

From these results we deduce that the enhanced 231 cm^{-1} band in the Raman spectra of As_2S_3 thin films is caused by an increase in the density of As–As bonds in photodarkened layers. The band is not as broad as the band at 231 cm^{-1} found in amorphous As (Lannin 1977, Davis 1981), which may be a result of the more molecular nature and the weaker coupling of As–As atoms into the amorphous network in photodarknened films. Since we have found that the intensity of the Raman band at 231 cm^{-1} is increased with photodarkening and decreased with annealing, this suggests that the reversible part of the photodarkening effect is associated with a redistribution of chemical bonds in As_2S_3 layers which involves an increase in the density of As–As bonds under illumination.

In well-annealed films of As_2S_3, the hetero-type bonds of As–S are preferred, and the reversible structural change connected with photodarkening can be described by

$$2|\text{As–S}| \rightarrow |\text{As–As}| + |\text{S–S}|. \qquad (1)$$

Equation (1) shows that the bond statistics of As_2S_3 films are shifted by strong illumination from a state which is close to the chemical ordered model towards a state described by the random network model. The randomness of the chemical bond distribution is therefore increased.

In a chemical approach the photodarkening process can be described as a photolytic reaction,

$$As_2S_3 \underset{A(T),\, h\nu_2,\, I_2}{\overset{h\nu_1,\, I_1}{\rightleftharpoons}} As_2S_{3-x} + xS, \qquad (2)$$

where I_i is the incident light intensity ($I_1 > I_2$), $h\nu_i$ is the incident light energy ($h\nu_2 \geqslant h\nu_1$; $h\nu_1 = E_g$ of the glass). $A(T)$ indicates thermal annealing at a temperature T. Similar suggestions have already been made by several authors, but mostly without the support of direct evidence.

The formation of homo-type bonds (As–As and S–S) from hetero-type bonds in As–S layers is possible without large structural rearrangement ; a proposed mechanism is illustrated in fig. 8. The final products of this reaction are probably As_n ($n \geqslant 2$) clusters.

The formation of relatively stable homo-type bonds in compound chalcogenides (for example, As–As bonds in As_2S_3), which corresponds to a decrease in the formal valence state of ' metallic ' atoms, is possibly the factor which

Fig. 8

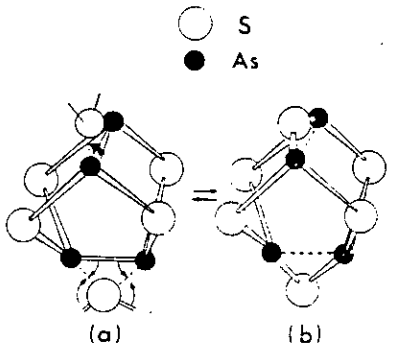

A simplified model illustrating the structural units in (*a*) photodarkened and (*b*) annealed As_2S_3 films. The formation of As_n clusters with $n \geqslant 2$ will be a further stage in the process.

enables the formation of two metastable states in these compounds. Photostructural effects have been found in chalcogenide systems containing As, Sb and Ge, and each of these elements can form lower-valence chalcogenides and relatively strong homo-type bonds.

The chemical reactions described by eqns. (1) and (2) are thermodynamically unfavourable (ΔG is positive). The As–As bonds or As clusters formed by photodarkening can be spontaneously 'dissolved' and converted back to As–S bonds. The rate of this process is slower at low temperature, and only in the vicinity of T_g, where the atoms are relatively mobile, can thermal bleaching 'dissolve' all types of As_n clusters ($n \geqslant 2$) and completely reverse the photodarkening process. At lower temperatures, where only partial photobleaching occurs, the smaller As_n clusters ($n = 2$) represented by single As–As bonds can probably be dissolved, and larger As clusters—for example, As_4 pyramids—may be relatively stable and form the steady-state part of the photodarkening effect. As the formation of As clusters involves the absorption of several photons, the density of As–As bonds at a given temperature and wavelength depends on the intensity of illumination. Changes in the density of As clusters, or of As–As bonds, which are directly related to changes in optical density, will be influenced by changing the intensity of the incident light or by the temperature of the layer (see figs. 2–4).

The photodarkening effect is thus a dynamic process, and some photobleaching of films can be observed even at room temperature (see figs. 3 and 4). The observed intensity of the 231 cm^{-1} Raman band is lower in samples measured several hours after photodarkening (fig. 6) than in samples photodarkened to saturation by the exciting wavelength used to record the Raman spectra.

The amorphous state contains many defects of local structure, and the energy of individual bonds has no sharp value. Thus, as we have found, even illumination of As_2S_3 layers with $h\nu < E_g$ can produce the photodarkening effect, but the change in transmissivity is lower than the change produced by

bandgap illumination. This result is also in accordance with the data obtained by Tanaka (1980).

In crystalline As_4S_n ($n=3, 4$), and probably in the amorphous As–S systems, As–As bonds are longer than As–S bonds (for example, in As_4S_4 As–As = 2·59 Å and As–S = 2·24 Å, and in As_4S_3 As–As = 2·45 Å and As–S = 2·21 Å; Porter and Sheldrick 1972). In our model the photodarkening is connected with the breaking of some As–S bonds. Instead of shorter As–S bonds, longer As–As bonds are formed. The reported increase in the thickness of As_2S_3 layers after illumination (Tanaka 1976, Hamaka *et al.* 1977), which was confirmed in this work, can be accounted for if it is assumed that a small fraction of the As–S bonds contribute to the change in thickness. Only changes in bond length perpendicular to the substrate plane contribute to the thickness change ΔX;

$$\Delta X = \Delta b \sin \psi, \tag{3}$$

where the change in bond length per bond, Δb, is given by

$$\Delta b = \tfrac{1}{2}(b_{\mathrm{As-As}} + b_{\mathrm{S-S}}) - b_{\mathrm{As-S}}, \tag{4}$$

and ψ is the angle between a given bond direction and the substrate plane. Thus, the mean value of ΔX is

$$\overline{\Delta X} = (\Delta b/\pi) \int_0^{\pi} \sin \psi \, d\psi = 2\Delta b/\pi. \tag{5}$$

A similar expression can be obtained for the average layer thickness $\overline{X_0}$ of the original As–S bonds;

$$\overline{X_0} = 2b_{\mathrm{As-S}}/\pi$$

and hence

$$\overline{\Delta X}/X_0 = \Delta b/b_{\mathrm{As-S}}. \tag{6}$$

For the bond lengths quoted above, and with $b_{\mathrm{S-S}} = 2{\cdot}2$ Å, these equations give $\overline{\Delta X}/X_0 = 0{\cdot}068$.

According to Hamaka *et al.* (1977), the relative change in thickness determind experimentally is 0·004, and hence the fraction of As–S bonds involved in the photostructural change is 0·004/0·068 = 0·059, approximately 6% of the total.

§ 5. Conclusions

We have found that the reversible part of the photodarkening effect observed in As_2S_3 films is accompanied by an increase in the Raman band with its maximum at 231 cm^{-1}. This was interpreted as an increase in the As–As bond density as a result of illumination. This experimental evidence supports previous speculative suggestions about bond redistribution or a photolytic chemical reaction connected with photo-darkening. The actual redistribution of chemical bond depends on the intensity and wavelength of the illumination, and also on the temperature of the film. Photodarkening is a dynamic equilibrium which can be shifted by changes in temperature and in the conditions of illumination. Our interpretation gives a structural meaning to the double-well model, and also predicts the increase in volume of illuminated films.

ACKNOWLEDGMENTS

The authors gratefully acknowledge the receipt of research grants from the Science and Engineering Research Council, and the cooperation of Dr. W. Taylor of the Physics Department of Edinburgh University in making available the experimental facilities for Raman spectroscopy.

REFERENCES

AVERJANOV, V. L., KOLOBOV, A. V., KOLOMIETS, B. T., and LYUBIN, V. M., 1980, *Phys. Stat. Sol.* (a), **57,** 81.

BERKES, J. S., ING, S. W., and HILLEGAS, W. J., 1971, *J. appl Phys.*, **42,** 4908.

BERTOLUZZA, A., FAGNANO, C., and MONTI, P., 1979, *Molecular Spectroscopy of Dense Phases*, edited by M. Grosman *et al.* (New York : Elsevier), p. 405.

DAVIS, E. A., 1981, *J. Phys., Paris*, **42,** C4, Suppl. No. 10, 855.

EWEN, P., 1978, Ph.D. Thesis, Edinburgh University.

GRIGOROVICI, R., and VANCU, A., 1981, *J. Phys., Paris*, **42,** C4, Suppl. No. 10, 391.

HAMAKA, H., TANAKA, K., and IIZIMA, S., 1977, *Solid St. Commun.*, **23,** 63.

KENEMAN, S. A., BORDOGNA, J., and ZEMEL, J. N., 1978 a, *J. opt. Soc. Am.*, **68,** 32 ; 1978 b, *J. appl. Phys.*, **49,** 663.

KOSEK, F., CIMPL, Z., MATYAS, M., and PISARCIK, M., 1982, *Czech. J. Phys.* B, **32,** 719.

KRASNOV, V. F., and REMESNIK, V. G., 1980, *Avtometroya*, **6,** 101.

LANNIN, J. S., 1977, *Phys. Rev.* B, **15,** 3836.

LUCOVSKY, G., and KNIGHTS, J. S., 1974, *Phys. Rev.* B, **10,** 4324.

NEMANICH, R. J., CONNELL, A. N., HAYES, T. M., and STREET, R. A., 1978, *Phys. Rev.* B, **18,** 6900.

PORTER, E. J., and SHELDRICK, G. M., 1972, *J. chem. Soc., Dalton Trans.*, p. 1347.

SOLIN, S. A., and PAPATHEODOROU, G. N., 1977, *Phys. Rev.* B, **15,** 2084.

TANAKA, K., 1976, *Structure and Excitation of Amorphous Solids*, edited by G. Lucovsky and F. L. Galeener, A.I.P. Conf. Proc. No. 31 (New York : American Institute of Physics), p. 148 ; 1980, *Solid St. Commun.*, **34,** 201.

TANAKA, K., and KIKUCHI, M., 1972, *Solid St. Commun.*, **11,** 1311.

TANAKA, K. and OHTSUKA, Y., 1978, *Thin Solid Films*, **48,** 17.